



Publicly Accessible Penn Dissertations


---

Summer 8-12-2011

# Investigating tRNA Release from the Bacterial Ribosome

Ian S. Farrell  
ifarrell@sas.upenn.edu

Follow this and additional works at: <http://repository.upenn.edu/edissertations>

 Part of the [Biochemistry Commons](#), and the [Molecular Biology Commons](#)

---

## Recommended Citation

Farrell, Ian S., "Investigating tRNA Release from the Bacterial Ribosome" (2011). *Publicly Accessible Penn Dissertations*. 376.  
<http://repository.upenn.edu/edissertations/376>

This paper is posted at ScholarlyCommons. <http://repository.upenn.edu/edissertations/376>  
For more information, please contact [libraryrepository@pobox.upenn.edu](mailto:libraryrepository@pobox.upenn.edu).

---

# Investigating tRNA Release from the Bacterial Ribosome

## Abstract

Translation of mRNA into proteins is integral in all living organisms, and takes place on the ribosome. In recent years, the X-ray crystal structures of biologically relevant ribosome complexes came into light, and the advance of kinetic studies was soon to follow, leading to a better understanding of the general ribosomal mechanism. However, there still remains some ambiguity in certain ribosome functions.

Ribosomal protein L1 initially became relevant in the early 1980s when it was determined that ribosomes lacking L1 showed a decreased capacity for *in vitro* protein synthesis. Later, it was shown that the L1-stalk is a highly mobile region of the ribosome, and that it may be involved in the release of deacylated-tRNA from the exit-site, after translocation. By using a fluorescently labeled L1 reconstituted ribosome as an E-site probe we were able to study the release of deacylated-tRNA from translocating ribosomes in a time-resolved manner. The movement of the L1-stalk with relation to the deacylated-tRNA was measured using fluorescence resonance energy transfer (FRET) measurements between labeled L1 and labeled tRNAs (L/t FRET). Further, the movement of deacylated-tRNA with relation to the P-site tRNA was measured using fluorescently labeled tRNAs (t/t FRET), and the release of deacylated-tRNA was measured using changes in anisotropy. We demonstrate that the deacylated-tRNA can be released from the ribosome via three possible different pathways, depending on the conditions. Further, in Chapter V, we begin to demystify the interaction that the E-site region of the ribosome has with deacylated-tRNAs in solution, and demonstrate the changes on deacylated-tRNA release when excess tRNAs are present.

The optimization of the creation of a viable E-site probe will prove to be important for future studies in both kinetic work and single molecule work when focusing on tRNA interaction with the E-site of the ribosome.

## Degree Type

Dissertation

## Degree Name

Doctor of Philosophy (PhD)

## Graduate Group

Chemistry

## First Advisor

Barry S. Cooperman

## Keywords

Ribosome, tRNA, E-site

## Subject Categories

Biochemistry | Molecular Biology

# INVESTIGATING tRNA RELEASE FROM THE BACTERIAL RIBOSOME

Ian S. Farrell

A DISSERTATION

in

Chemistry

Presented to the Faculties of the University of Pennsylvania

in

Partial Fulfillment of the Requirements for the Degree of Doctor of Philosophy

2011

Supervisor of Dissertation

---

Dr. Barry S. Cooperman  
Professor of Chemistry

Graduate Group Chairperson

---

Dr. Gary A Molander, Professor of Chemistry

Dissertation Committee

Dr. David W. Christianson, Professor of Chemistry

Dr. Ivan J. Dmochowski, Associate Professor of Chemistry

Dr. Yale E. Goldman, Professor of Physiology

Dedicated to my parents, Lynn and Jan Farrell, and my loving wife Kelli Farrell

## ACKNOWLEDGEMENTS

It is a pleasure and an honor to finally be able to acknowledge and thank the many people that have made this journey possible for me. First and foremost, this thesis would never have happened if it weren't for Dr. Barry S. Cooperman; his guidance and support proved to be invaluable during the trials and tribulations of this work. I can honestly say that he is one of the most intelligent people I know, and I can only strive to obtain the kind of well-rounded knowledge that Dr. Cooperman has for the world around him. Under his supervision, I believe I have obtained the skills necessary to further my career as a scientist, and a scholar.

I would like to show my gratitude towards our major collaborators with this project. In the text you will notice that a lot of materials were provided as kind gifts from other research labs, and instead of listing them all here, I would like to thank everyone. Dr. Yale Goldman is not only a committee member, but also a very close collaborator with the Barry Cooperman group, and his inspiring insights into my research have proved to be priceless. Dr. Akira Kaji is a close friend of the group, and his last minute questions during our group meetings always bring a finality to the presentations, and a smile to our faces.

In addition to Dr. Goldman, I would like to thank my committee members, Dr. David Christianson, and Dr. Ivan Dmochowski for their invaluable advice during my six years at Penn, through my annual (and sometimes bi-annual) committee meetings.

It is truly a pleasure to thank all of the current and past members of the Cooperman Group. Over the course of six years, you tend to witness many group

members enter and others leave. When I first joined the group, the advice of Nate Kreischer proved to stick with me throughout my PhD. studies, and helped me with my everyday work in the lab. Our technician in the lab, Nora Zuno, helped me with preparation and purification of ribosomes. Dr. Dongli Pan, Dr. Haiou Qin, and Dr. Hanqing Liu, were all senior members of the lab and helped me with everything from protein purification to kinetic scientist fits, if it weren't for these members of the group, I wouldn't be presenting here today. The current members of the group still provide engaging conversation and are extremely valuable to my growth as a scientist. Dr. Jaskiran Kaur, has forgotten more about tRNA aminoacylation, labeling, and purification than most people ever know in their lifetime, and I am honored to have learned these invaluable skills from her. Dr. Gabi Rosenblum, is not only a great scientist, working with really intriguing protein synthesis problems, but he is also a great friend, and I live vicariously through him and his adventures with his family on the weekends. Dr. Haibo Zhang has kept me company in the lonely hours before 8 AM in an otherwise empty department, and his contribution to the mRNA and ribosome purification fields in our lab has been excellent. Yuanwei Chen has been extremely helpful in developing the anisotropy studies in our lab, and performed the anisotropy measurements seen in Chapter IV. Wei Liu, Rong Shen, Dulce Alonso, and Michael Reiche have been incredible to work with, teach, and learn from, it is truly a great symbiotic relationship. Lastly, I'd like to thank a truly gifted undergraduate, Adriane Remiker, who started working under me with L1 studies, but has moved onto her own project. Adie has been a great friend, and an extremely good lab partner.

Last, but not least, doesn't begin to describe how much I need to thank my family and friends. I came into graduate school with a truly gifted class, and am fortunate to have found such great friends to share laughter, conversation, and even some science talk with over lunches and happy hours, Andre, Sara, Dan, Julie, Diana, and more recently, Emily, Ursula, Jerome, and Brian, thank you for keeping me grounded during this stressful time. Rob and Brandon, you two have been amazing friends, and I cannot wait to see where we all end up in 10 years, thank you for all your support and sometimes intelligent arguments during coffee breaks. Now to the nitty-gritty, Mom and Dad, without you guys I don't know how far I could have made it. You are truly an inspiration, and I hope I can be half as supportive to my children as you have been with me. Thank you, Thank you, Thank you. Mr. and Mrs. Quercetti, mom and dad, thank you for all of your support for both Kelli and myself during the past few years of graduate school, thesis writing, medical school, board exams, residency, etc... Your support and your open door at the beach have been greatly appreciated.

My wife, My life, My love, Kelli, you have no idea how grateful I am for your support and your love throughout these past six years. They have not been easy by any stretch of the imagination, but we have always persevered, and we are stronger for it. I cannot wait to start the rest of my life with you. I love you.

-Ian

## ABSTRACT

### INVESTIGATING tRNA RELEASE FROM THE BACTERIAL RIBOSOME

Ian S. Farrell  
Barry S. Cooperman

Translation of mRNA into proteins is integral in all living organisms, and takes place on the ribosome. In recent years, the X-ray crystal structures of biologically relevant ribosome complexes came into light, and the advance of kinetic studies was soon to follow, leading to a better understanding of the general ribosomal mechanism. However, there still remains some ambiguity in certain ribosome functions.

Ribosomal protein L1 initially became relevant in the early 1980s when it was determined that ribosomes lacking L1 showed a decreased capacity for *in vitro* protein synthesis. Later, it was shown that the L1-stalk is a highly mobile region of the ribosome, and that it may be involved in the release of deacylated-tRNA from the exit-site, after translocation. By using a fluorescently labeled L1 reconstituted ribosome as an E-site probe we were able to study the release of deacylated-tRNA from translocating ribosomes in a time-resolved manner. The movement of the L1-stalk with relation to the deacylated-tRNA was measured using fluorescence resonance energy transfer (FRET) measurements between labeled L1 and labeled tRNAs (L/t FRET). Further, the movement of deacylated-tRNA with relation to the P-site tRNA was measured using fluorescently labeled tRNAs (t/t FRET), and the release of deacylated-tRNA was measured using changes in anisotropy. We demonstrate that the deacylated-tRNA can be released from the ribosome via three possible different pathways, depending on the



conditions. Further, in Chapter V, we begin to demystify the interaction that the E-site region of the ribosome has with deacylated-tRNAs in solution, and demonstrate the changes on deacylated-tRNA release when excess tRNAs are present.

The optimization of the creation of a viable E-site probe will prove to be important for future studies in both kinetic work and single molecule work when focusing on tRNA interaction with the E-site of the ribosome.

## TABLE OF CONTENTS

CHAPTER I. INTRODUCTION.....	1
1.1 Protein Synthesis and the Ribosome.....	2
1.2 Ribosome Components.....	3
1.3 Bacterial Translation Cycle.....	4
1.3.1 Initiation.....	4
1.3.2 Peptide Elongation.....	4
1.3.3 Termination of Protein Synthesis and Ribosomal Recycling.....	5
1.3.4 Ribosome Movements During Translocation.....	6
1.4 Ribosome Structure.....	7
1.4.1 X-ray Crystallography.....	7
1.4.2 Cryoelectron Microscopy (Cryo-EM).....	9
1.5 Ribosome Protein L1.....	9
1.6 Deacylated-tRNA Release from the E-site.....	11
CHAPTER II. MATERIALS AND METHODS.....	25
2.1 Materials.....	26
2.1.1 Buffers.....	26
2.1.2 Reagents.....	28
2.2 Methods.....	29
2.2.1 Ribosome Preparations.....	29
2.2.1.1 70S Ribosomes from MRE 600 Cells.....	29
2.2.1.2 Subunits from MRE 600 Cells.....	30

2.2.1.3	70S Ribosomes From –L1 Cells.....	31
2.2.1.4	Subunits From –L1 Cells.....	31
2.2.2	mRNA Preparations.....	32
2.2.3	Protein Preparations.....	33
2.2.3.1	Preparation of Protein Factors.....	33
2.2.3.2	Preparation of Ribosomal Protein L1.....	34
2.2.3.2.1	Wild Type L1 Expression and Purification.....	34
2.2.3.3	Ribosomal Protein L1 Mutants.....	36
2.2.3.3.1	Primer Design For Site-directed Mutagenesis...	36
2.2.3.3.2	Mutagenesis.....	37
2.2.3.3.3	Fluorescent Dye Labeling of Mutated L1.....	38
2.2.3.3.4	Reconstitution of L1 into –L1 50S.....	39
2.2.3.4	Preparations of Crude Yeast and <i>E. coli</i> Aminoacyl RS....	40
2.2.4	tRNA Preparations.....	41
2.2.4.1	NaBH <sub>4</sub> Reduction of tRNAs to be Labeled.....	42
2.2.4.2	Aminoacylation of tRNAs.....	42
2.2.4.3	Hydrazide Labeling of Reduced tRNA.....	44
2.2.4.4	Rhodamine 110 Labeling of Reduced tRNA.....	44
2.2.5	Complex Formation.....	45
2.2.5.1	70S Initiation Complex (70SIC).....	45
2.2.5.2	Ternary Complex .....	46
2.2.5.3	PRE Complex.....	46
2.2.5.4	POST Complex.....	46

2.2.6 Equilibrium Assays.....	47
2.2.6.1 Filter Binding.....	47
2.2.6.2 Sucrose Cushion Pull Down.....	47
2.2.6.3 Puromycin Reactivity.....	48
2.2.6.4 FRET Measurements.....	48
2.2.7 Kinetic Assays.....	50
2.2.7.1 Ensemble FRET Experiments with Cy3 Dye as Donor.....	50
2.2.7.2 En. FRET Experiments with Rhd110 Dye as Donor.....	50
2.2.7.3 Anisotropy Measurements of tRNA <sup>fMet</sup> (Cy3).....	51
2.2.8 Rate Constant Estimation.....	52
CHAPTER III: OPTIMIZATION OF OVEREXPRESSION, PURIFICATION, AND	
RECONSTITUTION OF L1 MUTANTS.....	
3.1 Abstract.....	73
3.2 Introduction.....	74
3.3 Results.....	78
3.3.1 Optimization of L1 Overexpression.....	78
3.3.2 Optimization of L1 Purification.....	80
3.3.2.1 Metal Affinity Resin Optimization.....	81
3.3.2.2 Cell Lysis Optimization.....	81
3.3.2.3 MALDI Analysis .....	82

3.3.3 Optimization of Rb Recon. with Mutant and Labeled L1.....	82
3.3.3.1 –L1 70S Reconstitution.....	83
3.3.3.2 –L1 50S Reconstitution.....	84
3.4 Discussion.....	86
3.5 Conclusion.....	89
CHAPTER IV. THE CONDITIONS THAT AFFECT DEACYLATED tRNA	
MOVEMENT AFTER TRANSLOCATION.....	109
4.1 Abstract.....	110
4.2 Introduction.....	111
4.3 Results.....	114
4.3.1 L1 Interaction with tRNA <sup>fMet</sup> (L/t FRET).....	114
4.3.1.1 FRET Increase Upon Addition of TC to 70SIC.....	116
4.3.1.2 FRET Change Following Translocation.....	116
4.3.1.2.1 Buffer Conditions Affect Deacylated-tRNA-L1	
Movement.....	118
4.3.1.2.2 Peptidyl State of P-site tRNA Affects Deacylated-tRNA-	
L1 Movement.....	119
4.3.2 tRNA <sup>fMet</sup> Interaction with Phe-tRNA <sup>Phe</sup> (t/t FRET).....	121
4.3.2.1 In Buffer A, L1 Moves Away From Deacylated-tRNA <sup>fMet</sup>	
Prior to tRNA Release.....	122
4.3.2.2 In Buffer B, the tRNA Release Pathway is Dependent on	
P-site Peptidyl-state.....	123

4.3.3 Fluorescence Anisotropy Change of tRNA <sup>fMet</sup> (Cy3) After Translocation.....	125
4.3.4 Fitting of All Data to a Global Kinetic Scheme (EF-G Binding → Translocation) .....	126
4.3.4.1 Varying EF-G Concentration .....	127
4.3.5 Fitting of All Data to a Global Kinetic Scheme (Translocation → Deacylated-tRNA Release) .....	128
4.3.5.1 Global Fitting of Deacylated tRNA Release in Buffer A....	129
4.3.5.2 Global Fitting of Deacylated-tRNA Release in Buffer B (Peptidyl-tRNA in the P-site).....	129
4.3.5.3 Global Fitting of Deacylated-tRNA Release in Buffer B (Aminoacyl-tRNA in the P-site).....	130
4.4 Discussion.....	131
4.5 Conclusion.....	140
CHAPTER V: ADDITION OF DEACYLATED-tRNA IN SOLUTION ENHANCES THE SLOW RELEASE OF TRANSLOCATED DEACYLATED-tRNA <sup>fMet</sup> .....	171
5.1 Abstract.....	172
5.2 Introduction.....	172
5.3 Results.....	175
5.3.1 Preparation of a POST-1 Complex.....	175
5.3.2 The Extent of Competition Depends on the Concentration of the Added	

Deacylated-tRNA.....	176
5.3.3 Competition is Not Codon Specific.....	178
5.3.4 Addition of Ternary Complex Does Not Dramatically Enhance	
Deacylated-tRNA Release.....	178
5.4 Discussion.....	180
REFERENCES.....	197
APPENDIX 1 .....	212
APPENDIX 2 .....	221

## TABLE OF FIGURES

### CHAPTER I

Table 1.1 Components of <i>E. coli</i> Ribosomes.....	15
Figure 1.1 The Central Dogma of Molecular Biology .....	16
Figure 1.2 Aminoacyl-tRNA Charging Reaction .....	17
Figure 1.3 Overview of Bacterial Translation .....	18
Figure 1.4 Mechanism of EF-Tu Dependent Binding of Aminoacyl-tRNA to the Ribosomal A-site .....	19
Figure 1.5 Mechanism of Peptide Bond Formation .....	20
Figure 1.6 Mechanism of Translocation Showing Stepwise Movement of tRNA After GTP Hydrolysis .....	21
Figure 1.7 Relative Ribosomal Subunit Rotation .....	22
Figure 1.8 L1 Stalk Movements .....	23
Figure 1.9 Crystal Structure of L1 .....	24

### CHAPTER II

Table 2.1 Charging and Labeling Efficiencies of tRNAs .....	54
Table 2.2 Puromycin Reactivity of Ribosome Complexes .....	55
Figure 2.1 Separation of Purified –L1 Ribosomes .....	56
Figure 2.2 mRNA Purity and Activity .....	58
Figure 2.3 EF-Tu Activity Test Results .....	59
Figure 2.4 DNA and Protein Sequences of <i>E. coli</i> Ribosomal Protein L1 and	



Sequences of Single Mutant Primers .....	62
Figure 2.5 DNA Sequencing Results of the Single Mutants .....	64
Figure 2.6 Reconstitution Analyses of L1 and –L1 50S Subunits .....	65
Figure 2.7 Secondary Structures of tRNAs .....	66
Figure 2.8 FPLC Purification of Charged tRNAs .....	67
Figure 2.9 HPLC Purification of fMet-tRNA.....	68
Figure 2.10 HPLC Purification of Cy3-labeled tRNAs .....	69
Figure 2.11 SDS-PAGE Gel Electrophoresis Result of POST Complex.....	70
Figure 2.12 Schematic for A) Stopped Flow and B) Anisotropy Set-up.....	71
 <u>CHAPTER III</u>	
Table 3.1 Purification, Labeling, and Reconstitution Efficiency for L1 Preps.....	90
Table 3.2 Band Density Analysis for the Various Reconstitution Conditions.....	91
Figure 3.1 pET-16b Cloning Vector for L1 Expression.....	92
Figure 3.2 SDS-PAGE Analysis of Wild Type L1 During Overexpression.....	93
Figure 3.3 SDS-PAGE Analysis of Soluble L1 Created by Growth at Different Buffer Conditions.....	95
Figure 3.4 SDS-PAGE Analysis of L1 Purification Techniques.....	97
Figure 3.5 MALDI Analysis of T202C-L1 and T202C-L1 (Cy5).....	98
Figure 3.6 SDS-PAGE Analysis of Reconstituted 70S Ribosomes and Subunits...	99
Figure 3.7 SDS-PAGE Analysis of Incubation Time During L1 50S Recon.....	101
Figure 3.8 SDS-PAGE Analysis of Reconstitution Ratio of L1 and –L1 50S.....	102

Figure 3.9 SDS-PAGE Analysis of Incubation Temp on the Recon of L1 and and –L1 50S.....	103
Figure 3.10 SDS-PAGE Reconstitution of Wild Type L1 and Cy L1.....	105
Figure 3.11 [ <sup>35</sup> S]-fMet-tRNA <sup>fMet</sup> Binding to Ribosomes to Measure Activity.....	107
<u>CHAPTER IV</u>	
Table 4.1 Equilibrium FRET Efficiency Measurements .....	141
Table 4.2 Rate Constants Associated with the PRE-1 to POST-1 Translocation and tRNA Dissociation.....	144
Table 4.3 Binding Efficiencies of tRNA to Purified Ribosome Complexes.....	146
Table 4.4 Rate Constants for Global Scheme 4.1 .....	147
Table 4.5 Fluorescence Values for Global Fits.....	149
Table 4.6 FRET Efficiency Measurements for Equilibrium FRET and Stopped Flow FRET in PRE-1 and POST-1 States.....	151
Scheme 4.1 Global Scheme for Deacylated-tRNA Release from a Translocated Ribosome.....	153
Figure 4.1 Equilibrium FRET Efficiency Changes in Buffer A.....	155
Figure 4.2 Equilibrium FRET Efficiency Changes in Buffer B.....	156
Figure 4.3 FRET Efficiency Increase Associated with PRE-1 Formation.....	157
Figure 4.4 L/t FRET Efficiency Change Upon Translocation in Buffer A and Buffer B.....	158
Figure 4.5 L/t FRET Efficiency Change Upon Translocation in Buffer A.....	159

Figure 4.6 L/t FRET Efficiency Change Upon Translocation in Buffer B.....	160
Figure 4.7 t/t Equilibrium FRET Efficiency Change in Buffer B.....	161
Figure 4.8 L/t and t/t FRET Efficiency Change in Buffer A.....	162
Figure 4.9 t/t FRET Efficiency Change Upon Translocation in Buffer B.....	163
Figure 4.10 L/t and t/t FRET Efficiency Change in Buffer B.....	164
Figure 4.11 tRNA Release Measured by L/t FRET and Anisotropy Change.....	165
Figure 4.12 EF-G Concentration Dependent L/t FRET Efficiency Change.....	167
Figure 4.13 Global Fitting of L/t and t/t FRET Traces and Anisotropy.....	169
 <u>CHAPTER V</u>	
Table 5.1 tRNA Binding to POST-1 Complexes.....	185
Table 5.2 Apparent Rate Constants of tRNA <sup>fMet</sup> (Cy3) Release Upon Addition of Deacylated-tRNA and/or Ternary Complex.....	187
Figure 5.1 tRNA <sup>fMet</sup> (Cy3) Binding to a POST-1 Complex.....	188
Figure 5.2 Release of Deacylated-tRNA <sup>fMet</sup> (Cy3) from the E2-site as a Function of Added Deacylated-tRNA <sup>Lys</sup> Concentration .....	190
Figure 5.3 Deacylated-tRNA Binding to and Release From the E2-Site.....	192
Figure 5.4 Competition for the E2-site is Not Codon Specific .....	193
Figure 5.5 Addition of Ternary Complex Does Not Significantly Promote Additional Deacylated-tRNA Release.....	195

# **Chapter I: Introduction**

## 1.1 Protein Synthesis and the Ribosome

Deoxyribonucleic acids (DNAs), ribonucleic acids (RNAs), and proteins are known as the building blocks of life because they are responsible for storing and expressing the genetic information that makes up all living organisms. As described by the central dogma of molecular biology (**Crick, 1970**), DNAs are both replicated by DNA polymerases in order to preserve the genetic material (**Kornberg, 1969; Watson and Crick, 1953a; Watson and Crick, 1953b**), and transcribed into mRNAs by RNA polymerases. The mRNAs are subsequently translated into the amino acid sequences that compose proteins (**Figure 1.1**). DNA and mRNA are both composed of nucleotides containing the bases, adenine (A), cytosine (C), guanine (G), and either thymine (T) in DNA or uracil (U) in mRNA. The unique mRNA sequence is translated with the help of transfer RNA (tRNA) and the ribosome machinery. Initiation of ribosome mediated protein synthesis begins with recognition of an AUG mRNA codon, followed by triplets of nucleotides that code for different amino acids. The linker between the mRNA codon and the amino acid is tRNA. In bacterial cells there are about 40 tRNA molecules, each composed of about 76 nucleotides. Amino acids are added to a conserved -CCA end of the tRNA via an esterification utilizing amino acid-specific tRNA-synthetases and ATP (**Figure 1.2**). tRNA-synthetases have both a catalytic and editing site in order to ensure the correct amino acid addition to a specific tRNA. The tRNA also contains an anticodon stem-loop that recognizes the mRNA codon that codes for the specific amino acid. These steps ensure that the cognate amino acids get correctly added to the peptide chain.

## 1.2 Ribosome Components

The ribosome is a complex molecular machine that is utilized to translate mRNA sequences into specific polypeptides through repeated cycles of tRNA selection and peptide elongation. In both prokaryotes and eukaryotes the ribosome is made up of approximately two-thirds ribosomal RNA (rRNA) and one-third ribosomal proteins. My thesis work has been performed entirely with prokaryotic ribosomes. The *Escherichia Coli* (*E. Coli*) ribosome is a 2.5 MDa ribonucleoprotein assembly with a long dimension of ~200 Å, and a sedimentation coefficient of 70S. The ribosome is composed of a large (50S) and a small (30S) subunit. Each subunit can further be broken down into its rRNA and protein constituents. The large subunit is composed of 23S and 5S rRNA, and 34 different proteins labeled L1 through L36. Interestingly the Ser-2 of large subunit protein L12 can be acetylated to form L7, and the dimer formed between L7/L12 interacts with L10 to form what is called L8. The small subunit is composed of 16S rRNA, and 21 different proteins (S1-S21) (Table 1.1). Each ribosome has three main tRNA-binding sites; the aminoacyl (A) site, the peptidyl (P) site, and the exit (E) site located at the subunit interface. tRNAs progress through these sites in a stepwise fashion during the course of peptide elongation, as described below.

## 1.3 Bacterial Translation Cycle

### 1.3.1 Initiation

Protein synthesis in prokaryotic cells begins when mRNA binds to the 30S subunit of the ribosome. The anti-Shine-Dalgarno sequence at the 3' end of the 16S rRNA binds to the Shine-Dalgarno (SD) sequence of the mRNA and positions the AUG start codon in the P-site of the small subunit. With the help of three initiation factors (IF-1, IF-2, and IF-3) the initiator tRNA (fMet-tRNA<sup>fMet</sup>) binds to the AUG codon in a 30S pre- P-site, and the 50S subunit combines with the 30S initiation complex (30SIC) to form the 70SIC, placing fMet-tRNA<sup>fMet</sup> into the P-site. With an empty A-site, this initiation complex is ready to proceed to the peptide elongation phase of protein synthesis (Figure 1.3).

### 1.3.2 Peptide Elongation

Peptide elongation begins when a ternary complex consisting of elongation factor-Tu (EF-Tu) bound with GTP, and an aminoacyl-tRNA corresponding to cognate codon in the A-site arrive at the A-site of the ribosome. Proofreading at this point allows for discrimination between cognate and non-cognate codon-anticodon interactions. If the aminoacyl-tRNA anticodon is cognate with the mRNA in the A-site, GTP hydrolysis rapidly occurs allowing for tRNA accommodation into the A-site, and peptide bond formation (Pape et. al, 1998) (Figure 1.4, Figure 1.5). At this point the peptide and

nascent chain remain bound to the tRNA in the A-site while the deacylated-tRNA is located in the P-site. Experiments initially done by Noller and coworkers provided evidence that the tRNAs in a post-peptide bond formation, pre-translocation state can sample hybrid states in which the peptidyl-tRNA can simultaneously occupy the 30S A-site and the 50S P-site (A/P) and the deacylated tRNA can simultaneously occupy the 30S P-site and the 50S E-site (P/E) (**Moazed and Noller 1989**). Further single molecule evidence on pre-translocation ribosomes provided evidence that the classical (A/A, P/P) and the hybrid (A/P, P/E) tRNAs are in a dynamic equilibrium (**Blanchard et al., 2004**), next, elongation factor G (EF-G) bound with GTP facilitates the translocation of the tRNA<sup>fMet</sup>, and the new peptidyl-tRNA to the E and P-sites, respectively. This translocation proceeds via a kinetically competent intermediate (INT), in which the peptidyl-tRNA occupies the A/P hybrid state before completing translocation and occupying the P/P site (**Pan et al., 2007**) ([Figure 1.6](#)). The tRNA translocation is concomitant with mRNA movement by one codon, putting a new codon in the A-site, ready for the next cognate tRNA-ternary complex to enter and turnover the cycle (**Frank et al., 2007**). Elongation and translocation continue until a stop codon (UAA, UAG, or UGA) enters the A-site.

### **1.3.3 Termination of Protein Synthesis and Ribosomal Recycling**

Once a stop codon reaches the A-site of a ribosome, either release factor 1 (RF-1, stop codon UAA or UAG) or release factor 2 (RF-2, stop codon UAA or UGA) binds and catalyzes the hydrolysis of the ester bond between the completed protein and the P-site



tRNA, causing the release and final folding of the protein, and the rapid dissociation of the RF by RF-3 and GTP (**Zaviolov et al., 2002**). Finally, ribosome recycling factor (RRF), acting with EF-G and IF-3 removes the mRNA and tRNA from the ribosome and dissociates the 70S into the 30S and 50S subunits (**Reviewed by: Kisselev and Buckingham, 2000; Rao and Varshney, 2001; Vesper and Wilson, 2006**). At this point, the factors and subunits are ready to reinitiate protein synthesis.

#### **1.3.4 Ribosome Movements During Translocation**

The ribosome undergoes many conformational changes during translocation, not the least of which are subunit ratcheting and L1 stalk movement. Early cryo-electron microscopy (Cryo-EM) work demonstrated that the binding of EF-G.GTP to a pre-translocational ribosome induces a rotation of the 30S subunit relative to the 50S subunit of about 3°- 10° in the direction of mRNA movement (**Frank et al., 2000**) (**Figure 1.7**); further, the L1 stalk domain, consisting of ribosomal protein L1 and helices 76-78 of 23S rRNA moves ~20 Å towards the body of the ribosome (**Figure 1.8**) (**Valle et al., 2003; Frank et al., 2007; Connell et al., 2007**). These movements, along with the tRNA hybrid state formation, also seen in early cryo-EM structures, creates an “unlocked” ribosome formation from which translocation can occur. It was originally thought that addition of EF-G.GTP to a pre-translocation complex causes these unlocking movements; however, single-molecule fluorescence resonance energy transfer (smFRET) measurements later showed that individually, hybrid state formation (**Blanchard et al., 2004; Munro et al., 2007**), L1 stalk closure (**Fei et al., 2008; Cornish et al., 2009**), and

subunit ratcheting (Cornish et al, 2009) could be spontaneously achieved in pre-translocation complexes creating an equilibrium between locked and unlocked states. The manner in which these three structural transitions occur is highly debated, and still widely unknown. The current model is that these movements are uncoupled so that, although it is possible for all three to occur and create an unlocked complex in the absence of EF-G.GTP, it is a very low probability event. However, the presence of EF-G.GTP stabilizes a ratcheted conformation, in which the rate of P/E hybrid state formation and L1 stalk closure become accelerated (Munro et al., 2009, 2010).

## 1.4 Ribosome Structure

### 1.4.1 X-ray Crystallography

Ribosomeology was advanced exponentially in 2001 when Noller and coworkers first reported the low resolution structure of a 70S ribosome from *Thermus thermophilus* at 5.5 Å resolution (Yusupov et al., 2001). Previous to this, the essentially complete atomic structures of the 50S (*Haloarcula marismortui*, 2.4 Å, Ban et al., 2000) and 30S (*Thermus thermophilus*, 2.0 Å, Wimberly et al., 2000) subunits were solved, and are still currently used for the basis of phasing and/or molecular interpretation of all structures of the ribosome or its subunits. Cate and coworkers solved the first high-resolution structure of a 70S ribosome in 2005, with a 3.5 Å resolution structure of an empty *E. coli* ribosome (Schuwirth et al., 2005). However, more important to our work is the high-resolution structure of the ribosome with functional ligands attached; for example, the

*Thermus thermophilus* ribosome with mRNA and tRNA solved at 2.8 Å resolution by Ramakrishnan and coworkers in 2006 (Selmer et al., 2006). This particular structure shows the 70S ribosome reconstructed with mRNA, cognate A- and P-site tRNA, and non-cognate E-site tRNA in a pretranslocation complex. Also, the more recent high-resolution structures solved by Ramakrishnan and coworkers, with either EF-Tu.aminoacyl-tRNA (Schmeing et al., 2009), or EF-G (Gao et al., 2009) bound to the 70S ribosome, with the latter structure showing the ribosome stabilized in a post-translocation state, provides more insight into the elongation phase of protein synthesis.

Of particular interest to me is the structure of the highly mobile L1 stalk region on the ribosome. Because of the high mobility of this region, the L1-stalk (as well as the L7/L12 stalk) is partly or completely disordered in most high-resolution structures of the ribosome or the 50S subunit. However, the ribosomal protein L1 has been solved in isolation. The first structure of the *Thermus thermophilus* L1 was solved by Nikonov and colleagues at 1.86 Å resolution in 1996 (Nikonov et al., 1996); however, this structure did little to determine how the L1 interacted with the ribosome. It wasn't until 2003 when the structure of the *Sulfolobus acidocaldarius* L1 in complex with a specific 55-nucleotide fragment of 23S rRNA from *Thermus thermophilus* was solved at 2.65 Å resolution and was able to be incorporated into the *Thermus thermophilus* 70S structure, and the *Deinococcus radiodurans* 50S structure, that we had a good understanding of what L1 looked like on a ribosome (Nikulin et al., 2003). Later, a structure of the bacterial *Thermus thermophilus* L1 was modeled into the *E. coli* ribosome to provide an

even better look into the contacts between L1, tRNA and 23S rRNA (**Nevskaya et al., 2006**).

#### **1.4.2 Cryo-electron Microscopy (Cryo-EM)**

Cryo-EM has provided images of functional complexes of both prokaryotic and eukaryotic ribosomes with resolution below 10 Å (**Mitra and Frank, 2006; Halic et al., 2005; Chandramouli et al., 2008; Taylor et al., 2007; Li et al., 2008**). Although this resolution is well below the high resolution of X-ray crystallography, cryo-EM has the advantage of being able to image ribosomes frozen in specific functional states. As mentioned previously, this is of significant importance when looking at the movements associated with translocation, specifically hybrid state formation and L1 movement (Valle et al, 2003; Connell et al, 2007). Furthermore, a recent cryo-EM study showed the progression of tRNA movement during translocation in 50 distinct three-dimensional reconstructions, showing the tRNA in classical, hybrid and various novel intermediate states, that will prove to be useful to my thesis work (**Fischer et al., 2010**).

#### **1.5 Ribosomal Protein L1**

The ribosomal protein L1 is one of the largest proteins in the 50S subunit, and is located near the exit site on a protuberance that is also composed of helices 76-78 from the 23S rRNA. In *E. coli*, L1 is composed of 234 amino acids, and folds into two domains with both the N- and C-termini of the protein located in domain I (**Nikonov et**

**al., 1996).** Originally L1 was of profound interest because of its RNA binding activity. Not only does L1 bind rRNA in the L1 protuberance, it also has the ability to bind its own mRNA, thereby acting as its own repressor, and mediating autogenous regulation of translation by binding to a region within the leader sequence of the polycistronic mRNA of the L11 operon coding for ribosomal proteins L1 and L11 (**Gourse et al., 1986**). Early crystal structures were determined with the L1 protein bound to both mRNA (**Nevskaya et al., 2006**) and rRNA (**Nikulín et al., 2003**), at similar locations within domain I (**Figure 1.9**).

Early biochemical results showed that *E. coli* ribosomes lacking L1 displayed 40-60% reduced capacity for *in vitro* protein synthesis (**Subramanian and Dabbs, 1980**). It wasn't until two years later that the reason for the reduced protein synthesis was shown to be a direct result of L1 being important for the binding of tRNA to the ribosomal P-site (**Sander, 1982**).

The early cryo-EM information obtained by Valle and coworkers showed a large movement of the L1 protuberance towards the ribosome body upon binding of EF-G. This observation led to the hypothesis that, in the EF-G bound ribosome, the L1 protuberance makes a direct interaction with the elbow of a deacylated-tRNA in the P/E hybrid configuration and possibly is involved in translocation of the newly deacylated tRNA (**Valle et al., 2003**). These hypothesis were later corroborated with smFRET experiments in which the L1 protuberance was shown to occupy at least two (**Fei et al., 2008**), or three (**Cornish et al., 2009**) distinct structural states depending on the positions and acylation states of the tRNAs bound to the ribosome. For the majority of this thesis I

utilize a fluorescently labeled L1 that was originally introduced by Fei and coworkers, and was shown to be a more than adequate marker for probing the P- and E-site tRNA interaction with L1.

## **1.6 Deacylated-tRNA Release From the E-site**

Two fundamentally different roles of the E-site have been put forward. One, introduced by Nierhaus and colleagues, suggests an “allosteric three-site model” of elongation, characterized by the following four features. 1) The ribosome contains three tRNA-binding sites, A-, P-, and E-, the latter being specific for deacylated tRNA. 2) The deacylated-tRNA does not fall off during translocation but moves from P- to E- site. 3) The two tRNAs that are present on the ribosome both before and after translocation undergo codon-anticodon interaction. 4) The ribosome can adopt two conformational states, pre-translocational and post-translocational; the first of which has high affinities for tRNA in the A- and P-sites, and the latter, which has high affinities for tRNA in the P- and E-sites. (**Gnirke et al., 1989; Rheinberger and Nierhaus, 1986**). In contrast, Wintermeyer and colleagues proposed a second role of the E-site, suggesting that during translocation the deacylated-tRNA binds to the E-site transiently, promoting its release from the P-site (**Lill and Wintermeyer, 1987; Lill et al., 1988; Semenkov et al., 1996**). In this model, the E-site bound state exists as a transient intermediate, rather than a stable product of translocation. One of the largest inconsistencies between these two models is whether or not the deacylated-tRNA remains bound to the E-site after translocation; however, this contradiction can be explained by differences in preparation, specifically

buffer conditions. Nierhaus and colleagues worked with a more physiological buffer containing 4.5 mM  $Mg^{2+}$  and the polyamines spermine and spermidine, while Wintermeyer and colleagues primarily used a buffer with 7 mM  $Mg^{2+}$  and no polyamines. An experiment performed by Wintermeyer and colleagues, showed that either high  $Mg^{2+}$  (15-18 mM) or the presence of polyamines (as in Nierhaus's buffer conditions), results in less deacylated-tRNA from being released from the E-site instantaneously, whereas, in the buffer conditions with 7 mM  $Mg^{2+}$  and lacking polyamines, 85% of the deacylated-tRNA was released instantaneously (**Semenkov et al., 1996**). It is important to gain a better understanding of how deacylated-tRNA behaves in the E-site because the occupancy of the E-site has been linked to many different functions on the ribosome. For example, it has been postulated that an E-site occupied with a tRNA is involved in maintaining the reading frame at the decoding center (**Reviewed by: Nierhaus, 2006**). Further, occupancy at the E-site has been speculated to be involved in regulation of programmed frameshifting as seen on -1 frameshifting by Léger and colleagues (**Léger et al., 2007**), and +1 frameshifting by Liao and colleagues (**Liao et al., 2008**). Moreover, recent single molecule work done in our lab has shown that tRNA occupancy in the E-site inhibits EF-G assisted translocation (**Chen et al., Manuscript submitted**).

In the following thesis work, I will provide further evidence for three different pathways of deacylated-tRNA release from the ribosome by utilizing a fluorescently labeled ribosomal protein L1 as a specific E-site probe, and by following the FRET changes of fluorescently labeled tRNAs as they move into and out of the P/E hybrid state and E/E site. This site specifically labeled L1 has been shown to provide FRET interactions with labeled tRNA in the P/P, P/E, and E/E sites, the latter two having

similar FRET signals (**Fei et al., 2008**). Because of the highly mobile nature of the L1 protuberance, I also follow deacylated-tRNA release by FRET changes between the deacylated-tRNA and the peptidyl-tRNA in the P-site. By combining these two techniques along with the anisotropy change for a labeled deacylated-tRNA, I am able to provide distinct kinetic mechanisms for the release of deacylated-tRNA that depends on both buffer conditions and acylation state of the P-site tRNA that are novel, and that correspond nicely with the previous biochemical work, as well as current cryo-EM studies (**Agrawal et al., 1999; Fischer et al., 2010**).

In my most recent work, I studied the supposed allosteric interaction between the A-site and E-site tRNAs by measuring the rate of release of deacylated-tRNA through the loss of L1-tRNA FRET in a post-translocation complex. As mentioned above, Nierhaus and colleagues first introduced the theory of an “Allosteric Three-site Model” in 1986 (**Rheinberger and Nierhaus, 1986**). They utilized a poly-U mRNA and radioactively labeled tRNAs in order to show that addition of tRNA at the A-site, causes release of deacylated-tRNA from the E-site. This study drew criticisms in literature that reinterpreted the data as a chase of E-site tRNA by the deacylated tRNA present in the A-site substrate (**Robertson and Wintermeyer, 1987**). Baranov and Ryabova raised further criticism, and explained the data as a release and rebinding of the deacylated-tRNA to the A-site after translocation (**Baranov and Ryabova, 1988**). Both of these criticisms were valid considering the homopolymeric nature of the mRNA used, giving rise to the fact that all three binding sites contained the same codon, and it was virtually impossible to prove the site location of the deacylated-tRNA. These concerns were addressed in 1989, with the introduction of a heteropolymeric mRNA for translocation



studies. Nierhaus and colleagues showed that by adding an aminoacyl-tRNA that was non-cognate for the E-site to a translocated complex, the release of E-site tRNA was increased (**Gnirke et al., 1989**). They went on to state that a competition between the newly added tRNA and the E-site bound deacylated-tRNA was unlikely because the newly added tRNA is non-cognate for the E-site; a sound theory given the previous biochemical data (**Rheinberger et al., 1986**). However, in my following thesis work I will go on to show that even non-cognate tRNA is able to compete for replacement of the deacylated-tRNA in an E' (**Fischer et al., 2010**) or E2 (**Agrawal et al., 1999**) site that I claim the tRNA is located in under the above conditions. My work shows that addition of a ternary complex to a POST translocated complex does not drastically increase the amount of deacylated-tRNA that is released any more than is seen with only deacylated-tRNA added in excess to the complex.

	<b>Ribosome</b>	<b>Small Subunit</b>	<b>Large Subunit</b>
Sedimentation Coefficient	70S	30S	50S
Molecular Weight (kD)	2520	930	1590
<b>RNA</b>			
Major		16S, 1542 nts	23S, 2904 nts
Minor			5S, 120 nts
Molecular Weight (kD)	1664	560	1104
Proportion of Mass	66%	60%	70%
<b>Proteins</b>		21 polypeptides	34 polypeptides
Molecular Weight (kD)	857	370	487
Percentage of Mass	34%	40%	30%

**Table 1.1 Components of *E. coli* Ribosomes**

This table is adapted from (Voet et al., 2006).

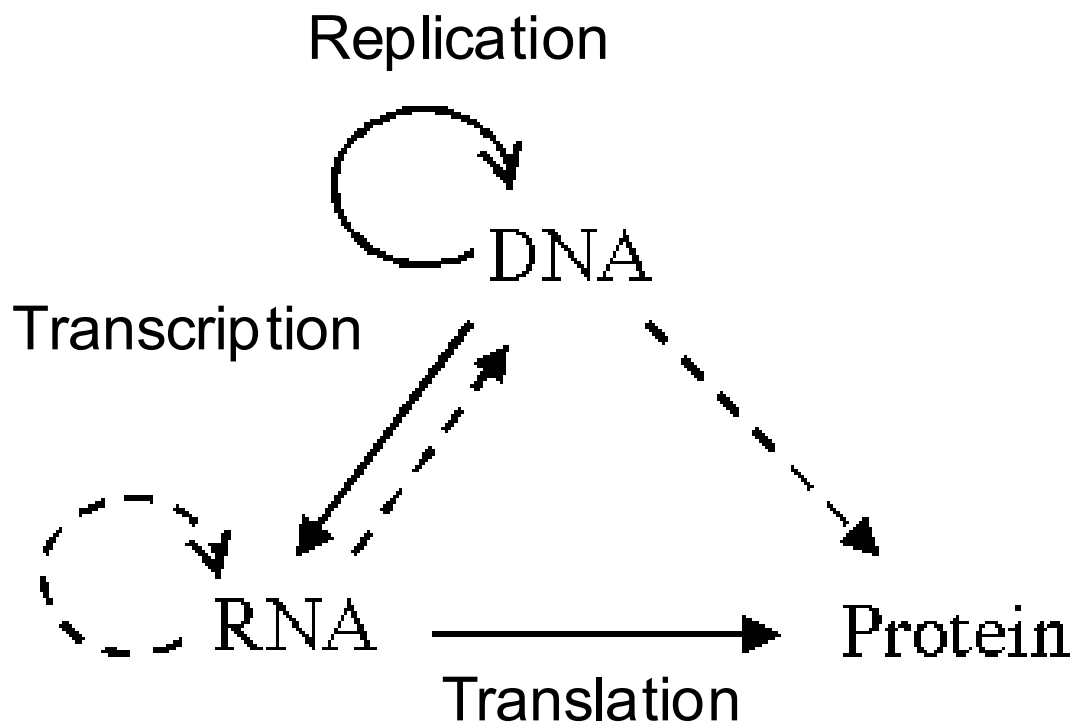


**Figure 1.1 The Central Dogma of Molecular Biology**

Figure adapted from (Crick, 1970)

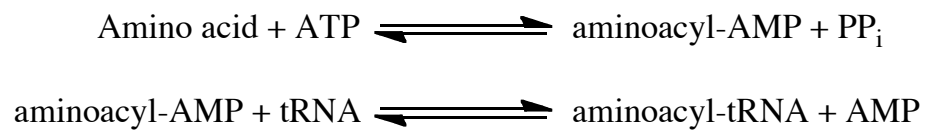
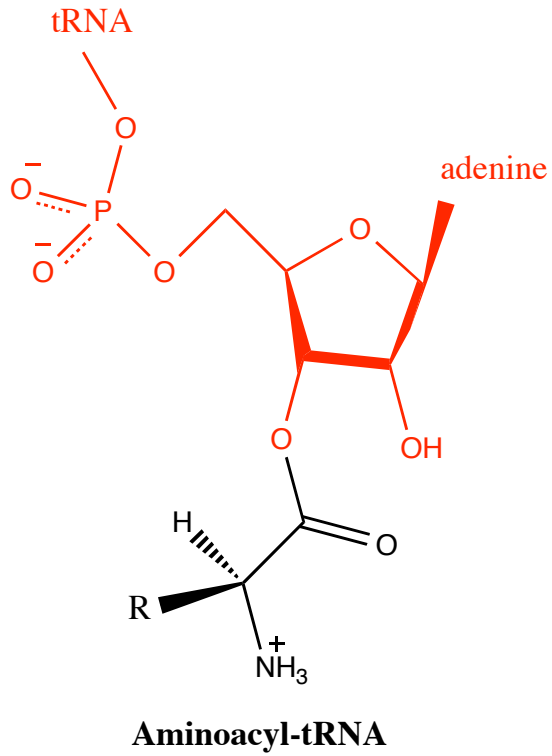


**Figure 1.2 Aminoacyl-tRNA Charging Reaction**

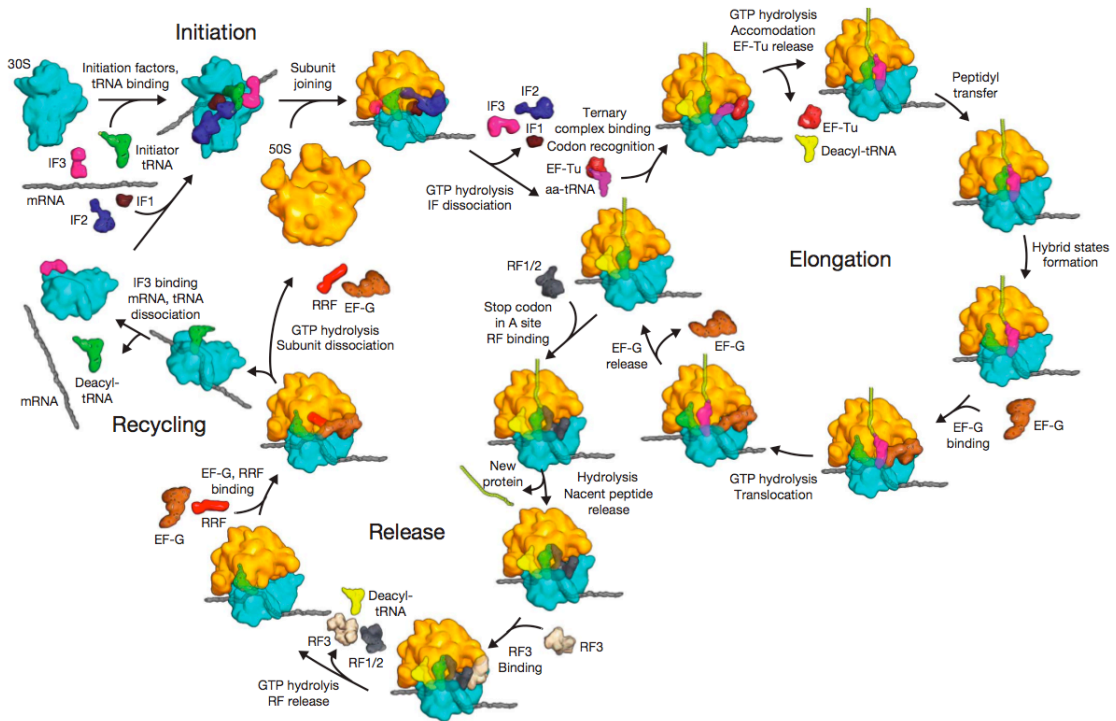


**Figure 1.3 Overview of Bacterial Translation**

This figure is taken from (Schmeing and Ramakrishnan, 2009).

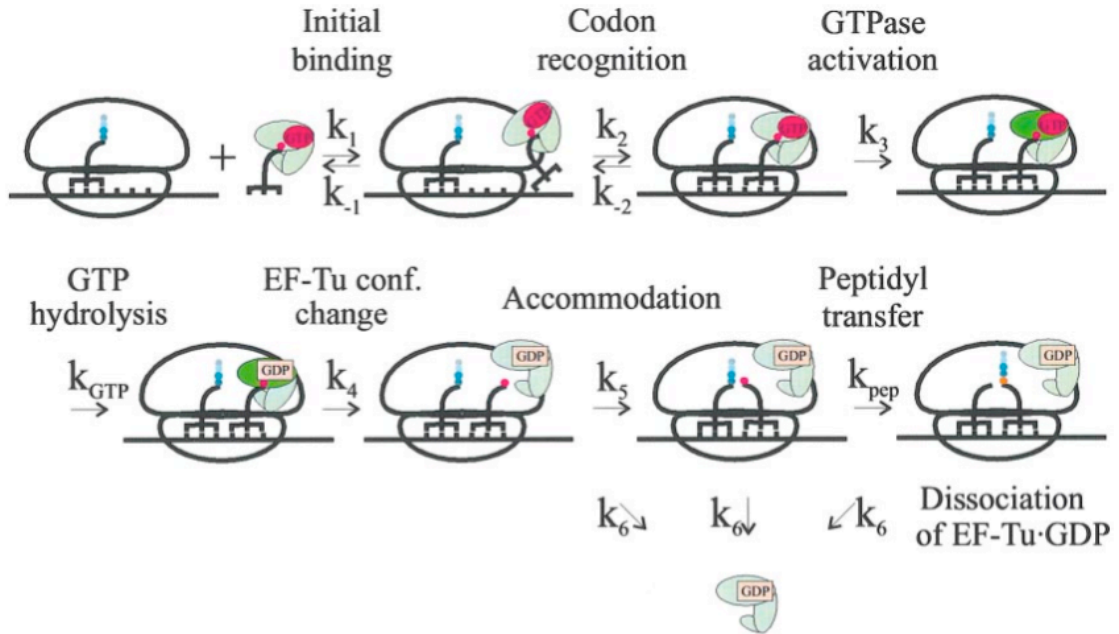


**Figure 1.4 Mechanism of EF-Tu-dependent Binding of Aminoacyl-tRNA to the Ribosomal A-site.** EF-Tu (light green) is depicted in three conformations: the GTP-bound form, the transient GTP-activated form on the ribosome (G domain dark green) and the GDP-bound form, which dissociates from the ribosome.

This figure is taken from (Pape et al., 1998).

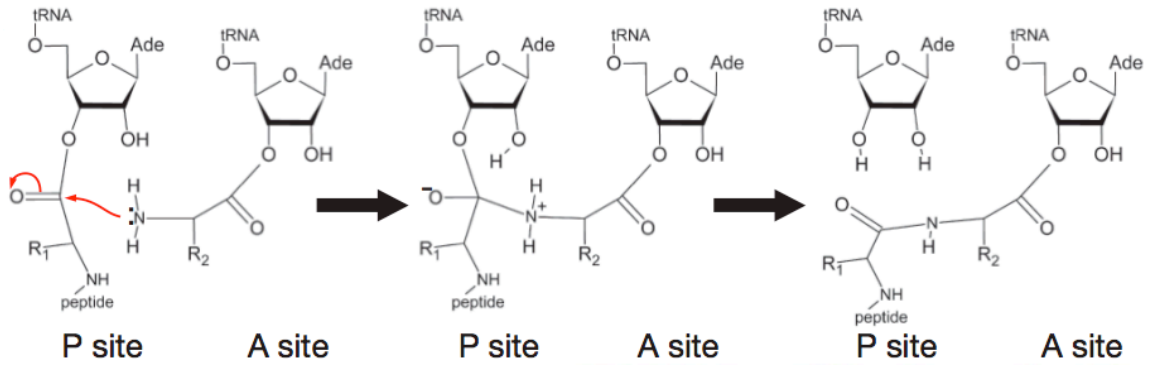


**Figure 1.5 Mechanism of Peptide Bond Formation**

This figure is taken from (Schmeing and Ramakrishnan, 2009).

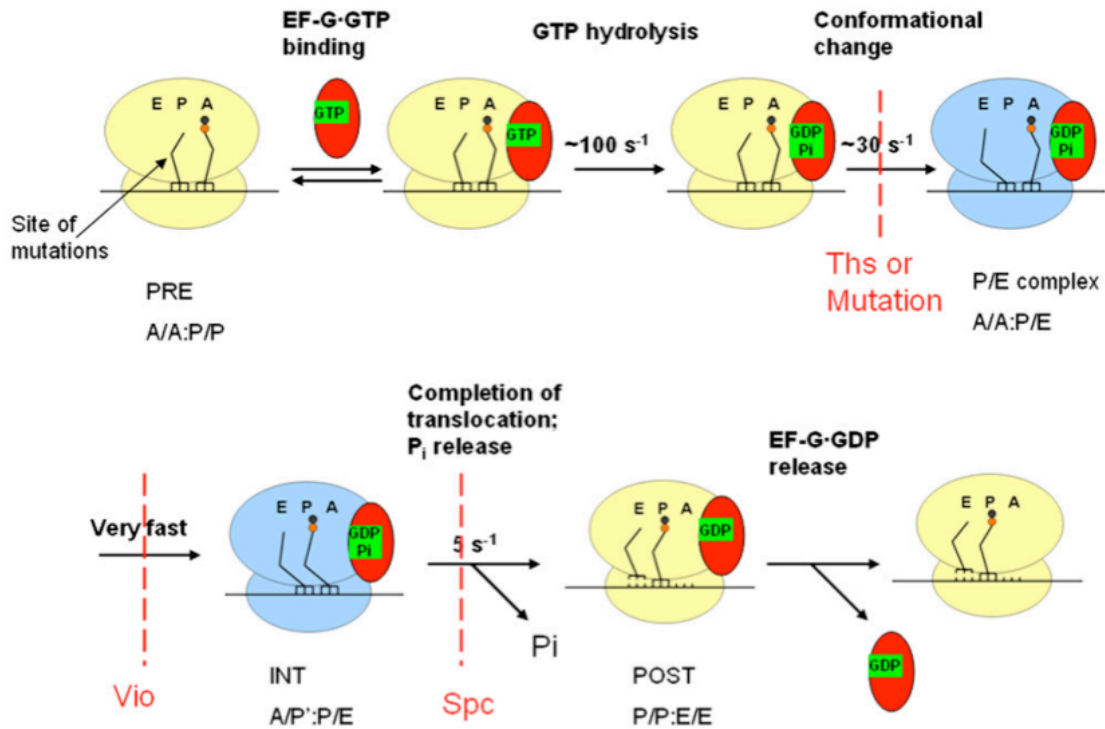


**Figure 1.6 Mechanism of Translocation Showing Stepwise Movement of tRNA After GTP Hydrolysis**

EF-G.GTP binding to the PRE complex and GTP hydrolysis are rapidly followed by formation of the INT which is more slowly converted to POST complex. Thiostrepton and viomycin inhibit INT formation, whereas spectinomycin selectively inhibits INT disappearance.

This figure and text is taken from (Pan et al., 2007).



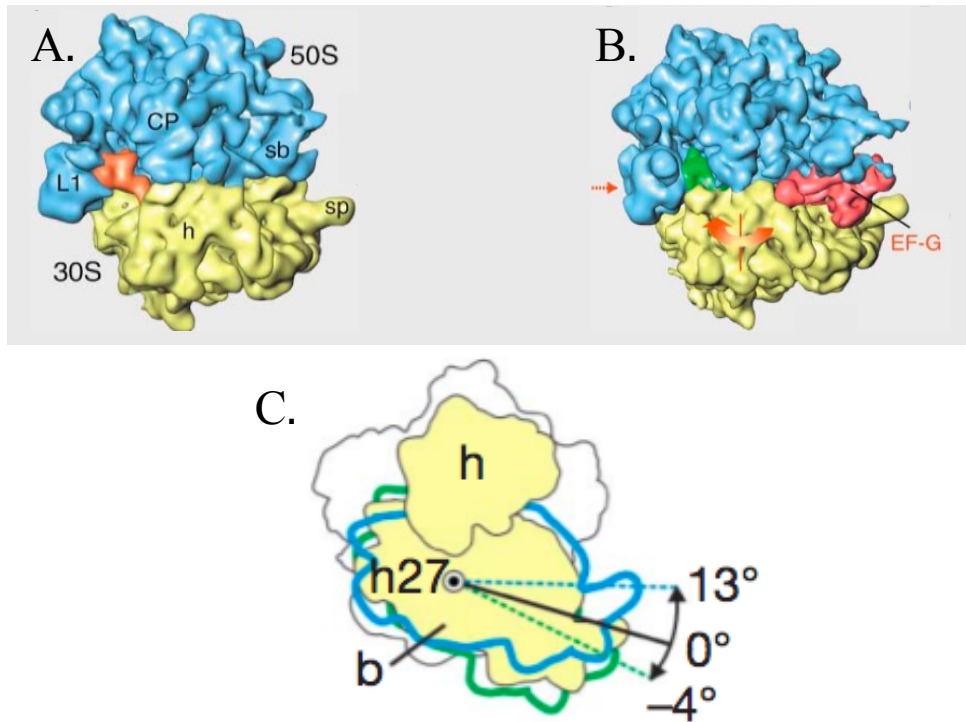


### Figure 1.7 Relative Ribosomal Subunit Rotation

**A and B:** Cryo-EM images of 70S-Puromycin samples before (**A**) and after (**B**) addition of EF-G.GDPNP, note the red arrows indicating the 30S subunit rotation, as well as the L1 protuberance movement. **C:** Schematic showing the rotation of the 30S subunit around the h27 helix.

This figure was adapted from (**A and B:** Valle et al., 2003, **C:** Fischer et al., 2010).

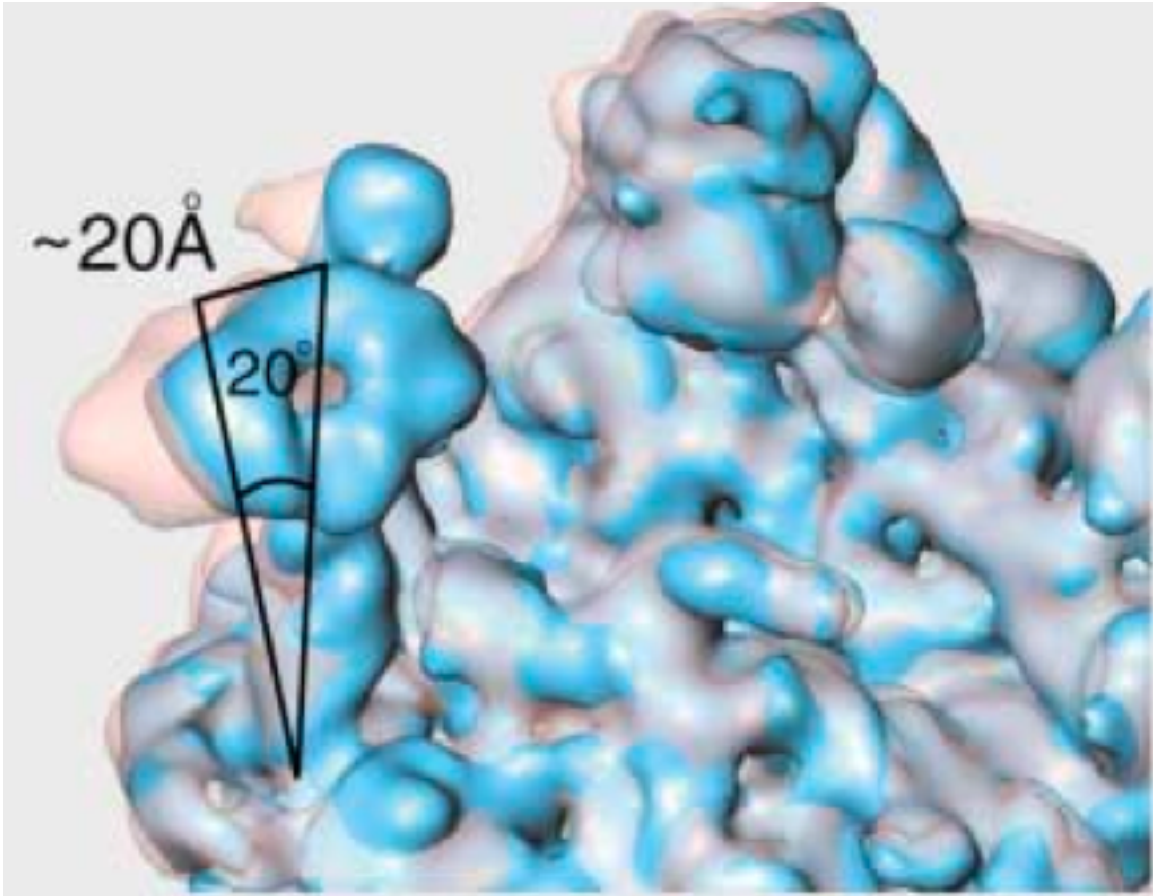


**Figure 1.8 L1 Stalk Movements**

Cryo-EM images of the 50S subunit in the open form without EF-G.GDPNP bound (semi-transparent pink) and the closed form with EF-G.GDPNP bound (solid blue).

This figure was taken from (Valle et al., 2003).

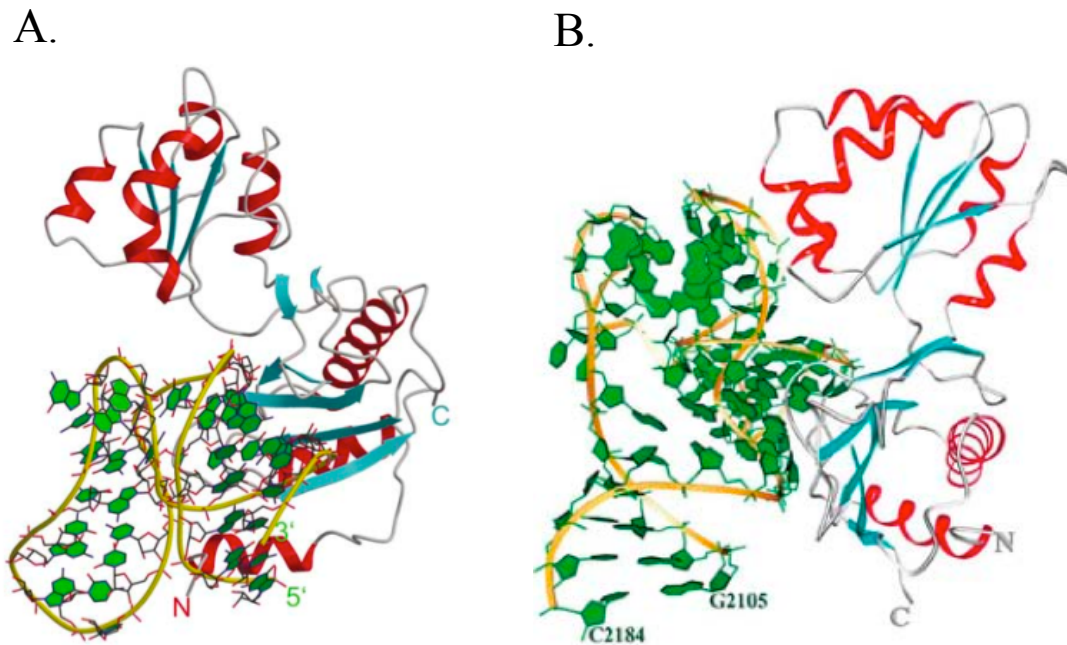


**Figure 1.9 Crystal Structure of L1**

The crystal structure of L1 bound to either **A)** mRNA or **B)** a 23S rRNA fragment.

This figure was adapted from **A.** Nevskaya et al., 2006; **B.** Nikulin et al., 2003

## **Chapter II: Materials and Methods**

## 2.1 Materials

### 2.1.1 Buffers

The following buffers were prepared in 18  $\Omega$  Milli-Q purified water, and the pH was adjusted at 25 °C, unless otherwise stated.

**Buffer A** (Wintermeyer Buffer): 50 mM Tris-HCl, pH 7.5, 30 mM NH<sub>4</sub>Cl, 70 mM KCl, 7 mM MgCl<sub>2</sub>, 1 mM DTT; T<sub>50</sub>A<sub>30</sub>K<sub>70</sub>M<sub>7</sub>D<sub>1</sub>

**Buffer B** (Nierhaus Buffer): 20 mM Hepes-KOH, pH 7.6 @ 0° C, 150 mM NH<sub>4</sub>Ac, 4.5 mM MgAc<sub>2</sub>, 4 mM  $\beta$ -mercaptoethanol, 2 mM spermidine, 0.05 mM spermine; H<sub>20</sub>A<sub>150</sub>M<sub>4.5</sub>B<sub>4</sub>S<sub>2</sub>Sp<sub>0.05</sub>

**Buffer C**: 50 mM Tris-HCl, pH 7.5, 5 mM NH<sub>4</sub>Ac, 100 mM KCl, 0.5 mM CaAc<sub>2</sub>, 15 mM MgAc<sub>2</sub>, 5 mM putrescine, 1 mM spermidine, 6 mM  $\beta$ -mercaptoethanol, T<sub>50</sub>A<sub>5</sub>K<sub>100</sub>Ca<sub>0.5</sub>M<sub>15</sub>P<sub>5</sub>S<sub>1</sub>B<sub>6</sub>

**Ribosome Lysis Buffer**: 20 mM Tris-HCl, pH 7.5, 100 mM NH<sub>4</sub>Cl, 10 mM MgAc<sub>2</sub>, 0.5 mM Ethylenediaminetetraacetic Acid (EDTA), 3 mM  $\beta$ -mercaptoethanol

**Ribosome Cushion Buffer**: 1.1 M Sucrose in 20 mM Tris-HCl, pH 7.5, 500 mM NH<sub>4</sub>Cl, 10 mM MgAc<sub>2</sub>, 0.5 mM (EDTA), 3 mM  $\beta$ -mercaptoethanol

**Ribosome Wash Buffer**: 20 mM Tris-HCl, pH 7.5, 500 mM NH<sub>4</sub>Cl, 10 mM MgAc<sub>2</sub>, 0.5 mM (EDTA), 3 mM  $\beta$ -mercaptoethanol

**70S TC Zonal Buffer**: 10 mM Tris-HCl, pH 7.5, 60 mM NH<sub>4</sub>Cl, 7 mM MgAc<sub>2</sub>, 0.25 mM EDTA, 3 mM  $\beta$ -mercaptoethanol

**MRE 600 Ribosome Storage Buffer:** 50 mM Tris-HCl, pH 7.5, 70 mM NH<sub>4</sub>Cl, 30 mM KCl, 7 mM MgAc<sub>2</sub>, 0.5 mM EDTA, 1 mM DTT

**MRE 600 Subunit Storage Buffer:** 20 mM Tris-HCl, pH 7.5, 100 mM NH<sub>4</sub>Cl, 10 mM MgCl<sub>2</sub>, 1 mM β-mercaptoethanol

**Subunit Separation Buffer:** 20 mM Tris-HCl, pH 7.5, 200 mM NH<sub>4</sub>Cl, 2 mM MgCl<sub>2</sub>, 2 mM β-mercaptoethanol

**L1 Lysis Buffer:** 50 mM NaH<sub>2</sub>PO<sub>4</sub>, pH 7.0, 300 mM NaCl, 1 mM PMSF

**L1 Wash Buffer:** 50 mM NaH<sub>2</sub>PO<sub>4</sub>, pH 7.0, 300 mM NaCl

**L1 Storage Buffer:** 20 mM Tris-HCl, pH 7.5, 400 mM NH<sub>4</sub>Cl, 4 mM MgCl, 0.2 mM EDTA, T<sub>20</sub>M<sub>4</sub>A<sub>400</sub>B<sub>4</sub>E<sub>0.2</sub>

**L1 Labeling Buffer:** 50 mM Tris-HCl, pH 7.5, 400 mM NH<sub>4</sub>Cl

**Reconstitution Buffer:** 10 mM Tris-HCl, pH 7.5, 150 mM NH<sub>4</sub>Cl, 8 mM MgAc<sub>2</sub>, 5 mM β-mercaptoethanol, T<sub>10</sub>MAc<sub>8</sub>A<sub>150</sub>B<sub>5</sub>

**Reconstitution Cushion Buffer:** 20 mM Tris-HCl, pH 7.5, 200 mM NH<sub>4</sub>Cl, 2 mM MgAc<sub>2</sub>, 2 mM β-mercaptoethanol, 1.1 M Sucrose

**Buffer RS1:** 0.02 M Tris-HCl, pH 7.3, 0.01 M MgCl<sub>2</sub>, 0.3 M NaCl, 0.5 mM EDTA, 6 mM β-mercaptoethanol

**Buffer RS2:** 50 mM Tris-HCl, pH 7.5, 10 mM MgCl<sub>2</sub>, 10 mM β-mercaptoethanol

**Buffer RS3:** 10 mM NaH<sub>2</sub>PO<sub>4</sub>, pH 7.2, 1 mM EDTA, 5 mM β-mercaptoethanol, 10% Glycerol

**Buffer D:** 20 mM NH<sub>4</sub>Ac, pH 5.0, 10 mM MgAc<sub>2</sub>, and 400 mM NaCl

**Buffer E:** 20 mM NH<sub>4</sub>Ac, pH 5.0, 10 mM MgAc<sub>2</sub>, and 400 mM NaCl, 30% ethanol  
(v/v)

**Buffer F:** 20 mM NH<sub>4</sub>Ac, pH 7.0, 10 mM MgAc<sub>2</sub>, and 400 mM NaCl

**Buffer G:** 20 mM NH<sub>4</sub>Ac, pH 7.0, 10 mM MgAc<sub>2</sub>, and 400 mM NaCl, 30% ethanol (v/v)

**Buffer H:** 50 mM NaAc, pH 5.0

**Buffer I:** 50 mM NaAc, pH 5.0, 1 M NaCl

**SOC Media:** 2% w/v bacto-tryptone, 0.5% w/v bacto-yeast extract, 10 mM NaCl, 2.5 mM KCl, 10 mM MgCl<sub>2</sub>, 20 mM glucose

### 2.1.2 Reagents

All aqueous solutions were prepared in diethyl pyrocarbonate (DEPC) treated water, in which 0.1% (v/v) DEPC (Sigma-Aldrich) was added to 18 Ω Milli-Q purified water, incubated overnight, and then autoclaved (**Sambrook and Russell, 2001**).

The *E. coli* tRNAs used as well as the Yeast tRNA<sup>Phe</sup> were purchased from Chemical Block (Moscow, Russia) and used without further purification, unless otherwise noted.

Rhodamine 110 (Rhd110) was purchased from Sigma-Aldrich. Rhd110, C<sub>20</sub>H<sub>15</sub>ClN<sub>2</sub>O<sub>3</sub>, M.W. 366.80, has maximum absorbance at 499 nm and maximum emission at 521 nm in methanol. The corresponding wavelengths in aqueous solution at

pH 7.0 are 496 nm (extinction coefficient, 90,000 cm<sup>-1</sup> M<sup>-1</sup>) and 530 nm, respectively.

The CyDye™ reagents used were purchased from GE Healthcare. Cy3 hydrazide, M.W. 765.95, has a maximum absorbance at 550 nm (extinction coefficient, 150,000 M<sup>-1</sup> cm<sup>-1</sup>), and a maximum emission at 570 nm. The Cy5 hydrazide, M.W. 791.99, has a maximum absorbance at 649 nm (extinction coefficient, 250,000 M<sup>-1</sup> cm<sup>-1</sup>), and a maximum emission at 670 nm. The Cy3 and Cy5 maleimide dyes, M.W. 791.0 and 817.0 respectively, have the same spectroscopic properties as the hydrazide cohorts.

Stock solutions of ampicillin and chloramphenicol (Sigma-Aldrich) were made in water to 20 mg/mL and 15 mg/mL, respectively. Stock solutions of puromycin were made in the respective buffers prior to use and the pH was adjusted to 7.5.

Stock solutions of ATP were made to 100 mM and the pH was adjusted to 7.5. Stock solutions of 100 mM GTP were purchased from GE.

## **2.2 Methods**

### **2.2.1 Ribosome Preparations**

#### **2.2.1.1 70S Ribosomes From MRE 600 Cells**

Tight-coupled 70S ribosomes were prepared from *E. coli* MRE 600 cells as described (**Rodnina and Wintermeyer, 1995**) with slight modifications. Approximately 65 g of frozen cells (15-L culture) were resuspended in 100 mL of Ribosome Lysis Buffer and opened by French press (SML Instruments, Inc.) at 10 K-12 K psi. To eliminate cell debris, the opened cells were centrifuged at 15 K rpm for 30 min (SS-34



rotor) then the supernatant was removed and re-centrifuged for 60 min in an SS-34 rotor. The supernatant, now called S30, was layered on top of 22 mL of Ribosome Cushion Buffer and centrifuged at 30 K rpm, for 21 hours, in a Ti 45 Beckman rotor. The supernatant of this centrifugation (S100) is removed and used to prepare aminoacyl-tRNA synthetases. The pellets were resuspended in 35 mL of Ribosome Wash Buffer, transferred to SS34 centrifuge tubes, and centrifuged at 15 K rpm for 15 min to remove any left over debris. The supernatant was layered on top of 10 mL of Ribosome Cushion Buffer and centrifuged at 30 K rpm for 21 hours in a Ti 45 Beckman rotor. This step was repeated two more times and the final pellets were resuspended in 70S TC Zonal Buffer. The tight-coupled 70S ribosomes were isolated from the subunits by zonal centrifugation in a Beckman Ti 50 rotor (20 K rpm, 16 hours) on a gradient from 10% to 50% sucrose in the desired buffer for future experiments. Concentration was determined by  $A_{260}$  with 1  $A_{260}$  equal to 26 pmol 70S.

#### **2.2.1.2 Subunits from MRE 600 Cells**

Ribosomes were prepared as described above; however, after the final centrifugation, the pellets were resuspended in Subunit Separation Buffer. The lower  $Mg^{2+}$  concentration of the Subunit Separation Buffer will facilitate the subunit dissociation and allow purification of 30S and 50S. The subunits were then separated from the 70S and each other by zonal centrifugation in a Beckman Ti 50 rotor (20 K rpm, 16 hours) on a gradient from 7.4% to 50% sucrose in Subunit Separation Buffer. The concentration was determined for the 30S and 50S using  $A_{260}$  with 1  $A_{260}$  equaling 39 pmol 50S and 78 pmol 30S.

### **2.2.1.3 70S Ribosomes From –L1 Cells**

Cells for ribosomes lacking the large subunit protein L1 (MV17-10, originally used by **Subramanian and Dabbs, 1980**) were a kind gift from Dr. Knud Nierhaus (Max-Planck Institute, Germany), and were grown in 15 L Luria-Bertani (LB) media for 18 hours. Approximately 65 g of the frozen cells were resuspended in Ribosome Lysis Buffer, and then the protocol for purification of MRE-600 70S was followed until the Zonal centrifugation. Prior to the zonal centrifugation, an analytical 70S TC separation was performed using Zonal Buffer containing either 1, 6, 7, or 8 mM  $Mg^{2+}$  in order to determine the optimum  $Mg^{2+}$  concentration for 70S TC formation. 70S ribosomes were the dominant form at  $Mg^{2+}$  concentrations above 6 mM; therefore, the zonal centrifugation was performed with 6 mM  $Mg^{2+}$ , just like for the MRE 600 ribosomes. Absence of the L1 protein as determined by SDS-PAGE analysis of the 70S –L1 ribosomes proved inconclusive due to the similar, SDS-PAGE analyzed, molecular weights of L1 (26,700 Da), S2 (28,300 Da), S3 (28,200 Da), and especially S4 (26,700 Da). Therefore, subunit separation was necessary in order to conclude that L1 was indeed absent.

### **2.2.1.4 Subunits from –L1 Cells**

The –L1 ribosomes were prepared as described above, and resuspended in Subunit Separation Buffer. The –L1 ribosomal subunits were then separated from the 70S by zonal centrifugation in a Beckman Ti 50 rotor (20 K rpm, 16 hours) on a gradient from 7.4% to 50% sucrose in Subunit Separation Buffer (**Figure 2.1 A**). The 30S and 50S were collected and the 50S were analyzed by SDS-PAGE to ensure that the subunits

lacked ribosomal protein L1 (Figure 2.1 B).

### 2.2.2 mRNA Preparations

mRNA022 was prepared by transforming pTZ118 plasmid containing the 022 sequence under a T7 promoter (provided by C. Gualerzi, University of Camerino) into JM109 cells. The plasmid was extracted from cells using Qiagen Plasmid Maxi kit, and linearized by the restriction enzyme HindIII. *In vitro* transcription was conducted using the EPICENTRE Ampliscribe T7 Flash Transcription Kit. mRNA was isolated from other components in the reaction mixture by precipitation with 2.5 M pre-chilled LiCl on ice for 30 min, and then ethanol precipitated two times (2.5 volume of 95% ethanol, and 1/10 volume of 0.3 M NaAc (pH 5.2), > 1 hour at -20°C). The purity was confirmed by urea-PAGE (Figure 2.2 A) and  $A_{260}/A_{280}$  ( $2.0 \pm 0.2$ ) and the concentration was determined by  $A_{260}$  using the extinction coefficient of 0.04 mg/ $A_{260}$ .

022MFK-mRNA was purchased from Dharmacon (Lafayette, CO) with the sequence GGG AAG GAG GUA AAA AUG UUU AAA CGU AAA UCU ACU (initiator codon underlined). Both the transcribed mRNA022 and the purchased 022MFK-mRNA were tested for activity by the amount of [ $^{35}$ S]-fMet-tRNA<sup>fMet</sup> bound to the ribosome as a function of mRNA concentration (Figure 2.2 B).

## 2.2.3 Protein Preparations

### 2.2.3.1 Preparation of Protein Factors

The cloned elongation factors EF-G (*E. coli*) and EF-Tu (*S. aureus*), C-terminally His-tagged, were provided as kind gifts from Drs. Wilson and Noller (University of California, Santa Cruz), and Dr. M. Sassanfar (Harvard University), respectively. Dr. T. Ueda (University of Tokyo) kindly provided the *E. coli* N-terminal His-tagged initiation factors, IF-1, IF-2, and IF-3. Finally, Dr. Y.M. Hou provided the PheRS and LysRS. The protein factors were all purified (by me: EF-Tu, EF-G; or by others in the lab: Initiation factors) from either Ni-NTA (Qiagen) or TALON Superflow (Clontech) metal affinity columns. The EF-G underwent further purification via FPLC Mono-Q column using a gradient of 50 mM - 350 mM KCl in 50 mM Tris-HCl (pH 7.5), 10 mM MgCl<sub>2</sub>, 0.5 mM EDTA, and 6 mM 2-mercaptoethanol. The proteins were dialyzed against Buffer A lacking Mg<sup>2+</sup> overnight, and then dialyzed against Buffer A for 3 hours. The Bradford Assay (Bradford, 1976) was used to determine the final protein concentrations, and SDS-PAGE was used to ensure the final purity of the protein factors.

As with the mRNA, the activity of each of the initiation factors was determined by measuring the amount of [<sup>35</sup>S]-fMet-tRNA<sup>fMet</sup> bound to tight-coupled 70S ribosomes. Each of the initiation factors measured promoted initiator tRNA binding to the ribosome to reach a plateau of ~0.5-0.6 [<sup>35</sup>S]-fMet-tRNA<sup>fMet</sup> /70S. The remaining unbound ribosomes are a result of either inactive ribosomes, or the binding of the non-radioactive tRNA<sup>fMet</sup>.

The activity of EF-Tu was measured by binding of [<sup>14</sup>C]-GDP. Varying amounts of

purified EF-Tu were added to an excess of [<sup>14</sup>C]-GDP, in 20 mM Tris-HCl, pH 7.6, 100 mM NH<sub>4</sub>Cl, 10 mM MgCl<sub>2</sub>, and incubated for 20 min at room temperature. The EF-Tu. [<sup>14</sup>C]-GDP complexes were collected on 0.45 μm nitrocellulose filters (Millipore), and washed with 4 x 1 mL of the above buffer. The concentration of active EF-Tu measured via this assay is then used to determine the corrected EF-Tu concentration used in all future experiments and is typically 65-75% of those determined by Bradford Assay. (Figure 2.3)

### **2.2.3.2 Preparation of Ribosomal Protein L1**

#### **2.2.3.2.1 Wild Type L1 Expression and Purification**

The expression and purification of L1 was optimized through various growing conditions and purification techniques and is summarized in Chapter III. Below are the best conditions for growing and purification.

A clone of the *E. coli* ribosomal protein L1 was a kind gift from Dr. R. Zimmerman (University of Massachusetts). The cells were initially grown on an LB-agar plate containing 50 μg ampicillin/mL at 37 °C overnight. A single colony was selected from the plates, and grown in 5 mL LB containing 50 μg ampicillin/mL at 37 °C for 18 hours, until the solution became visibly cloudy with cell density. Pre-warmed large-scale LB growths were then inoculated with 1/1000 volume of the overnight culture, and grown to an OD<sub>595</sub> of ~0.8. IPTG was added to a final concentration of 1 mM, and the growth temperature was dropped to ~20 °C, in order to limit the amount of L1 inclusion bodies, and grown for 18 hours. The cells were centrifuged into a pellet, quick-frozen and stored at -80 °C.

Approximately 8 g of frozen cells were resuspended in 30 mL L1 Lysis buffer with 1/100 Protease Inhibitor Cocktail Set 1 (Calbiochem) by light vortexing and homogenizer. French press (12 K- 16 K psi), performed 3 times, was used to open the cells which were then centrifuged at 16,000 rcf (relative centrifugal force, as measured by:  $RCF = [r (2\pi N)^2]/g$ ; where r is the rotational radius of the rotor, N is rotational speed, and g is the earth's gravitational acceleration. rcf can be used in place of rpm when the rotor used for the centrifugation changes, both rpm and rcf are readily available readouts on the centrifuge) for 20 mins at 4 °C. The supernatant was then added to TALON Superflow (Clontech) resin which was previously washed three times with ~10 bed volumes of L1 Wash Buffer. The supernatant/resin mixture was gently agitated for 60 min at 4 °C on a platform shaker. The mixture was gently centrifuged at 700 rcf for 5 min to pellet the resin, and the supernatant was removed and saved for SDS-PAGE analysis. The resin was washed with 10 bed volumes of L1 Wash Buffer for 10 min at 4 °C, and again centrifuged at 700 rcf for 5 min. The above was repeated 2 more times for a total of 3 washes. After the final wash, the resin was resuspended in ~15-20 mL of Wash Buffer and put into a column for elution. The His-tagged L1 was eluted from the resin using a 25 mM, 50 mM, 150 mM, and 300 mM imidazole stepwise gradient in L1 Wash Buffer. The fractions containing L1, as determined by 12% SDS-PAGE (Figure 3.4 B), were pooled and dialyzed against L1 Storage Buffer without  $Mg^{2+}$  overnight, then against L1 Storage Buffer for 3 hours. The dialyzed samples were concentrated through 4-mL Millipore centrifugal tubes with a molecular weight cutoff of 10,000 in a SLA-1500 rotor at 7500 rcf. The concentration of the final sample was determined through Bradford Assay, using bovine serum albumin (BSA) as the standard. The Coomassie

Brilliant Blue G-250 (Bradford reagent) reacts primarily with arginine, and less so with histidine, lysine, tyrosine, tryptophan, and phenylalanine that are present in the analyzed protein. Known concentrations of BSA are used to make a standard curve to determine the concentration of the L1 protein; therefore, it is advantageous if the L1 has similar features to BSA. BSA and L1 contain similar percentages of Arg (BSA: 4.3%; L1: 4.7%), Lys (BSA: 9.9%; L1: 9.8% ), and Trp (BSA: 5.6%; L1: 5.5%) out of total protein; however, BSA contains ~2-3 times more of the other reactive amino acids. Therefore, BSA may provide a fairly accurate standard curve for reading of L1 concentration, and, if anything, underestimates the L1 concentration. Other measurements also provide information about the accuracy of the concentration of L1. During reconstitution of a labeled L1 in to –L1 50S subunits, when analyzed by SDS-PAGE, the L1:50S ratio is 1:1 (Section 2.2.3.3.4) and the label:50S depends solely on the labeling efficiency of the L1. Therefore, it would appear that the calculation to determine labeling efficiency (using the L1 concentration from the Bradford Assay) is accurate. Previously, L1 concentration has been determined by “Folin Phenol Reagent” (Dabbs et al., 1981), but more recent concentration determinations have not been mentioned.

### **2.2.3.3 Ribosomal Protein L1 Mutants**

#### **2.2.3.3.1 Primer Design For Site-directed Mutagenesis**

The Stratagene QuickChange Site-Directed Mutagenesis Kit was utilized to construct five mutations of L1 (S40C, K54C, V177C, T202C, V221C). According to the kit’s manual, the following principles were followed when designing primers: 1) Both of the mutagenic primers must contain the desired mutation and anneal to the same

sequence on opposite strands of the plasmid. 2) Primers should be between 25 and 45 bases in length, with a melting temperature ( $T_m$ ) of  $\geq 78$  °C. The following calculation was used to determine  $T_m$  for the primers.

$$T_m = 81.5 + 0.41(\%GC) - 675/N \quad \text{Equation 2.1}$$

, where N is the primer length in bases, and % GC is a whole number. 3) The desired mutation should be in the middle of the primer with ~10-15 bases of correct sequence on both sides. 4) The primers optimally should have a minimum GC content of 40% and should terminate in one or more C or G bases (Figure 2.4).

#### **2.2.3.3.2 Mutagenesis**

In a 50 uL reaction volume, 50 ng of double-stranded template L1 DNA, 125 ng of each plasmid, 1 uL dNTP mix, 5 uL of the 10x reaction buffer, enough DEPC H<sub>2</sub>O to reach 50 uL, and lastly 1 uL of 25 U/mL pFu Turbo DNA polymerase were prepared for PCR. The PCR thermocycler was set up for three segments: 1) 1 cycle at 95 °C for 30 sec; 2) 16 cycles at 95 °C for 30 sec, 55 °C for 1 min, and 68 °C for 7 min; 3) 1 cycle at 4 °C for 10 min; however, the sample can be left at 4 °C up to at least 18 hours. After the PCR reaction was complete, 1 uL 10 U/μL Dpn I restriction enzyme were added directly to each amplification reaction, and incubated at 37 °C for one hour in order to digest the parental DNA.

Transformation was performed by adding 1 uL of the Dpn I digested PCR product



to 50  $\mu$ L of XL1-Blue super-competent cells in pre-chilled 14-mL polypropylene round-bottom tubes and incubating on ice for 30 min. The transformation reactions were heat shocked at 42 °C for 45 sec and then kept on ice for 2 min. 0.9 mL SOC media, pre-heated to 42 °C, was added to the tube and incubated at 37 °C for one hour. 50  $\mu$ L of the transformed cells were added to LB-agar plates containing ampicillin (20  $\mu$ g/mL) and tetracycline (10  $\mu$ g/mL), and allowed to incubate for 24-36 hours. Single colonies were inoculated into 6 mL of LB broth and grown overnight. 1 mL of the cell cultures were used to make glycerol stocks, and the remaining 5 mL were prepared for sequence analysis. Plasmid DNA was extracted and purified from the overnight culture by a QIAprep Spin Miniprep Kit (Qiagen), and then sent for sequence analysis (Figure 2.5).

#### **2.2.3.3.3 Fluorescent Dye Labeling of Mutated L1**

The single mutations of L1 were over-expressed and purified similarly to the wild type L1, and concentrated to  $\sim$  2 mg/mL in 0.5 mL L1 Storage Buffer. The concentrated mutant L1 was exchanged into L1 Labeling Buffer by using a NAP-5 (GE-Healthcare) column, which was pre-washed and pre-equilibrated with 10 mL of the L1 Labeling Buffer. The protein was eluted with 1 mL of the L1 Labeling buffer. *Tris*(2-carboxyethyl)phosphine (TCEP) was added to the exchanged protein to a final concentration of 1 mM. A 1-mg package of Amersham Cy3- or Cy5-maleimide mono-reactive dye (GE-Healthcare) was resuspended in 50  $\mu$ L dry dimethylformamide (DMF). The dye was added to the L1 drop-wise and incubated in a 37 °C shaking water bath for one hour. Adding  $\beta$ -mercaptoethanol to a final concentration of 43  $\mu$ M, and shaking at room temperature for 10 min, stopped the reaction. During the incubation, a 30 mL

Sephadex G-25 column was pre-washed with 60 mL Milli Q-H<sub>2</sub>O, and pre-equilibrated with >75 mL of the L1 Storage Buffer. After the reaction was stopped, the reaction mixture was added to the G-25 column in order to remove the excess Cy-dye. The labeled protein elutes out of the column first and the fractions that were high in A<sub>552</sub> (Cy3) or A<sub>652</sub> (Cy5) were collected and pooled. The pooled fractions were concentrated in 4-mL Millipore centrifugal tubes with a molecular weight cutoff of 10,000 in a SLA-1500 rotor at 7500 rcf, and analyzed by Bradford Assay for protein concentration, and A<sub>552</sub> or A<sub>652</sub> for the dye concentration. Typical Cy/L1 ratios were  $0.6 \pm 0.2$  (Table 3.1). It was shown previously that it is possible to separate labeled from unlabeled L11 using FPLC separation; therefore, several attempts were made in order to separate the labeled L1 from unlabeled L1 using similar techniques, but all proved to be unsuccessful. Further, the labeled T202C-L1 (Cy5) was analyzed using MALDI (Section 3.3.2.3, Figure 3.5), and showed an increase of approximately 750 Da for the labeled sample, which corresponds nicely with the molecular weight of the Cy5 dye.

#### **2.2.3.3.4 Reconstitution of Cy-Labeled L1 into 50S of –L1 Subunits**

Initial attempts to reconstitute either the wild type, mutated, or labeled L1 into 70S –L1 ribosomes resulted in non-specific binding of the L1 to the ribosome, as seen through control experiments (Section 3.3.3.1, Figure 3.6). Therefore, reconstitution was performed using the 50S subunits of the –L1 ribosomes; this change not only doesn't show non-specific binding of the L1, but also allows the reconstitution to be observed via SDS-PAGE analysis. Wild type, mutated, or labeled L1 was added in a 2x excess of the 50S subunits lacking L1 in Reconstitution Buffer to a total of 150 uL, and incubated at 37

°C for 15 min. The mixture was layered above 400  $\mu$ L Reconstitution Cushion Buffer, and centrifuged at 110 K rpm for 40 min (S120-AT2 rotor). The resulting pellet was resuspended in Buffer A, B, or C, and analyzed by SDS-PAGE. In all cases, except the S40C mutant, the L1 band in the reconstituted samples revealed ~1:1, 50S to L1 reconstitution, where band density in the SDS-PAGE gels was used to determine reconstitution efficiency (Table 3.2). Specifically, the ratio of band density from L1/L2 was determined for the reconstituted samples, and compared to the ratio of L1/L2 for the wild type 70S ribosomes. The ratio of these two numbers determined the reconstitution efficiency. In the cases where a labeled L1 was used, the Cy5 : 50S ratio was  $0.6 \pm 0.2$  depending solely on the labeling efficiency of the L1 (Figure 2.6).

#### 2.2.3.4 Preparations of crude Yeast and *E. Coli* Aminoacyl Synthetases

The procedure of Kemkhadze and coworkers was followed to prepare *E. coli* aminoacyl-tRNA synthetases (Kemkhadze et al., 1981). The S-100 fraction obtained from the ribosome preparation in Section 2.2.1.1 was dialyzed against Buffer RS1, and approximately 375  $A_{280}$  units were loaded onto a 50 mL DEAE-Cellulose column (2 cm x 20 cm) that was first equilibrated with Buffer RS1. The loaded sample was then eluted from the column with Buffer RS1. Fractions determined to have a  $A_{280}/A_{260}$  greater than 1.5 were pooled, frozen, and kept at -80 °C in small aliquots. Bradford Assay determined protein concentrations.

Crude yeast aminoacyl-tRNA synthetases were prepared as described (Lagerkvist and Waldenstrom, 1964). Approximately 6 g of dry yeast from *Saccharomyces cerevisiae*, Type II (Sigma) was added to 40 mL of pre-chilled Buffer RS2, and incubated

at 4 °C for 20 min. The yeast cells were opened by French press at 10-12 K psi repeated 4 times, and, in an SS34 rotor, were centrifuged at 12 K rpm for 30 min. The supernatant was re-centrifuged at 12 K rpm for another 30 min (SS34 rotor). At 4 °C, 1/10 volume of 10% streptomycin sulfate in Buffer RS2 was added drop-wise with stirring to the supernatant in order to precipitate the nucleic acids. The sample was then centrifuged at 12 K rpm for 1.5 hours (SS34 rotor). Ammonium sulfate fractionation was utilized to partially purify the synthetases by the following procedure. Ceramic mortar and pestle were used to grind the ammonium sulfate powder, which was then slowly added with intense stirring to the supernatant to a concentration of 50% (313 g/L). After all the ammonium sulfate is dissolved, the solution was stirred for 40 min at 4 °C. The solution was then centrifuged at 12 K for 1.5 hours (SS34 rotor). The pellet was dissolved in 80 mL of Buffer RS3, and dialyzed against 3 L of Buffer RS3 for 3 x 1 hour. The sample was then quick-frozen and kept at -80 °C in small aliquots.

#### **2.2.4 tRNA Preparations**

In Chapters IV and V, I utilize initiator tRNA<sup>fMet</sup> in a variety of states: 1) highly charged and highly labeled; 2) highly charged and unlabeled; and 3) uncharged and highly labeled. The synthesis of the highly charged and highly labeled tRNA<sup>fMet</sup> can be thought of as a three-step procedure, involving NaBH<sub>4</sub> reduction, labeling with the Cy-hydrazide, and aminoacylation using S100 for synthetase. The optimal order of these reactions was determined by Pan and coworkers, where they found that reduction-charging-labeling gives the best results (**Pan et al., 2009**). For the highly charged and

unlabeled, only the charging was necessary; for the uncharged and highly labeled, labeling immediately followed the reduction. Further, in order to obtain high stoichiometry of charging or of labeling, HPLC purification was necessary following either or both of the steps. Elongator tRNA<sup>Phe</sup>, tRNA<sup>Lys</sup>, and tRNA<sup>Arg</sup> are also used in either charged and labeled, or only charged states as described below (Figure 2.7).

#### 2.2.4.1 NaBH<sub>4</sub> Reduction of tRNAs to be Labeled

The tRNAs utilized in this work were either labeled with Rhodamine 110 (Rhd110), Cy3 hydrazide, or Cy5 hydrazide, at the dihydrouridine position(s) in the D-loop of the tRNA. In order for either of these reactions to take place, the dihydrouridine(s) had to be reduced with NaBH<sub>4</sub>, to form 3-ureidopropanol, which was then replaced by the label. This reduction to create tRNA(red) was carried out by incubating the tRNA (2.5 mg/mL), and NaBH<sub>4</sub> (10 mg/mL, added from 100 mg/mL in 0.01 M KOH), in 40 mM Tris-HCl (pH 7.5) at 0 °C for 60 min in a total volume of 400 μL. Three ethanol precipitations then followed in order to remove any unreacted NaBH<sub>4</sub>.

#### 2.2.4.2 Aminoacylation of tRNAs

Unlabeled tRNA<sup>fMet</sup> or tRNA<sup>fMet</sup>(red) was charged and formylated with partially purified *E. coli* tRNA synthetase from S100 (described above) which contain MetRS and formyl-transferase. The reaction was carried out with 15-20 μM tRNA<sup>fMet</sup> or tRNA<sup>fMet</sup>(red), 720 μM folic acid (as formyl donor), 67 μM [<sup>35</sup>S]-methionine (~300 cpm/pmol) and between 1/5-1/20<sup>th</sup> total volume of the crude *E. coli* tRNA synthetase (as optimized for each batch) in 100 mM Tris-HCl (pH 7.8), 4 mM ATP, 20 mM MgCl<sub>2</sub>, 1 mM EDTA, 10 mM KCl, 7 mM β-mercaptoethanol, and 0.005 units/uL of inorganic

pyrophosphatase (TIPP) for 30 min at 37 °C. The aminoacylation reactions for *E. coli* tRNA<sup>Lys</sup> and tRNA<sup>Arg</sup>, were similar except 100 μM [<sup>3</sup>H]-Lys or [<sup>3</sup>H]-Arg were used, respectively.

Unlabeled tRNA<sup>Phe</sup> or tRNA<sup>Phe</sup>(red) was charged using purified yeast tRNA synthetase containing PheRS. The reaction was performed with 20-30 μM tRNA<sup>Phe</sup> or tRNA<sup>Phe</sup>(red), 100 μM [<sup>3</sup>H]-Phe (~200 cpm/pmol) and between 1/5 and 1/20<sup>th</sup> total volume of yeast tRNA synthetase (optimized for each batch) in 100 mM Tris-HCl, 10 mM ATP, 50 mM MgCl<sub>2</sub>, 2.5 mM EDTA, 3 mM β-mercaptoethanol, and 0.005 units/uL of TIPP for 30 min at 37 °C.

The above charging reactions were quenched with the addition of 1/10 volume of 20% KAc pH 5.0, and extracted with 1 volume of Tris saturated phenol (pH 4.2 +/- 0.2) to remove proteins, followed by an extraction with 1 volume of chloroform to remove any remaining phenol. The samples were then ethanol precipitated and the pellets were resuspended in 800 μL of either Buffer D for HPLC purification or Buffer H for FPLC purification.

The aminoacylated-tRNAs were further purified from poly-adenine byproducts through FPLC Mono-Q chromatography starting with a 15 mL wash with 50 mM NaAc (pH 5.0) followed by a linear gradient of 0-1 mM NaCl in 50 mM NaAc (pH 5.0) (Figure 2.8). As seen in Chapter IV, the ribosome is not blind to the aminoacylation state of the initiator tRNA. Through the inherent difficulties associated with fully charging tRNA it was determined that separation of fMet-tRNA<sup>fMet</sup> from tRNA<sup>fMet</sup> is necessary, and this is possible through HPLC purification using C18/15μm column chromatography (Waters)

with a gradient of 6-21% ethanol in Buffer D (Figure 2.9). The fractions were pooled and ethanol precipitated based on charging efficiency.

#### 2.2.4.3 Hydrazide Labeling of Reduced tRNA

Labeling of either charged or uncharged tRNA(red) with Cy3- or Cy5-hydrazide occurs at the now fully reduced dihydrouridine sites in the tRNA (fMet: 20, Phe: 16/17, Lys: 16/17/20). The pellet of a dried tRNA(red) was resuspended in the smallest volume possible (typically 5-10  $\mu$ L) of 0.1 M sodium formate (pH 3.7). Cy3 or Cy5 dye (resuspended from dry sample to  $\sim$ 200-300 mM in DMSO) was added to a final concentration of approximately 120-200 mM and incubated at 37  $^{\circ}$ C for 2 hours, followed by vacuum drying. The dried sample was resuspended in 400  $\mu$ L water and 1/10 volume 20% KAc (pH 6.5), and ethanol precipitated three times to remove any excess dye. Purification of labeled tRNAs from unlabeled tRNAs was accomplished through HPLC using the same column as above with a gradient of 0-30% ethanol in Buffer F at 4  $^{\circ}$ C (Figure 2.10). This separation technique was used for all combinations of charged and uncharged tRNA<sup>fMet</sup>, and tRNA<sup>Phe</sup>. In each case the fractions were pooled, and in the case of the charged tRNAs separated based charging efficiency (typically 0.8-0.9 : 1) and labeling efficiency (fMet-tRNA<sup>fMet</sup>:  $\sim$ 1:1, Phe-tRNA<sup>Phe</sup>  $\sim$ 1.5:1). Or in the case of the uncharged tRNAs, separated based only on labeling efficiency (tRNA<sup>fMet</sup>: 1:1) (Table 2.1).

#### 2.2.4.4 Rhodamine 110 Labeling of Reduced tRNA

0.1 mg/mL of either charged or uncharged tRNA(red) was added to 850  $\mu$ L of 0.1 M sodium formate (pH 3.0). 100  $\mu$ L of 8 mg/mL rhodamine 110 in methanol was added

dropwise to the tRNA mixture and incubated at 37 °C for 90 min. The reaction was stopped by adding 120 µL of 2M Tris-HCl (pH 7-8) and then performing a phenol and chloroform extraction as seen above. The labeling reaction was analyzed by spectrophotometer and typically resulted in labeling efficiencies of Rhd110: Phe-tRNA<sup>Phe</sup> of 0.45:1 and Rhd110 : tRNA<sup>Lys</sup> of 0.65:1 (Table 2.1).

## 2.2.5 Complex Formation

All of the following complexes were incubated in a 37 °C water bath. The complexes were purified using ultracentrifugation in the Sorvall Discovery M120SE ultracentrifuge with an S120-AT2-0372 rotor. The 70SIC, PRE-1, and POST-1 complexes were analyzed by tRNA binding and puromycin reactivity towards each species, which will be discussed later.

### 2.2.5.1 70S Initiation Complex (70SIC)

Activated ribosomes were made by preheating mutant-50S or mutant-labeled 50S (2 µM) with 30S subunits (3 µM) for 10 min in either Buffer A or Buffer B. The resulting activated ribosomes were incubated with mRNA (8-12 µM, depending on mRNA batch), IF 1 (3 µM), IF 2 (3 µM), IF 3 (3 µM), GTP (1 mM) and either charged and labeled, charged and unlabeled, uncharged and labeled, or uncharged and unlabeled, tRNA<sup>fMet</sup> (3 µM) and incubated in Buffer A or B for 25 min. Initiation complexes were purified by ultracentrifugation through 1.1 M sucrose cushion in either Buffer A or B at 450,000 rcf for 40 min at 4 °C. fMet-tRNA<sup>fMet</sup> binding to the ribosome was determined through measuring [<sup>35</sup>S]-fMet-tRNA<sup>fMet</sup> per ribosome, and/or label per ribosome; when



using HPLC purified tRNA, stoichiometries of tRNA bound were typically 0.7 : 1 and 0.8 : 1, respectively. However, the tRNA binding was strongly influenced by buffer and aminoacylation of initiator tRNA (Section 4.3.1.2.2, Table 4.3).

#### 2.2.5.2 Ternary Complex

Ternary complex was formed by incubating EF-Tu (6  $\mu$ M) with unlabeled or labeled Phe-tRNA<sup>Phe</sup>, Lys-tRNA<sup>Lys</sup>, or Arg-tRNA<sup>Arg</sup> (3  $\mu$ M), GTP (1 mM), phosphoenoyl pyruvate (PEP, Roche Diagnostics, 1.5 mM), and pyruvate kinase (Roche Diagnostics, 0.015 mg/mL) in either Buffer A or B for 5 min.

#### 2.2.5.3 PRE Complex

Incubating unpurified initiation complex with ternary complex for 1 min formed pre-translocation (PRE-1) complexes. The PRE-1 complexes were purified in the same manner as the 70SIC, and resulted in similar fMet-tRNA<sup>fMet</sup> binding efficiencies. A-site binding was measured by the amount of fMet-[<sup>3</sup>H]-Phe/Lys/Arg-tRNA<sup>Phe/Lys/Arg</sup> bound to the ribosome, and typically resulted in  $\sim 0.6 - 0.7$  [<sup>3</sup>H]-tRNA / ribosome (Table 4.3).

#### 2.2.5.4 POST Complex

Post-translocation (POST-1) complexes were formed by incubating an unpurified PRE-1 complex with EF-G (2 : 1 for EF-G : 70S) and GTP (1 mM) for 1 min. The POST complexes were purified in the same manner as the previous complexes. Further, when measuring the transition from POST-1 to PRE-2 (Section 5.3.4), it is necessary to ensure that all EF-G has been removed from the POST-1 sample. To ensure ribosome purification from EF-G,  $\sim 30$  pmol of purified POST complex was analyzed on a 12% SDS-PAGE gel and compared to unpurified POST, and EF-G alone (Figure 2.11). As is

evident in this figure, the ultracentrifugation of the POST complex through a sucrose cushion is effective in removing EF-G.

## **2.2.6 Equilibrium Assays**

### **2.2.6.1 Filter Binding**

Filter binding was used to determine the amount of tRNA bound to the ribosome, to determine initial charging efficiency of reactions in cooperation with TCA precipitation, and to determine the activity of EF-Tu. To determine the amount of tRNA bound to the ribosome, the sample was filtered through a nitrocellulose filter (pore size 0.45  $\mu\text{m}$ , from Millipore), followed by 6 washes with 1 mL of either Buffer A or B. Initial tRNA charging efficiency is determined by first incubating 15  $\mu\text{L}$  of the charging mixture with 400  $\mu\text{L}$  of pre-chilled 5% TCA on ice for 60 mins. That mixture is then passed through a nitrocellulose filter (pore size 0.45  $\mu\text{m}$ , from Millipore), and washed six times with 1 mL of 5% TCA. Determination of the activity of EF-Tu also uses filter binding and was described above (2.2.3.1).

### **2.2.6.2 Sucrose Cushion Pull Down**

Filter binding to determine the binding of tRNA has its benefit in that it uses very little sample and is relatively quick; however, the results vary greatly with the technique used in washing and filtering the sample. In order to obtain a more accurate and precise measure of tRNA binding, a sucrose cushion pull down is performed. However, it should be mentioned that some amount of tRNA that is loosely bound to the ribosome is lost

during sucrose cushioning, which is not lost during filter binding. However, to determine the amount of [<sup>35</sup>S]-fMet-tRNA<sup>fMet</sup> bound to a 70SIC, the 70SIC is made as above with a final amount of ribosome of approximately 40 pmol. The complex is then layered onto a 1.1 M sucrose cushion in either Buffer A or B, and centrifuged at 450,000 ref for 40 min at 4 °C. The pellet is then resuspended in either Buffer A or B, and a small aliquot is tested for radioactivity in the scintillation counter (Beckman LS6500).

### **2.2.6.3 Puromycin Reactivity**

Puromycin is an A-site-specific antibiotic that forms a peptide bond with peptidyl-tRNA in the P-site, but has almost no reactivity toward peptidyl-tRNA in the A-site. For the experiments presented here, the puromycin reactivity was only measured at equilibrium to provide further evidence of the tRNA location in the complexes. For example, each of the complexes that were used in my experiments were tested for puromycin reactivity by incubating 0.1 μM complex with 5 mM puromycin (from 20 mM stock) for 15 s at 25 °C, the reaction was stopped with 0.3 M sodium formate (pH 5.0), and extracted with ethyl acetate. The organic phase was analyzed in the scintillation counter to determine the amount of peptidyl-puromycin formed per ribosome (Table 2.2).

### **2.2.6.4 FRET Measurements**

Equilibrium FRET measurements were made on a photon-counting instrument (Fluorolog-3 spectrofluorometer, Horiba Jobin Yvon, USA). Typically three fluorescence traces were averaged for each result. The experiments were performed at 25 °C by connecting the instrument to a circulating water bath. The majority of the kinetic studies that were done were first tested at equilibrium because of the small amount of material

needed for these studies. The results of these equilibrium studies can be seen in Chapter 4.

The complexes that utilized a Cy3/Cy5 FRET pair were excited at 518 nm (excitation band pass of 2 nm) and the emission spectrum from 550-750 nm was recorded. For the equilibrium FRET, complexes containing only Cy3 (D\*A), only Cy5 (DA\*), both dyes (D\*A\*), and no dyes (DA) were measured. The DA sample was subtracted from all other traces to correct for light scattering and background fluorescence, and relative FRET efficiency changes were determined by [equation 2.2](#):

$$E = \frac{DA^{*'}_A - DA^*_A}{DA^*_A} \times \left[ \frac{1}{DonorEfficiency} \right] \times \left[ \frac{1}{AcceptorEfficiency} \right] \quad \text{Equation 2.2}$$

$$DA^{*'}_A = D^* A^*_A - \left[ D^* A^*_D \times \frac{D^* A_A}{D^* A_D} \right]$$

Where E is the FRET efficiency, DA\*' is the extracted acceptor emission as calculated by the bottom equation. D\*A\*(A) is a sample with both donor and acceptor labeled, measured at the acceptor peak, D\*A\*(D) is the same complex measured at the donor peak. The DA\* indicates a sample in which only the acceptor is labeled, and a D\*A indicates a sample where only the donor is labeled. The donor efficiency and acceptor efficiency are measured as the amount of donor/70S and acceptor/70S in the purified complexes. (Values and a sample calculation can be seen in [Table 4.1](#), [Figure 4.1-4.2](#)).

The complexes that utilized the Rhd110/Cy3 FRET pair were excited at 480 nm (excitation band pass of 2 nm) and the emission spectrum from 500-750 nm (emission band pass of 2 nm) was recorded. The complexes containing only Rhd110 (D\*A), only Cy3 (DA\*), both dyes (D\*A\*), and no dyes (DA) were measured, and relative FRET changes were determined by comparing all three traces after subtraction of DA. The relative FRET was determined as above for the Cy3 donor experiments, except the acceptor peak occurs at 566 nm and the donor peak at 532 nm (Table 4.1, Figure 4.7).

## **2.2.7 Kinetic Assays**

Changes in fluorescence and anisotropy after rapid mixing were measured using a KinTek stopped flow spectrofluorometer model SF-2004 (Figure 2.12 A). In a stopped flow apparatus, two solutions are rapidly mixed and the reaction times are measured by fluorescence or anisotropy change. In our instrument, the dead time is ~2 ms, giving us sufficient time resolution for most of the changes we monitor.

### **2.2.7.1 Ensemble FRET experiments with Cy3 dye as donor**

Experiments were performed in the KinTek stopped flow spectrofluorometer with an excitation of 530 nm, the donor Cy3 fluorescence was measured in PMT-1 with a 570 +/- 10 nm band pass filter, and the acceptor Cy5 fluorescence was measured in PMT-2 with a 680 +/- 10 nm band pass filter (slit width of 1.56 nm for the excitation). In some instances complexes were created with only Cy3 (donor alone, D\*A) or only Cy5 (acceptor alone, DA\*) in order to determine cross talk between the channels (i.e. donor

excitation being read in the acceptor channel); however, because of the spectroscopic properties of the FRET pair, the overlap is minimal. In most cases, at least 10 traces were taken and averaged per experiment.

### **2.2.7.2 Ensemble FRET experiments with Rhd110 dye as donor**

Experiments were performed using the KinTek stopped flow spectrofluorometer with an excitation of 480 nm. The donor, in this case Rhd110, fluorescence was measured in PMT-1 with a 520 +/- 10 nm band pass filter, and the acceptor Cy3 fluorescence was measured in PMT-2 with a 570 nm long-pass filter (slit width of 1.56 nm for the excitation). In all instances the Rhd110 (donor alone D\*A) complex was measured in order to determine the overlap of the Rhd110 emission in the Cy3 channel. Unlike the Cy3/Cy5 FRET pair, the Rhd110/Cy3 FRET pair has considerable overlap, and thus the acceptor channel needs to be corrected by looking at the 4 traces utilized in the bottom half of [Equation 2.2](#): 1) Donor and acceptor labeled, measured at the donor channel,  $D^*A^*_{(D)}$ ; 2) Donor and acceptor labeled, measured at the acceptor channel,  $D^*A^*_{(A)}$ ; 3) Donor labeled, measured at the donor channel,  $D^*A_{(D)}$ ; and 4) Donor labeled, measured at the acceptor channel,  $D^*A_{(A)}$ . Where  $D^*A^*_{(A)}$  is the corrected acceptor channel used to determine FRET efficiency change.

### **2.2.7.3 Anisotropy Measurements of tRNA<sup>fMet</sup> (Cy3) Release**

In Chapter IV, preliminary fluorescence anisotropy measurements are used in order to determine the rate at which a deacylated-tRNA<sup>fMet</sup> (Cy3) is released from the ribosome. Fluorescence anisotropy is a useful method to study molecular interactions by monitoring changes in apparent size of fluorescently labeled molecules, in this case the

interaction between a fluorescent tRNA and the ribosome. Losses in fluorescence anisotropy indicate that the fluorescent tRNA has gone from a bound to unbound state, and provides a direct measurement of tRNA release from the ribosome. The PRE-1 complexes used in Chapter IV were prepared as described above, and the KinTek stopped flow was equipped with polarizing filters to allow anisotropy measurements (Figure 2.12 B). Anisotropy measurements utilize four fluorescence intensities and the value is calculated by equation 2.3.

$$Anisotropy = \frac{I_{VV} - GI_{VH}}{I_{VV} + GI_{VH}} \quad \text{Equation 2.3}$$

$$G = \frac{I_{HV}}{I_{HH}}$$

Where,  $I_{VV}$  stands for intensity with vertically polarized excitation and vertically polarized emission,  $I_{VH}$  stands for intensity with vertically polarized excitation and horizontally polarized emission, and so on.  $G$  is a measure of the sensitivity difference between the two PMTs used for obtaining the data.

## 2.2.8 Rate Constant Estimation

In Chapter IV, the data presented were fit both to triple exponential (Figures 4.4-4.6, 4.8-4.11) and to the global Scheme 4.1 (Figures 4.12, 4.13) using the program

Scientist (MicroMath Research, LC). Fitting of the data to a triple exponential (Equation 2.6) yielded apparent rate constants presented in Table 4.1. Whereas fitting to Scheme 4.1, yielded rate constants presented in Table 4.3.

In Chapter V, the data presented in Figures 5.2A, 5.3, 5.4, and 5.5 were fit to either a single exponential (Equation 2.4) or a double exponential (Equation 2.5) in Scientist, and yielded apparent rate constants presented in Table 5.2.

$$y = y_0 + A_1 e^{-k_{app1}t} \quad \text{Equation 2.4}$$

$$y = y_0 + A_1 e^{-k_{app1}t} + A_2 e^{-k_{app2}t} \quad \text{Equation 2.5}$$

$$y = y_0 + A_1 e^{-k_{app1}t} + A_2 e^{-k_{app2}t} + A_3 e^{-k_{app3}t} \quad \text{Equation 2.6}$$



tRNA	Charge	Label	[ <sup>3</sup> H]/[ <sup>35</sup> S]- aa : tRNA FPLC Purified	[ <sup>3</sup> H]/[ <sup>35</sup> S]- aa : tRNA HPLC Purified	Dye : tRNA	Dye : tRNA HPLC Purified
<b>fMet</b>	Yes	No	0.4±0.1	0.8±0.1	-	-
	Yes	Cy3	0.4±0.1	0.8±0.1	0.3±0.1	1.0±0.1
	No	Cy3	-	-	0.3±0.1	1.0±0.1
<b>Phe</b>	Yes	No	0.3±0.1	0.8±0.1	-	-
	Yes	Cy3	0.3±0.1	0.8±0.1	0.4±0.1	1.4±0.1
	Yes	Rhd110	0.3±0.1	0.8±0.1	0.4±0.1	-
<b>Lys</b>	Yes	No	0.15±0.05	-	-	-
	No	Rhd110	-	-	0.6±0.1	1.5±0.1
<b>Arg*</b>	Yes	No	0.25	-	-	-
	Yes	Cy3	0.40	-	0.50	-

\*The Arg-tRNA<sup>Arg</sup> was only charged one time, and only charged and labeled one time.

**Table 2.1 Charging and labeling efficiencies of tRNAs**

Different species of tRNAs were made and purified by either HPLC or FPLC, the resulting charging efficiencies and labeling efficiencies are shown in this table. In general, HPLC purification of charged tRNA and/or labeled tRNA gave efficiencies greater than FPLC purification due to the higher separation of the HPLC. The >1 labeling

efficiencies of Phe and Lys can be attributed to the tRNA having more than one dihydrouridine.

<b>Complex</b>	<b>Buffer</b>	<b>peptidyl-Puro : 70S</b>
<b>70SIC</b>	A	0.36±0.05
	B	0.30±0.05
<b>PRE-1</b>	A	0.03±0.01
	B	0.02±0.01
<b>POST-1</b>	A	0.35±0.05
	B	0.32±0.05
<b>PRE-2</b>	A	0.05±0.01
	B	0.05±0.01

**Table 2.2 Puromycin Reactivity of Ribosome Complexes**

Equilibrium puromycin reactivity was measured for each of the complexes made to ensure that the correct complex was created. For the 70SIC complex, puromycin forms a peptide bond with [<sup>35</sup>S]-fMet to create [<sup>35</sup>S]-fMet-Puromycin. [<sup>35</sup>S]-fMet-Puromycin per 70S ribosome was measured to determine puromycin reactivity. Puromycin is unable to react with a PRE-1 or PRE-2 complex and the levels shown in the table are similar to background. In the POST-1 complex puromycin reacts with the [<sup>35</sup>S]-

fMet-[<sup>3</sup>H]-Phe, to create [<sup>35</sup>S]-fMet-[<sup>3</sup>H]-Phe-Puromycin, and either the radioactive fMet or radioactive Phe is used to measure reactivity.

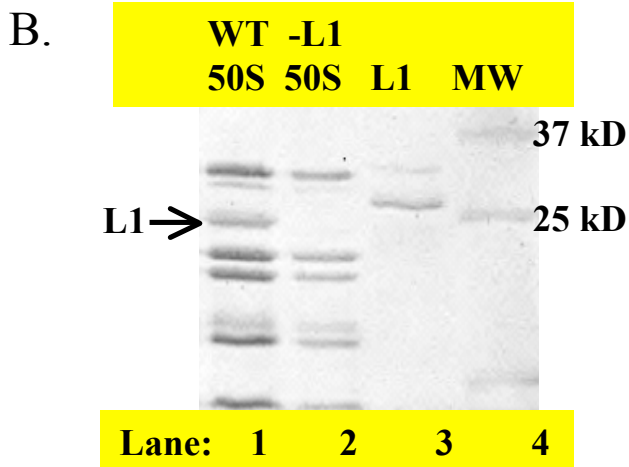
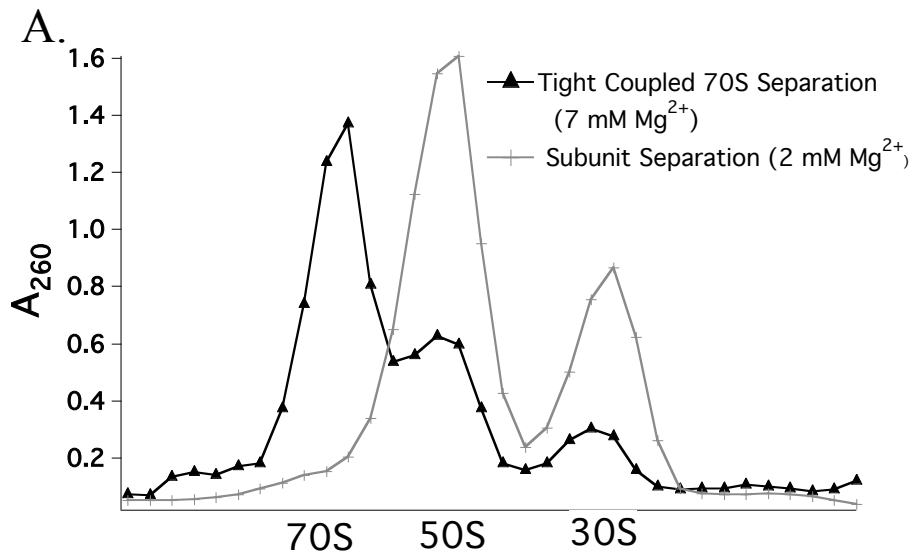
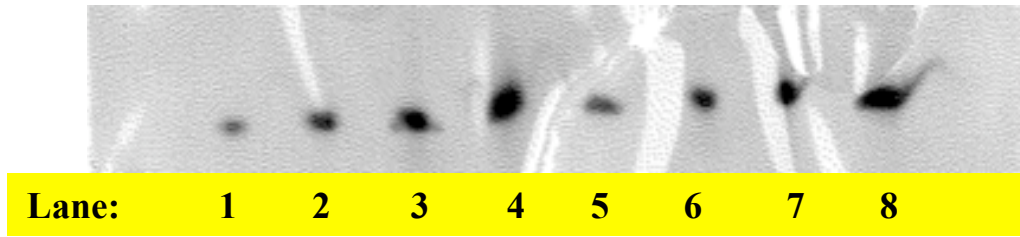


**Figure 2.1 Separation of Purified -L1 Ribosomes**

After purification, the -L1 ribosomes were separated to collect either tight coupled 70S (black triangles) or 50S and 30S subunits (grey crosses). Approximately 30 pmol of the

50S subunits were then analyzed on a 12% SDS-PAGE gel (**B**). **Lane 1:** MRE-600 50S subunits (~30 pmol); **Lane 2:** -L1 50S subunits; **Lane 3:** Purified L1 (~20 pmol); **Lane 4:** Molecular Weight Marker. Notice that in Lane 2 the band for L1 is missing. The apparent increase in molecular weight in the L1 band between Lane 1 and Lane 3 is attributed to the 10x-His-tag and linker associated with the Lane 3 purified L1 protein.

A.



B.

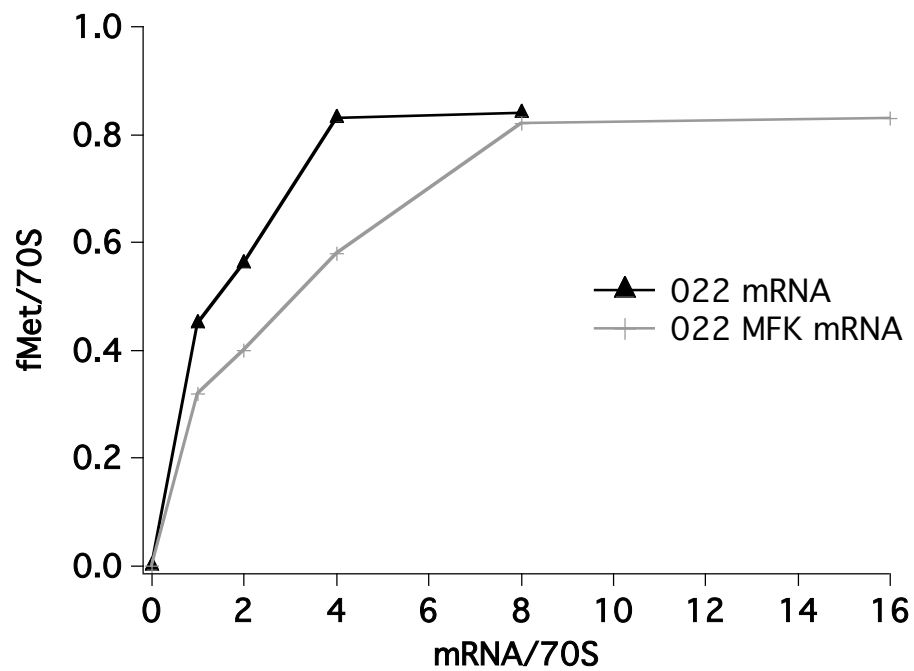


### Figure 2.2 mRNA Purity and Activity

**A:** Transcribed mRNA022 (Lane 1-4, increasing amounts, 0.5, 1, 2, 4  $\mu\text{g}$ ) was loaded on to a 6% SDS-UREA gel, and run against the same amounts of known mRNA022 (lane 5-8), and stained with a methanol blue stain. **B:** mRNA promotes the binding of [ $^{35}\text{S}$ ]-fMet-tRNA<sup>fMet</sup> that normally reaches a plateau of 0.7 – 0.9 fMet per ribosome. A number at the plateau that is less than one is a result of either inactive

ribosomes, or the binding of the non-radioactive tRNA<sup>fMet</sup>. This assay was used to determine the correct concentration of mRNA to add in order to reach the optimum fMet-tRNA<sup>fMet</sup> binding.

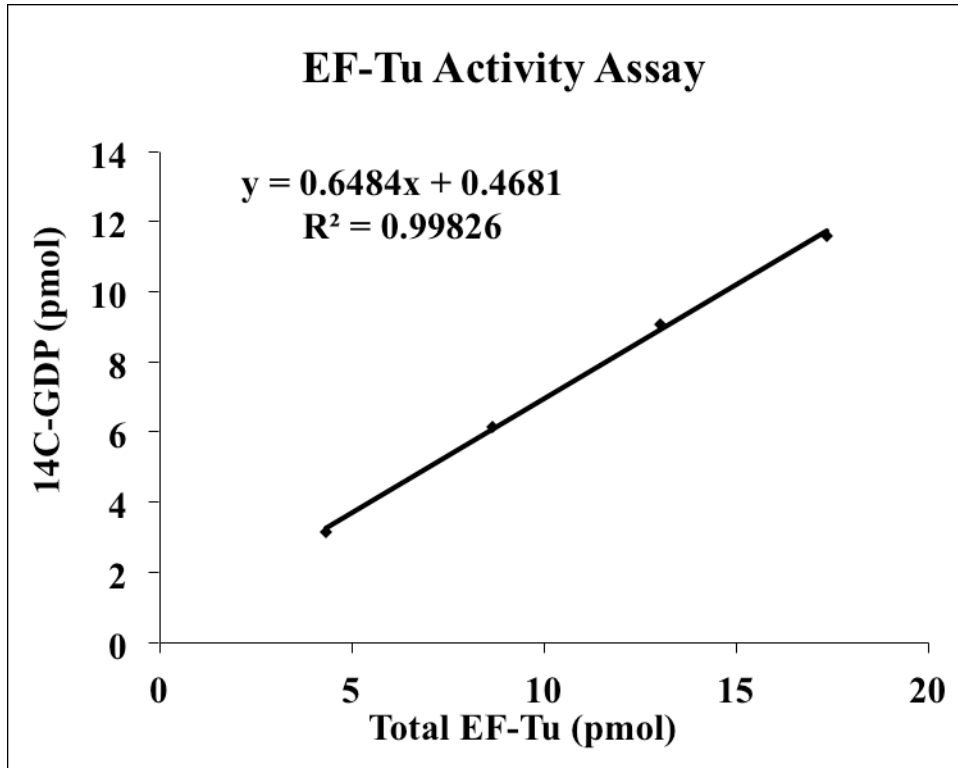


**Figure 2.3 EF-Tu Activity Test Results**

Increasing amounts of EF-Tu were incubated with a saturating amount of [<sup>14</sup>C]-GDP. The EF-Tu.GDP complex was collected on nitrocellulose filters and the amounts were determined by radioactive counts. The active concentration of EF-Tu was determined by the slope of a linear fitting and was determined to be 64.8% as active as

the total amount of EF-Tu as determined by Bradford Assay. Typical EF-Tu preparations yield 60-70% active EF-Tu.

## DNA Sequence

```
1   ATGGCTAAAC TGACCAAGCG CATGCGTGTT ATCCGCGAGA AAGTTGATGC
51  AACCAAACAG TACGACATCA ACGAAGCTAT CGCACTGCTG AAAGAGCTGG
101 CGACTGCTAA ATTCGTAGAA AGCGTGGACG TAGCTGTTAA CCTCGGCATC
151 GACGCTCGTA AATCTGACCA GAACGTACGT GGTGCAACTG TACTGCCGCA
201 CGGTACTGGC CGTTCGGTTC GCGTAGCCGT ATTTACCCAA GGTGCAAACG
251 CTGAAGCTGC TAAAGCTGCA GGCGCAGAAC TGGTAGGTAT GGAAGATCTG
301 GCTGACCAGA TCAAGAAAGG CGAAATGAAC TTTGACGTTG TTATTGCTTC
351 TCCGGATGCA ATGCGCGTTG TTGGCCAGCT GGGCCAGGTT CTGGGTCCGC
401 GCGGCCTGAT GCCAAACCCG AAAGTGGGTA CTGTAACACC GAACGTTGCT
451 GAAGCGGTTA AAAACGCTAA AGCTGGCCAG GTTCGTTACC GTAACGACAA
501 AAACGGCATC ATCCACACCA CCATCGGTAA AGTGGACTTT GACGCTGACA
551 AACTGAAAGA AAACCTGGAA GCTCTGCTGG TTGCGCTGAA AAAAGCAAAA
601 CCGACTCAGG CGAAAGGCGT GTACATCAAG AAAGTTAGCA TCTCCACCAC
651 CATGGGTGCA GGTGTTGCAG TTGACCAGGC TGGCCTGAGC GCTTCTGTAA
701 ACTAA
```

## *E. Coli* L1 Sequence

```
1   makltkrmrv irekvdatkq ydineaiall kelatakfve svdvavnlgi darksdqnv
61  gatvlphgtg rsvrvavftq ganaeaakaa gaelvgmedl adqikkgemn fdvviaspda
121 mrvvgqlgqv lgprglmpnp kvgtvtpnva eavknakagq vryrndkngi ihttigkvd
181 dadklkenle allvalkkak ptqakgvyik kvsisttmga gvavdqagls asvn
```

## Primers

### S40C (AGC→TGC)

Forward: 5' GCGACTGCTAAATTCGTAGAA**TGCGTGGACGTAGCTGTTAACC** 3'

Reverse: 5' GGTTAACAGCTACGTCCAC**GCA**TTCTACGAATTTAGCAGTCGC 3'

GC content: 48.84%	Location: 50-92
Melting temp: 83.9°C	Mismatched bases: 1
Length: 43 bp	Mutation: Substitution
5' flanking region: 21 bp	Forward primer MW: 13282.76 Da
3' flanking region: 21 bp	Reverse primer MW: 13162.70 Da

### K54C (AAA→TGC)

Forward: 5' CTCGGCATCGACGCTCGT**TGCTCTGACCAGAACGTACGTG** 3'

Reverse: 5' CACGTACGTTCTGGTCAG**AGCA**ACGAGCGTCGATGCCGAG 3'

GC content: 60.00%	Location: 142-181
Melting temp: 81.2°C	Mismatched bases: 3
Length: 40 bp	Mutation: Substitution
5' flanking region: 18 bp	Forward primer MW: 12249.07 Da
3' flanking region: 19 bp	Reverse primer MW: 12347.13 Da

### V177C (GTG→TGC)

Forward: 5' CCACACCACCATCGGTA**ATGCGACTTTGACGCTGACAAAC** 3'

Reverse: 5' GTTTGTCAGCGTCAAAGT**CGCA**TTTACCGATGGTGGTGTGG 3'

GC content: 51.22%	Location: 113-153
Melting temp: 78.9°C	Mismatched bases: 3
Length: 41 bp	Mutation: Substitution
5' flanking region: 19 bp	Forward primer MW: 12492.28 Da
3' flanking region: 19 bp	Reverse primer MW: 12718.36 Da

### T202C (ACT-->TGC)

Forward: 5'GCTGAAAAAAGCAAAACCG**TGCCAGGCGAAAGGCGTGTAC**

Reverse: 5'GTACACGCCTTTCGCCTGGC**ACGG**TTTTGCTTTTTTCAGC

GC content: 52.50%	Location: 585-624
Melting temp: 78.4°C	Mismatched bases: 3
Length: 40 bp	Mutation: Substitution
5' flanking region: 19 bp	Forward primer MW: 12406.20 Da
3' flanking region: 18 bp	Reverse primer MW: 12187.03 Da

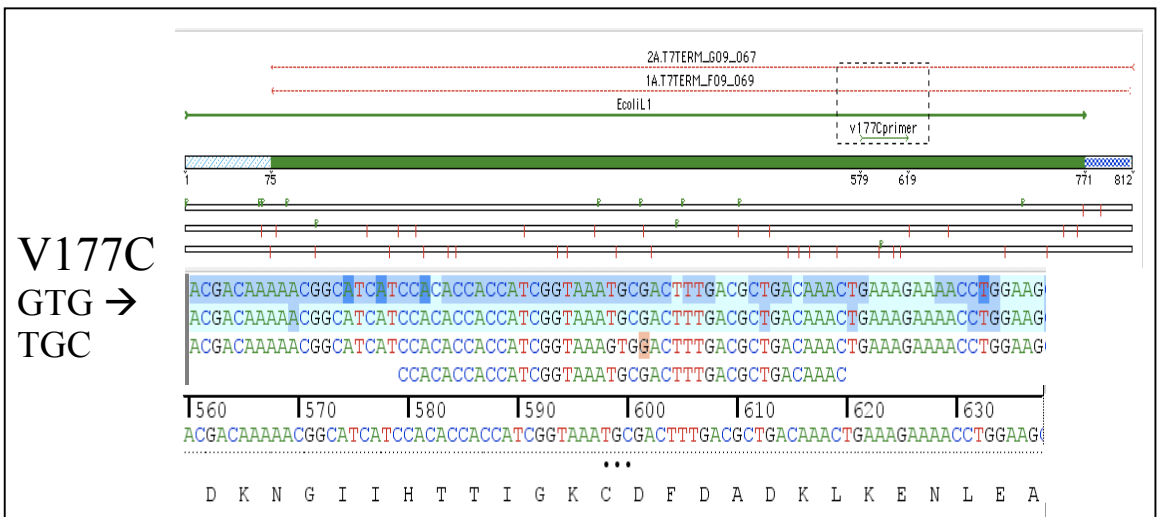
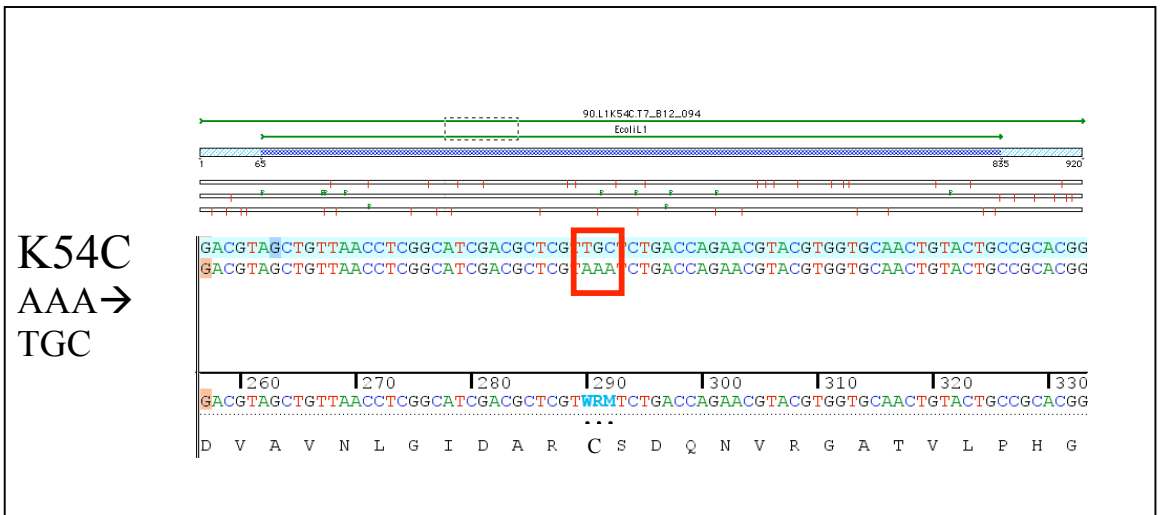
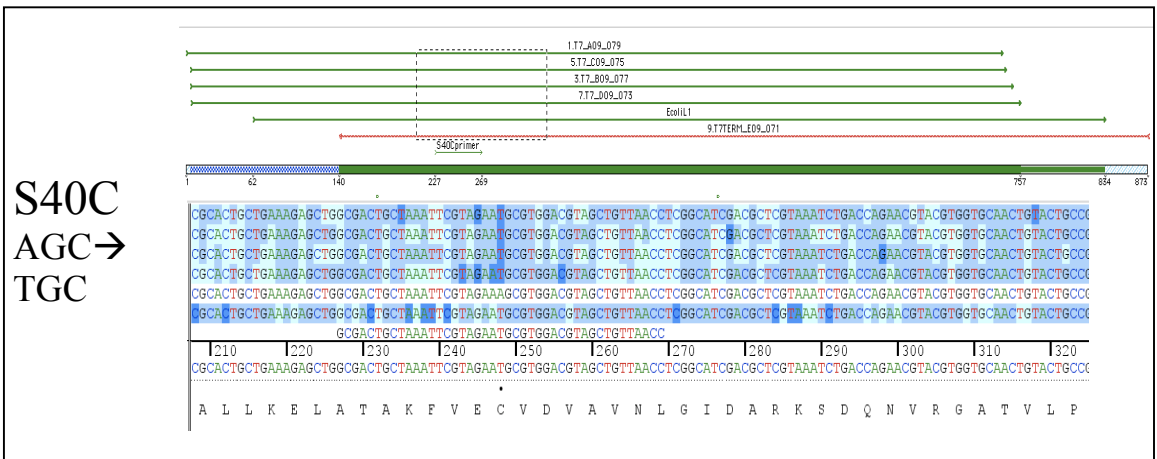


**V221C (GTT→TGT)**Forward: 5' CACCATGGGTGCAGGT**TGT**GCAGTTGACCAGGCTGReverse: 5' CAGCCTGGTCAACTGC**ACA**ACCTGCACCCATGGTG

GC content: 60.00%	Location: 98-132
Melting temp: 80.8°C	Mismatched bases: 2
Length: 35 bp	Mutation: Substitution
5' flanking region: 16 bp	Forward primer MW: 10844.13 Da
3' flanking region: 17 bp	Reverse primer MW: 10662.05 Da

**Figure 2.4 DNA and protein sequences of *E. coli* ribosomal protein L1 and sequences of the single mutant primers**

Mutants are indicated in the DNA and protein sequence, S40C (blue), K54C (orange), V177C (red), T202C (pink), V221C (green), and the start codon is underlined in the DNA sequence. Single mutant primers were designed using the program PrimerX (<http://www.bioinformatics.org/primerx/>) under the specifications for the Stratagene Quickchange site directed mutagenesis kit.



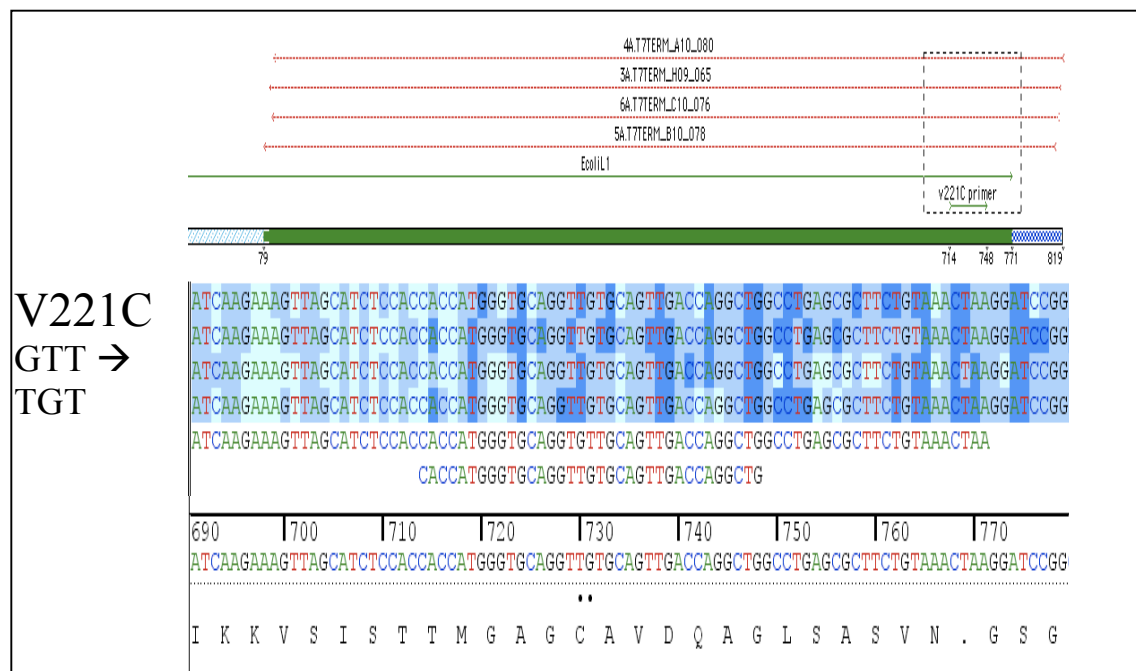
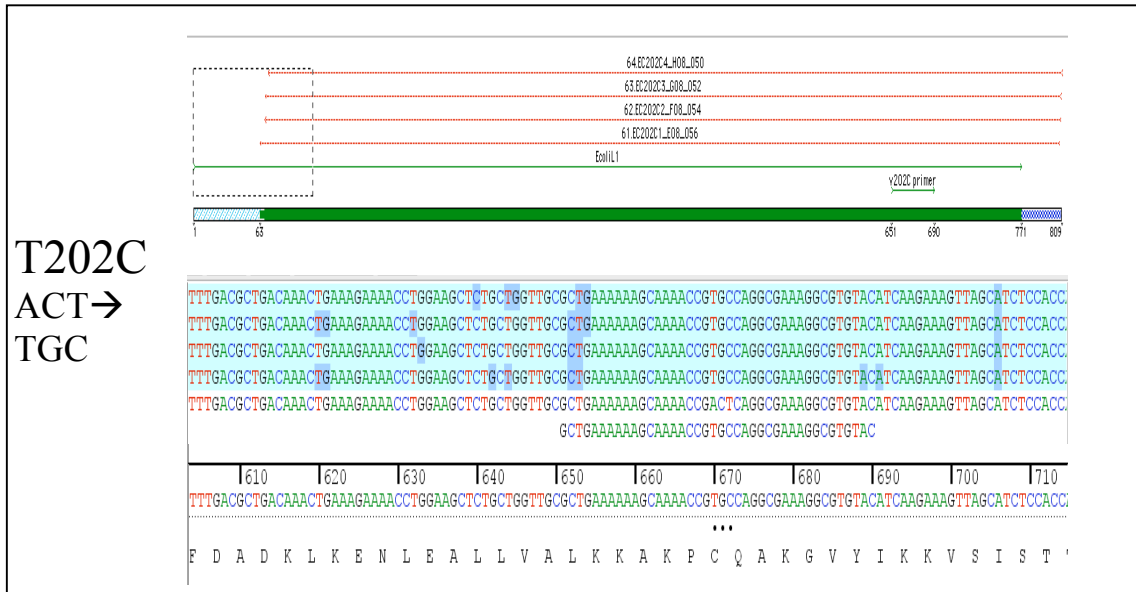


**Figure 2.5 DNA Sequencing Results of the Single Mutants**

The single mutant primers were used to create mutant strains that were sequenced using the T7 promoter or T7 terminator sequences as a sequencing primer depending on the location of the mutant within the plasmid. Early mutants in the sequence like S40C

and K54C utilized the T7 promoter primer, where as the other mutants used the T7 terminator primer.

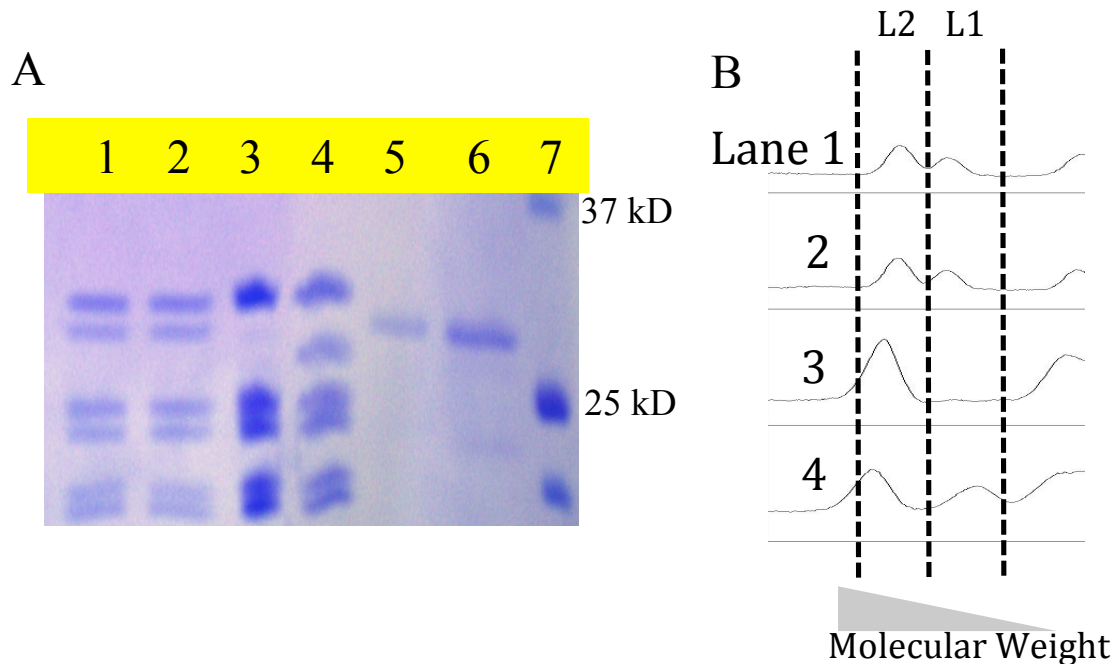


**Figure 2.6 Reconstitution analyses of L1 and -L1 50S subunits**

-L1 50S subunits were reconstituted with T202C-L1 (Lane 1 A, B) and T202C-L1 (Cy5) (Lane 2 A, B). An SDS-PAGE gel was used to analyze the reconstitution by comparing the reconstituted samples (Lane 1 and 2) to wild type 50S subunits (Lane 4), 50S subunits lacking L1 (Lane 3), T202C-L1 (Lane 5) and T202C-L1 (Cy5) (Lane 6). Reconstitution with both the T202C-L1 (Cy5) and T202C-L1 samples reached 1:1 when analyzed by band density. When the labeled T202C-L1 (Cy5) was reconstituted, the Cy5 : 50S ratio was  $0.6 \pm 0.2$ , depending exclusively on the labeling efficiency of the L1 protein.

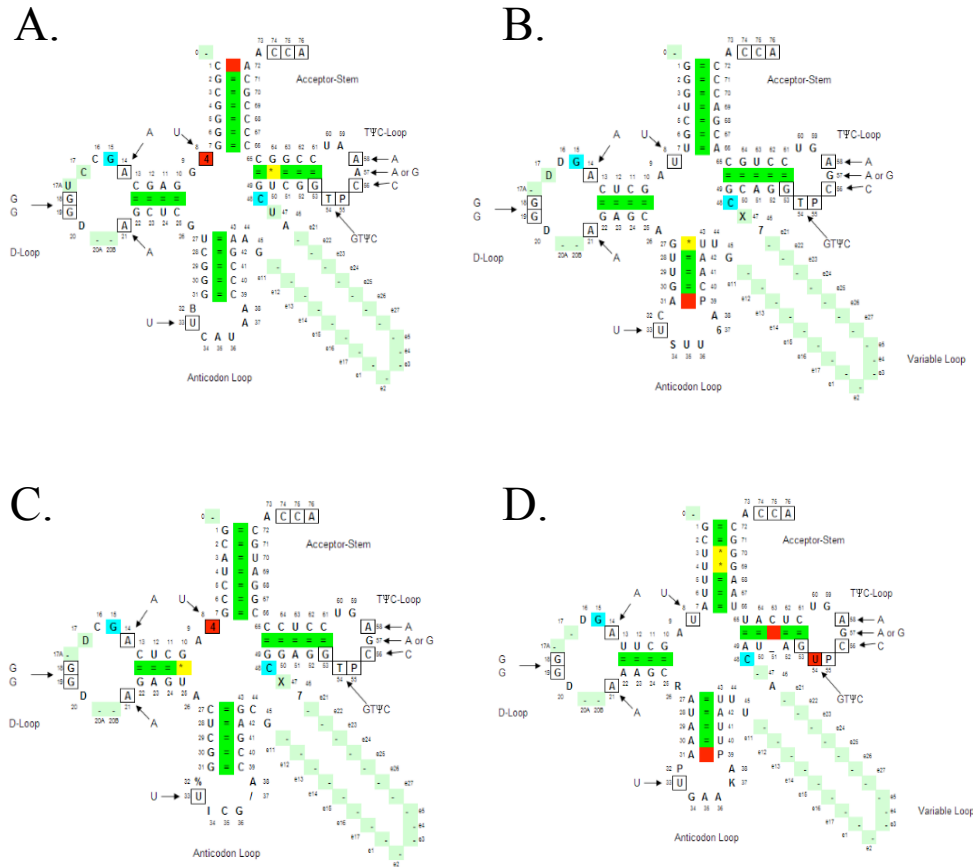


**Figure 2.7 Secondary Structures of tRNAs**

Cloverleaf structures of **A)** initiator tRNA<sup>fMet</sup>, **B)** tRNA<sup>Lys</sup>, **C)** tRNA<sup>Arg</sup> from *E. coli*, and **D)** tRNA<sup>Phe</sup> from yeast.

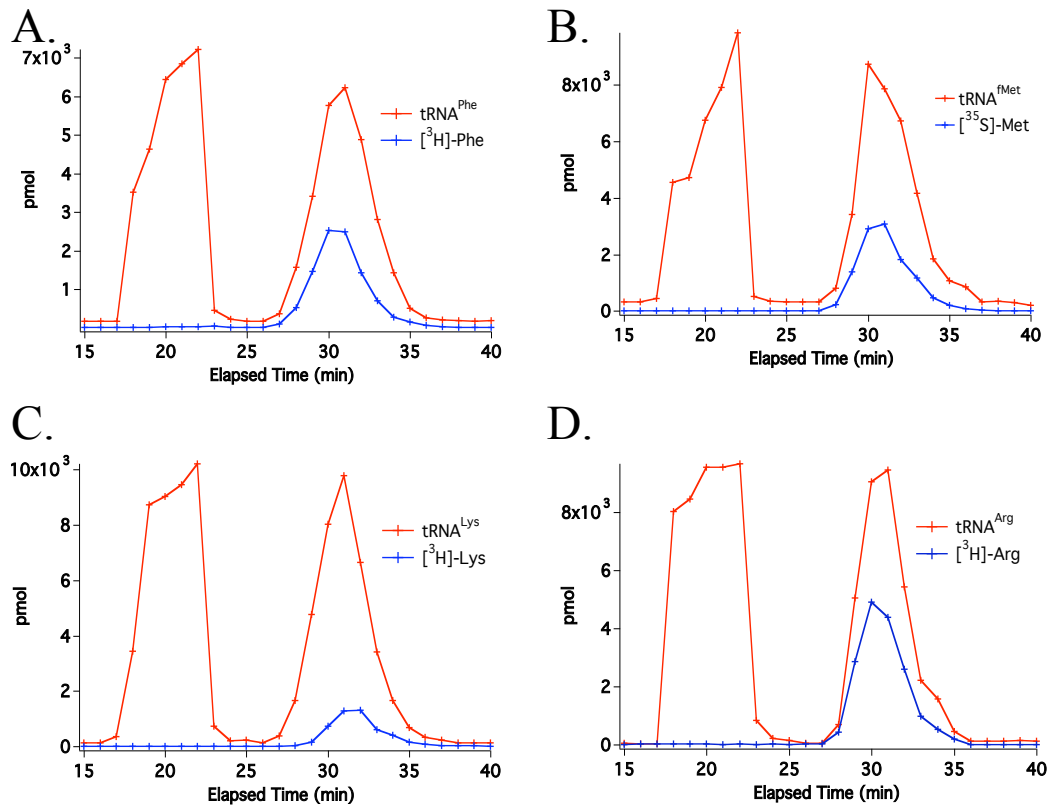


**Figure 2.8 FPLC Purification of Charged tRNAs**

The above traces are examples for purification of tRNA from the poly-adenine byproduct (elapsed time ~18-23 min). The FPLC purification does not separate charged tRNA from uncharged tRNA, thus collection of the tRNA peak (elapsed time ~26-35 min) results in only the inherent charging efficiencies as evidenced by comparison of tRNA concentration versus amino acid concentration. A) fMet-tRNA<sup>fMet</sup>: total tRNA (~0.35:1); B) Phe-tRNA<sup>Phe</sup>: total tRNA (~0.4:1); C) Lys-tRNA<sup>Lys</sup>: total tRNA (~0.2:1); and C) Arg-tRNA<sup>Arg</sup>: total tRNA (~0.6:1).

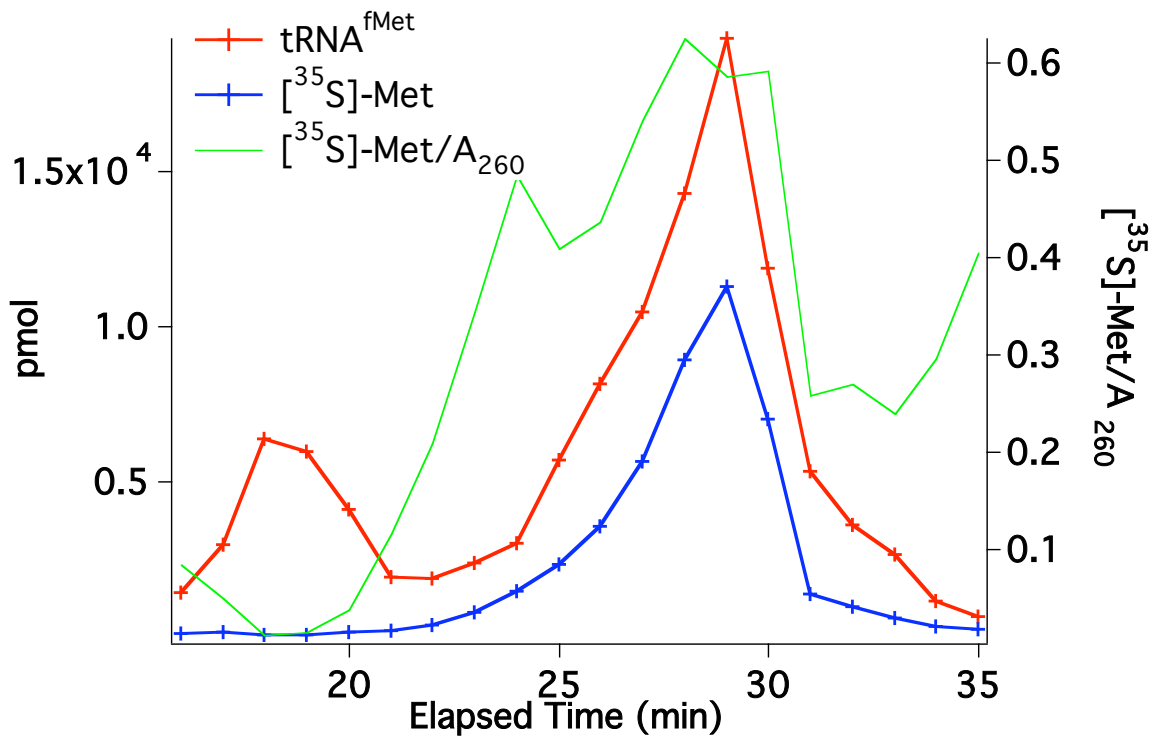


**Figure 2.9 HPLC Purification of fMet-tRNA<sup>fMet</sup>**

HPLC purification of tRNA<sup>fMet</sup> (elapsed time ~18-19 min) from fMet-tRNA<sup>fMet</sup> (elapsed time ~25-30 min) resulted in a sample that contained a ratio of [<sup>35</sup>S]-Met : tRNA<sup>fMet</sup> of ~0.8 : 1. The poly-adenosine peak as well as an earlier tRNA<sup>fMet</sup> peak is not shown here.

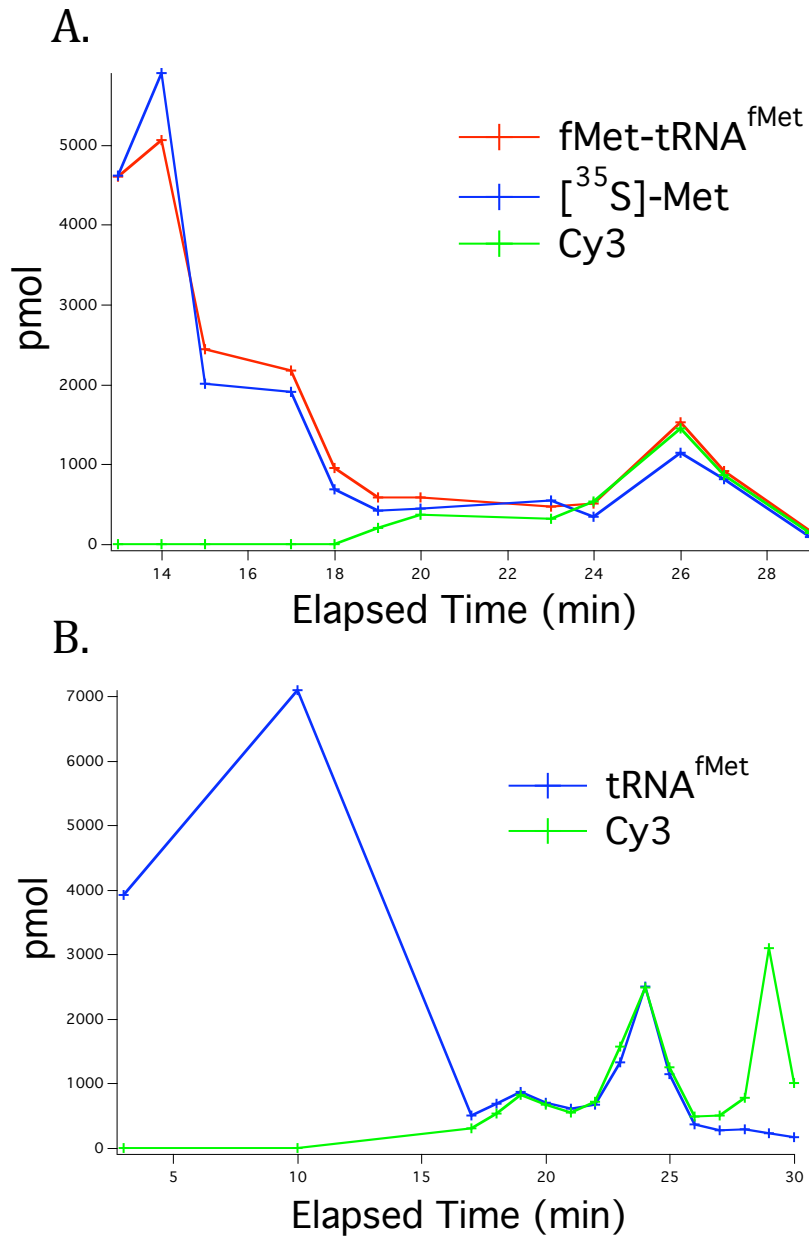


**Figure 2.10 HPLC Purification of Cy3-labeled tRNAs**

HPLC purification of Cy3-hydrazide labeled fMet-tRNA<sup>fMet</sup> (Cy3) (A) or tRNA<sup>fMet</sup> (Cy3) (B). In both cases the labeled tRNA (elapsed time A: ~26 min; B: ~24-



25 min) came out after the unlabeled tRNA and resulted in labeling efficiencies of Cy3:tRNA of 1:1. There is a free dye peak seen in B that is also seen in A, but it is not shown on the plot.

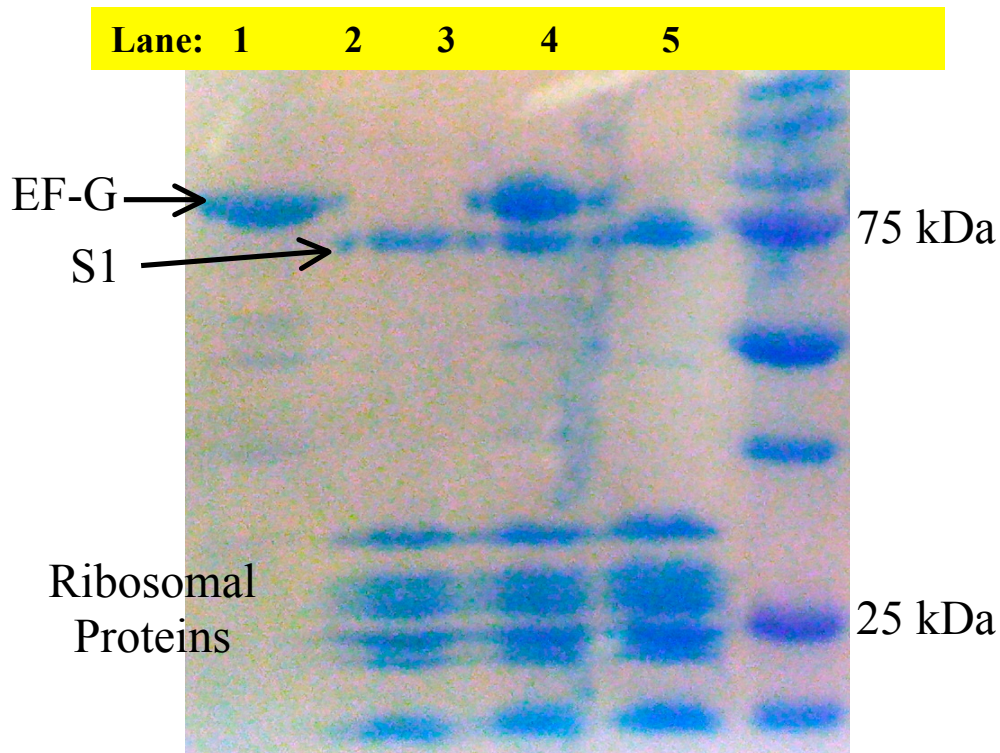
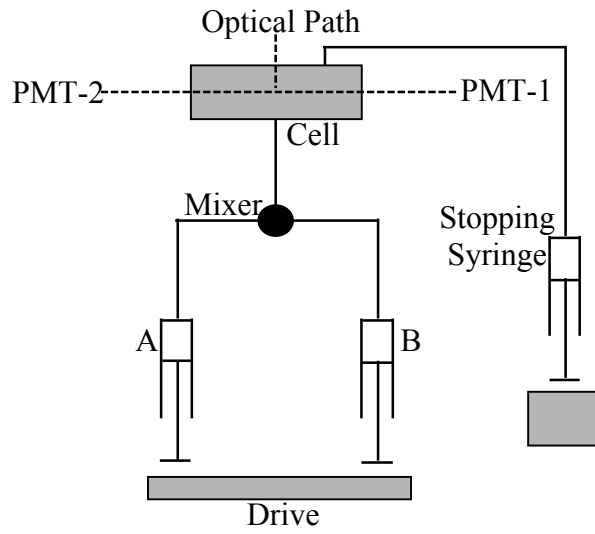


**Figure 2.11 SDS-PAGE Gel Electrophoresis Result of POST Complex Preparation**

Approximately 30 pmol of ribosome complexes were loaded to a 12% SDS-PAGE gel. Lane 1: EF-G (39 pmol); Lane 2: 70S; Lane 3: EF-G (39 pmol) and 70S (30 pmol) added together; Lane 4: POST complex after sucrose cushion; Lane 5: Molecular Weight Marker. The highest molecular weight ribosomal protein S1 is present in lanes 2-4 indicating the presence of ribosomes. EF-G is present in lanes 1, and 3, but is absent in lane 2 and 4, which clearly shows that the sucrose cushion has removed most of the EF-G protein at least beyond the detection limit of the gel.

A.



B.

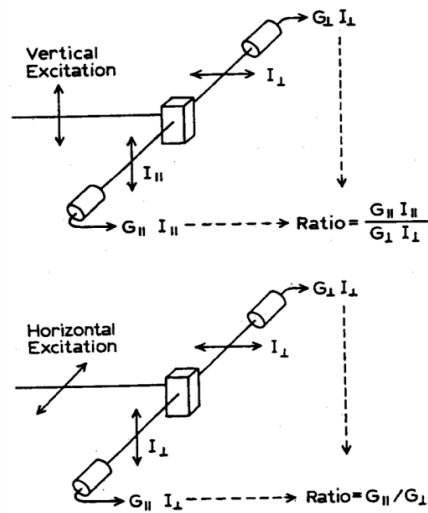


Figure 2.12 Schematic for A) Stopped Flow and B) Anisotropy Set-up

# **Chapter III: Optimization of Overexpression, Purification, and Reconstitution of L1 Mutants**

### 3.1 Abstract

Obtaining pure samples of reconstituted ribosomes with modified L1 in an efficient manner was required for the success of the following research. It is for this reason that it was necessary to spend time discovering the optimal conditions for L1 overexpression, L1 purification, and ribosome reconstitution with the mutant and/or labeled L1. Here we discuss a variety of conditions to increase the protein yield by overexpression, and optimize the purification of an active, native ribosomal protein L1. By following suggestions from a review written by Sørensen and Mortensen, it was determined that the most efficient way to increase yields of native L1 was to lower the temperature at which overexpression occurred to  $\sim 20$  °C (**Sørensen and Mortensen, 2005**). This resulted in yields of purified usable L1 of  $\sim 2$  mg/L of culture, which, when overexpressed on a large (15-L) scale provided plenty of pure L1. Once the L1 was overexpressed, French press or a commercially available Bug Buster® Master Mix was used to lyse the cells. Both methods proved to be viable means of opening the cells to obtain soluble protein. Purification was then optimized, and the TALON resin was determined to provide the highest yield of pure L1.

Once overexpression and purification of the wild type L1 were optimized, the mutants (S40C, K54C, V177C, T202C, and V221C-L1) were created and either labeled with a dye functionalized with a maleimide (Cy3, Cy5, or Cy5.5) or left underivatized. These mutants, either labeled or unlabeled, were then reconstituted into –L1 ribosomes. By optimizing the previous work of Odom et al., reconstitution into –L1 50S subunits was determined to be the most efficient method for creating pure reconstituted ribosomes

(Odom et al., 1990). Further, the reconstituted 50S ribosomes were used to create ribosomal complexes, and T202C-L1 (Cy5) and K54C-L1 (Cy5) were shown to be useful probes for P- and E-site tRNA movement.

### 3.2 Introduction

Much of the work in the biochemical field requires a reliable source for expression of proteins from a variety of species. In the early 1980s the utilization of expression vectors containing an IPTG-inducible promoter based on the *lac* operon became a popular way to control high-level expression of foreign proteins in *E. coli* (Amann et al., 1983; Amann and Brosius, 1985; Sambrook and Russell, 2001). These vectors use the cell's own RNA polymerase to express a gene downstream of the *lac* promoter; however, this could cause further problems when the RNA polymerase is needed to express the cell's own genes, possibly leading to leaky expression. This problem was solved with the use of expression systems utilizing the bacteriophage T7 promoter (Tabor and Richardson, 1985; Studier and Moffatt, 1986). These expression systems use the bacteriophage T7 RNA polymerase, and only recognize the bacteriophage T7 promoters, therefore limiting the amount of non-specific expression. In order to use the T7 promoter expression system, two things are required: 1) bacteriophage T7 RNA polymerase, which is the product of T7 gene *I*; and 2) a plasmid vector containing a bacteriophage T7 promoter upstream of the target gene (Sambrook and Russell, 2001). The expression system in the following work uses the bacteriophage T7 RNA polymerase from the competent *E. coli* BL21 (DE3) cells (Stratagene). The BL21

(DE3) cells contain the T7 gene *l* that is under control of the IPTG-inducible *lacUV5* promoter. The plasmid vector utilized for expression of L1 is the pET-16b vector. The pET series of vectors, originally developed by Studier *et al.*, contains the T7 promoter region and various cut sites downstream to insert the target gene (**Studier et al., 1990**). Specifically, the pET-16b cloning and expression region contains the T7 promoter, a *lac* operator, a sequence coding for a 10x His-tag, followed by multiple cloning sites in which the L1 gene was inserted between the NdeI (5' end) and BamHI (3' end), and finally the T7 terminator (**Figure 3.1**). Proper expression of the L1 gene, and eventually the L1 mutants, is necessary in order to successfully put together fluorescently labeled 50S complexes, and therefore, the proper mix of vector and competent cell is critical.

The overexpression of a protein, either foreign or native, to high levels in *E. coli* often leads to the formation of insoluble intracellular aggregates of the expressed protein called inclusion bodies (**Williams et al., 1982; for reviews please see Marston, 1986; Hartley and Kane, 1988; Marston and Hartley, 1990; Georgiou and Valax, 1996; Sambrook and Russell, 2001**). It is unclear what determines whether an overexpressed protein forms an inclusion body or folds properly and remains soluble. However, the available evidence suggests that inclusion bodies arise by the aggregation of partially folded and malformed polypeptides, and is not a result of insolubility or instability of the native protein (**Sambrook and Russell, 2001**). It was previously reported that, when overexpressed, *E. coli* L1 forms inclusion bodies, instead of the soluble folded protein (**Köhler et al., 1998**). Therefore, in addition to optimizing the overexpression machinery for L1, it is also necessary to optimize the conditions of growth to ensure proper folding of the protein, thus limiting the inclusion bodies. Here, I show that by lowering the

temperature of the growth, it is possible to limit the amount of L1 in inclusion bodies, thus increasing the amount of soluble protein.

The next step necessary to obtaining L1-reconstituted ribosomes for use in future studies is separating L1 from all other soluble proteins. In the case of L1, a 10x-His-tag on the N-terminus of the protein is employed. Immobilized-metal affinity chromatography (IMAC) was first used to purify proteins in 1975, and utilized the chelating ligand iminodiacetic acid (IDA) charged with metal ions in order to purify different peptides and proteins (**Porath et al., 1975**). Since the first IMAC purification techniques were used, many more have been discovered, including but not limited to Ni-NTA (Qiagen) and TALON (Clontech). Ni-NTA was first used in the late 1980s and utilizes nitrilotriacetic acid (NTA) which forms a tetradentate with a metal ion, occupying four of the six ligand binding sites in the coordination sphere of the Ni, thereby allowing two sites to coordinate with the His-tag of the protein (**Hochuli, 1989; Qiagen Manual**). In 1991, the TALON IMAC resin was introduced and utilizes a special tetradentate metal chelator that holds the electropositive metal in an electronegative pocket allowing it to bind metal ions, specifically, cobalt. This binding pocket is an octahedral structure in which four of the six metal coordination sites are occupied by the TALON resin ligand. The TALON resin has the advantage of enhancing the accessibility of the bound metal ion to the polyhistidine-tagged protein. The coordination profile of the TALON Resin ligand and cobalt is more specific for polyhistidine-tagged proteins than the Ni-NTA resin, and therefore limits the undesirable tendency to bind unwanted proteins with histidine residues (**Clontech manual**). Both of these IMAC resins have their advantages

and disadvantages, and here it is determined which purification method works best with L1 and L1 mutants.

The purified mutant proteins were labeled at the new cysteine position by maleimide functionalized dyes, specifically Cy3 and Cy5. The labeling procedure is very straightforward and did not necessitate any further optimization resulting in dye:L1 ratios around 0.6-0.8 (Section 2.2.3.3.3 and [Table 3.1](#)). Futile attempts to separate unlabeled L1 away from labeled L1 using FPLC separation were made, and eventually it was decided that further attempts would prove unproductive because extremely highly labeled L1 was not needed for future studies.

Finally, the mutant and/or fluorescently labeled L1 were reconstituted into ribosomes lacking L1. In 1980, Subramanian and coworkers obtained a spontaneous mutant ribosome that was found to lack L1. The mutant ribosome was found to have a reduced level of protein synthesis that is fully restored upon addition of purified L1 to the mutant (**Subramanian and Dabbs, 1980; Dabbs et al., 1981**). However, reconstitution efficiency was difficult to determine, and the reconstituted ribosome was only shown to be functionally active. Here, the most efficient reconstitution for WT, mutant, and fluorescently labeled L1 into  $-L1$  ribosomes or subunits was determined to be an incubation with at least 2x excess L1 to  $-L1$  50S at 37 °C for 15 min.

Initial equilibrium FRET studies were performed using the mutants V177C-L1 (Cy3), or V221C-L1 (Cy3) as the acceptor, and fMet-tRNA<sup>fMet</sup> (Rhd 110) as the donor. After multiple attempts it was determined that the Rhd110/Cy3 FRET pair was not optimal for FRET studies. Even though preliminary data showed FRET efficiency



changes upon ternary complex addition to 70SIC and translocation, the inherent overlap between the Cy3 and Rhd110 dye made FRET efficiency calculations more difficult. However, the Rhd110/Cy3 FRET pair is used later for tRNA/tRNA FRET experiments, and the signal overlap is addressed. The S40C-L1 (Cy3) mutant studies were dropped after it became obvious that the reconstitution with this mutant was not readily possible.

Fluorescently labeled T202C-L1 has been shown to be a useful probe for P- and E-site tRNA in single molecule experiments (Fei et al., 2008). After optimizing the procedures leading up to the final T202C-L1 (Cy Dye)-50S subunit, it is important to show that this particular construct is able to work as effectively on an ensemble experiment scale. Steady-state spectrofluorometer experiments (Fluorolog-3 spectrofluorometer, Horiba Jobin Yvon, USA) were conducted to determine the equilibrium FRET efficiency changes for tRNAs translocating through the ribosome in both Buffer A and Buffer B. Not only was it determined that the T202C-L1 (Cy Dye) 50S was an appropriate probe for P- and E-site tRNA, it was also shown that buffer conditions play an important role in the release of deacylated-tRNA.

### **3.3 Results**

#### **3.3.1 Optimization of L1 Overexpression**

Initial overexpression of wild type ribosomal protein L1 was performed at 37 °C for four hours after induction and resulted in little protein, and almost no soluble protein after cell lysis. In order to optimize protein recovery from overexpression, an initial time

course study was performed. A 5-mL culture was grown overnight, and then 1 L of Luria Bertani media was inoculated with 1:1000<sup>th</sup> volume of the overnight growth (2.2.3.2.1), and grown to an  $OD_{595} = 0.80$  at which time, the 1 L culture was induced with IPTG (1 mM). During overexpression, small aliquots were selected at 1, 2, 4, 6, and 20 hours, and run on a 12% SDS-PAGE gel to determine the level of overexpression (Figure 3.2). As evidenced by the gel, allowing the protein to express for at least 18-20 hours provides the optimum level of overexpression.

Although overexpressing for longer periods of time may allow more protein to be made, the amount of native soluble protein after cell lysis still remains a problem. There are two approaches that can be taken to redirect the protein from inclusion bodies into soluble proteins; either the protein can be refolded from inclusion bodies, or the expression strategy can be modified to obtain expressed protein that is more soluble. Therefore, a multifaceted approach was taken to solve the problem of aggregated, misfolded, and, most likely, inactive L1. First, an attempt to simply purify the denatured protein, and then refold it through a series of dialysis steps (independent communication with Jingyi Fei) proved to be more difficult and less efficient than previously believed. Thus, growth conditions, specifically temperature and media type, were varied in order to limit the amount of protein in inclusion bodies created during overexpression (**Review by Sørensen and Mortensen, 2005**). Four different growth media were examined: 1) LB, 2) LB + 0.5% glycerol, 3) Terrific Broth (TB), and 4) TB + 0.5% glucose. Each of these media were inoculated with the same overnight cell culture and allowed to reach an  $OD_{595} = 0.8$  before IPTG induction. Immediately after IPTG induction, the temperature of the overexpression was either left at 37 °C or dropped to 20 °C, resulting in a total of

eight growth conditions; however, TB growth medium in the absence of 0.5% glucose resulted in no protein expression, and thus no further analysis was done using this medium, leaving six conditions. After an overnight overexpression, the cells were centrifuged to obtain the cell pellet, which was resuspended and the cells were lysed via French Press as described in 2.2.3.2.1. The insoluble cellular material was separated from the soluble protein via centrifugation, and both the insoluble pellet, and the soluble supernatant were analyzed on an SDS-PAGE gel (Figure 3.3). It is apparent that, aside from the TB media, the other media (LB, LB + 5% glycerol, or TB + 5% glucose) does not have a big influence on overexpression; however, the temperature decrease during overexpression strongly increases the amount of soluble protein produced. All further overexpressions were performed in LB media simply because other growths in the lab use LB media, and therefore, sterilized media is readily available. Also the overexpressions were at 20 °C after addition of IPTG to limit the inclusion bodies.

### 3.3.2 Optimization of L1 Purification

To facilitate purification, the *E. coli* L1 construct used in this work is equipped with a 10x-His-tag on the N-terminus. Initial purification was performed much like the other His-tag purifications in the lab by utilizing the Ni<sup>2+</sup>-NTA resin (Qiagen); however, after optimization, a Co<sup>2+</sup> based resin (TALON, Clontech) was determined to provide better coordination to the polyhistidine tags. Further, along with lysis by French press, a lysis procedure utilizing a commercially available protein extraction kit called Bug Buster® Master Mix (Novagen) was tested for opening the cells.

### 3.3.2.1 Metal Affinity Resin Optimization

Initially the same amount of harvested L1 overexpressed cells was resuspended and lysed using the French press, and the soluble proteins were purified by running the supernatant through either Ni<sup>2+</sup>-NTA resin, or TALON resin. The His-tagged L1 protein bound to the resin, and was eluted by an increasing amount of imidazole in a stepwise gradient using (25, 50, 150 and 300 mM imidazole). The resulting fractions were run on a 12% SDS-PAGE gel to determine which fractions contain the pure, eluted, His-tagged L1 (Figure 3.4 A, B). In accordance with the gels, the TALON resin provides a better purification and separation of the L1 from the other soluble proteins. The TALON resin inherently provides a better environment for both binding of only the His-tagged protein and purified elution. The Co<sup>2+</sup> core specifically binds only histidines that are neighboring, essentially eliminating the amount of nonspecific binding of other proteins to the resin. Since only the His-tagged protein binds the resin, the elution conditions can be less stringent resulting in a more highly purified sample.

### 3.3.2.2 Cell Lysis Optimization

In order for the soluble proteins to be harvested, the cell must first be lysed, and cell debris must be separated from the proteins. There are numerous ways to lyse the cell; however, I utilize two different methods, French press and Bug Buster® Master Mix, in order to obtain the soluble protein. Both cell lysis methods result in soluble L1 that is ready to be purified through the TALON resin. The advantage of the French press is that it is cost efficient and is able to handle large volumes of cell re-suspension; however,

sometimes for analytical studies only a small volume is needed, in these cases the Bug Buster® Master Mix is the best choice because it is quick and does not require use of a large instrument. In **Figure 3.4 B and C**, the SDS-PAGE gel clearly shows pure protein elutions after both French press and Bug Buster® Master Mix treatment. The preliminary purifications were done using wild type L1; however, the L1 mutants described below were all purified in a similar manner, and the pure mutant proteins were labeled with maleimide dyes without the need for further optimization (**Table 3.1**).

### **3.3.2.3 MALDI Analysis of Pure and Labeled Mutant L1 (T202C)**

The molecular masses of purified T202C-L1 samples, both labeled with Cy5-maleimide and unlabeled were determined by MALDI (**Figure 3.5**). MALDI of the unlabeled T202C-L1 resulted in a strong peak at 27,296 Da in strong accordance with the theoretical molecular weight of the mutant L1 with 10x His-tag and linker. Further, the Cy5 labeled T202C-L1 resulted in 2 peaks, one indicating the unlabeled portion of the sample at 27,296 Da, and the other indicating the labeled sample with a molecular weight of 28,045 Da. The increased molecular weight of ~750 Da corresponds to the molecular weight of the added Cy5-Maleimide dye (Section 2.1.2).

### **3.3.3 Optimization of Ribosome Reconstitution with Mutant and Labeled L1**

Odom and coworkers first performed the reconstitution of fluorescently labeled L1 into the ribosome in 1990, when they added a fluorescein-L1 to 50S subunits (**Odom et. al., 1990**). Using their protocol as a guide, the optimal conditions of the reconstitution for the mutant and fluorescently labeled L1 were determined; however, many factors play

a role in determining the best protocol for reconstitution. For instance, reconstitution into –L1 70S tight coupled ribosomes has the advantage of saving a week’s worth of time by not having to separate the ribosome into subunits; however, as mentioned previously, checking reconstitution efficiency is then not possible with SDS-PAGE because of the similar molecular weights of L1, S2, S3, and S4, although, this is not a problem when using fluorescently labeled L1. As was discovered during the optimization, reconstituting –L1 70S has the additional problem of non-specific binding of L1 to other locations on the ribosome, resulting in false positive results for reconstitution.

### **3.3.3.1 –L1 70S Reconstitution**

As seen in section 2.2.3.3.4, ribosome reconstitution involves an incubation of an excess of either WT, mutant, or fluorescently labeled L1 with –L1 ribosomes, followed by a sucrose cushion to remove any excess L1 and/or fluorescent dye. Initial reconstitution was attempted on –L1 70S with T202C-L1 (Cy5), and the reconstitution efficiency was measured by  $A_{260}$  (for ribosome) :  $A_{652}$  (for Cy5), allowing the measurement of the amount of Cy5 per ribosome (~0.7-0.8 : 1). However, as it was alluded to earlier, reconstitution could not be monitored by SDS-PAGE gel, and therefore, a direct measurement of L1 : 70S could not be obtained. In order to determine if the L1 protein was indeed being reconstituted, and to rule out that either the Cy5-L1 or the Cy5 alone was binding non-specifically to the ribosome, the reconstituted 70S was separated into 50S and 30S subunits by decreasing the  $Mg^{2+}$  concentration, and then separating the subunits via a sucrose gradient. Upon SDS-PAGE analysis of the subunits, it became apparent that L1 was indeed not being correctly reconstituted into the –L1 70S, and was

in fact only binding transiently, resulting in a false positive for Cy3:70S, that was not actually reconstitution (Figure 3.6). Thus, reconstitution into –L1 50S and then subunit association with 30S is necessary in order to obtain the correctly reconstituted ribosomes.

### 3.3.3.2 –L1 50S Reconstitution

Reconstituting L1 into –L1 50S has the distinct advantage of allowing monitoring via SDS-PAGE gel analysis because there are no other 50S subunit proteins that have a molecular weight close to that of L1; therefore, SDS-PAGE analysis provides a very nice reporter of the reconstitution efficiency of the reaction. The efficiency can be directly determined by comparing the band density of the reconstituted L1 to the band density of L2. This ratio can be compared to the L1:L2 ratio in a wild type 50S subunit, and the closer these two numbers become, the better the reconstitution (Table 3.2). With this in mind, the optimal conditions necessary for reconstitution were determined, specifically, incubation time, L1 : –L1-50S ratio, and incubation temperature.

T202C-L1 mutants were reconstituted into –L1 50S subunits in a ratio of 2:1 and incubated at 37° C for 5, 10, 15, and 30 min, before being purified through a sucrose cushion, and analyzed on a 12% SDS-PAGE gel (Figure 3.7). As evidenced from the gel, the reconstitution efficiency reached a maximum at 15 min; therefore, all future reconstitutions were incubated for 15 min (Table 3.2).

Because the –L1 50S can be made on a larger scale, pure mutant L1 or pure mutant fluorescently labeled L1 is a limiting reagent when determining how much reconstituted ribosomes can be made. Thus, in order to limit waste, it was important to determine the most efficient ratio of L1 to –L1-50S for reconstitution. T202C-L1 and –

L1-50S were combined in ratios of: 1:0 (control), 1:1, 2:1, 3:1, and 5:1, and incubated for 15 min at 37 °C before being purified by centrifugation through a sucrose cushion, and analyzed on a 12% SDS-PAGE gel (Figure 3.8). As expected, the control that only contained T202C-L1 did not pellet through the cushion, ensuring that all the L1 seen in the gel is indeed reconstituted in the ribosome. Further, the reconstitution efficiency reached approximately 90-100% when starting with a two times excess of L1 over –L1 50S. The efficiency only increased a little bit when adding three times excess, and then plateaued (Table 3.2).

Even though a reconstitution efficiency of approximately 100% was reached using an incubation with a 3 times excess of L1 at 37 °C for 15 min, it would be useful to obtain a similarly highly reconstituted sample using less L1. Therefore, a 1:1 ratio of T202C-L1 to –L1 50S was used and incubated for 15 min at 25 °C, 37 °C, and 45 °C, followed by purification through a sucrose cushion. The resulting reconstituted ribosomes were analyzed on a 12% SDS-PAGE gel, and it was determined that changing the incubation temperature does not result in further reconstitution; therefore, it is necessary to use a 2-3 fold excess of L1 (depending on availability of L1) in order to obtain approximately 100% reconstitution (Figure 3.9, Table 3.2).

In addition to using the mutant T202C-L1 and T202C-L1 (Cy5), reconstitutions of S40C-L1 (Cy3), K54C-L1 (Cy5), V177C-L1 (Cy3), V221C-L1 (Cy3) were all done with a 2 times excess of L1 : 50S and incubated for 15 min at 37 °C (Figure 3.10). These samples were all analyzed by SDS-PAGE for reconstitution efficiency, and spectrophotometrically for label per 50S (Table 3.1). All the labeled mutants besides the



S40C-L1 (Cy3) were able to be adequately reconstituted into the -L1 50S, and were used for further equilibrium FRET experiments (See Appendix).

Previously, it had been shown the ribosomes lacking L1 resulted in lower binding of initiator tRNA. In order to test the functional activity of the reconstituted ribosomes, an assay was designed to determine the binding of [<sup>35</sup>S]-fMet-tRNA<sup>fMet</sup> to the reconstituted ribosomes. As seen in [Figure 3.11](#), initiator tRNA binding to -L1 ribosomes was very low, but binding was recovered to near wild-type efficiency when using the fully reconstituted ribosomes. As expected, the complexes made with ribosomes supposedly reconstituted with S40C (Cy3), did not regain binding efficiency.

### **3.4 Discussion**

The ability to effectively and efficiently reconstitute a site-specifically labeled L1 into a ribosome is a very useful tool for the future investigation of tRNA progression through the ribosome. Fluorescently labeled L1 on the ribosome has been previously used for single molecule work in other labs; however, their methods of expression, purification, and reconstitution proved to be too inefficient for use on the much larger scale that is necessary for ensemble work. By optimizing all the steps to work in our facilities, creating a probe to monitor tRNA near the exit site of the ribosome is now a very simple task. Fluorescently labeled L1 is currently being used for both ensemble FRET studies (Cy5), as well as single molecule studies (Cy3). Further, work is progressing using the fluorescent ribosomes to monitor translation in a cell free transcription/translation system.

The overexpression of L1 was initially tested on the wild type L1 obtained from Dr. Robert Zimmermann; however, after expression was optimized, the single site directed mutant L1 (S40C, K54C, V177C, T202C, V221C), was overexpressed with similar results as the wild type. The overexpression of the wild type L1 along with all 5 mutants initially resulted in very high levels of inclusion body formation, which was also noted in **Fei et al., 2008**. Fei and coworkers were able to overcome this by purifying the denatured insoluble L1 and then refolding after purification; however, for our needs, this process was deemed inefficient. By simply lowering the temperature of the growth after induction with IPTG, the amount of soluble L1 was increased dramatically, allowing the purification of active, soluble L1 for use in future studies. As mentioned above, inclusion bodies typically result from misfolded proteins, not necessarily unstable proteins; therefore, by lowering the growth temperature and essentially slowing down the overexpression, we were able to limit the amount of misfolded proteins, resulting in more soluble L1.

Purification of the wild type, S40C, V177C, and V221C was attempted using the Ni-NTA resin, but the purification using this procedure was very poor. Therefore, purification was moved to the TALON resin system for all five mutant L1 samples. The use of the TALON cobalt resin resulted in much cleaner purification, and therefore, a higher yield of usable protein. The better purification with the TALON resin is most likely attributed to the inherently better coordination of the cobalt metal ion to the resin, resulting in more specific binding of polyhistidine residues, and limiting the nonspecific binding of proteins or peptides containing native histidines.

Initial studies were performed using the S40C, V177C, and V221C mutants (see Appendix); however, it became obvious that the most viable mutant for my studies was the T202C-L1 mutant. The S40C-L1 mutant did not reconstitute into –L1 50S to a high enough extent (Table 3.1, Figure 3.11); and the V177C-L1 (Cy3) and V221C-L1 (Cy3) mutants showed limited FRET efficiency changes when analyzed with fMet-tRNA<sup>fMet</sup> (Rhd110). However it is very possible that, using what we currently have learned with the T202C-L1 (Cy5) mutant, the V177C and V221C mutants could still be very viable options for P- and E-site probes in the future. Further, very promising preliminary results have been seen with the K54C-L1 (Cy5) mutant, in which it can be easily labeled and reconstituted into –L1 50S, and has also shown the ability to act as a probe for P- and E-site tRNAs, possibly in a different manner than the T202C-L1 mutant.

Nonetheless, throughout this thesis the T202C-L1 (Cy5) ribosome is utilized to measure FRET changes from Cy3 labeled initiator tRNA. In separate single molecule work, T202C-L1 (Cy3) ribosomes are used with Cy5 and Cy5.5 labeled tRNAs. In both cases, the reconstitution of T202C-L1 (Dye) to ribosomes is very close to 1:1 and the label to ribosomes is solely dependent on the labeling efficiency of the dye to L1 (typically 0.6-0.8). Further, a functional assay in which the binding of [<sup>35</sup>S]-fMet-tRNA<sup>fMet</sup> to –L1 ribosomes, MRE-600 wild type ribosomes, or reconstituted ribosomes was measured, and proved that the reconstitution described above results in a ribosome that actively binds initiator tRNA to an extent similar to the wild type ribosome. tRNA binding per ribosome appears to be less than one because of the low (~30%) charging efficiency of the [<sup>35</sup>S]-fMet-tRNA<sup>fMet</sup> in addition to the notion that the undetectable tRNA<sup>fMet</sup> also binds to the P-site.

### **3.5 Conclusion**

We have developed a method to efficiently overexpress, purify, label, and reconstitute ribosomal protein L1 into a –L1 strand of ribosomes, allowing us to use the labeled L1 as a probe for measuring tRNA movement on the ribosome as it approaches the exit site. The labeled ribosomes are currently being used in ensemble as well as single molecule two and three color FRET experiments. By optimizing the steps leading to the site specifically labeled L1 in the ribosome, we were able to obtain a large amount of L1-labeled ribosome in order to do multiple ensemble studies without having to go through the process of overexpressing and purifying the L1 on a regular basis. The method for limiting inclusion bodies during expression is dependent of the protein being studied; however, the use of TALON resin for purification is most likely universally better and has been applied to the purification of other His-tagged proteins in the lab including EF-Tu, L11, and the initiation factors.

<b>L1</b>	<b>Purification Efficiency (mg/L)</b>	<b>Cy:L1 Labeling Efficiency</b>	<b>Cy:50S Reconstitution Efficiency</b>	<b>Approximate L1:50S Reconstitution Efficiency</b>
<b>Wild Type</b>	2.3 ± 0.2	N/A	N/A	1:1
<b>S40C</b>	1.3 ± 0.7	Cy3: 0.7 ± 0.2	0.5 ± 0.1	0:1
<b>K54C</b>	2.3*	Cy5: 0.5 ± 0.1	0.5 ± 0.2	1:1
<b>V177C</b>	1.3 ± 0.3	Cy3: 0.60 ± 0.05	0.6 ± 0.1	1:1
<b>T202C</b>	1.5 ± 0.5	Cy5: 0.6 ± 0.2	0.6 ± 0.2	1:1
<b>V221C</b>	0.7 ± 0.3	Cy3: 0.6 ± 0.2	0.6 ± 0.1	1:1

\*K54C-L1 mutant was only purified one time.

### **Table 3.1 Purification, Labeling, and Reconstitution Efficiency for L1**

#### **Preparations**

The wild-type L1 and L1 mutants were overexpressed for 18 hours in LB media at 25 °C. The cells were opened with French Press and purified using TALON (Co<sup>2+</sup>) resin yielding the above efficiencies of pure protein to amount of overexpression media. The mutant L1 samples were labeled with Cy maleimide dye and efficiency was measured spectrophotometrically. The mutant, labeled L1 samples were then reconstituted into – L1 50S subunits by incubation with a 2x excess of L1 at 37 °C for 15 min. Reconstitution was measured spectrophotometrically to obtain the Cy:50S ratio, and by SDS-PAGE analysis to obtain the approximate L1:50S efficiency. All but the S40C-L1 mutant reconstituted to almost 100% when measured by L1:50S, and the Cy:50S efficiencies were typically limited by the labeling efficiency of the L1.

<b>Incubation Time (min)</b>		<b>Reconstituted L1:L2 Band Density Ratio</b>	<b>Reconstitution Efficiency*</b>
5	37 °C 2:1 (L1:50S)	0.33	0.44
10		0.34	0.44
15		0.51	0.68
30		0.22	0.29
<b>Incubation L1 : 50S Ratio</b>			
1:1	37 °C 15 min	0.23	0.36
2:1		0.49	0.76
3:1		0.65	1.0
5:1		0.68	1.0
<b>Incubation Temperature (°C)</b>			
25	1:1 (L1:50S) 15 min	0.21	0.28
37		0.20	0.26
45		0.28	0.38

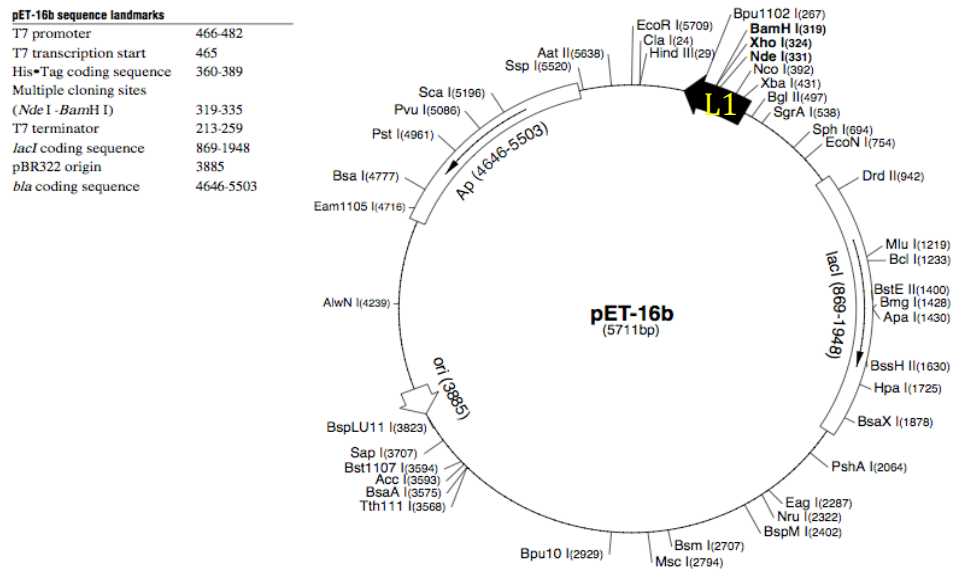
\*Reconstitution Efficiency was determined by Reconstituted L1:L2 ratio divided by wild type 50S L1:L2 ratio of 0.65-0.75 depending on the gel.

### **Table 3.2 Band Density Analysis for the Various Reconstitution**

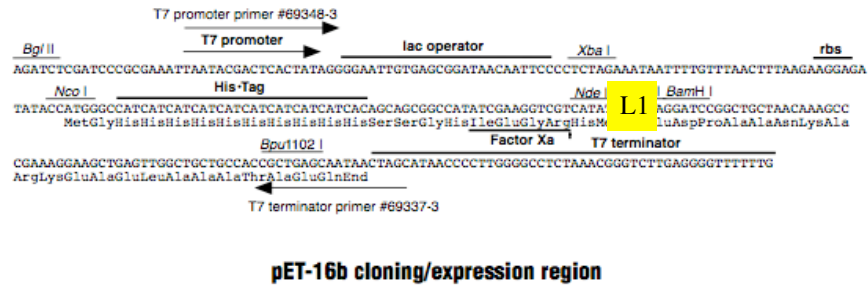
#### **Conditions.**

The gels seen in Figures 3.7-3.9 were analyzed using the software Image J to obtain the density of the bands corresponding to L1 and L2. L2 was used as a normalizing agent for ribosome concentration.

A.



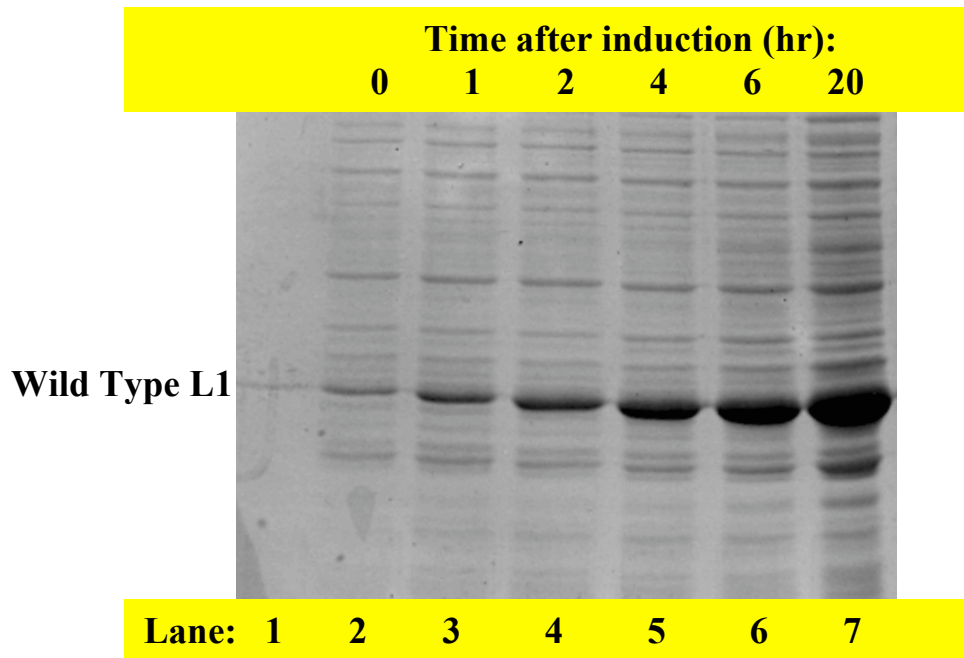
B.



**Figure 3.1 pET-16b Cloning Vector for L1 Expression**

L1 was cloned into the pET-16b *E. coli* vector using the 5' Nde I and 3' BamHI cut sites to incorporate the L1 gene. The vector (A) contains an N-terminal 10x-His-tag and the T7 promoter/terminator sequence for efficient overexpression. (B) The expression sequence highlights the important aspects of the vector, as well as indicates positions for sequencing primers when determining accuracy of the mutations.

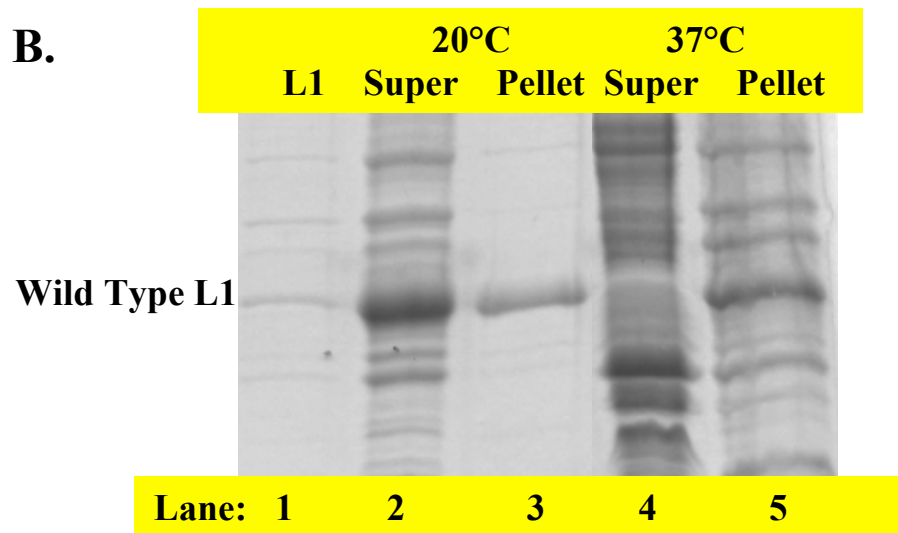
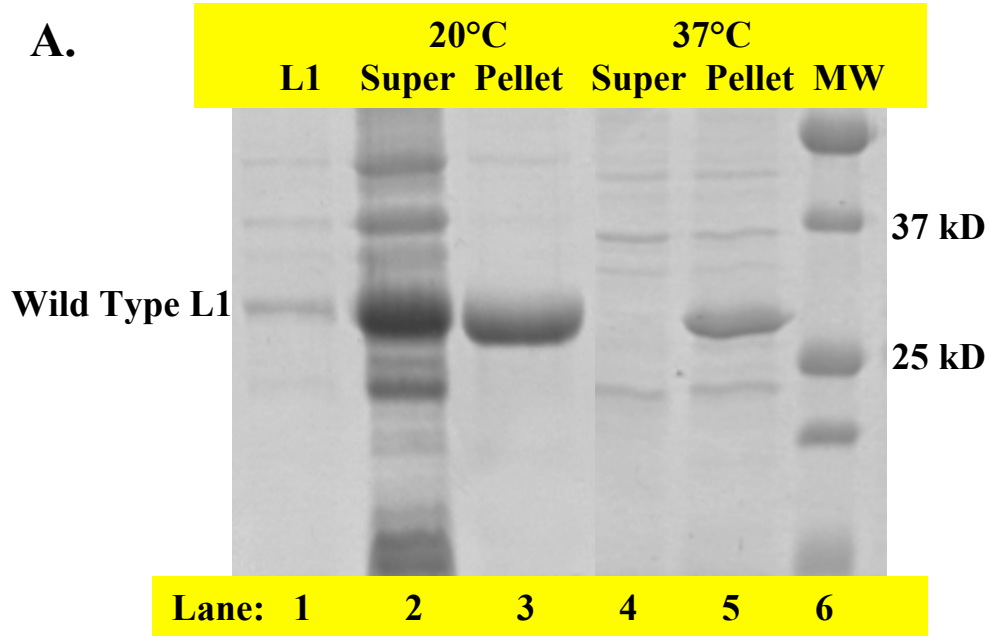
Figure is adapted from Novagen pET-16b vector manual.



**Figure 3.2 SDS-PAGE Analysis of Wild Type L1 During Overexpression**

An aliquot of 10  $\mu$ L of growth media were collected and loaded onto a 12% SDS-PAGE gel after IPTG induction. **Lane 1:** Purified wild type L1 (~20 pmol); **Lane 2:** Aliquot of the growth media at  $OD_{595} = 0.8$ , immediately prior to addition of IPTG; **Lane 3-7:** aliquots of the protein overexpression media after 1, 2, 4, 6 and 20 hours following the addition of IPTG. The band corresponding to L1 (approximately 27,000 Da) increases as the overexpression time increases, leading to a maximum amount of protein after overexpression for at least 20 hours. Protein amounts for overexpression times longer than 20 hours were not determined.





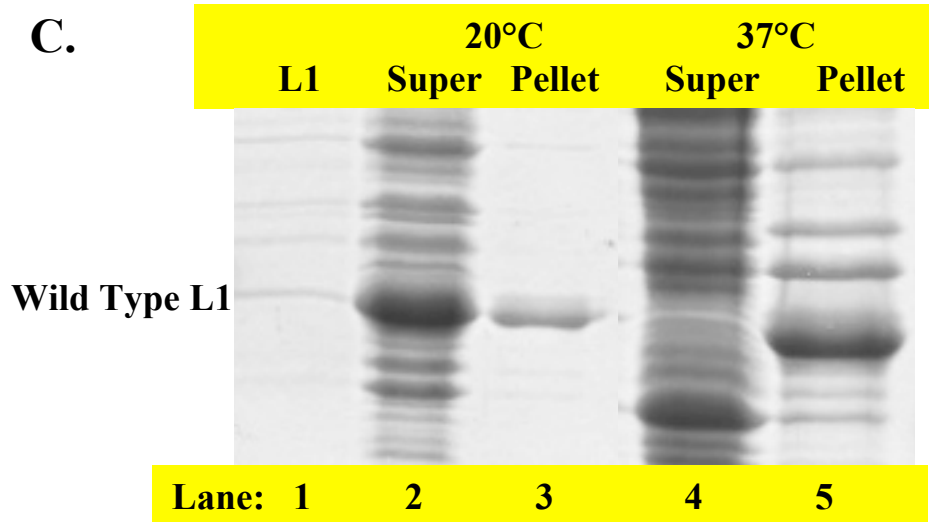


**Figure 3.3 SDS-PAGE Analysis of Soluble L1 Created by Growth at Different Buffer Conditions**

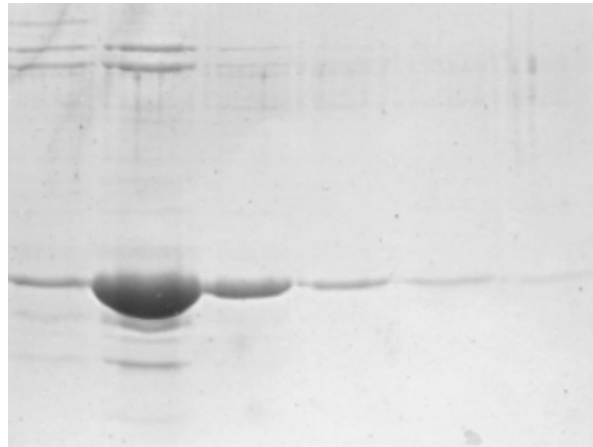
Overexpression of L1 results in soluble active L1 and/or denatured inclusion bodies of L1. Multiple growth media (**A:** Luria Bertani (LB); **B:** LB + 5% Glycerol, **C:** Terrific Broth + 5% Glucose) and temperatures (20 °C and 37 °C) were tested to determine the optimum conditions for limiting inclusion bodies, and thus increasing the amount of useful protein. After 18 hours of induction, the cells were harvested, opened, and the soluble protein (**Super**) was separated from the cell debris and inclusion bodies (**Pellet**) by centrifugation. A 10 µL aliquot of the supernatant was loaded to a 12% SDS-PAGE gels (**Lanes 2 and 4**). The pellet was resuspended in a denaturing buffer containing 8 M Urea, and a 10 µL aliquot was taken and loaded onto the gels (**Lanes 3 and 5**). In addition to a protein standard (**A: Lane 6**), a previously purified wild type L1 sample was added as a marker for L1 (**Lane 1**). As evidenced in all three growth media, the amount of soluble L1 is increased when the protein is overexpressed at 20 °C. It

should be mentioned that a fourth growth media, Terrific Broth, was tested but resulted in no protein overexpression, and thus is left out of this comparison.

**A.**

Imidazole Concentration

Wild Type L1

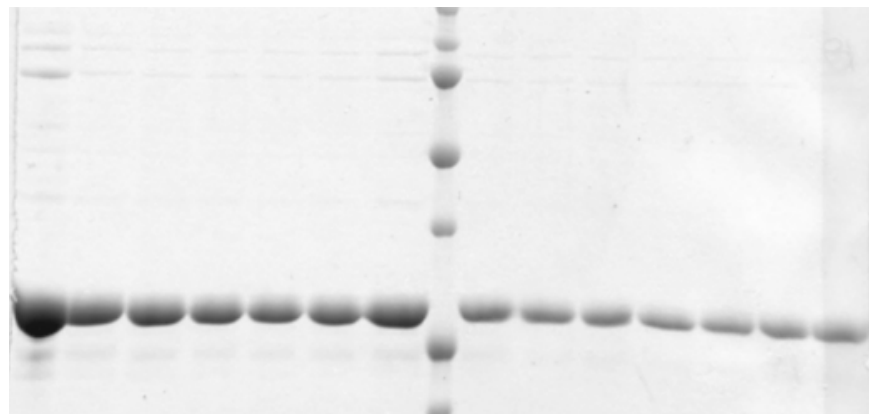


Lane: 1 2 3 4 5 6

**B.**

Imidazole Concentration

Wild Type L1



Lane: 1 2 3 4 5 6 7 8 9 10 11 12 13 14 15

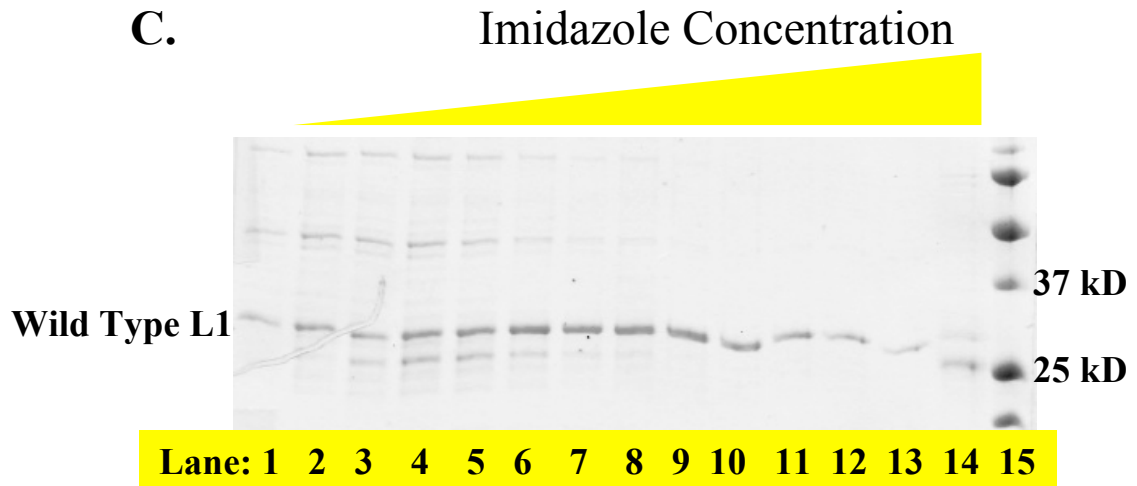


**Figure 3.4 SDS-PAGE Analysis L1 Purification Techniques**

After overexpression, the cells were opened by French Press (**A and B**) or Bug Buster® Master Mix (**C**). Either a TALON Co<sup>2+</sup> column (**B and C**) or Ni<sup>2+</sup>-NTA column (**A**) was used to bind the His-tag of the overexpressed L1. A stepwise gradient of 25 mM to 300 mM imidazole (25, 50, 150, 300 mM) was used to elute the L1 from the column, 1-mL fractions were collected and 10 µL aliquots were loaded to a 12% SDS-PAGE gel for analysis. A previously purified L1 sample was used as a marker (**Lane 1**), and a protein standard was also used in **B: Lane 8, and C: Lane 15**. As is evidenced by the gels, the TALON resin (**B and C**) provided a more pure L1 sample, and both French Press and Bug Buster® Master Mix were viable options for opening the cells.

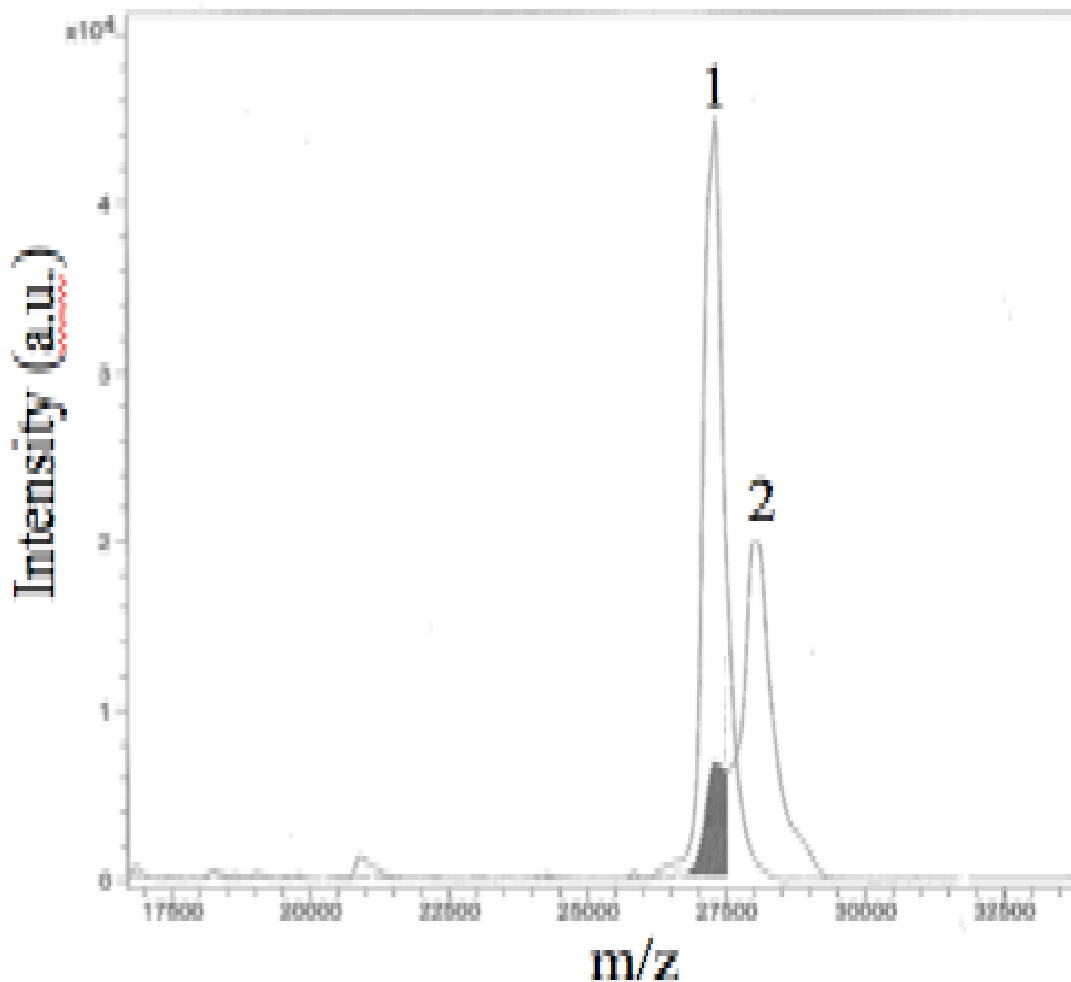


**Figure 3.5 MALDI Analysis of T202C-L1 and T202C-L1 (Cy5)**

MALDI analysis was performed on T202C-L1 (Peak 1) and T202C-L1 (Cy5) (Peak 2) using sinapic acid as the matrix on a Bruker Daltonics MALDI TOF MS. Approximately 4-8 pmol of protein was combined with excess sinapic acid in order to obtain the peaks. Peak 1 corresponds to the unlabeled T202C-L1 with a molecular weight of 27296, and the shaded region represents the unlabeled portion of T202C-L1 (Cy5). Peak 2 represents the labeled portion of T202C-L1 (Cy5) with a corresponding

molecular weight of 28045, approximately 750 Da higher than the unlabeled peak. Corresponding directly to the molecular weight of the Cy5 maleimide dye.

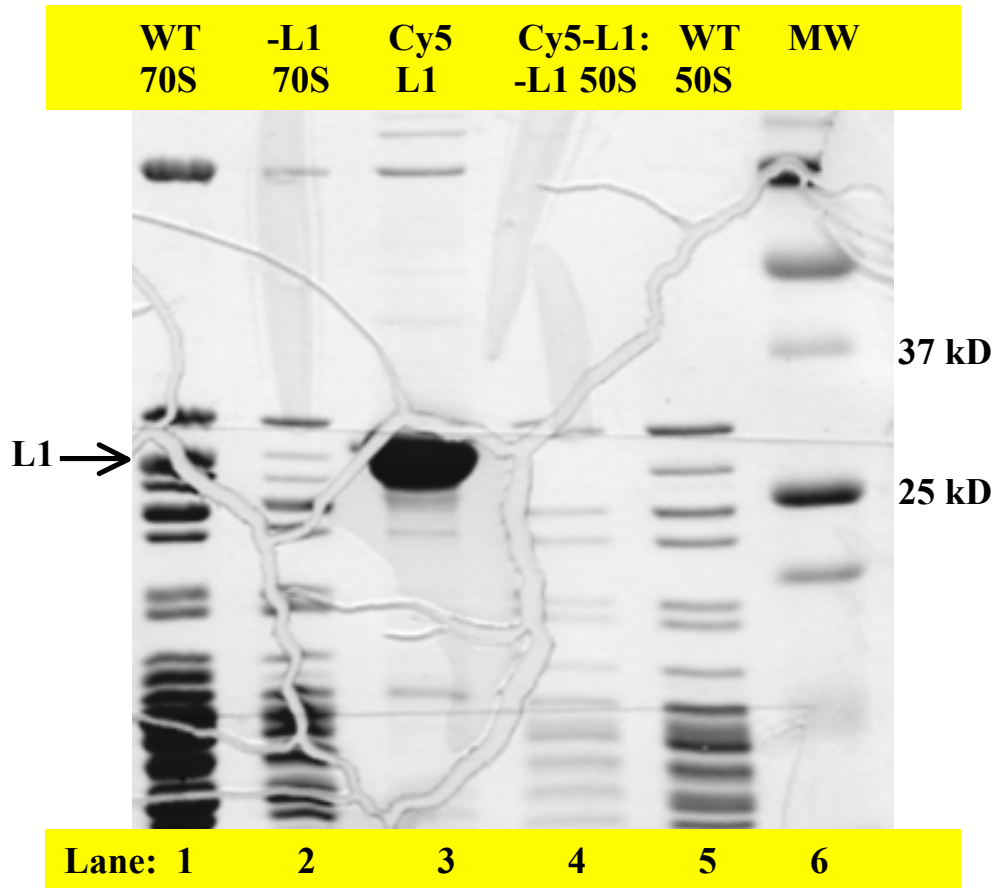


**Figure 3.6 SDS-PAGE Analysis of Reconstituted 70S Ribosomes and Subunits**

Approximately 20 pmol of ribosomes were loaded onto a 12% SDS-PAGE gel to analyze the presence or absence of L1 after a reconstitution into -L1 70S and subsequent subunit separation. T202C-L1 (Cy5) was reconstituted into -L1 70S and purified by centrifugation through a sucrose cushion. The ribosome pellet was resuspended in buffer

containing 1 mM  $Mg^{2+}$  in order to separate the subunits, and then the subunits were each purified through a sucrose gradient in order to obtain pure 30S and pure 50S. The purified 50S (**Lane 4**) was shown to not contain L1, and therefore to not have actually been reconstituted. **Lane 1:** wild type 70S; **Lane 2:** -L1 70S, take note that it is difficult to see that L1 is missing due to the presence of either S2, S3 and/or S4 which have similar molecular weights as L1; **Lane 3:** T202C-L1 (Cy5); **Lane 4:** Purified 50S subunits from the reconstitution of T202C-L1 (Cy5) and -L1 70S, notice that there is no band corresponding to L1; **Lane 5:** Purified wild type 50S subunits from wild type 70S; **Lane 6:** Protein standard.

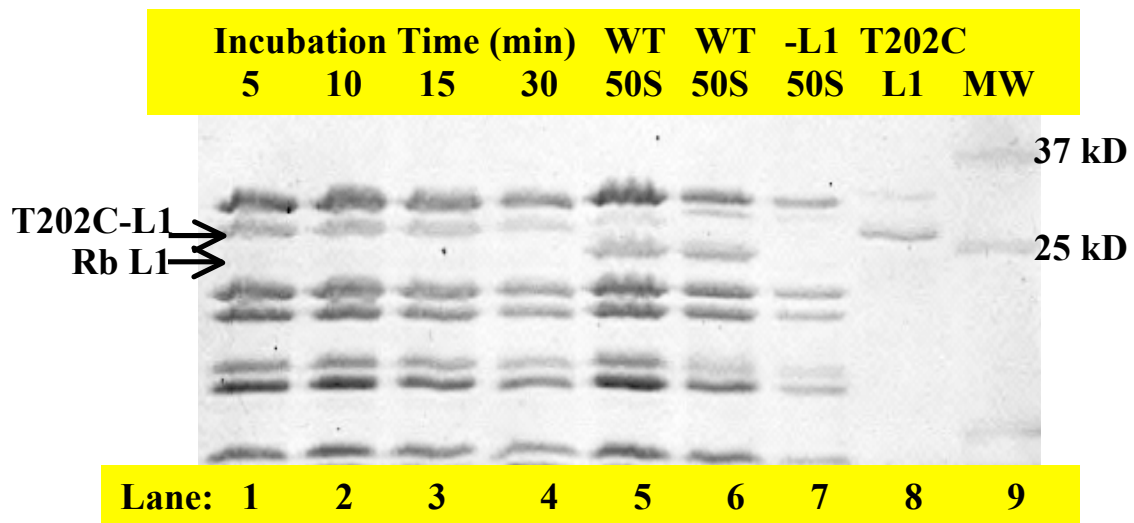


**Figure 3.7 SDS-PAGE Analysis of Incubation Time During T202C-L1: - L1 50S Reconstitution.**

Approximately 20 pmol (unless otherwise noted) of 50S subunits were loaded to a 12% SDS-PAGE gel. T202C-L1 was added in excess to -L1 50S subunits and incubated for 5, 10, 15, or 30 min at 37 °C, followed by purification through sucrose cushion centrifugation (**Lanes 1-4**). **Lane 5**: MRE-600 50S (~50 pmol); **Lane 6**: MRE-600 50S; **Lane 7**: -L1 50S incubated without L1 for 15 min. The apparent density around where L1 appears is caused by contaminating 30S ribosomal protein either S3 or S4 (the presence of contaminating S30 is confirmed by the presence of a slight amount of S1 at approximately 65 kDa, not shown); **Lane 8**: T202C-L1 incubated without ribosomes or subunits for 15 min, but not centrifuged; **Lane 9**: Protein standard. It should be noted that the L1 band in Lanes 1-4 and 7 has a higher molecular weight than that of the MRE-600 50S because the purified mutant L1 contains a 10x-His-tag in addition to a linker between the tag and the protein. Band density analysis of the L1 band was normalized to



the density of the L2 band to determine reconstitution efficiency. The ratio of L1:L2 band density was used as a measure of reconstitution efficiency, and normalized to the L1:L2 ratio of the wild type 50S (see [Table 3.2](#)).

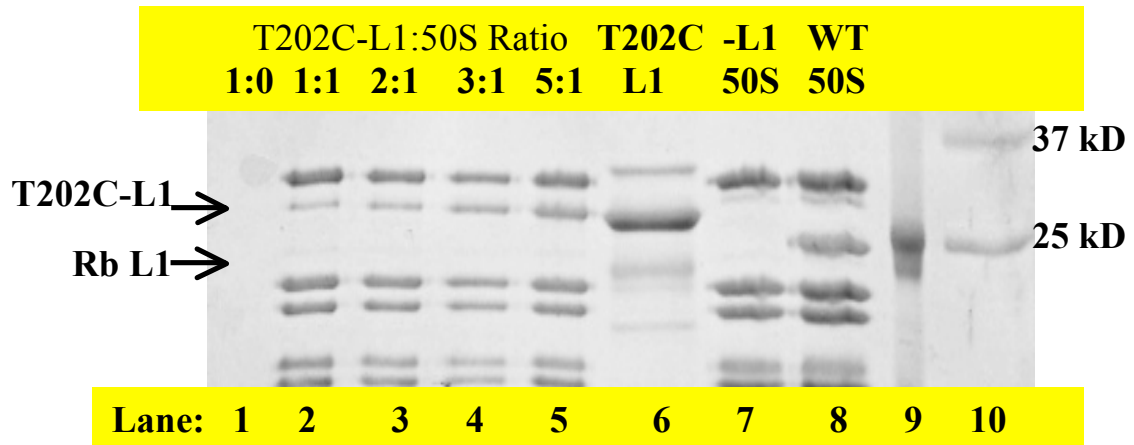


**Figure 3.8 SDS-PAGE Analysis of Reconstitution Ratio of T202C-L1 and -L1 50S Subunits**

Approximately 20 pmol of 50S subunits were loaded onto a 12% SDS-PAGE gel, and the reconstitution of T202C-L1 into -L1 50S was analyzed based on the L1:L2 band density ratio, normalizing to the MRE-600 50S L1:L2 band density. T202C-L1 was incubated with -L1 50S for 15 min at 37 °C at increasing ratios of T202C-L1 : -L1 50S, and purified through a sucrose cushion centrifugation. **Lane 1:** 40 pmol of T202C-L1 was incubated without 50S subunits, and centrifuged through the sucrose cushion as a control to ensure that L1 does not pellet on its own; **Lanes 2-5:** Increasing ratios of T202C-L1 to -L1 50S; **Lane 6:** T202C-L1; **Lane 7:** -L1 50S; **Lane 8:** MRE-600 50S; **Lane 9:** Rainbow Molecular Weight Marker; **Lane 10:** Protein standard. Although the

L1 band may appear darkest for the 5:1 reconstitution, the ratio of L1:L2 is the same for the 3:1 reconstitution, and only slightly lower for 2:1; therefore, further reconstitutions were performed at either 2:1 or 3:1.

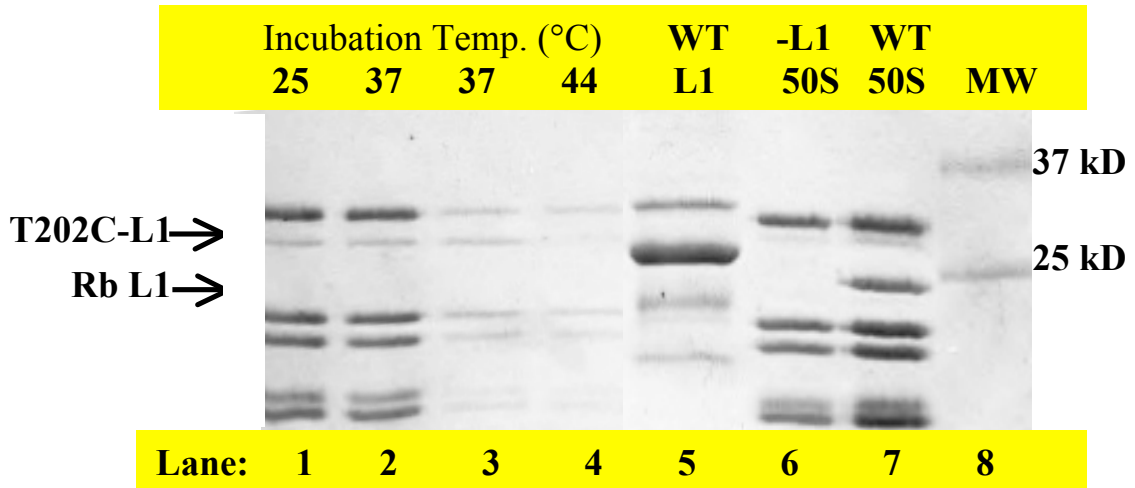
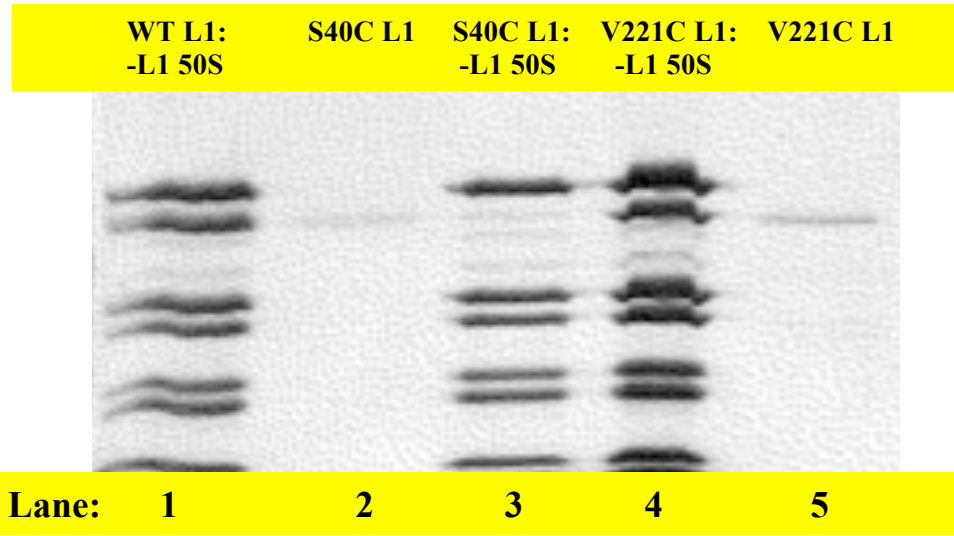


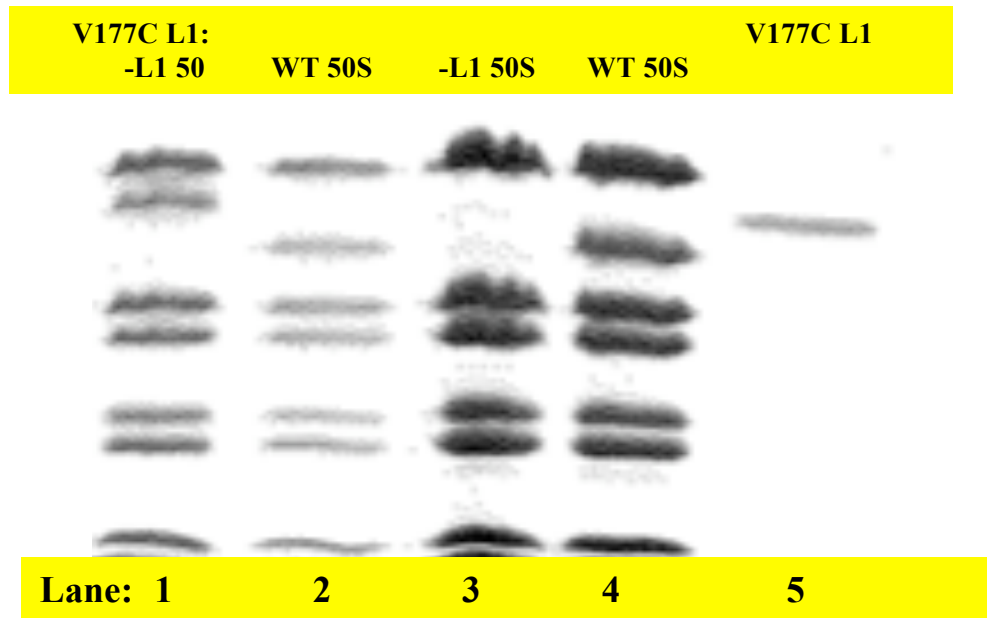
**Figure 3.9 SDS-PAGE Analysis of Incubation Temperature on the Reconstitution of T202C-L1 with -L1 50S**

T202C-L1 was incubated with -L1 50S at a ratio of 1:1 for 15 min at various temperatures in order to determine if complete reconstitution could be achieved while using less L1. After reconstitution, the samples were purified through sucrose cushion centrifugation and loaded (~20 pmol) onto a 12% SDS-PAGE gel. Although reconstitution occurred, the ratio of L1:L2 was not increased by varying temperature; therefore, a beginning ratio of T202C-L1 : -L1 50S of  $\geq 2:1$  must be used to achieve 1:1 reconstitution.

**A.**



**B.**



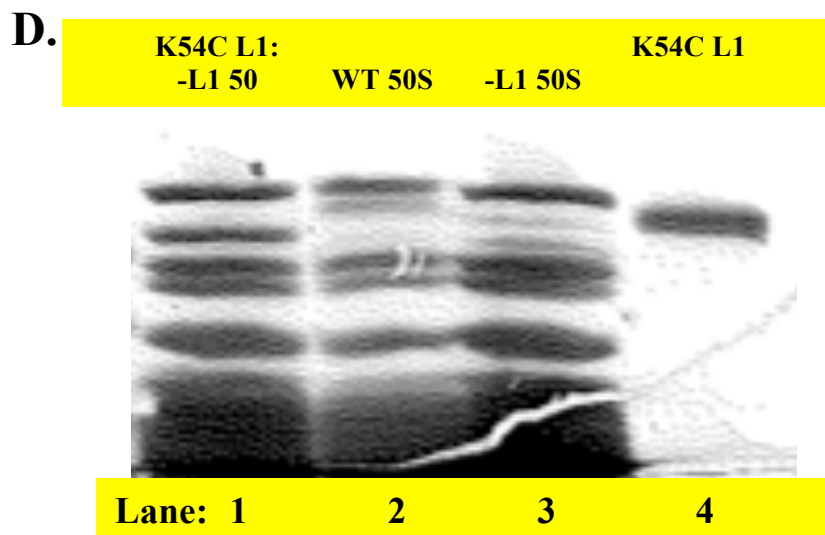
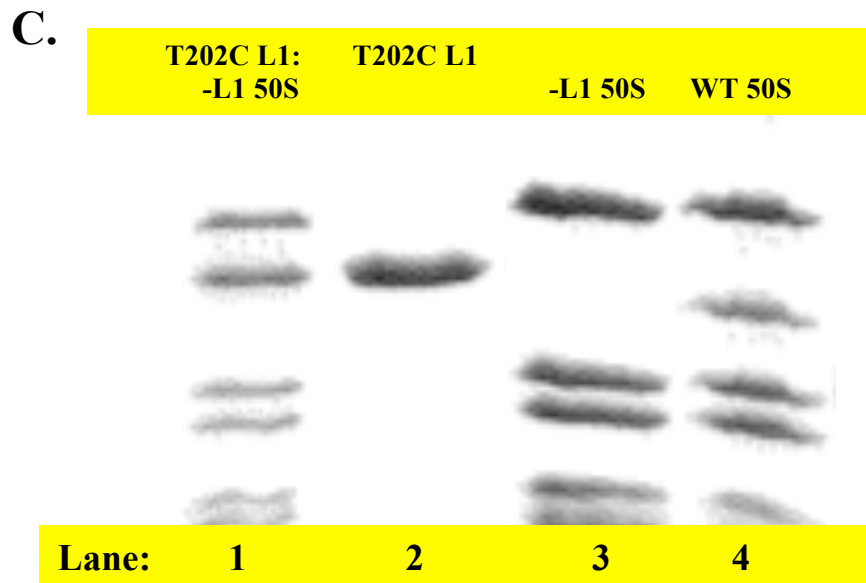


**Figure 3.10 SDS-PAGE Reconstitution Analysis of Wild Type L1 and Cy-Labeled Mutant L1**

Wild type, S40C (Cy3), K54C (Cy5), V177C (Cy3), T202C (Cy5), and V221C (Cy3) L1 was reconstituted into -L1 50S subunits by incubating a 2x excess of L1 with -

L1 50S for 15 min at 37 °C. Approximately 30 pmol of reconstituted ribosomes were added to a 12% SDS-PAGE gel for analysis. **A)** Ribosomes reconstituted with wild type L1 (**Lane 1**), Cy3-S40C L1 (**Lane 3**), and Cy3-V221C (**Lane 4**) were run on a 12% gel, notice that the S40C-L1 (Cy3) does not reconstitute into the -L1 50S subunits; therefore, this mutant was no longer used. The wild type, and V221C-L1 (Cy3) reconstituted to approximately 1:1. **B)** Ribosomes reconstituted with V177C-L1 (Cy3) (**Lane 1**) were loaded to a 12% gel, and compared to MRE-600 50S (**Lane 2 and 4**), -L1 50S (**Lane 3**), and V177C-L1 (**Lane 5**). The L1 band in the reconstituted sample runs higher than in the MRE-600 50S sample because of the increased molecular weight due to the 10x His-tag, linker, and dye in the L1 that is reconstituted, this trend is seen in all of the reconstituted samples. **C)** Ribosomes reconstituted with Cy5-T202C-L1 (**Lane 1**) were loaded to a 12% gel, and compared to MRE-600 50S (**Lane 4**), -L1 50S (**Lane 3**), and T202C-L1 (**Lane 2**). **D)** Ribosomes reconstituted with K54C-L1 (Cy5) (**Lane 1**) were loaded to a 12% gel, and compared to MRE-600 50S (**Lane 2**), -L1 50S (**Lane 3**), and K54C-L1 (**Lane 4**).

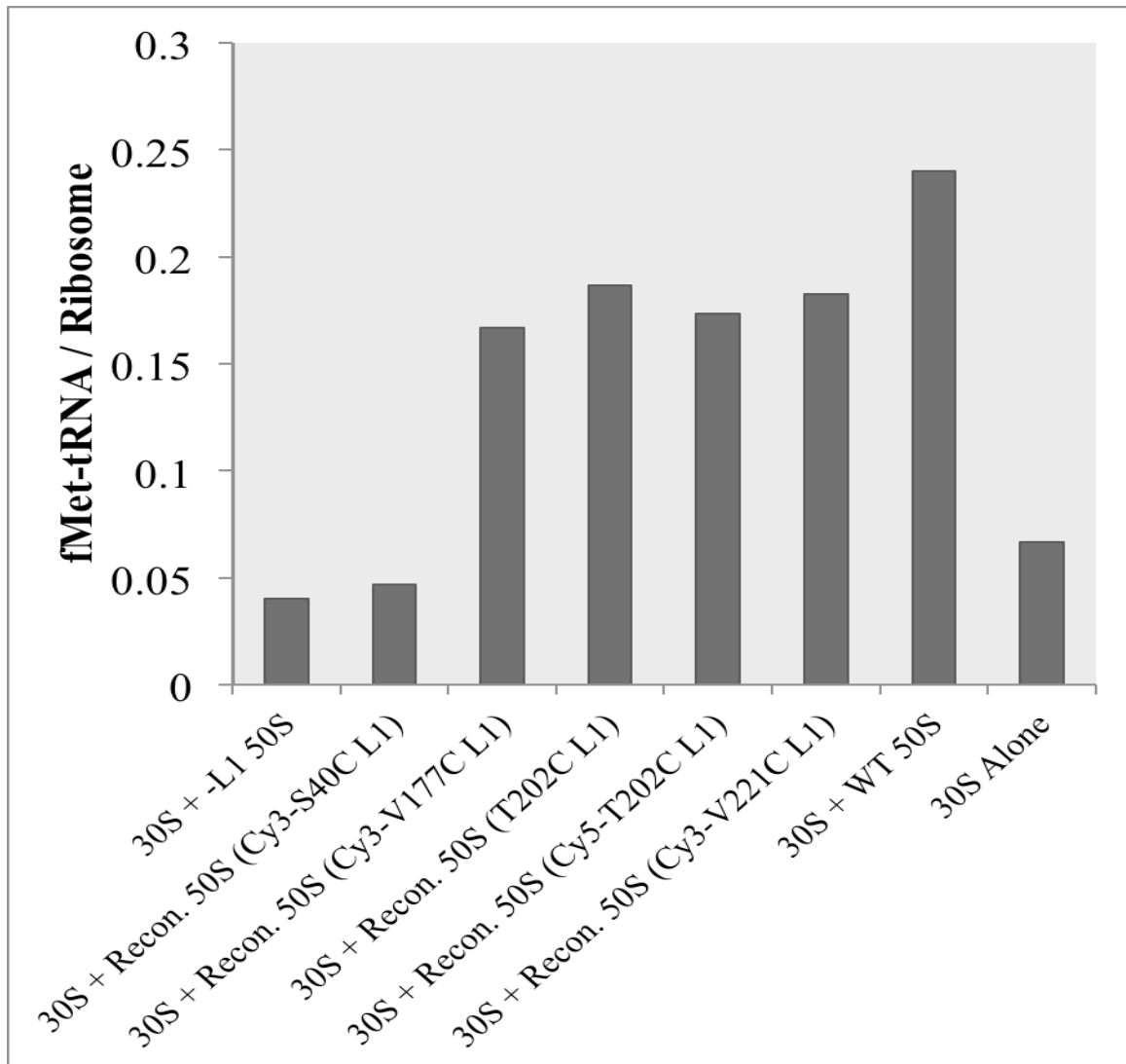


**Figure 3.11 [<sup>35</sup>S]-fMet-tRNA<sup>fMet</sup> Binding to Ribosomes to Measure Activity**

30S subunits were incubated with an excess of 50S subunits, mRNA, and [<sup>35</sup>S]-fMet-tRNA<sup>fMet</sup> for 5 min at 37 °C, followed by a filter binding to remove any unbound tRNA, and analysis by radioactive counting. As seen here, ribosomes lacking L1, and 30S subunits without 50S have reduced tRNA binding efficiencies; however, upon

reconstitution of V177C-L1 (Cy3), T202C-L1, T202C-L1 (Cy5), or V221C-L1 (Cy3) with –L1 50S, the binding efficiency increases to almost wild type levels. However, as indicated in the SDS-PAGE gel analysis, the S40C-L1 (Cy3) did not reconstitute in the –L1 50S. Further, for the wild type subunits, binding is not 1:1 because of the low aminoacylation efficiency of the fMet-tRNA<sup>fMet</sup>, and the fact that initiator tRNA binds the P-site independent of its acylation state. Therefore, it is probable that the undetectable tRNA<sup>fMet</sup> is also binding to P-site.

**Chapter IV: The Conditions that Affect  
Deacylated-tRNA Movement After Translocation**



## 4.1 Abstract

The occupancy of the E-site has previously been postulated to be linked to fidelity of cognate tRNA selection at the ribosomal decoding site, preserving the reading frame, regulating programmed frameshifting, and determining the preference of the ribosome for binding either EF-Tu or EF-G. Therefore, it is important to better understand how tRNA behaves while in the E-site. Three experimental procedures were utilized in order to determine how deacylated-tRNA<sup>fMet</sup> leaves the E-site of the ribosome. 1) The FRET efficiency changes between T202C-L1 (Cy5) ribosomes and tRNA<sup>fMet</sup> (Cy3); 2) The FRET efficiency changes between tRNA<sup>fMet</sup> (Cy3) and tRNA<sup>Phe</sup> (Rhd110); and to a lesser extent, 3) The anisotropy loss from the translocated tRNA<sup>fMet</sup> (Cy3) as it dissociates from the ribosome. When using 70SICs created with fMet-tRNA<sup>fMet</sup> (Cy3) in the P-site and T202C-L1 (Cy5) ribosomes, the addition of ternary complex results in an increase in FRET efficiency because of both the tRNA<sup>fMet</sup> (Cy3) adoption of a P/E-hybrid, and the L1-stalk movement towards the body of the ribosome into a closed conformation. This FRET efficiency is eventually lost when either the L1-stalk moves away, or the deacylated-tRNA dissociates. Three different pathways were demonstrated that allow the deacylated-tRNA<sup>fMet</sup> to dissociate from the E-site; 1) the L1-stalk moves away from the body of the ribosome into an “out” conformation before the deacylated-tRNA<sup>fMet</sup> dissociates; 2) the L1-stalk moves away at a similar time as the deacylated-tRNA<sup>fMet</sup> dissociation; or, 3) the deacylated-tRNA<sup>fMet</sup> moves along with the L1-stalk into an apparent E2-site as the L1 moves to the “out” conformation. In all the cases, the release

of deacylated-tRNA<sup>fMet</sup> from the E-site proceeds at similar rates; however, the rates of dissociation from E-site and E2 site are quite different.

## 4.2 Introduction

Ribosomal protein L1 was first observed as a biochemically relevant protein in the early 1980s when Subramanian and coworkers discovered that ribosomes lacking L1 displayed a 40-60% reduced capacity for *in vitro* protein synthesis (**Subramanian et al., 1980**). Later in the 1980s, it was discovered that L1 was important for the binding of tRNA to the ribosomal P-site (**Sander, 1982**). A long period passed before Nikonov and coworkers finally crystallized an isolated *E. coli* L1 in 1996, and it wasn't until the early 2000's that the structure of L1 on the ribosome really came into focus (**Nikonov et al., 1996; Valle et al., 2003; Yusupov et al., 2001; Selmer et al., 2006**). With the known structure came more biochemical work, specifically in the single molecule field when Fei and coworkers used a labeled T202C-L1 to help determine the motions of a ratcheting ribosome (**Fei et al., 2008**). In the present work, we determine how L1 movement relates to the mechanism of deacylated-tRNA<sup>fMet</sup> dissociation from the E-site of the ribosome.

The L1-stalk, comprised of ribosomal protein L1 and helices 76-78 from the 23S rRNA, is a highly mobile region of the 50S subunit. Previous X-ray crystallography and cryo-EM work has shown that the movement of the L1-stalk is highly linked to both the positions and acylation state of tRNAs on the ribosome. The L1-stalk occupies an “out” state when the ribosomes have vacant E-sites or in isolated 50S subunits (**Korostelev et al., 2008; Harms et al., 2001**). When deacylated-tRNA is bound in the E-site the L1-

stalk moves inward by ~30-40 Å to the “in” conformation (**Korostelev et al., 2006; Selmer et al., 2006**). A third position for the L1-stalk, the “overly closed,” determined by Cornish and coworkers, occurs when the tRNA adopts a P/E-hybrid conformation, and requires a further movement of ~15-20 Å towards the body of the ribosome. (**Cornish et al., 2009; Valle et al., 2003; Gao et al., 2003**). It has been hypothesized that the L1-stalk moves with the deacylated-tRNA as it moves from P/E to E/E-sites, and then has to move to an “out” conformation in order for the deacylated-tRNA to release. The behavior of deacylated-tRNA as it reaches the E-site is important because E-site occupancy has been linked to accuracy at the decoding site (**Nierhaus, 2006; Zaher and Green, 2009**), regulation of programmed frameshifting (**Leger, M. et al., 2007; Liao, et al., 2008**), and determination of the preference for the ribosome to bind either EF-Tu or EF-G (**Wilson and Nierhaus, 2006**). In the following work, I demonstrate that deacylated-tRNA<sup>fMet</sup> leaves the E-site of the ribosome via at least three distinct pathways, each one favored by different buffer conditions and peptidyl-state of P-site tRNA.

Results presented in Chapters II and III demonstrate that it is possible to prepare reconstituted 50S ribosomes containing either labeled or unlabeled T202C-L1. Here, we use these ribosomes, along with highly labeled tRNAs, to measure the FRET efficiency and anisotropy changes associated with tRNA release from the E-site of the translocated ribosome.

The highly mobile nature of the L1-stalk and the mobile nature of the deacylated-tRNA after translocation make it difficult to determine which physical movement the FRET efficiency change is associated with; therefore, two different FRET efficiency

measurements were taken: 1) FRET between the deacylated-tRNA<sup>fMet</sup> (Cy3) donor and the T202C-L1 (Cy5) acceptor (L/t FRET); and, 2) FRET between the (fMet)-Phe-tRNA<sup>Phe</sup> (Rhd110) acceptor (which may or may not be present as a dipeptide depending on the set up of the experiment) and the deacylated-tRNA<sup>fMet</sup> (Cy3). In a translocated ribosome the (fMet)-Phe-tRNA<sup>Phe</sup> (Rhd110) is in the P-site and the deacylated-tRNA<sup>fMet</sup> (Cy3) is, at least initially, in the E-site. The L/t FRET experiments provide information about the movement of the L1-stalk relative to the deacylated-tRNA<sup>fMet</sup>; the t/t experiment uses a relatively rigidly bound P-site tRNA ((fMet)-Phe-tRNA<sup>Phe</sup>) as a marker for when deacylated-tRNA<sup>fMet</sup> leaves the E-site (loss of FRET efficiency) (See Section 4.3.2.1).

Preliminary fluorescence anisotropy measurements were utilized to monitor the release of deacylated-tRNA from the ribosome, exploiting the decrease in anisotropy that accompanies tRNA dissociation from the ribosome. Here, we were able to relate the apparent rate constant for tRNA dissociation with values associated for the FRET efficiency losses in order to determine a distinct kinetic pathway for each set of conditions (Buffer A, peptidyl-tRNA in the P-site after translocation from PRE-1 to POST-1; Buffer B, peptidyl-tRNA in the P-site; and, Buffer B, aminoacyl-tRNA in the P-site). Our results provide clear, biochemical evidence for a second E-site, the E<sup>'</sup>- or E2- site, that may have initially been described by Robertson and colleagues in early biochemical data, and incorrectly named the E-site (**Robertson et al., 1986; reviewed by Burkhardt et al., 1998**). Later, cryo-EM work characterized the additional exit binding position as the E<sup>'</sup>- or E2-site (**Agrawal et al., 1999, Fischer et al., 2010**).

## 4.3 Results

### 4.3.1 L1 Interaction with tRNA<sup>fMet</sup> (L/t FRET)

FRET efficiency between T202C-L1 on the 50S subunit and either fMet-tRNA<sup>fMet</sup> or tRNA<sup>fMet</sup> (depending on the progression of the elongation cycle) was measured using T202C-L1 (Cy5) and (fMet)-tRNA<sup>fMet</sup> (Cy3). 70S initiation complexes (70SIC, 4.3.1.1), pre-translocation complexes (PRE-1), and post-translocation complexes (POST-1, Chapter 5), were made and utilized in the following work in order to better understand what affects the release of deacylated-tRNA<sup>fMet</sup> after the first round of translocation. In this chapter, except where noted, PRE-1 complexes were created and purified via sucrose cushion centrifugation.

In order to establish preliminary FRET efficiency values between T202C-L1 (Cy5) ribosomes and fMet-tRNA<sup>fMet</sup> (Cy3), equilibrium FRET experiments were performed on 70SICs, PRE-1, and POST-1 complexes (Figure 4.1, 4.2). 70SICs were prepared in either Buffer A or Buffer B with D\*A\*: T202C-L1 (Cy5) ribosomes and highly charged fMet-tRNA<sup>fMet</sup> (Cy3) initiator tRNA; D\*A: T202C-L1 ribosomes and fMet-tRNA<sup>fMet</sup> (Cy3) initiator tRNA; DA\*: T202C-L1 (Cy5) ribosomes and fMet-tRNA<sup>fMet</sup> initiator tRNA; and, DA: T202C-L1 ribosomes and fMet-tRNA<sup>fMet</sup> initiator tRNA and purified via sucrose cushion centrifugation; PRE-1 complexes were made by adding excess ternary complex to the 70SICs, and POST-1 complexes were made by adding excess ternary complex and EF-G to the 70SICs. Measurements were made in parallel on the D\*A\*, D\*A, DA\*, and DA samples for each ribosome complex. The

signal for the corresponding blank sample (DA) was subtracted from each D\*A\*, D\*A, and DA\* to correct for light scattering and background fluorescence. The efficiency of energy transfer was determined through acceptor fluorescence enhancement at 667 nm, and calculated by equation 2.2, as seen in [Table 4.1](#). Traces corresponding to D\*A\*, D\*A, and DA\*, as well as, the fitted donor contribution, and the extracted acceptor emission are seen in [Figure 4.1](#) for Buffer A, and [Figure 4.2](#) for Buffer B. Fitted donor contribution is determined by multiplying the D\*A fluorescence by the ratio of D\*A\* and D\*A at 567 nm, and the extracted acceptor was determined by subtracting the fitted donor from the D\*A\* fluorescence. As evidenced in [Figure 4.2](#), the apparent FRET efficiency decreases approximately 2-fold upon addition of EF-G.GTP to a PRE-1 complex in Buffer B. According to previous single-molecule FRET efficiency studies between tRNA and L1, there is no FRET efficiency change associated with translocation ([Fei et al., 2008](#)). Therefore, I interpret the retention of FRET signal after translocation as indicating that tRNA is not fully released from the POST-1 state. This is not seen in Buffer A because the deacylated-tRNA is not stably bound in the E-site under these conditions. Although equilibrium FRET experiments were not performed starting with uncharged-tRNA<sup>fMet</sup>, Appendix 2 contains other examples for FRET efficiency changes in Buffer A and Buffer B starting with 70SICs containing ~25% charged fMet-tRNA<sup>fMet</sup>. Unlike the time-resolved studies seen later in this chapter (Section 4.3.1), apparent FRET efficiency does not depend on initiator tRNA charging efficiency in Buffer B for equilibrium experiments.

#### 4.3.1.1 FRET Increase Upon Addition of Ternary Complex to 70SIC (70SIC → PRE-1)

In both Buffer A and Buffer B, a significant increase in FRET efficiency is seen when a Phe-tRNA<sup>Phe</sup>.EF-Tu.GTP ternary complex (0.5 μM) is added to a 70SIC (0.1 μM) containing fMet-tRNA<sup>fMet</sup> (Cy3) and T202C-L1-50S (Cy5). This is not only obvious in the equilibrium FRET experiments (Figure 4.1 D, 4.2 D), but also in a time-resolved stopped flow experiment where ternary complex (0.5 or 1.0 μM; Buffer A and Buffer B, respectively) was added to the sucrose purified 70SIC (0.25 μM) (Figure 4.3). In the equilibrium FRET experiments, the FRET efficiency calculated for the PRE-1 complex in Buffer A and Buffer B was 0.73 and 0.90, respectively (Table 4.1, Equation 2.2). These values are similar to the 0.8 that was shown for a PRE complex in previous single molecule work. This work also showed that a deacylated-tRNA<sup>fMet</sup> in the PRE complex would fluctuate between hybrid (FRET= 0.8) and classical states (Fei et. al., 2008). Population of a high FRET state is observed in ensemble studies as a net FRET efficiency increase between L1 and deacylated-tRNA on PRE-1 complex formation that is caused by L1 movement towards the body of the ribosome and deacylated-tRNA adopting a P/E hybrid conformational state.

#### 4.3.1.2 FRET Efficiency Change Following Translocation (PRE-1 → POST-1)

PRE-1 complexes were created and purified to remove any excess tRNA and factors that are unbound to the ribosome. Previous single molecule work has shown that the FRET efficiency between deacylated-tRNA in a P/E hybrid state and T202C-L1 does not change during translocation because the L1 moves along with the elbow region of the

tRNA (**Fet et al., 2008**). In the L/t FRET experiments, the addition of EF-G.GTP (1.0  $\mu\text{M}$  unless otherwise noted) to purified PRE complexes (0.25  $\mu\text{M}$ ), results in a lag that can be attributed to the rate-limiting translocation step in the majority of the experiments ( $k_{\text{app}}$ , **Table 4.2**). In all experiments the rate constant for the lag associated with translocation is between 3.3  $\text{s}^{-1}$  for complexes in Buffer B, and 8  $\text{s}^{-1}$  for complexes in Buffer A. For the complexes in Buffer A, the translocation rate is in agreement with the previously measured translocation rates upon addition of 1  $\mu\text{M}$  EF-G.GTP, of  $\sim 7.8 \text{ s}^{-1}$  (**Pan et al., 2007**). Although, the translocation of mRNA has previously been shown to be similar in both buffer conditions (**Liu et al., 2010**), a decrease in translocation rate by a factor of  $\sim 2$  has been shown here for Buffer B and will be explained in the Discussion. Following the lag, the rate and amplitude of L/t FRET efficiency loss are highly dependent on both buffer conditions and the aminoacylation state of the tRNA occupying the P-site as seen in **Table 4.2**.

The L/t FRET traces (as well as the t/t FRET traces seen in Section 4.3.2, and anisotropy change traces seen in Section 4.4.3) were all initially fit to a triple exponential curve using Scientist (MicroMath):

$$y = y_o + A_1 e^{-k_{\text{app}1} t} + A_2 e^{-k_{\text{app}2} t} + A_3 e^{-k_{\text{app}3} t} \quad (\text{Equation 4.1})$$

As mentioned earlier, the  $k_{\text{app}1}$  in the L/t FRET experiments was attributed to the lag between the L1 and the deacylated-tRNA<sup>fMet</sup> before separation occurs. Depending on the



conditions, the major change in the FRET efficiency is represented by either  $k_{app2}$  or  $k_{app3}$  as seen below and in [Table 4.2](#).

#### 4.3.1.2.1 Buffer Conditions Affect Deacylated-tRNA-L1 Movement

[Figure 4.4](#) directly compares the tRNA-L1 FRET efficiency loss between Buffers A and B upon addition of EF-G.GTP (1.0  $\mu$ M) to a PRE-1 complex (0.25  $\mu$ M) containing tRNA<sup>fMet</sup> (Cy3) and T202C-L1 (Cy5) that was made from a 70SIC using highly charged fMet-tRNA<sup>fMet</sup> (Cy3). After a lag ( $k_{app1}$ ), the fluorescence loss of the acceptor was measured to determine the L/t FRET efficiency loss, after  $\sim$ 10 s the full FRET efficiency is lost in Buffer A, as is evidenced by the D\*A\* sample reaching the same level as the DA\* sample ([Figure 4.1, 4.4](#)). The amplitude difference of the FRET efficiency change between the two buffer conditions can be attributed to deacylated-tRNA binding to E-site more tightly in Buffer B ([Semenkov et al., 1996](#)), so that, following translocation, it is not fully released. Indeed, retention of FRET signal in Buffer B reflects the establishment of an equilibrium between tRNA release (giving rise to a FRET efficiency loss) and deacylated-tRNA rebinding (refer to section 5.3.2).

Buffer A contains 7.5 mM Mg<sup>2+</sup> and no polyamines, and the lag phase corresponding to translocation is  $k_{lapp} = 7.6 \text{ s}^{-1}$ ; further, the major loss of FRET efficiency, as indicated by the loss of acceptor fluorescence, has an apparent rate constant of  $k_{app2} = 4.71 \text{ s}^{-1}$ . In Buffer B, containing 4.5 mM Mg<sup>2+</sup> and polyamines, the translocation rate is slower ( $k_{lapp} = 3.6 \text{ s}^{-1}$ ) and the major loss of FRET efficiency is also slower, with an apparent rate constant of  $k_{app2} = 1.6 \text{ s}^{-1}$ . The loss of FRET efficiency can be accounted for in two ways: 1) L1 movement away from the E-site tRNA and/or, 2) tRNA release from

the ribosome. Because both labeled species, L1 and tRNA, are mobile, further experiments need to be conducted to determine which is indeed causing the loss of FRET efficiency. Distinguishing between these two possibilities is addressed later in this chapter (**Section 4.3.2**).

#### **4.3.1.2.2 Peptidyl State of P-site tRNA Affects Deacylated-tRNA-L1 Movement**

The ability to aminoacylate a tRNA<sup>fMet</sup> to a very high level requires meticulous work and HPLC separation to attempt to remove the uncharged tRNA<sup>fMet</sup>. To this date, the best charging efficiency achieved for fMet-tRNA<sup>fMet</sup> was 70-80%. Non HPLC-purified samples reached ~30-40% charging.

In Buffer A, the charging efficiency of fMet-tRNA<sup>fMet</sup>, and thus occupancy of peptidyl-tRNA in the P-site upon translocation, does not make a difference in rate of the L1-tRNA FRET efficiency decrease (**Figure 4.5, Table 4.2**). However, it does make a difference in the amplitude of the acceptor fluorescence change (**Table 4.2**). The amplitude of the fluorescence change increases approximately proportionally as the charging efficiency increases (25% charging: 0.33, 70% charging: 0.65, 78% charging: 0.70).

A possible explanation is that the uncharged tRNA<sup>fMet</sup> does not bind to the P-site as tightly, and thus does not survive the sucrose cushion purification of the PRE-1 state. Direct evidence for this is seen when preparing the PRE-1 complexes from 70SIC containing deacylated-tRNA<sup>fMet</sup> (Cy3). When the 70SIC complexes were prepared, half were purified via centrifugation through a sucrose cushion, and the other half were treated with ternary complex to make PRE-1 complexes, and then subjected to sucrose

cushion purification. In both cases the ribosome pellets were resuspended in Buffer A, and tRNA<sup>fMet</sup> (Cy3) in the 70SIC remained bound to the ribosome through the sucrose cushion (~0.60 Cy3 / ribosome), whereas very little tRNA<sup>fMet</sup> (Cy3) was bound in the PRE-1 complex (~0.06 Cy3 / ribosome) (Table 4.3, 70S IC: Row 1; PRE: Row 4), indicating that the binding of deacylated-tRNA<sup>fMet</sup> to a P-site in a PRE-1 complex is less stable than in a 70SIC. Initially this result was surprising because previous single molecule work has shown that FRET efficiency is retained between P-site deacylated-tRNA<sup>fMet</sup> and A-site Phe-tRNA<sup>Phe</sup> after purification through size exclusion spin columns at varying concentrations of Mg<sup>2+</sup> and no polyamines (Kim et al., 2007); however, the above experiment has been repeated multiple times and deacylated-tRNA<sup>fMet</sup> continues to be unstably bound. It is possible that sucrose cushion purification is more stringent than size exclusion spin columns, and therefore, less stably bound tRNA is removed via sucrose cushion, but not size exclusion columns.

In Buffer B both highly charged and completely uncharged initiator tRNAs remain bound to PRE complexes at similar levels (~0.4-0.7 Cy3/70S, Table 4.3). It is possible that the binding of a deacylated-tRNA<sup>fMet</sup> to the P-site in a PRE-1 complex is stronger in Buffer B versus Buffer A, allowing the purification of a PRE-1 complex with aminoacyl-Phe-tRNA<sup>Phe</sup> in the A-site in Buffer B, but not in Buffer A.

Using a PRE complex formed from a 70SIC containing uncharged tRNA<sup>fMet</sup> (Cy3), in Buffer B, results in a P-site that is filled with aminoacyl-tRNA upon translocation, and a biphasic change in the FRET efficiency between T202C-L1 (Cy5) and tRNA<sup>fMet</sup> (Cy3). After the initial lag ( $k_{app1}$ ) phase that follows EF-G.GTP addition,

only a small fraction of the FRET efficiency loss is attributed to rapid tRNA release ( $k_{app2} = 1.17 \text{ s}^{-1}$ ), and the major change is the second phase that occurs with an apparent rate constant of  $k_{app3} = 0.022 \text{ s}^{-1}$ . Using a PRE complex formed with highly charged fMet-tRNA<sup>fMet</sup> (Cy3) results in a P-site that is filled with a peptidyl-tRNA upon translocation, and after the initial lag ( $k_{1app}$ ), the first phase is the major change with an apparent rate constant approximately 75 times faster ( $k_{app2} = 1.6 \text{ s}^{-1}$ ) than the major change seen when aminoacyl-tRNA is in the P-site ( $k_{app2} = 0.022 \text{ s}^{-1}$ ) (Figure 4.6, Table 4.2).

In all three conditions: 1) Buffer A, 2) Buffer B, peptidyl-tRNA in the P-site, and 3) Buffer B, aminoacyl-tRNA in the P-site, the L/t FRET efficiency loss occurs in three phases. For all three conditions, the first phase is a lag phase with a  $k_{1app}$  similar to the translocation rate. For conditions 1 and 2, the second phase is the major change in which the L/t FRET efficiency decreases at a rate depending on the buffer ( $k_{app2}$ ), and the third phase is a smaller, slower loss of FRET efficiency that is attributed to slow tRNA release ( $k_{app3}$ ). However, in condition 3, the second phase is a small change where only a fraction of the L/t FRET signal is lost, and the slower third phase is the much larger FRET efficiency change.

#### 4.3.2 tRNA<sup>fMet</sup> Interaction with Phe-tRNA<sup>Phe</sup> (t/t FRET)

The changes in L/t FRET efficiency, although interesting, do not provide enough information in order to fully understand the tRNA movement and subsequent release of deacylated-tRNA<sup>fMet</sup> after translocation. Definitive statements for the tRNA movement in L/t experiments is difficult due to the inherent movements of both labels; therefore, a

complex with a relatively stably-bound FRET donor in the P-site of a POST complex (Phe-tRNA<sup>Phe</sup> (Rhd110)) was used to monitor movement of acceptor tRNA<sup>fMet</sup> (Cy3) away from the P-site of the ribosome. Preliminary equilibrium FRET efficiency measurements seen in [Figure 4.7](#), were taken for purified PRE-1 complexes, and purified PRE-1 complexes with EF-G.GTP (1  $\mu$ M), where the acceptor was limiting. The FRET efficiency value was determined as above for the L/t experiments, except using Cy3/Rhd110 as the FRET pair. The PRE-1 complex has a FRET efficiency of  $\sim 0.53$  as determined by equation 2.2 ([Table 4.1](#)), which is in agreement with previous single molecule work ([Chen et al., 2011](#)). For the kinetic experiments, PRE-1 complexes were isolated using sucrose cushion centrifugation, and the t/t movement was measured upon addition of EF-G.GTP (1.0  $\mu$ M unless otherwise noted), and fit to equation 4.1. In addition to monitoring the donor channel increase and acceptor channel decrease during FRET efficiency loss, calculations were performed in order to eliminate contributions to acceptor intensity due to acceptor fluorescence resulting from direct excitation from the laser and donor fluorescence leakage into the acceptor channel (Equation 2.2, Section 2.2.7.2).

#### **4.3.2.1 In Buffer A, L1 Moves Away From Deacylated-tRNA<sup>fMet</sup> Prior to tRNA Release**

A tRNA translocated from the A- to P- site remains in the P/P-site, and maintains a fairly stable conformation, as seen in the X-ray crystallographic structure of a POST-1 complex with deacylated-tRNA in the P-site (B-factor =  $86 \text{ \AA}^2$ , indicating a rms displacement of  $\sim 1 \text{ \AA}$ ) ([Gao et al., 2009](#)). Also, Fischer and coworkers use cryo-EM to

see three different POST complexes and there is no indication of movement in the P-site tRNA between the complexes (**Fischer et al., 2010**). For these reasons, any loss in FRET efficiency between tRNA<sup>fMet</sup> (Cy3) and fMet-Phe-tRNA<sup>Phe</sup> (Rhd110) should reflect movement of tRNA<sup>fMet</sup> (Cy3) away from the P-site of the ribosome. 70SICs containing fMet-tRNA<sup>fMet</sup> (Cy3) and T202C-L1 50S were incubated with ternary complex containing Phe-tRNA<sup>Phe</sup> (Rhd110) to create PRE-1 complexes, which were subsequently purified through sucrose cushion centrifugation. EF-G.GTP (1  $\mu$ M) was stopped flow added to the purified PRE-1 complexes (0.25  $\mu$ M) in Buffer A; the resulting FRET efficiency losses were monitored as acceptor fluorescence losses and were fit to a triple exponential curve (Equation 4.1). As seen in **Figure 4.8**, there is a brief initial lag in which the FRET efficiency does not change which corresponds to  $k_{app1}$ , followed by the major FRET efficiency decrease that occurs with an apparent rate constant of  $k_{app2} = 1.4 \text{ s}^{-1}$ , approximately 3.5 times slower than the loss of L/t FRET efficiency under the same conditions (**Table 4.2**). Therefore, when considering the major FRET efficiency changes for the t/t and L/t experiments, it is reasonable to assume that the L1-stalk is moving away from the deacylated-tRNA<sup>fMet</sup> prior to its release from the ribosome (see Discussion, **Scheme 4.1**).

#### **4.3.2.2 In Buffer B, the tRNA Release Pathway is Dependent on P-site Peptidyl-state**

As seen before, the L/t FRET efficiency change in Buffer B depends heavily on whether the P-site is occupied with fMet-Phe-tRNA<sup>Phe</sup> or Phe-tRNA<sup>Phe</sup> (**Figure 4.6**). In contrast, **Figure 4.9** shows that the t/t FRET efficiency change shows only weak dependence on the P-site tRNA peptidyl state. The t/t FRET efficiency changes can be

compared to the L/t FRET efficiency changes under the same conditions in order to better understand the movement of the deacylated-tRNA<sup>fMet</sup> after translocation.

When EF-G.GTP is added to PRE-1 complexes containing tRNA<sup>fMet</sup> (Cy3) and fMet-Phe-tRNA<sup>Phe</sup> (Figure 4.10 A), only a fraction of the t/t FRET signal is rapidly lost ( $k_{app1} = \sim 28 \text{ s}^{-1}$ ), with the major loss of FRET efficiency having an apparent rate constant of  $k_{app2} = 1.6 \text{ s}^{-1}$ , approximately the same apparent rate constant as the major L/t FRET efficiency loss seen under the same conditions (Table 4.2). Also, similar to the L/t FRET efficiency loss, a slower minor FRET efficiency loss is seen with an apparent rate constant of  $k_{app3} = 0.20 \text{ s}^{-1}$ . The simplest model for understanding the major FRET efficiency changes seen in the t/t and L/t experiments is that the deacylated-tRNA<sup>fMet</sup> loss in FRET efficiency from L1 and from P-site peptidyl-tRNA is concomitant with the release of deacylated-tRNA from the ribosome (Scheme 4.1, see discussion).

When EF-G.GTP is added to PRE-1 complexes containing tRNA<sup>fMet</sup> (Cy3) and Phe-tRNA<sup>Phe</sup> (Figure 4.10 B,C), the t/t FRET efficiency changes are basically similar to what is seen in Figure 4.10 A. They can still be fit to a triple exponential curve (Equation 4.1) with only a fraction of the t/t FRET signal is lost in the first rapid change ( $k_{app1} = \sim 17 \text{ s}^{-1}$ ) and the major loss occurring in the second phase  $k_{app2} = 1.3 \text{ s}^{-1}$ , that is followed by a slower ( $k_{app3} = 0.24 \text{ s}^{-1}$ ) smaller loss. However, the L/t FRET efficiency changes are quite different from what is seen in Figure 4.10 A, with the major L/t FRET efficiency loss occurring >50 times slower than the major FRET efficiency loss associated with the t/t FRET. Thus, the movement of deacylated-tRNA away from the P-site is at a rate that is similar to the movement away in other conditions, but much faster than the loss in FRET

efficiency from L/t. This indicates that the tRNA is remaining bound to the L1 stalk and moving away from the E-site, possibly into a secondary E2-site that retains FRET efficiency with T202C-L1, but loses FRET efficiency with P-site tRNA (**Fischer et al., 2010; Agrawal et al., 1999**).

### 4.3.3 Fluorescence Anisotropy Change of tRNA<sup>fMet</sup> (Cy3) After Translocation

Fluorescence anisotropy is a useful tool for measuring of the apparent size of a fluorescently labeled molecule. By using Cy3 labeled initiator tRNA, it was possible to monitor the  $k_{\text{off}}$  rates of the deacylated-tRNA<sup>fMet</sup> upon translocation in Buffer B. The bound and free states of the tRNA each have an intrinsic polarization value: a higher value for the bound state and a lower value for the free state; thus, by looking at the decrease in anisotropy of the labeled tRNA it is possible to have a direct measurement of tRNA release. Anisotropy measurements utilize four fluorescence intensities, and the value is calculated by equation 4.2.

$$\text{Anisotropy} = \frac{I_{VV} - GI_{VH}}{I_{VV} + GI_{VH}} \quad \text{Equation 4.2}$$

$$G = \frac{I_{HV}}{I_{HH}}$$

Where,  $I_{VV}$  stands for intensity with vertically polarized excitation and vertically polarized emission,  $I_{VH}$  stands for intensity with vertically polarized excitation and



horizontally polarized emission, and so on.  $G$  is a measure of the sensitivity difference between the two PMTs used for obtaining the data.

Initial equilibrium anisotropy measurements were taken on PRE-1 complexes (bound), and POST-1 complexes (unbound) to determine the maximum loss of anisotropy for the translocation and release, these experiments were performed in Buffer A to ensure release, and the anisotropy loss was approximately  $0.05 \pm 0.01$ , from 0.31 to 0.26 (**Yuanwei Chen, work in progress**). PRE-1 complexes were created using 70SICs that were made with unlabeled T202C-L1 ribosomes and either deacylated-tRNA<sup>fMet</sup> (Cy3), or highly charged fMet-tRNA<sup>fMet</sup> (Cy3) in Buffer B, and the anisotropy changes were monitored upon stopped flow addition of EF-G.GTP (1.5  $\mu$ M). As expected, the anisotropy change for both complexes made with tRNA<sup>fMet</sup> (Cy3) and fMet-tRNA<sup>fMet</sup> (Cy3) was significantly less than that seen in Buffer A due to the inherent equilibrium of binding and release of deacylated-tRNA in the E-site in Buffer B as seen in the FRET studies. Unfortunately, this led to difficulty in analyzing the overall anisotropy changes, and this analysis is still ongoing. However, preliminary results show that in **Figure 4.11**, the anisotropy change resulting from a POST-1 complex containing P-site Phe-tRNA<sup>Phe</sup> mimics the major L/t FRET efficiency loss, with  $k_{app3} = \sim 0.052 \text{ s}^{-1}$  (**B**) (**Table 4.2**).

#### **4.3.4 Fitting of All Data to a Global Kinetic Scheme (EF-G Binding $\rightarrow$ Translocation)**

A major goal in this research was to find a general kinetic scheme for the release of deacylated-tRNA<sup>fMet</sup> that would fit all the data obtained quantitatively. In order for the

scheme to be valid, not only did the data collected here need to fit properly, but also the results of previous work needed to be accommodated. Rates of EF-G.GTP binding, hydrolysis, and conformational change were all first performed by Savelsbergh and coworkers at 37 °C (Savelsbergh et al., 2003); however, since the work shown here is at 25 °C, the following results have been used (Pan et al., 2006). At 25 °C in Buffer A with coumarin labeled EF-G, EF-G.GTP binding and dissociation occur at rates of  $30 \mu\text{M}^{-1} \text{s}^{-1}$  and  $25 \text{s}^{-1}$ , respectively, and binding is followed almost immediately by hydrolysis at  $\sim 100 \text{s}^{-1}$  (Seo et al., 2006; Pan et al., 2006; Pan et al., 2007). Conformational change within the EF-G.GDP.Pi complex follows hydrolysis and occurs at  $\sim 30 \text{s}^{-1}$ . This conformational change is indistinguishable from a tRNA movement creating a P/E complex, as both steps are inhibited by thiostrepton (ThS) and occur at similar rates (Seo et al., 2006, Pan et al., 2007). A very fast conversion from the P/E complex to an INT complex directly precedes translocation.

#### 4.3.4.1 Varying EF-G Concentration

In order to better understand the early steps of EF-G.GTP addition to a PRE-1 complex, increasing concentrations of EF-G.GTP were added to the PRE-1 complexes discussed above, and the FRET efficiency changes were monitored. In all cases (A, B, and C), the curves were fit to the global Scheme 4.1, where the hydrolysis and conformational change steps leading up to translocation described above were combined into  $k_3$ . When fitting the concentration dependent data to Scheme 4.1,  $k_4$  through  $k_9$  were held constant and the data for  $k_1$  through  $k_3$  were fit to the Scheme. In Buffer A (A), at higher concentrations of EF-G (2.0-5.0  $\mu\text{M}$ ) a very rapid ( $\sim 29 \mu\text{M}^{-1} \text{s}^{-1}$ ) increase in

FRET efficiency is seen (Figure 4.12 A) upon binding of EF-G.GTP. At lower EF-G concentrations (0.5-1  $\mu\text{M}$ ) this increase is only seen as a lag because the higher FRET intermediate does not have time to build up before L1 movement. Further, the GTP hydrolysis and conformational change steps are combined into ( $k_3$ ), and result in a rate constant of  $\sim 25 \text{ s}^{-1}$  (Tables 4.4, 4.5).

In Buffer B, using PRE-1 complexes created with 70SICs containing highly charged fMet-tRNA<sup>fMet</sup> (Cy3) and T202C-L1 (Cy5) ribosomes, only two EF-G concentrations were examined, but both were fit to Scheme 4.1 as above (Figure 4.12 B). Under these conditions, addition of 5  $\mu\text{M}$  EF-G results in a small increase in FRET efficiency. The rate constant for the binding was determined to be  $\sim 44 \mu\text{M}^{-1} \text{ s}^{-1}$ , and  $k_3 = 25 \text{ s}^{-1}$  (Tables 4.4, 4.5).

In Buffer B, using PRE-1 complexes created with 70SICs containing deacylated-tRNA<sup>fMet</sup> (Cy3) and T202C-L1 (Cy5) ribosomes, increasing concentrations of EF-G were added to the PRE-1 complex (Figure 4.12 C). The curves were all fit to the global Scheme 4.1, as above, where  $k_4$ - $k_9$  were all held constant. Like in Buffer A, the binding of EF-G resulted in an increase in FRET efficiency ( $k_1 = \sim 26 \mu\text{M}^{-1} \text{ s}^{-1}$ ) at higher concentrations, and a  $k_3$  of  $\sim 25 \text{ s}^{-1}$  (Tables 4.4, 4.5).

#### **4.3.5 Fitting of All Data to a Global Kinetic Scheme (Translocation Through Deacylated-tRNA Release)**

The results obtained by the EF-G concentration dependence studies for the early steps after EF-G addition were set into Scheme 4.1, and the remaining steps  $k_4$ - $k_9$  were

determined by fitting the L/t and t/t FRET traces from [Figure 4.8](#) and [Figure 4.10](#) to the global [Scheme 4.1](#). The results from these fittings are seen in [Tables 4.4, 4.5](#), and summarized below.

#### 4.3.5.1 Global Fitting of Deacylated-tRNA Release in Buffer A

[Scheme 4.1](#) represents the steps leading up to deacylated-tRNA release from the ribosome after addition of EF-G.GTP. From what we know about the triple exponential fits of the L/t and t/t FRET efficiency data in Buffer A, tRNA release should follow pathway 1 with the rate constants  $k_6$  and  $k_8$  dominating the L/t and t/t FRET efficiency changes, respectively. As seen in [Figure 4.13 A](#) and [Table 4.4](#), initial translocation occurs with a rate constant of  $k_4 = 8.2 \text{ s}^{-1}$ , and after reaching a POST-1 state, the rate constant  $k_6 = 5.10 \text{ s}^{-1}$  corresponds to the movement of the L1-stalk into an out position, followed by deacylated-tRNA<sup>fMet</sup> release via a rate constant  $k_8 = 1.07 \text{ s}^{-1}$ . Additionally, in both t/t and L/t FRET experiments, a slower release follows pathway 2, and is seen as  $k_5 = 0.65 \text{ s}^{-1}$ . It can be said that the deacylated-tRNA release follows a dominant pathway 1, but there is also a minor pathway 2, in which less deacylated-tRNA is released with a slower rate.

#### 4.3.5.2 Global Fitting of Deacylated-tRNA Release in Buffer B (Peptidyl-tRNA in the P-site)

Using what was learned by fitting the L/t and t/t FRET experiments to a triple exponential curve above ([Figure 4.10 A](#)), both sets of data were fit to [Scheme 4.1](#), holding  $k_1 - k_3$  constant with values observed above (4.3.4.1). After translocation ( $k_4 =$

3.34 s<sup>-1</sup>), the majority of the release of deacylated-tRNA<sup>fMet</sup> followed pathway 2, and was dominated by the rate constant  $k_5 = 1.60 \text{ s}^{-1}$ , with very little release following any of the other pathways as seen in [Figure 4.13 B](#), and [Table 4.4](#). It should be noted, that since the initial charging efficiency of the fMet-tRNA<sup>fMet</sup> was 78%, approximately 22% of the ribosomes still contain aminoacyl-tRNA in the P-site after translocation; therefore, it is possible that a small fraction, undetectable in this Scheme, is following pathway 3, as described below.

#### **4.3.5.3 Global Fitting of Deacylated-tRNA Release in Buffer B (Aminoacyl-tRNA in the P-site)**

The rate constants obtained by fitting the L/t and t/t FRET traces to triple exponential curves above ([Figure 4.10 B, C](#)), shows that in global [Scheme 4.1](#) the majority of the release of deacylated-tRNA<sup>fMet</sup> follows pathway 3, in which the deacylated-tRNA moves out along with the L1-stalk and is then slowly released ( $k_7$  and  $k_9$ ). Indeed, when the L/t and t/t FRET traces were fit to [Scheme 4.1](#), the major release was seen by  $k_7 = 1.30 \text{ s}^{-1}$  and  $k_9 = 0.020 \text{ s}^{-1}$ , with a minor release being seen via pathway 2,  $k_5 = 0.74 \text{ s}^{-1}$  ([Figure 4.13 C](#), [Table 4.4](#)).

## **4.4 Discussion**

Both the Cy5-labeled and unlabeled T202C-L1 ribosomes have been shown to be readily accessible and able to bind initiator tRNA to near wild type efficiency (**Chapter 3**). Further, this particular mutant has been shown to be a very good indicator of tRNA movement between the P/P and E/E-tRNA binding sites as seen in both single molecule

work (Fei et al., 2008, Ben Stevens manuscript in progress), equilibrium FRET, and the stopped flow kinetic FRET. Further, the ability to prepare tRNAs that are highly labeled with either hydrazide dyes, or rhodamine 110 and highly aminoacylated was essential to being able to discover different pathways by which tRNA can leave the E-site of the ribosome.

The L1 stalk has been shown to occupy at least two (Fei et al., 2008) or three (Cornish et al., 2009) distinct conformations depending on the positions and acylation-state of the tRNAs bound to the ribosome. The L1-stalk occupies an “open” (out) state when the ribosomes have vacant E-sites or in isolated 50S subunits (Korostelev et al., 2008; Harms et al., 2001) and this is most likely the position for the sucrose-purified 70SIC ribosomes used here. When deacylated-tRNA<sup>fMet</sup> is bound in the E-site, the L1-stalk moves inward by ~30-40 Å (Korostelev et al., 2006; Selmer et al., 2006) and this is the most likely position of the stalk directly after translocation when the E-site is occupied with the translocated deacylated-tRNA<sup>fMet</sup>. A third position for the L1-stalk, the “overly closed,” determined by Cornish and coworkers, requires a further movement of ~15-20 Å towards the body of the ribosome and occurs when a tRNA adopts the P/E-hybrid conformation (Cornish et al., 2009; Valle et al., 2003; Gao et al., 2003). This is most likely the position of the stalk directly after addition of ternary complex to a 70SIC resulting in the increase in FRET efficiency described above.

In a 70SIC complex, the L1 stalk remains in an “out” conformation at least until peptide bond formation, at which point the now deacylated-tRNA<sup>fMet</sup> can adopt a hybrid P/E conformation. It is this movement of deacylated-tRNA<sup>fMet</sup>, along with the movement

of the L1 into an “overly-closed” conformation, which results in the increase in FRET efficiency seen in [Figures 4.1-4.3](#). During translocation, the L1/tRNA interaction from P/E-hybrid to E/E-site does not change, as first seen in single molecule work by [Fei et al., 2008](#), and as shown here by a L/t FRET efficiency lag. The FRET efficiency for the PRE-1 complex has been calculated from equilibrium FRET and stopped flow FRET experiments and is approximately  $0.8 \pm 0.1$  in Buffer A, and  $\sim 0.90 \pm 0.03$  in Buffer B. This FRET efficiency, first seen in the PRE-1 state, remains relatively unchanged until either deacylated-tRNA dissociation or conformational change, at which time the POST-1 FRET efficiency either goes to 0 as in Buffer A, or decreases to approximately 0.5 in Buffer B. As mentioned before, the remaining FRET efficiency in the POST-1 complex in Buffer B is caused by rebinding of deacylated-tRNA to the E-site. The measured values for the PRE-1 complex are similar to FRET efficiency values seen previously in single molecule work ([Table 4.6](#)).

### **EF-G.GTP Binding → Translocation**

Two different variables, buffer conditions and P-site peptidyl-state, with two possibilities were tested above; however, for one of the buffer conditions (A) we could only study the peptidyl-tRNA because the aminoacyl-tRNA did not remain bound to the PRE-1 complex through sucrose cushioning. Therefore, three different complexes were used to determine the possible pathways in which deacylated-tRNA can dissociate from the ribosome. In all three pathways, the steps leading up to translocation did not change, and were in accordance with previous literature ([Pan et al., 2007](#)). L/t FRET

experiments with addition of multiple concentrations of EF-G to PRE-1 complexes were used in order to better understand the early stages of POST-1 formation.

As seen in [Figure 4.12](#), the addition of EF-G.GTP at high concentrations (2.0  $\mu\text{M}$ -5.0  $\mu\text{M}$ , in most cases) resulted in a net FRET efficiency increase between L1 and deacylated-tRNA at a rate constant of  $\sim 30 \mu\text{M}^{-1} \text{s}^{-1}$ . Interestingly, this increase in FRET efficiency is associated with the binding of EF-G rather than with conformational change step ( $k_3$ ) ([Table 4.5](#)). For samples with peptidyl-tRNA ([A and B](#)), the FRET efficiency increase in Buffer A is greater than it is in Buffer B. For the PRE-1 complex, the FRET efficiency value in Buffer A is 0.8 ([Figure 4.1](#)) and in Buffer B it is 0.9 ([Figure 4.12 A, B, Table 4.6](#)). It is possible that more deacylated-tRNA samples the higher FRET state in Buffer B prior to addition of EF-G.GTP, and therefore, less of an increase is observed after addition of EF-G.GTP. Prior to EF-G.GTP addition, the L1-stalk fluctuates between “in” and “out” conformations, while the now deacylated-tRNA fluctuates between classic (P/P) and hybrid (P/E) conformations. A deacylated-tRNA in the P/E hybrid state will show a FRET signal with the L1-stalk that moves into the “in” conformation. Upon addition of EF-G.GTP, the equilibrium between classic and hybrid states shifts towards the hybrid, resulting in a net increase in average FRET efficiency between the L1 and deacylated-tRNA, as seen in [Figure 4.12](#). Indeed, in Buffer A, the increase in FRET efficiency leads to a FRET efficiency value of  $\sim 1$ , similar to the FRET efficiency value seen for the PRE-1 state in Buffer B. At lower concentrations of EF-G.GTP, the intermediate in which an increased fraction of the complexes is hybrid does not have a chance to build up, thus the binding is observed as a lag (as is seen in all other L/t experiments presented here). After EF-G.GTP binding, GTP hydrolysis occurs, followed



by a series of conformational changes (which were all fit to a single rate constant,  $k_3$ ), and translocation, none of which affect the L/t FRET signal (Table 4.5) because the distance between the L1-stalk and the deacylated-tRNA in the P/E state does not change when the tRNA is translocated to the E/E state.

### **Translocation → Deacylated-tRNA Release**

By using the L/t and t/t FRET efficiency changes, three different pathways for deacylated-tRNA<sup>fMet</sup> release from the E-site have been discovered. As seen above, during the steps leading up to translocation and the steps immediately after translocation, the conformation of the ribosome is the same for each pathway; the L1-stalk is in towards the body of the ribosome ( $L_i$ ) and the deacylated-tRNA is in the E-site (E). After release, the tRNA is off of the ribosome ( $E_o$ ) and the L1-stalk has moved out ( $L_o$ ). Pathway 1) the L1-stalk moves to the open conformation first ( $L_o$  E), and then deacylated-tRNA<sup>fMet</sup> is released from the ribosome ( $L_o$   $E_o$ ); 2) the L1/tRNA interaction is lost at a similar time as tRNA release occurs ( $L_o$   $E_o$ ); and 3) the L1-stalk moves to an open conformation ( $L_o$ ) and remains in contact with the deacylated-tRNA<sup>fMet</sup> that has now moved into an apparent E2-site ( $E_2$ ) and is then released very slowly ( $E_o$ ) (Scheme 4.1).

The first pathway, in which the L1-stalk moves out prior to deacylated-tRNA<sup>fMet</sup>, was discovered by monitoring translocation and release in Buffer A. Buffer A has previously been shown to cause tRNA in the E-site to be released rapidly. However, the timing of the release was never determined (Semenkov et al., 1996). In the PRE-1 complex, the FRET efficiency between deacylated-tRNA<sup>fMet</sup> (Cy3) and T202C-L1 (Cy5) is approximately 0.73, as measured by L/t equilibrium FRET (Figure 4.1). Upon

translocation, this FRET efficiency value does not change; therefore, under these conditions, in which EF-G.GTP (1  $\mu$ M) is added to the PRE-1 complex, the only change in FRET efficiency is when either the L1-stalk moves away, or the tRNA is released. Prior to the major FRET efficiency loss, a lag phase is indeed seen in the L/t FRET; this lag corresponds to the events leading up to and including the rate limiting translocation and has an apparent rate constant of 8.2  $s^{-1}$ , which is in accordance with translocation rates of  $\sim 7.8 s^{-1}$  measured in similar conditions by Pan and coworkers (**Pan et al., 2007**). Two-thirds of the release of deacylated-tRNA in Buffer A follows pathway 1, in which the L1-stalk moves away prior to the release of deacylated-tRNA. Therefore, the loss in FRET efficiency seen in the L/t FRET traces is due to the movement of the L1-stalk to an out conformation. The movement from an in conformation to an out conformation is approximately 30-40 Å, which increases the distance between the dyes from  $\sim 40$  Å to  $\sim 70-80$  Å. With a Förster  $R_0$  of approximately 50 Å (**Fei et al., 2008**) for the Cy3/Cy5 FRET pair, this increase in distance takes a theoretical FRET efficiency from  $\sim 0.80$  to  $\sim 0.05$  (Distance =  $R_0 \cdot (1/E-1)^{1/6}$ ), values that correspond very nicely with the values observed (**Table 4.6**). After the L1-stalk moves out, deacylated-tRNA dissociation is seen by the loss of t/t FRET efficiency with a rate constant of  $\sim 1.6 s^{-1}$ .

The second pathway, is one in which the L1 moves away from the tRNA at a similar apparent rate constant as the tRNA releases off of the ribosome, and was discovered by monitoring translocation and deacylated-tRNA<sup>fMet</sup> release in Buffer B. In order to obtain complexes which release deacylated-tRNA<sup>fMet</sup> via this pathway, PRE-1 complexes had to be prepared using 70SICs which contained highly charged (>75%) fMet-tRNA<sup>fMet</sup>, because ribosomes that bind deacylated-tRNA<sup>fMet</sup> in the 70SIC favor

release from pathway 3, as discussed later. The only definitive statement that can be made about ribosomes that follow this pathway of deacylated-tRNA<sup>fMet</sup> release from the E-site is that the deacylated-tRNA<sup>fMet</sup> dissociates from the ribosome at an apparent rate constant of  $\sim 1.6 \text{ s}^{-1}$ , as seen by the global fitting to [Scheme 4.1](#) of the L/t and t/t FRET traces. There are four sets of circumstances that could occur to cause all of these rate constants to be similar, and none of them can be positively ruled out using this set of experiments: 1) The L1-stalk outward movement, and the dissociation of the deacylated-tRNA<sup>fMet</sup> are concerted movements; 2) The deacylated-tRNA<sup>fMet</sup> loss occurs while the L1-stalk is “in” and the dissociation of tRNA causes the decrease in L/t and t/t FRET efficiency; 3) The L1-stalk and the deacylated-tRNA<sup>fMet</sup> move out together in a rate-determining step that is followed by rapid deacylated-tRNA<sup>fMet</sup> release from the E2-site, so that L/t and t/t FRET efficiency decrease at indistinguishable rates; or 4) The L1-stalk moves out first in a rate-determining step that is followed by rapid deacylated-tRNA<sup>fMet</sup> dissociation from the E-site. It is very unlikely that the two events occur concertedly, and from the evidence seen in the crystal structures when the E-site is unoccupied (L1-stalk in an open conformation), and from the other pathways presented here, it is unlikely that the L1-stalk remains in an in conformation while tRNA releases; therefore, the first two options are improbable. This leaves options 3) and 4), which we are unable to distinguish between to the precision of the rate constants measured here. Fei and coworkers used single molecule FRET to monitor a similar release of deacylated-tRNA after translocation, with a dipeptide in the P-site. Their results indicate that the L1-stalk moves out, prior to the release of deacylated-tRNA, similar to pathway 1; however, their buffer conditions (with polyamines, 15 mM Mg<sup>2+</sup>) cause the translocation reaction as well as the

release to slow down drastically at roughly  $0.1 \text{ s}^{-1}$ , and  $0.06 \text{ s}^{-1}$ , respectively based on lifetimes. (Fei et al., 2008). It is possible that the pathway 2 seen here, is indeed similar to what they observe, but here it is on a much faster time scale, and thus tRNA dissociation and L1-stalk movement appear as concerted movements.

The third pathway, in which the tRNA moves away from the body of the ribosome with the L1-stalk, was discovered by monitoring translocation and deacylated-tRNA<sup>fMet</sup> release in Buffer B. This pathway is favored by ribosomes that initiate protein synthesis using a deacylated-tRNA<sup>fMet</sup>, so that, upon translocation, the P-site contains only an aminoacyl-tRNA. For ribosomes that follow this pathway, after the deacylated-tRNA<sup>fMet</sup> loses contact with the P-site tRNA, it remains in contact with the L1-stalk as the stalk moves from a closed ( $L_i$ ) to an open ( $L_o$ ) position. This movement of tRNA with the L1-stalk is believed to put the deacylated-tRNA into a position similar to the E2-site ( $E_2$ ) seen in recent cryo-EM images (Fischer et al., 2010). The distance between the dihydrouridine (and therefore Cy3) at position 20 of the tRNA<sup>fMet</sup> in the E/E-site, and the dihydrouridines at position 16/17 (Rhd110) of tRNA<sup>Phe</sup> in the P/P-site is  $\sim 45 \text{ \AA}$ . If the deacylated-tRNA<sup>fMet</sup> were indeed moving to the E2-site, the anticodon stem loop and the elbow region would move away from the P-site tRNA. Although it is currently not possible to obtain distance calculations because the coordinates are not available, it is likely that this movement would cause the loss of FRET efficiency that is seen in the t/t FRET measurements. The loss in t/t FRET efficiency observed in the ribosomes that follow this pathway occurs at a rate constant that is very similar to that seen for the loss in t/t FRET efficiency for the other pathways ( $\sim 1.6 \text{ s}^{-1}$ ); therefore, the release of deacylated-tRNA<sup>fMet</sup> from the E-site is the same for all three pathways. The L1-stalk

movement, and the interaction of the tRNA with the L1-stalk is dependent on (in these cases) the buffer conditions and the peptidyl-state of the P-site tRNA after translocation. In this pathway, the deacylated-tRNA<sup>fMet</sup> remains in contact with the L1 stalk as it moves to an open conformation, and occupies the E2-site. The E2-site, according to cryo-EM images, does not have any codon/anticodon interactions between the tRNA and mRNA; therefore, under these conditions the tRNA in the E2-site may be very easily displaced by any deacylated-tRNA in solution (as seen in Chapter 5). However, under these conditions in which there are no excess deacylated-tRNAs, it is possible for the tRNA to remain bound to the E2-site for a long time, as seen with the slow loss of L/t FRET efficiency and the major fluorescence anisotropy change that is seen on the same time scale ( $\sim 0.02 \text{ s}^{-1}$ ).

Although it has been shown that the three different conditions favor three different major pathways of deacylated-tRNA release, it should be mentioned that a minor, less significant pathway is also followed in each case. The probability of a deacylated-tRNA releasing via any of the three specific pathways varies based on the conditions.

As previously mentioned in Section 1.6, the function and occupancy of the E-site has been highly debated in the literature. In one case the E-site acts as a stable binding site in which a translocated deacylated-tRNA can remain bound to the E-site in Buffer B even after sucrose centrifugation (**Gnirke et al., 1989**). In light of the findings that peptidyl-state of the P-site tRNA affects the release of deacylated-tRNA<sup>fMet</sup> from the E-site (or E2-site) in Buffer B, the stable binding of E-site tRNA described above was

explored. The current results indicate that when peptidyl-tRNA is in the P-site, deacylated-tRNA<sup>fMet</sup> dissociates from the ribosome relatively rapidly, whereas, when aminoacyl-tRNA is in the P-site, deacylated-tRNA<sup>fMet</sup> dissociates from the ribosome much more slowly. The complexes used by Nierhaus and colleagues utilize a POST translocation state that has an N-acetyl-acyl-tRNA in the P-site, and show that this particular complex has a stable binding of E-site tRNA. It is possible that N-acetyl-acyl-tRNA in the P-site favors release of deacylated-tRNA via pathway 3 in [Scheme 4.1](#), which would allow the stable binding of the deacylated-tRNA after translocation.

The second role of the E-site, proposed by Wintermeyer and colleagues, is that it acts as a transient intermediate (**Lill and Wintermeyer, 1987; Lill et al., 1988; Semenov et al., 1996**). This work, performed mostly in Buffer A, shows in a non-time resolved manner, that approximately 85% of the deacylated-tRNA is released “instantaneously” upon translocation (**Semenov et al., 1996**). Our results agree in showing release of deacylated-tRNA<sup>fMet</sup> via pathway 1 ([Scheme 4.1](#)).

As mentioned previously, it is important to better understand the function of the E-site because its occupancy has been implicated in preventing amino acid misincorporation and random frameshifting (**Nierhaus, 2006; Devaraj et al., 2009; Sergiev et al., 2005**), as well as assisting in programmed frameshifting (**Leger et al., 2007, Liao et al., 2008**). To this end, it is possible that all three pathways observed here are viable options for deacylated-tRNA release, and the probability of release via any one pathway is dependent on conditions that may favor or disfavor changes in protein synthesis, such as frameshifting.

## 4.5 Conclusions

By utilizing a site specifically labeled L1 mutant, and reconstituting it into –L1 50S subunits, I was able to create a probe for EF-G.GTP binding and deacylated-tRNA release from the ribosome. Using this labeled ribosome along with t/t FRET and preliminary fluorescence anisotropy, three possible pathways for deacylated-tRNA<sup>fMet</sup> release from the E-site (or E2-site) were discovered. 1) The L1 stalk moves from a closed to an open position prior to release of deacylated-tRNA<sup>fMet</sup>; 2) The L1 stalk moves from a closed to an open position with a rate constant similar to that for the release of deacylated-tRNA<sup>fMet</sup>; and, 3) The deacylated-tRNA<sup>fMet</sup> moves with the L1-stalk as it moves away from the body of the ribosome into an E2-site and is then released very slowly. All three of these pathways are viable options for deacylated-tRNA release and the probability of release via any one pathway is dependent on experimental conditions.

**A**

Buffer	Complex	Cy5/ 70S	Cy3/ 70S	D*A* (A) x10 <sup>5</sup>	D*A* (D) x10 <sup>6</sup>	D*A (A) x10 <sup>4</sup>	D*A (D) x10 <sup>6</sup>	Ext. A (A) x10 <sup>5</sup>	DA* (A) x10 <sup>5</sup>	FRET
A	70SIC			1.95	1.54	4.85	1.51	1.45	1.62	~0
	PRE-1	0.64	0.78	2.66	1.41	4.85	1.51	2.21	1.62	<b>0.73</b>
	POST-1			1.79	1.54	4.85	1.51	1.29	1.62	~0
B	70SIC			1.66	1.46	4.84	1.50	1.90	1.53	~0
	PRE-1	0.66	0.75	2.68	1.45	4.84	1.50	2.21	1.53	<b>0.90</b>
	POST-1			2.35	1.43	4.84	1.50	1.89	1.53	<b>0.48</b>
B (t/t)	PRE-1	<b>Rhd</b> <b>/70S</b>	0.64	15.7	1.25	66.3	1.76	11.0	92.7	<b>0.53</b>
	POST-1	0.53		13.0	1.69	66.3	1.76	6.65	75.0	~0

**B**

$$DA^*{}' = D^* A^*{}'_A - \left[ D^* A^*{}'_D \times \frac{D^* A_A}{D^* A_D} \right]$$

$$BufferA1 : DA^*{}' = 26.6 - \left[ 141 \times \frac{4.85}{151} \right] = 22.07$$

$$BufferB1 : DA^*{}' = 26.8 - \left[ 145 \times \frac{4.84}{150} \right] = 22.12$$

$$E = \frac{DA^*{}'_A - DA^*{}_A}{DA^*{}_A} \times \left[ \frac{1}{Cy5/70S} \right] \times \left[ \frac{1}{Cy3/70S} \right]$$

$$BufferA1 : E = \frac{22.07 - 16.2}{16.2} \times \left[ \frac{1}{0.64} \right] \times \left[ \frac{1}{0.78} \right] = 0.73$$

$$BufferB1 : E = \frac{22.12 - 15.3}{15.3} \times \left[ \frac{1}{0.66} \right] \times \left[ \frac{1}{0.75} \right] = 0.90$$

**Table 4.1 Equilibrium FRET Efficiency Measurements**

70SICs were made for L/t FRET analysis using fMet-tRNA<sup>fMet</sup> (Cy3) as the donor and T202C-L1-50S (Cy5) as the acceptor. Equilibrium FRET measurements were taken



using a Spectrofluorometer to determine the FRET efficiency at different stages of translocation. The samples were excited at 518 nm and FRET efficiency was measured as acceptor fluorescence change at 667 nm. D\*A\*, D\*A, DA\*, and DA samples were prepared for each complex, and the DA background was subtracted for all samples prior to analysis. The t/t sample was prepared similarly, using Phe-tRNA<sup>Phe</sup> (Rhd110) as the donor and fMet-tRNA<sup>fMet</sup> (Cy3) as the acceptor, exciting at 480 nm, and measuring acceptor fluorescence at 567 nm. The efficiency of energy transfer was calculated via Equation 2.2, reshown here as a sample calculation for FRET efficiency in the PRE-1 complex in Buffers A and B (**B**). Where E is the FRET efficiency, DA\* is the extracted acceptor emission as calculated by the bottom equation. D\*A\*<sub>(A)</sub> is a sample with both donor and acceptor labeled, measured at the acceptor peak, D\*A\*<sub>(D)</sub> is the same complex measured at the donor peak. The DA\* indicates a sample in which only the acceptor is labeled, and a D\*A indicates a sample where only the donor is labeled. The donor efficiency and acceptor efficiency are measured as the amount of donor/70S and acceptor/70S in the purified complexes.

Exp.	Buffer	Charging Efficiency of fMet-tRNA <sup>fMet</sup> in 70S IC	k <sub>1app</sub>	k <sub>2app</sub>	k <sub>3app</sub>
1 (L/t)	A	25%	13.2 ± 0.4 (lag)	<b>4.7 ± 0.1 (0.33)</b>	0.71 ± 0.02 (0.29)
34 (L/t)	A	70%	7.7 ± 0.1 (lag)	<b>4.67 ± 0.08 (0.65)</b>	0.544 ± 0.006 (0.30)
41 (L/t)	A	78%	7.6 ± 0.1 (lag)	<b>4.7 ± 0.1 (0.70)</b>	0.54 ± 0.01 (0.30)
32 (t/t)	A	70%	13.3 ± 0.4 (lag)	<b>1.38 ± 0.01 (0.53)</b>	0.293 ± 0.003 (0.27)
44 (t/t)	A	78%	14.5 ± 0.4 (lag)	<b>1.44 ± 0.03 (0.52)</b>	0.27 ± 0.02 (0.29)
13 (L/t)	B	0%	1.7 ± 0.3 (lag)	1.8 ± 0.3 (0.26)	<b>0.018 ± 0.001 (0.74)</b>
30 (L/t)	B	0%	1.28 ± 0.07 (lag)	1.17 ± 0.06 (0.20)	<b>0.022 ± 0.004 (0.70)</b>
39 (L/t)	B	0%	2.5 ± 0.2 (lag)	0.5 ± 0.1 (0.28)	<b>0.030 ± 0.008 (0.69)</b>
28 (t/t)	B	0%	17 ± 1 (0.10)	<b>1.24 ± 0.06 (0.51)</b>	0.238 ± 0.007 (0.31)
38 (t/t)	B	0%	17 ± 2 (0.12)	<b>1.24 ± 0.02 (0.37)</b>	0.238 ± 0.006 (0.13)
12 (L/t)	B	78%	2.5 ± 0.1 (lag)	<b>1.57 ± 0.08 (0.62)</b>	0.11 ± 0.03 (0.14)
26 (L/t)	B	70%	3.6 ± 0.3 (lag)	<b>1.6 ± 0.1 (0.61)</b>	0.26 ± 0.03 (0.11)

40 (L/t)	B	78%	$5.5 \pm 0.1$ (lag)	<b><math>1.6 \pm 0.3</math></b> <b>(0.61)</b>	$0.27 \pm 0.07$ (0.14)
24 (t/t)	B	70%	$28 \pm 3$ (0.10)	<b><math>1.69 \pm 0.06</math></b> <b>(0.55)</b>	$0.20 \pm 0.01$ (0.11)
42 (t/t)	B	78%	$25 \pm 2$ (0.17)	<b><math>1.04 \pm 0.02</math></b> <b>(0.59)</b>	$0.22 \pm 0.03$ (0.12)
64 (Anis.)	B	0%	$1.2 \pm 0.4$ (lag)	$0.48 \pm 0.06$ (0.20)	<b><math>0.052 \pm 0.002</math></b> <b>(0.70)</b>

\*Amplitude changes appear in parenthesis, major change appears in bold

**Table 4.2 Rate Constants Associated with PRE-1 to POST-1 Translocation and tRNA Dissociation**

PRE-1 complexes were made by incubating 70SIC containing (fMet)-tRNA<sup>fMet</sup> (Cy3) at varying aminoacylation efficiencies, and either T202C-L1 50S (t/t) or T202C-L1 (Cy5) 50S (L/t) with ternary complexes containing either Phe-tRNA<sup>Phe</sup> (Rhd110) (t/t) or Phe-tRNA<sup>Phe</sup> (L/t). The PRE-1 complex used for the anisotropy study were created from 70ICS containing uncharged tRNA<sup>fMet</sup> (Cy3) and unlabeled T202C-L1 ribosomes. The FRET efficiency and anisotropy changes were all fit to a triple exponential curve using Scientist (MicroMath) with the major change for each experiment appearing in bold.

Fig.	Purified Complex	Buffer	Initial fMet Charging	fMet/ PRE	Phe/ PRE	Cy3/PRE (tRNA <sup>fMet</sup> )	Rhd/PRE (tRNA <sup>Phe</sup> )
	70SIC	A	0	0	--	0.58*	--
4.3	70SIC	A	25	0.52	--	0.42	--
4.3	70SIC	B	78	0.45	--	0.36	--
	PRE-1	A	0	0	0.19	0.06*	--
4.5	PRE-1	A	25	0.39	0.70	0.39	--
4.4, 4.5	PRE-1	A	70	0.45	0.67	0.53*	--
4.5, 4.8, 4.12A, 4.13A	PRE-1	A	78	0.58	0.61	0.62*	--
4.6, 4.10B/ C, 4.12C, 4.13C	PRE-1	B	0	0	0.35	0.57*	--
	PRE-1	B	25	0.34	0.31	0.46	--
4.4, 4.6, 4.10A, 4.12B, 4.13B	PRE-1	B	78	0.52	0.37	0.70*	--
	PRE-1	A	0	0	0.20	0.06*	0.16
	PRE-1	A	70	0.47	0.76	0.63*	0.54
4.8,	PRE-1	A	78	0.57	0.73	0.65*	0.50

4.13A							
4.9, 4.10B/ C, 4.11, 4.13C	PRE-1	B	0	0	0.41	0.52*	0.35
	PRE-1	B	70	0.48	0.47	0.43*	0.45
4.9, 4.10A, 4.13B	PRE-1	B	78	0.50	0.51	0.46*	0.53

\*HPLC purified, highly labeled tRNA<sup>fMet</sup>

**Table 4.3 Binding Efficiencies of tRNA to Purified Ribosome Complexes**

Complexes were created and purified through sucrose cushion centrifugation. The ribosome concentration was determined by  $A_{260}$ , and was then analyzed for tRNA binding by measuring the radioactive amino acid on the tRNA, or for label by measuring, Cy3 concentration by  $A_{552}$ , or Rhd110 concentration by  $A_{512}$ .

	$k_1$ ( $\mu\text{M}^{-1}\text{s}^{-1}$ )	$k_2$ ( $\text{s}^{-1}$ )	$k_3$ ( $\text{s}^{-1}$ )	$k_4$ ( $\text{s}^{-1}$ )	$k_5$ ( $\text{s}^{-1}$ )	$k_6$ ( $\text{s}^{-1}$ )	$k_7$ ( $\text{s}^{-1}$ )	$k_8$ ( $\text{s}^{-1}$ )	$k_9$ ( $\text{s}^{-1}$ )
<b>A</b>	$29 \pm 1$ (-0.33)	$24 \pm 2$	$25.3 \pm 0.1$	$8.2 \pm 0.1$ (lag)	$0.65 \pm 0.02$ (L/t:0.26) (t/t:0.29)	$5.10 \pm 0.04$ (0.73)	$\sim 0$	$1.07 \pm 0.02$ (0.64)	$\sim 0$
<b>B</b>	$41 \pm 8$ (-0.03)	$44 \pm 14$	$25 \pm 2$	$3.34 \pm 0.09$ (lag)	$1.60 \pm 0.01$ (L/t:0.60) (t/t:0.59)	$\sim 0$	$\sim 0$	$\sim 0$	$\sim 0$
<b>C</b>	$25 \pm 2$ (-0.20)	$25 \pm 4$	$25 \pm 2$	$1.27$ (lag)	$0.74 \pm 0.01$ (L/t:0.33) (t/t:0.31) (Anis: 0.30)	$\sim 0$	$1.30 \pm 0.01$ (0.51)	$\sim 0$	$0.020 \pm 0.001$ (L/t: 0.66) (Anis: 0.70)

\*Amplitude changes are shown in parenthesis, and negative values indicate an increase in FRET efficiency. Amplitude changes were

\* $k_1, k_3$  amplitude changes were determined by the L/t FRET experiment where 5.0  $\mu\text{M}$  EF-G was added.

\* $k_4, k_5, k_6, k_9$  amplitude changes were determined by the L/t FRET (and Anisotropy in C, 1.5  $\mu\text{M}$  EF-G) experiment where 1.0  $\mu\text{M}$  EF-G was added in traces fit to a triple exponential.

\* $k_7, k_8$  amplitude changes were determined by the t/t FRET experiment where 1.0  $\mu\text{M}$  EF-G was added in traces fit to a triple exponential.

**Table 4.4 Rate Constants for Global Scheme 4.1**

L/t and t/t FRET traces were fit to the global Scheme 4.1 using Scientist. **A)** PRE-1 complexes made in Buffer A; **B)** PRE-1 complexes made in Buffer B with peptidyl-tRNA in the P-site (after translocation); and **C)** PRE-1 complexes made in Buffer B with

aminoacyl-tRNA in the P-site (after translocation). Rate constants for the steps leading up to translocation ( $k_4$ ) were fit to scheme 4.1 using EF-G concentration dependent data seen in **Figure 4.12**, and previous literature values, while holding  $k_4$ - $k_9$  constant. Then, the L/t and t/t FRET traces were all fit to the global Scheme 4.1 while holding the early steps constant ( $k_1$ - $k_3$ ). For each complex tested (A, B, and C) the L/t and t/t data fit to the scheme showed that the majority of deacylated-tRNA was released via 1 of 3 different pathways (**bold**), with a slower release resulting from heterogeneity in the sample (**red**).

<b>Fig</b>	<b>Exp.</b>	<b>FA</b>	<b>FC</b>	<b>FD</b>	<b>FE</b>	<b>FF</b>	<b>FG</b>	<b>FH</b>
<b>4.12</b>	L/t	4.0*	3.9 ±	2.2 ±	2.3 ±	n.d.	n.d.	n.d.

<b>A</b>	0.5 $\mu$ M		0.4	0.3	0.4			
	1.0 $\mu$ M	4.0*	5.7 $\pm$ 0.2	2.3 $\pm$ 0.2	2.4 $\pm$ 0.2	n.d.	n.d.	n.d.
	2.0 $\mu$ M	4.0*	6.0 $\pm$ 0.2	3.2 $\pm$ 0.2	2.8 $\pm$ 0.2	n.d.	n.d.	n.d.
	5.0 $\mu$ M	4.0*	5.7 $\pm$ 0.1	3.7 $\pm$ 0.1	3.0 $\pm$ 0.1	n.d.	n.d.	n.d.
<b>4.12 B</b>	L/t 1.0 $\mu$ M	4.0*	4.01 $\pm$ 0.02	4.02 $\pm$ 0.01	3.76 $\pm$ 0.01	n.d.	n.d.	2.17 $\pm$ 0.01
	5.0 $\mu$ M	4.0*	4.08 $\pm$ 0.01	4.03 $\pm$ 0.01	3.85 $\pm$ 0.01	n.d.	n.d.	2.62 $\pm$ 0.01
<b>4.12 C</b>	L/t 0.5 $\mu$ M	4.0*	4.03 $\pm$ 0.05	4.09 $\pm$ 0.01	4.11 $\pm$ 0.02	n.d.	n.d.	10 $\pm$ 0.3
	1.0 $\mu$ M	4.0*	4.03 $\pm$ 0.03	3.97 $\pm$ 0.01	4.16 $\pm$ 0.01	n.d.	n.d.	12 $\pm$ 0.3
	2.0 $\mu$ M	4.0*	3.96 $\pm$ 0.02	4.01 $\pm$ 0.01	4.17 $\pm$ 0.02	n.d.	n.d.	14 $\pm$ 0.3
	5.0 $\mu$ M	4.0*	4.28 $\pm$ 0.02	3.98 $\pm$ 0.01	4.01 $\pm$ 0.01	n.d.	n.d.	7.5 $\pm$ 0.3
<b>4.13 A</b>	L/t	4.0*	4.0*	4.0*	4.0*	2.95 $\pm$ 0.03	n.d.	2.6 $\pm$ 0.1
	t/t	4.07 $\pm$ 0.02	3.74 $\pm$ 0.06	4.09 $\pm$ 0.03	3.76 $\pm$ 0.03	3.48 $\pm$ 0.03	n.d.	3.1 $\pm$ 0.1
<b>4.13 B</b>	L/t	4.0*	4.0*	4.0*	4.0*	n.d.	n.d.	n.d.
	t/t	4.00 $\pm$ 0.01	3.93 $\pm$ 0.03	3.88 $\pm$ 0.01	3.78 $\pm$ 0.01	n.d.	n.d.	n.d.
<b>4.13 C</b>	L/t	4.0*	4.0*	4.0*	4.0*	n.d.	3.93 $\pm$ 0.01	3.32 $\pm$ 0.02
	t/t	4.00 $\pm$ 0.01	4.01 $\pm$ 0.01	3.89 $\pm$ 0.01	3.75 $\pm$ 0.01	n.d.	n.d.	n.d.

\*Fixed values



### **Table 4.5 Fluorescence Values for Global Fits**

Fluorescence values of traces fit to global **Scheme 4.1**. In the table above, the complexes that are n.d. (not determined) are complexes that don't build up during the course of the reaction.

Figure	Experiment	Buffer	PRE FRET Efficiency Value ( $t_0$ )	Apparent POST FRET Efficiency Value ( $t_{10s}$ )
4.1	Equil; HC; L/t	A	0.7	0
4.2	Equil; HC; L/t	B	0.9	0.5
4.4, 4.8	SF; HC; L/t	A	1.0	0
4.4, 4.6, 4.10	SF; HC; L/t	B	0.95	0.53
4.6, 4.10	SF; UC; L/t	B	0.93	0.55*
4.7	Equil; HC; t/t	B	0.53	0
4.9, 4.10A	SF; HC; t/t	B	0.52	0.15
4.9, 4.10B,C	SF; UC; t/t	B	0.91	0.07
4.12 A	SF; HC; L/t (5 uM EF.G)	A	0.80/1.0**	0.12
4.12 B	SF; HC; L/t (5 uM EF.G)	B	0.95/0.96**	0.46
4.12 C	SF; UC; L/t (5 uM EF.G)	B	0.93/0.97**	0.6****
Chen et al, (submitted)	sm FRET t/t	-	0.5	
Fei et al., (2008)	sm FRET L/t	PA	0.8	0.8
Stevens et al., (submitted)	sm FRET L/t	TAM15	0.5	0.75

**Abbreviations:** Equil: Equilibrium FRET; SF: Stopped Flow FRET; HC: Starting with highly charged fMet-tRNA<sup>fMet</sup>; UC: Starting with uncharged tRNA<sup>fMet</sup>; smFRET: Single Molecule FRET; PA: Polyamine Buffer (polyamines, and 15 mM Mg<sup>2+</sup>); TAM15: 20

mM Tris-HCl (pH 7.5), 15 mM Mg(OAc)<sub>2</sub>, 30 mM NH<sub>4</sub>Cl, 70 mM KCl, 0.75 mM EDTA, 1 mM DTT, 0.2% (w/v) Tween 20.

\*POST fluorescence value for FRET calculation was taken at t= 90s.

\*\* X/Y, where X is the FRET at t=0 and Y is the FRET at the peak of the increase, in B, the change in FRET value may not be significant.

\*\*\*POST fluorescence value for FRET calculation was taken at t= 30s

**Table 4.6 FRET Efficiency Measurements for Equilibrium FRET and Stopped Flow FRET in PRE-1 and POST-1 States.**

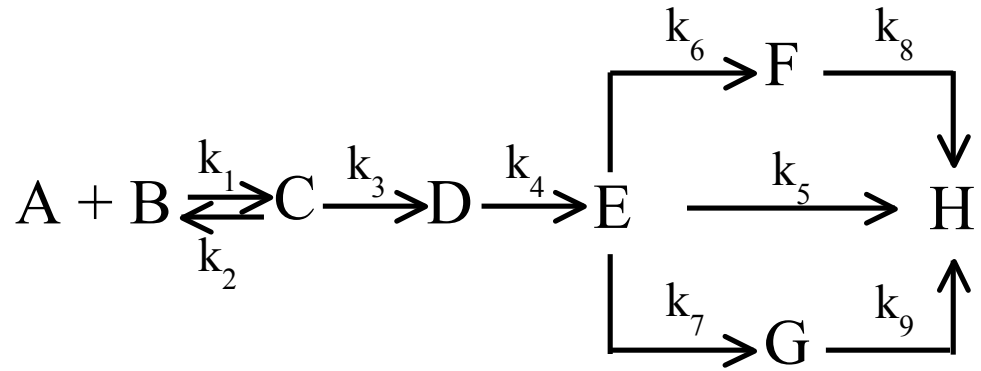
It is possible to obtain FRET efficiency measurements the experiments presented here. The equilibrium FRET calculation is done as shown in [Table 4.1](#). To obtain FRET efficiency measurements from stopped flow data, the PRE-1 state is defined at t = 0s, before EF-G.GTP is added:

$$PRE\_FRET = \frac{D^* A^*_{(t0)} - DA^*_{(t0)}}{DA^*_{(t0)}} \times \left( \frac{1}{DonorEfficiency} \right)$$

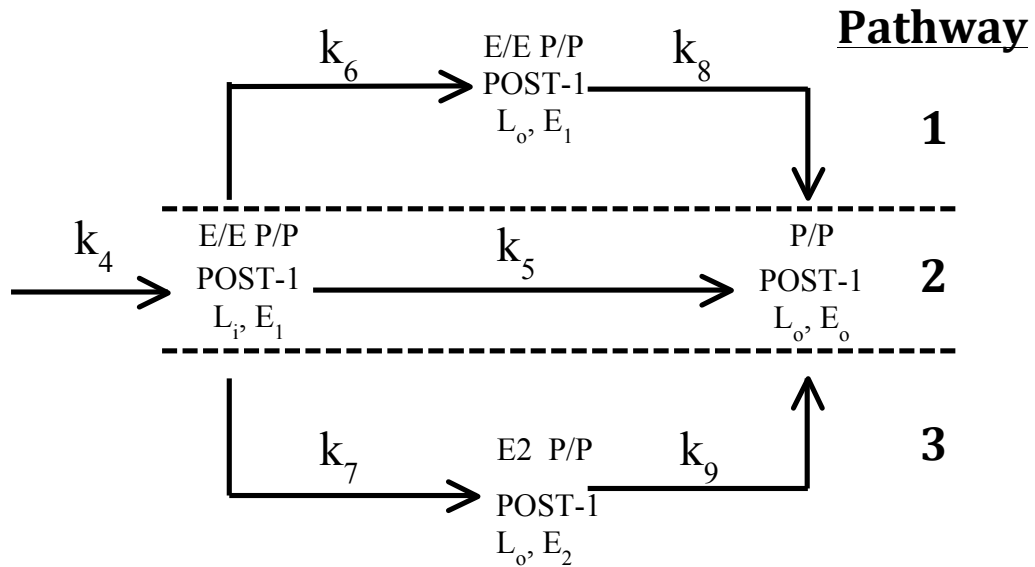
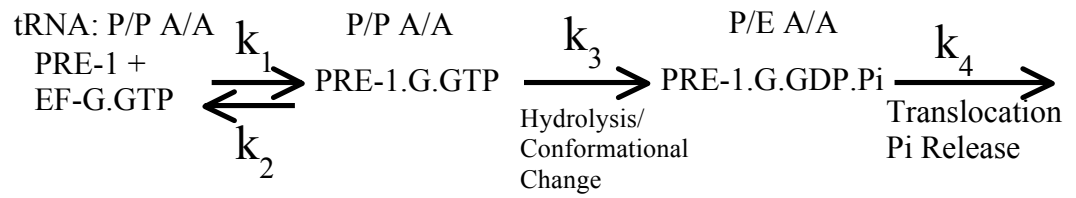
$$POST\_FRET = \frac{D^* A^*_{(tx)} - DA^*_{(tx)}}{DA^*_{(tx)}} \times \left( \frac{1}{DonorEfficiency} \right)$$

Where, D\*A\* is a sample containing both donor and acceptor dyes, and DA\* is a sample containing only the acceptor dye. The POST FRET efficiency is calculated similarly, using times after the translocation has occurred.

A.



B.



## **Scheme 4.1 Global Scheme for Deacylated-tRNA Release From a Translocated Ribosome**

**A)** The L/t and t/t FRET data that was originally fit to triple exponential curves (Figures 4.8 and 4.10), was fit to this global scheme using Scientist. Further, EF-G concentration dependent L/t FRET data was used to help find the rate constants associated with EF-G binding ( $k_1$  and  $k_2$ ) and hydrolysis/conformational change  $k_3$ . With these rate constants known,  $k_4$  through  $k_9$  were determined by fitting the L/t and t/t FRET traces for each complex to the scheme, and the pathway for deacylated-tRNA release was elucidated from these fits. **B)** The same scheme as A, but with the corresponding states of the ribosome and tRNA.  $L_i$ : L1-stalk “in”;  $L_o$ : L1-stalk “out”;  $E_1$ : deacylated-tRNA in the E site;  $E_2$ : deacylated-tRNA in the E2 site; and  $E_o$ : deacylated-tRNA off the ribosome.

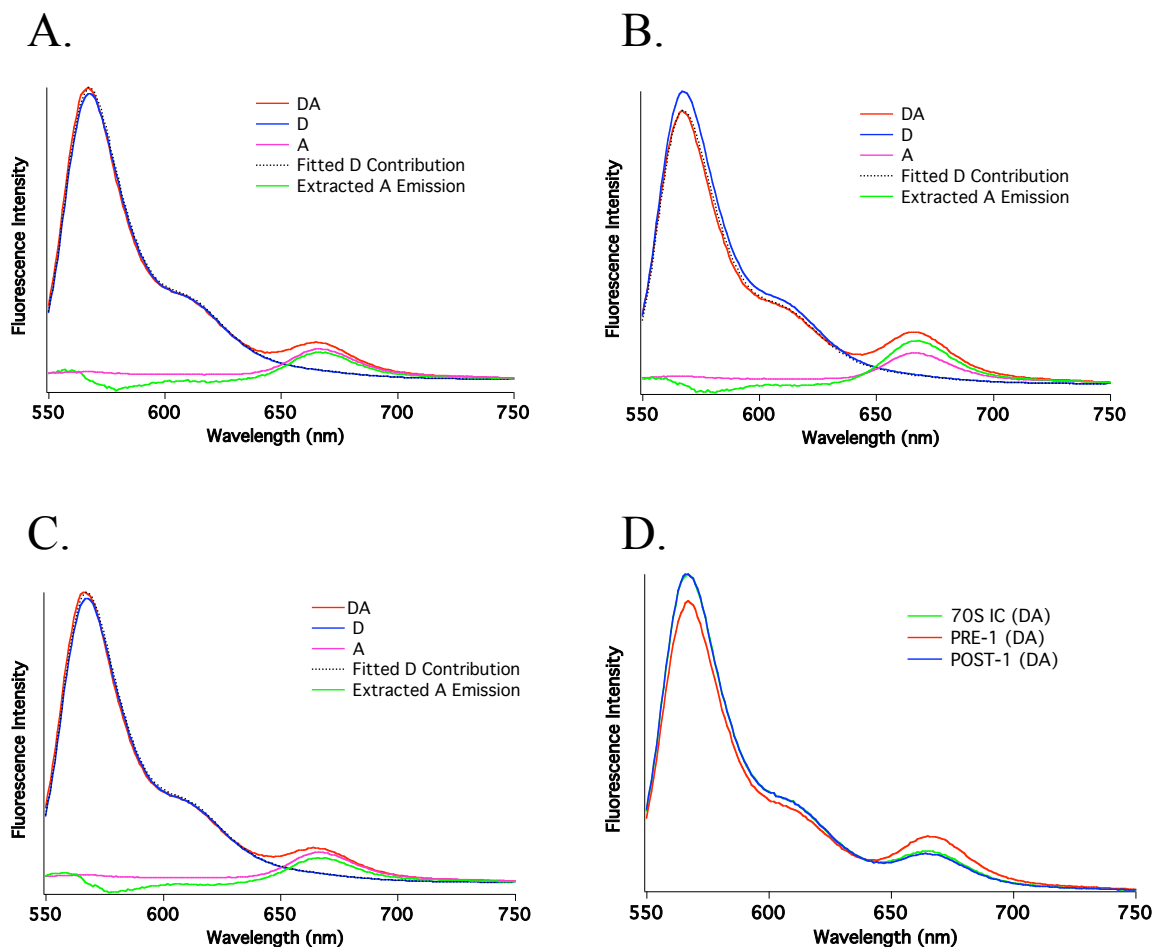


**Figure 4.1 Equilibrium FRET Efficiency Changes in Buffer A**

70SICs were made for FRET analysis using fMet-tRNA<sup>Met</sup> (Cy3) as the donor and T202C-L1-50S (Cy5) as the acceptor, and purified through a sucrose cushion. Equilibrium FRET measurements were taken using a spectrofluorometer to determine the FRET efficiency at different stages of translocation (**A: 70SIC** (0.1  $\mu$ M), **B: PRE-1** (70SIC + Phe-tRNA<sup>Phe</sup>.EF-Tu.GTP (0.25  $\mu$ M)), **C: POST-1** (70SIC + Phe-tRNA<sup>Phe</sup>.EF-Tu.GTP (0.25  $\mu$ M) + EF-G.GTP (0.25  $\mu$ M))). The samples were excited at 518 nm and FRET efficiency was measured as acceptor fluorescence change at 667 nm. D\*A\*, D\*A, DA\*, and DA samples were prepared for each complex, and the DA background was

subtracted for all samples prior to analysis. Fitted D contribution and extracted A emission were determined for each stage, and the efficiency of energy transfer was determined by equation 2.2. The DA samples are plotted together for each ribosome complex in **D**.

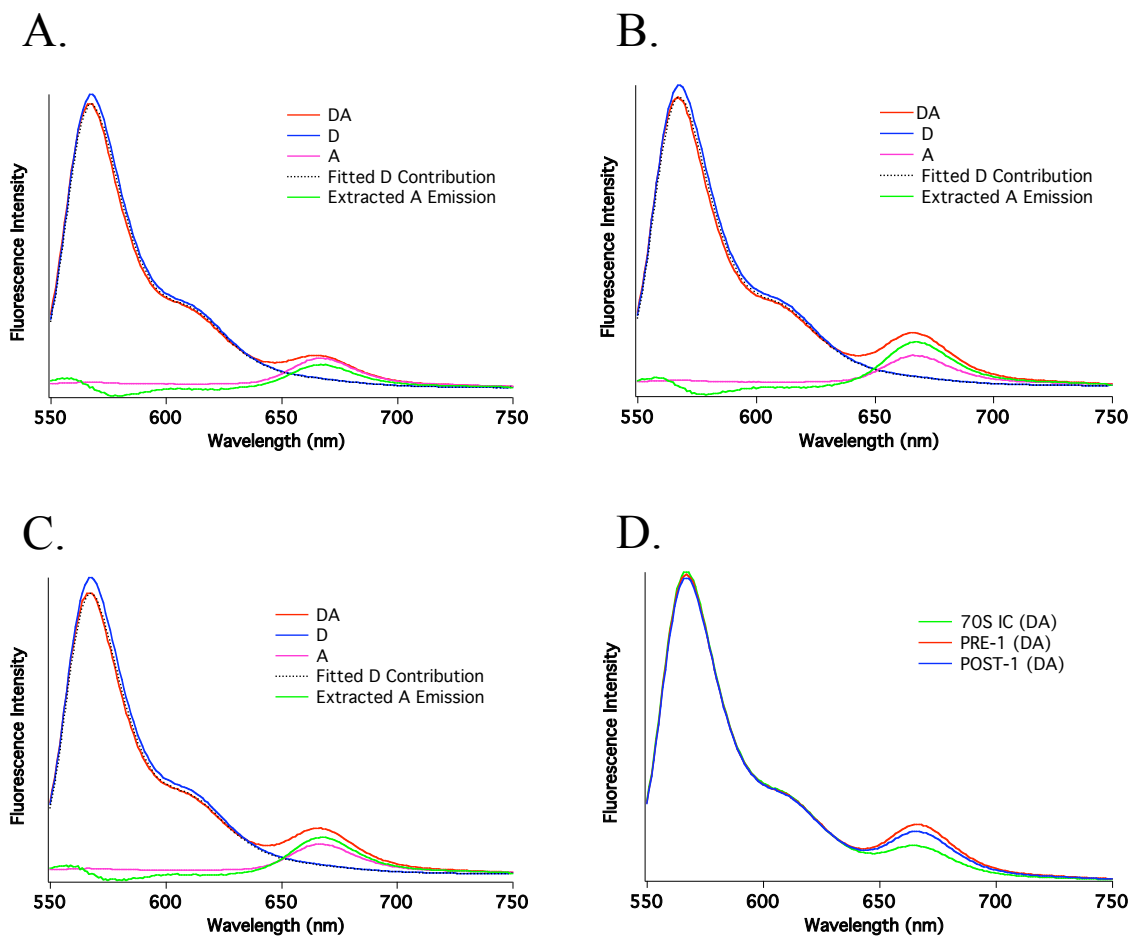


**Figure 4.2 Equilibrium FRET Efficiency Changes in Buffer B**

Complexes were made and analyzed in the same way as Figure 4.1, except they were made in Buffer B. Notice in **C and D** that the FRET efficiency is not completely lost due to the rebinding of deacylated-tRNA to the E-site in Buffer B.

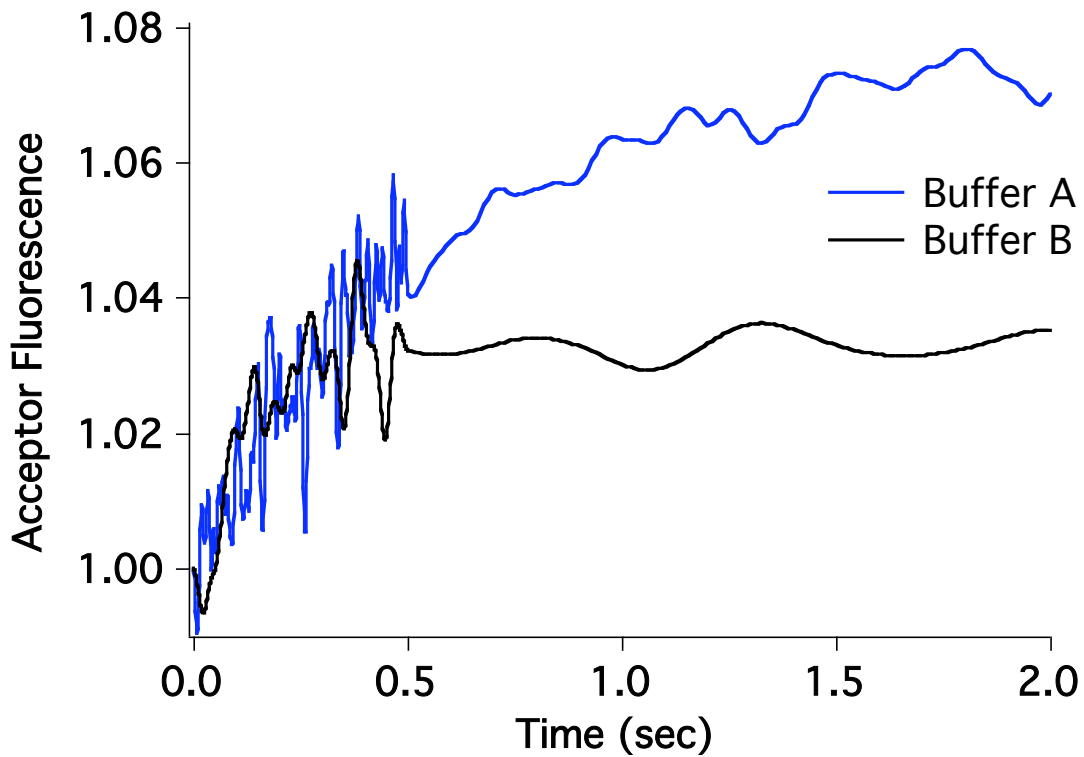


**Figure 4.3 FRET Efficiency Increase Associated with PRE-1 Formation**

70SIC was created in either Buffer A or Buffer B with highly charged fMet-tRNA<sup>fMet</sup> (Cy3) and T202C-L1 (Cy5) ribosomes. Phe-tRNA<sup>Phe</sup>.EF-Tu.GTP ternary complex (0.5  $\mu$ M for Buffer A, and 1.0  $\mu$ M for Buffer B) was stopped flow added to the 70S IC (0.25  $\mu$ M). tRNA<sup>fMet</sup> (Cy3) in the PRE-1 complex was excited at 540 nm and the emission of the Cy5 acceptor was monitored at  $680 \pm 10$  nm to determine FRET efficiency change, and is seen here.



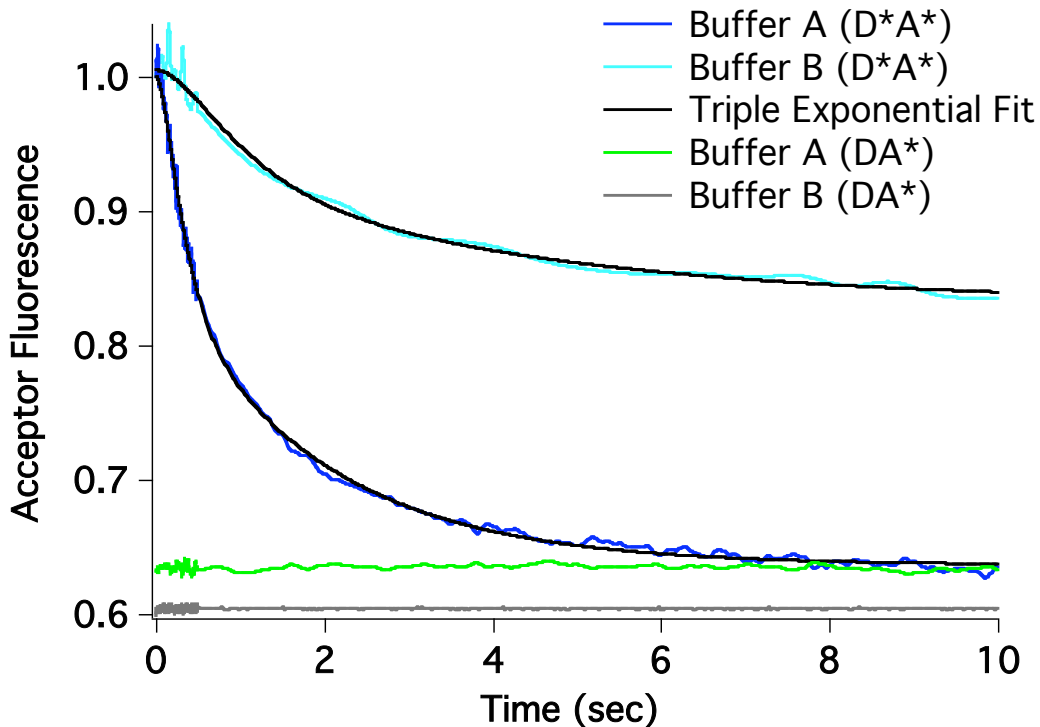


**Figure 4.4 L/t FRET Efficiency Change Upon Translocation in Buffer A and Buffer B**

1.0  $\mu\text{M}$  EF-G.GTP was rapidly mixed in a stopped flow spectrophotometer with a PRE-1 complex (0.25  $\mu\text{M}$ ) that was created from a 70SIC containing highly charged fMet-tRNA<sup>fMet</sup> (Cy3) and T202C-L1 (Cy5) ribosomes in Buffer A or B. tRNA<sup>fMet</sup> (Cy3) in the PRE-1 complex was excited at 540 nm and the emission of the Cy5 acceptor was monitored at  $680 \pm 10$  nm to determine FRET efficiency change. D\*A\* samples contain both Cy5 and Cy3 labels, whereas DA\* samples contain only Cy5. Background (DA) traces were subtracted from all samples, and the D\*A\* samples were normalized to 1.0. The DA\* samples were compensated for the normalization by dividing by the D\*A\* fluorescence at time 0. After  $\sim 10$  s in Buffer A, tRNA is completely released from the

ribosome resulting in no FRET; however, in Buffer B, FRET remains due to the equilibrium established between release and rebinding of deacylated-tRNA. The D\*A\* traces were both fit to a triple exponential curve using Scientist.

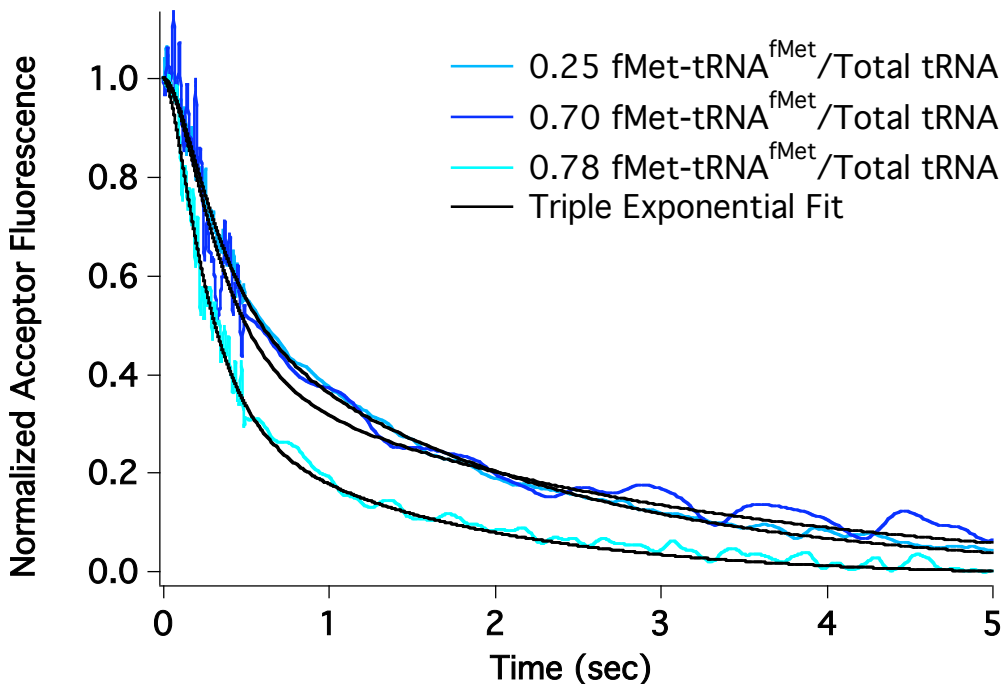


**Figure 4.5 L/t FRET Efficiency Change Upon Translocation in Buffer A**

1.0  $\mu\text{M}$  EF-G.GTP was rapidly mixed in a stopped flow spectrophotometer with a PRE-1 complex (0.25  $\mu\text{M}$ ) that was made from 70SIC complexes containing fMet-tRNA<sup>fMet</sup> (Cy3) charged to different levels, and ribosomes containing T202C-L1 (Cy5) 50S in Buffer A. tRNA<sup>fMet</sup> (Cy3) in the PRE-1 complex was excited at 540 nm and the emission of the Cy5 acceptor was monitored at  $680 \pm 10$  nm to determine FRET efficiency change. The FRET efficiency changes were fit to a triple exponential curve

using Scientist. Unlike Buffer B, the level of charging efficiency of the initiator tRNA does not affect the apparent rate constant of the major FRET change in Buffer A.

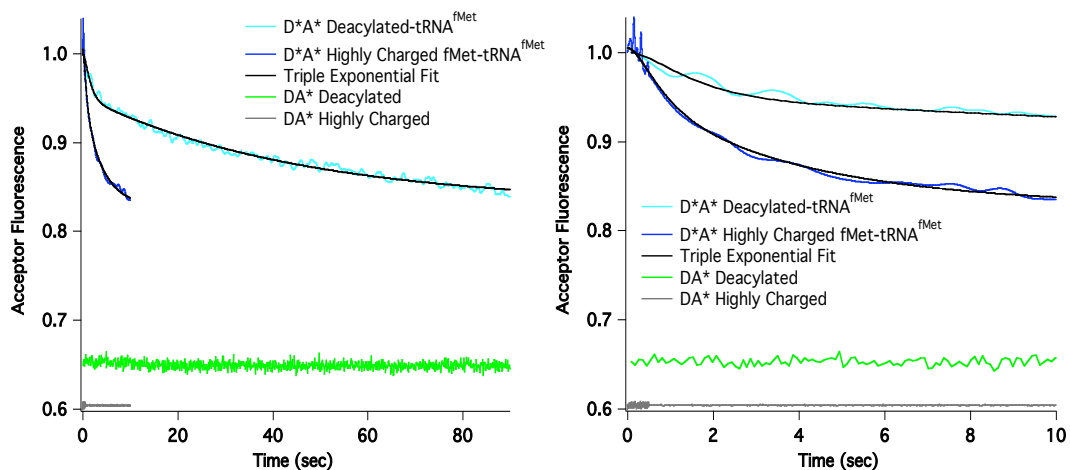


**Figure 4.6 L/t FRET Efficiency Change Upon Translocation in Buffer B**

1.0  $\mu\text{M}$  EF-G.GTP was rapidly mixed in a stopped flow spectrophotometer with a PRE-1 complex (0.25  $\mu\text{M}$ ) that was made from 70SIC complexes containing either highly charged fMet-tRNA<sup>fMet</sup> (Cy3) or deacylated-tRNA<sup>fMet</sup> (Cy3), and ribosomes containing T202C-L1 (Cy5) 50S in Buffer B. tRNA<sup>fMet</sup> (Cy3) in the PRE-1 complex was excited at 540 nm and emission was measured at  $570 \pm 10$  nm. The emission of the Cy5 acceptor was monitored at  $680 \pm 10$  nm and is shown here fitted to a triple exponential curve using Scientist. Acceptor alone (DA\*) samples are also shown to indicate the FRET Efficiency = 0 fluorescence.

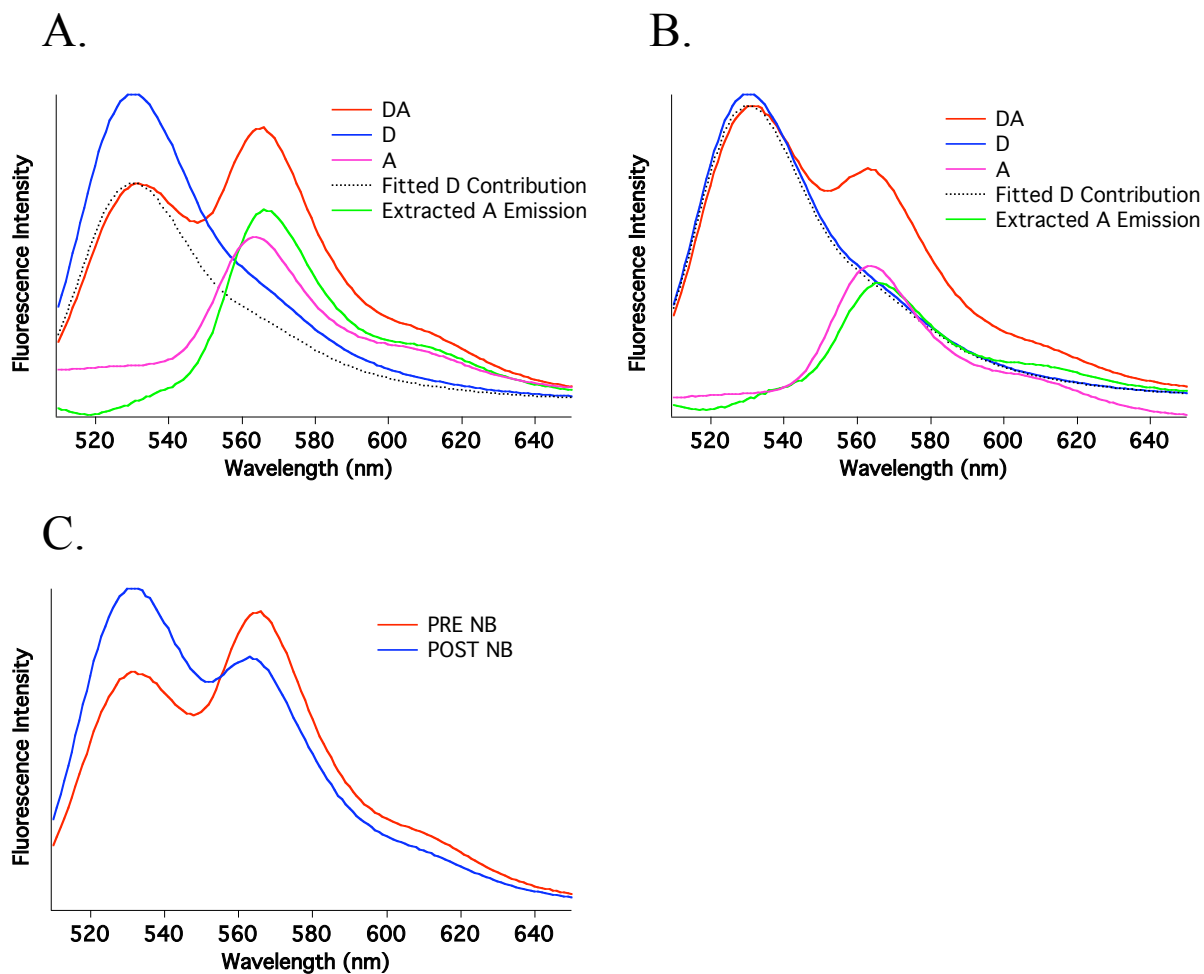


**Figure 4.7 t/t Equilibrium FRET Change in Buffer B**

PRE-1 complexes were made for FRET analysis using Phe-tRNA<sup>Phe</sup> (Rhd110) as the donor and fMet-tRNA<sup>fMet</sup> (Cy3) as the acceptor, and purified through a sucrose cushion. Equilibrium FRET measurements were taken using a spectrofluorometer to determine the FRET efficiency at different stages of translocation (**A: PRE-1** (0.1 μM), **B: POST-1** (PRE-1 + EF-G.GTP (0.25 μM)). The samples were excited at 480 nm and FRET efficiency was measured as acceptor fluorescence change at 567 nm. D\*A\*, D\*A, DA\*, and DA samples were prepared for each complex, and the DA background was

subtracted for all samples prior to analysis. Fitted D contribution and extracted A emission were determined for each stage, and the efficiency of energy transfer was determined by equation 2.2. The DA samples are plotted together for each ribosome complex in C.

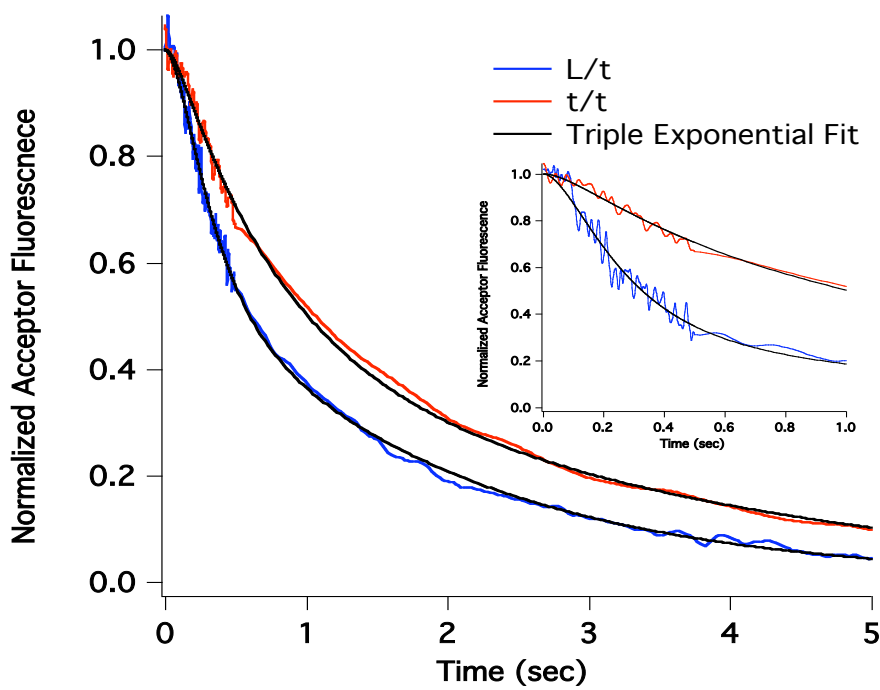


**Figure 4.8 L/t and t/t FRET Efficiency Change in Buffer A**

The L/t FRET efficiency change is monitored as described in Figure 4.2. For the t/t FRET experiments, 1.0  $\mu\text{M}$  EF-G.GTP was rapidly mixed with 0.25  $\mu\text{M}$  PRE-1 complex that was made from a 70SIC complex containing highly charged fMet-tRNA<sup>fMet</sup> (Cy3), Phe-tRNA<sup>Phe</sup> (Rhd110), and T202C-L1 50S ribosomes. The donor fMet-Phe-tRNA<sup>Phe</sup> (Rhd110) was excited at 480 nm and emission was measured at  $525 \pm 10$  nm,

the acceptor emission was monitored at  $570 \pm 10$  nm and is shown here. The L/t FRET was fit to a triple exponential curve as seen in Figure 4.2, and the t/t was also fit to a triple exponential using Scientist.

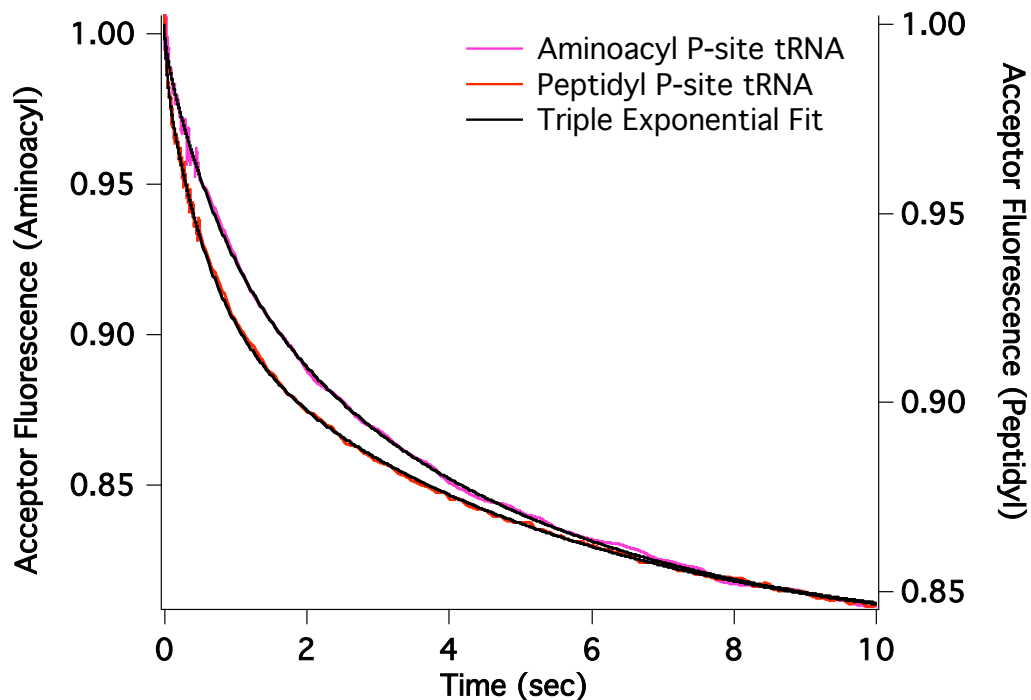


**Figure 4.9 t/t FRET Efficiency Change Upon Translocation in Buffer B**

For the t/t FRET experiments,  $0.25 \mu\text{M}$  PRE-1 complex made from a 70SIC containing either highly charged fMet-tRNA<sup>fMet</sup> (Cy3) or deacylated-tRNA<sup>fMet</sup> (Cy3), Phe-tRNA<sup>Phe</sup> (Rhd110), and T202C-L1-50S ribosomes. The PRE-1 complex was rapidly mixed with  $1.0 \mu\text{M}$  EF-G.GTP in a stopped flow experiment. The donor (fMet)-Phe-tRNA<sup>Phe</sup> (Rhd110) was excited at  $480$  nm and emission was measured at  $525 \pm 10$  nm,

the acceptor emission was monitored at  $570 \pm 10$  nm and is shown here. The t/t FRET efficiency changes were both fit to a triple exponential curve using Scientist.

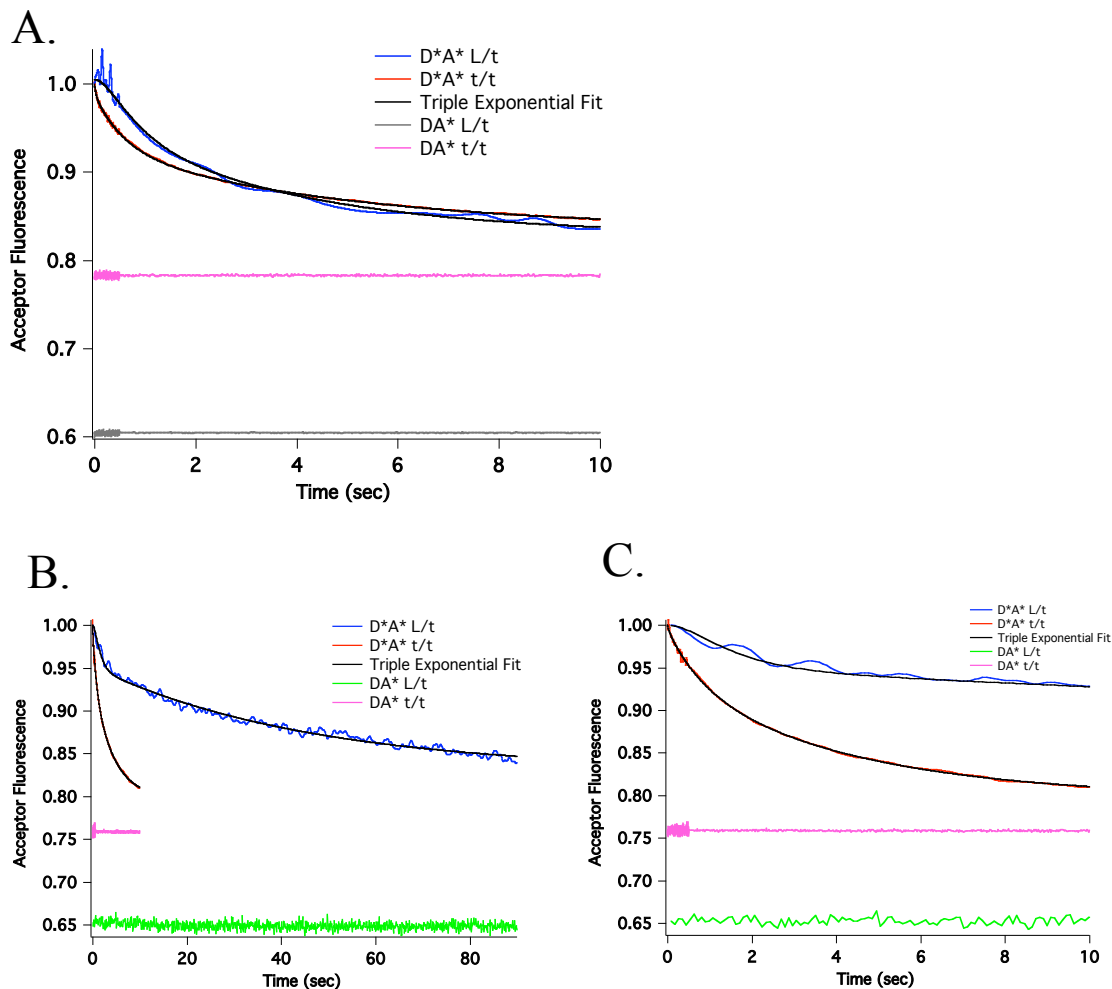


**Figure 4.10 L/t and t/t FRET Efficiency Change in Buffer B**

The complexes used in the L/t FRET experiments are made, and the efficiency change is monitored as described in [Figure 4.6](#). For the t/t FRET experiments,  $1.0 \mu\text{M}$  EF-G.GTP was rapidly mixed with  $0.25 \mu\text{M}$  PRE-1 complex made from a 70SIC containing highly charged fMet-tRNA<sup>fMet</sup> (Cy3) (**A**) or deacylated-tRNA<sup>fMet</sup> (Cy3) (**B and C**), and T202C-L1-50S ribosomes. The donor (fMet)-Phe-tRNA<sup>Phe</sup> was excited at

480 nm and emission was measured at  $525 \pm 10$  nm, the acceptor emission was monitored at  $570 \pm 10$  nm and is shown here. Acceptor alone (DA\*) samples are also shown to indicate the FRET Efficiency = 0 fluorescence. The L/t FRET efficiency changes were fit to a triple exponential curve as in Figure 4.4, and the t/t FRET efficiency changes were also fit to a triple exponential curve using Scientist.

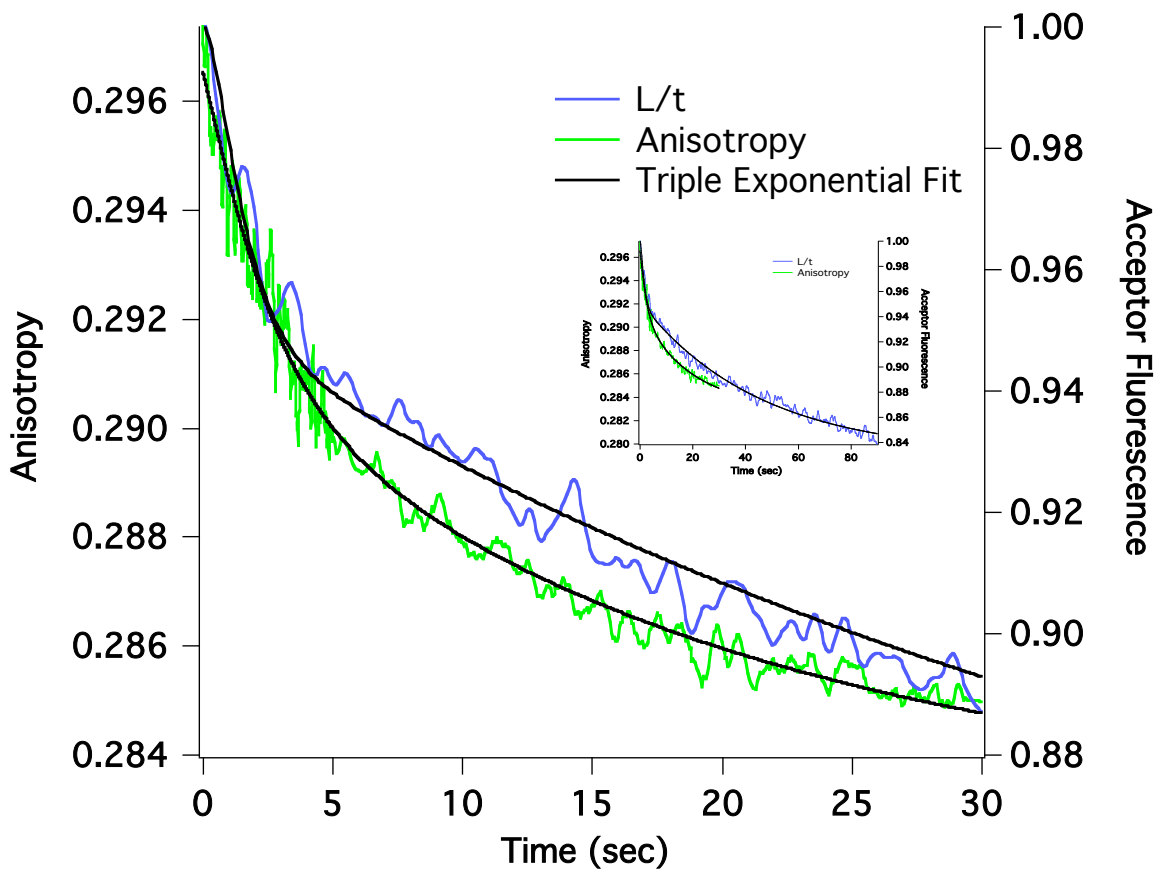
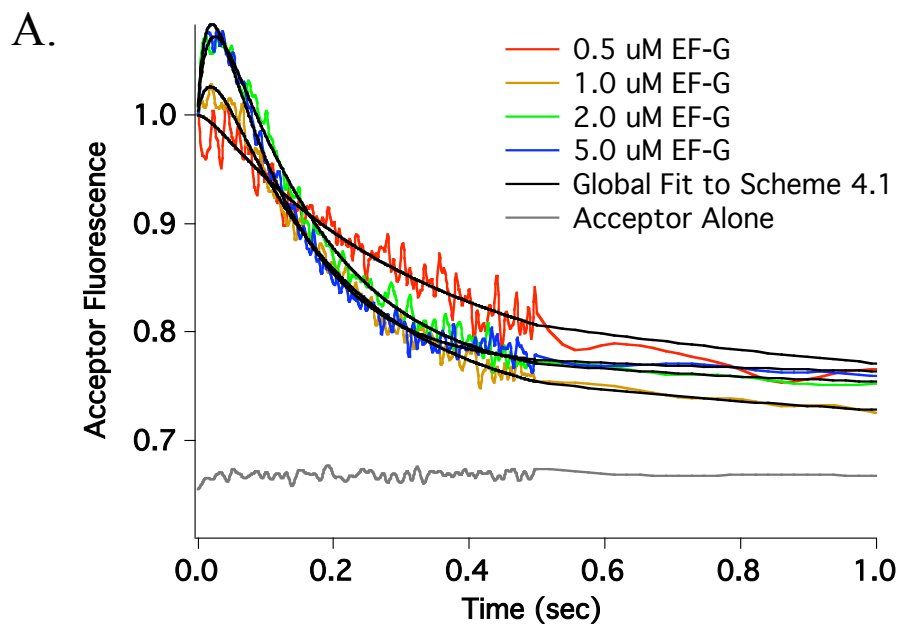


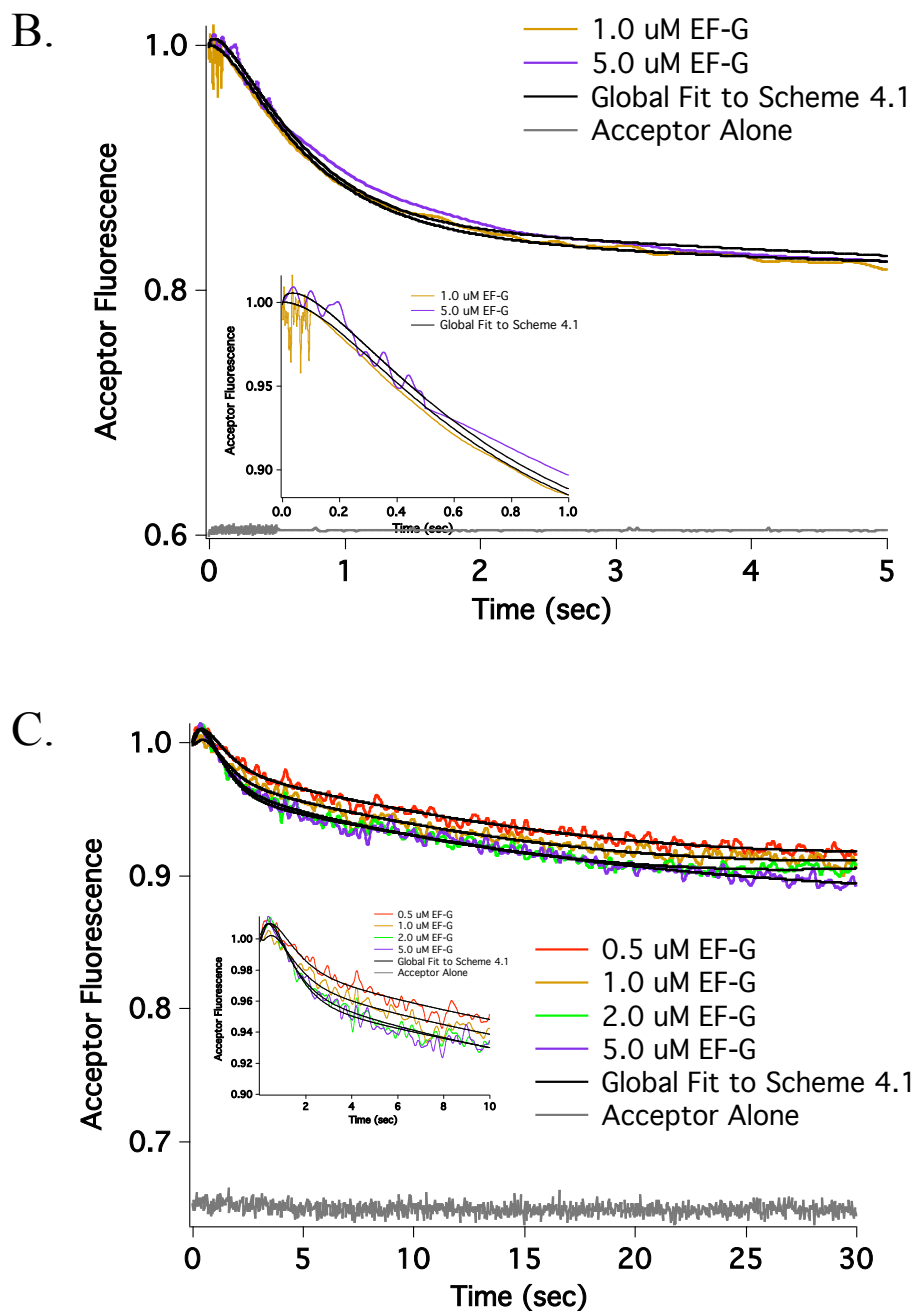
**Figure 4.11 tRNA Release Measured by L/t FRET and Anisotropy Change**

To measure the L/t FRET efficiency change,  $1.0 \mu\text{M}$  EF-G.GTP was rapidly mixed in a stopped flow spectrophotometer with a PRE-1 complex ( $0.25 \mu\text{M}$ ) that was made from 70SIC complexes containing deacylated-tRNA<sup>fMet</sup> (Cy3), and ribosomes



containing T202C-L1 (Cy5) 50S in Buffer B. The resulting trace was fit to a triple exponential using Scientist. For anisotropy change experiments, 1.5  $\mu\text{M}$  EF-G.GTP was rapidly mixed with 0.25  $\mu\text{M}$  PRE-1 complex made from a 70SIC containing deacylated-tRNA<sup>Met</sup> (Cy3), and unlabeled T202C-L1-50S ribosomes in Buffer B. Anisotropy change was measured using a polarizing excitation at 540 nm, and monitored with polarizers on the PMT at  $570 \pm 10$  nm; the changes were fit to a triple exponential curve. It should be noted that the L/t FRET efficiency change was monitored when 1.0  $\mu\text{M}$  EF-G.GTP was added to 0.25  $\mu\text{M}$  PRE-1 complex, whereas 1.5  $\mu\text{M}$  EF-G.GTP was added to the PRE-1 complex for the anisotropy experiments. However, as seen in (Figure 4.12) EF-G concentration does not significantly affect the release of deacylated-tRNA.

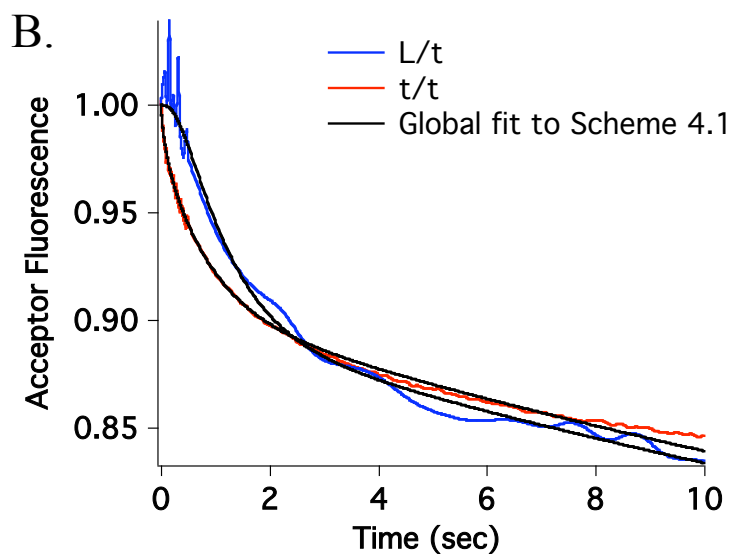
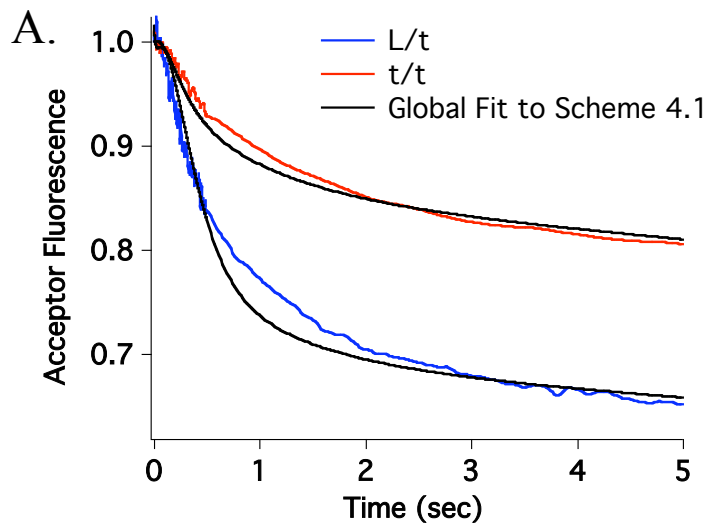




**Figure 4.12 EF-G Concentration Dependent L/t FRET Efficiency Change**

The L/t FRET efficiency change is monitored for PRE-1 complexes that were made from 70SIC complexes containing either highly charged fMet-tRNA<sup>fMet</sup> (Cy3) (**A and B**), or deacylated-tRNA<sup>fMet</sup> (Cy3) (**C**), and T202C-L1 (Cy5) ribosomes in either

Buffer A (**A**) or Buffer B (**B and C**). Acceptor alone ( $DA^*$ ) samples are also shown to indicate the FRET Efficiency = 0 fluorescence. In all three conditions, the FRET efficiency changes were fit to global **Scheme 4.1**, where  $k_4$  through  $k_9$  were held constant, while  $k_1$  through  $k_3$  were fit under these conditions.



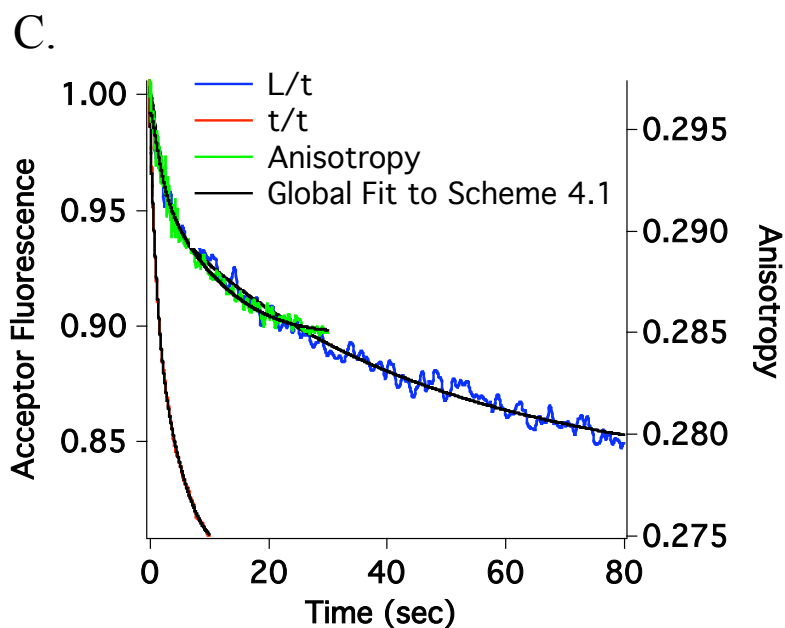


**Figure 4.13 Global Fitting of L/t and t/t FRET Traces and Anisotropy**

The traces shown in kinetic FRET experiments above were initially fit to triple exponential curves with the apparent rate constants seen in [Table 4.2](#). Here, those traces were fit to the global [Scheme 4.1](#) and followed different pathways for deacylated tRNA release depending on the ribosome complex and buffer conditions. **A)** 1.0  $\mu\text{M}$  EF-G.GTP was added to 0.25  $\mu\text{M}$  PRE-1 complexes in Buffer A as described in [Figure 4.8](#); **B)** 1.0  $\mu\text{M}$  EF-G.GTP was added to 0.25  $\mu\text{M}$  PRE-1 complexes as described in [Figures 4.10 A](#); **C)** 1.0  $\mu\text{M}$  EF-G.GTP was added to 0.25  $\mu\text{M}$  PRE-1 complexes as described in [Figures 4.10 B/C](#). Both the L/t and t/t FRET traces for each complex were fit to the Scheme to elucidate the major pathway for deacylated-tRNA release. The fluorescence anisotropy trace was created as in [Figure 4.11](#), and also fit to the Scheme. Complexes from **A** mostly followed pathway 1, with a less significant and slower release via pathway 2. Complexes

from **B** followed pathway 2, and complexes from **C** mostly followed pathway 3, with a less significant release via pathway 2 as well.

**Chapter V: Addition of Deacylated-tRNA in Solution  
Enhances the Slow Release of Translocated Deacylated-  
tRNA<sup>fMet</sup>**

## 5.1 Abstract

The ribosomes which follow pathway 3 described in Chapter IV have an apparent problem to overcome in that the deacylated-tRNA remains bound to the E2-site for too long to be viable *in vivo*. However, the above experiments were done in conditions in which there were no outside factors competing for the tRNA binding site, or ternary complexes binding to the A-site. It is possible that deacylated-tRNA in solution can compete for the E2-site, and/or ternary complex binding to the A-site could allosterically affect the release of tRNA from the E/E2-site. Here, it is shown that there is indeed a competition between deacylated-tRNAs for binding to the ribosome that affects the release of tRNA. Further, this competition, rather than an allosteric interaction between A- and E-sites, seems to provide the major affect on deacylated-tRNA release.

## 5.2 Introduction

In Chapter IV it was shown that tRNA could leave the E-site of the ribosome via three different pathways, each one distinct in the movement of the L1-stalk in relation to the deacylated-tRNA. The first two pathways show that deacylated-tRNA<sup>fMet</sup> can dissociate from the ribosome at a reasonable rate ( $\sim 1-2 \text{ s}^{-1}$ ); however, the third pathway holds the deacylated-tRNA<sup>fMet</sup> in what is presumed to be the E2-site as seen in cryo-EM images (Agrawal et al., 1999; Fischer et al., 2010). Although it would be troublesome for a translating ribosome to only slowly release a translocated

tRNA, one must remember that in the above experiments, there were no deacylated-tRNAs, and no additional ternary complexes present. *In vivo* there is on the order of 200  $\mu$ M tRNA (**Dong et al., 1996**), and available ternary complex ready to continue translation. Therefore, it is possible that, even though the ribosomes following pathway 3 (Chapter 4) appear to hold onto the deacylated-tRNA for an excessively long time, *in vivo* the deacylated-tRNA<sup>fMet</sup> is in an equilibrium between bound and unbound states, and this equilibrium can be affected by competition between other deacylated-tRNAs present in the cell.

In order to test whether or not the dissociation of deacylated-tRNA<sup>fMet</sup> from ribosomes following pathway 3 is affected by the presence of deacylated-tRNA in the solution, POST-1 complexes were prepared in conditions that favor pathway 3. Such complexes were rapidly mixed with various concentrations of deacylated-tRNA<sup>Lys</sup> or tRNA<sup>Tyr</sup>, and the changes in fluorescence were recorded in a stopped flow spectrofluorometer. Both the loss of FRET between T202C-L1 (Cy5) and translocated tRNA<sup>fMet</sup> (Cy3), and the gain of FRET between T202C-L1 (Cy5) and added tRNA<sup>Lys</sup> (Cy3) were measured in order to determine if there were indeed a competition for the apparent E2-site. According to the cryo-EM images, there should be no codon-anticodon interaction with tRNAs in the E2-site. Therefore, we tested the codon dependence of the competition between the deacylated-tRNA<sup>fMet</sup> (Cy3) and the added deacylated-tRNAs.

Further, the supposed allosteric interaction between the A-site and the E-site as first proposed by Nierhaus and colleagues (**Rheinberger and Nierhaus, 1986**),



and as later seen in single molecule work by Chen and colleagues (**Chen et al., submitted manuscript**) was tested under these conditions. The presence of an allosteric interaction between an A-site and E-site by way of negative cooperativity would allow better accuracy of selection of aminoacyl-tRNAs while preventing binding of non-cognate codons in the decoding process. Further, by constantly maintaining 2 codon-anticodon interactions, it may help keep the messenger RNA in frame during translation (**Nierhaus, 1990; Rheinberger, 1991**). The criticism against interpreting the results of Rheinberger and Nierhaus as reflecting an allosteric interaction was that the release of translocated E-site tRNA was coming from a competition with deacylated-tRNA in the solution (**Robertson and Wintermeyer, 1987**). Here, we find that deacylated-tRNA in solution does indeed provide the major affect on the release of tRNA; however, there is possibly a small additional affect when ternary complex is also added, presumably via binding to the A-site.

In the preliminary work presented here, it appears that there is a competition between deacylated-tRNA for a site near the labeled L1 that is not codon dependent. However, the data here have yet to be incorporated into a general kinetic scheme, and further work needs to be completed in order to determine the exact mechanism for this competition.

## 5.3 Results

### 5.3.1 Preparation of a POST-1 Complex

Unless otherwise specified, T202C-L1 (Cy5) POST-1 complexes were made in Buffer B for the following experiments, starting with 70SICs containing deacylated-tRNA<sup>fMet</sup> (Cy3). Addition of EF-Tu.GTP.Phe-tRNA<sup>Phe</sup> and EF-G.GTP resulted in POST-1 complexes that were purified through sucrose to remove any excess factors and tRNA (Section 2.2.5.4). Table 5.1 presents the binding efficiencies for the tRNA<sup>fMet</sup> (Cy3) to the ribosome, in what is assumed to be the E2-site, and Phe-tRNA<sup>Phe</sup> to the P-site in the purified complexes; further, to ensure the complexes are indeed POST-1, puromycin reactivity was tested. The untranslocated PRE-1 complex does not react with puromycin (~0.02 aminoacyl-puro/70S); however, upon addition of EF-G.GTP the resulting POST-1 complex regains reactivity to a level similar to that seen in 70SIC (~0.3 aminoacyl-puro/70S), indicating that the A-site is indeed unoccupied (Table 2.2). A complex created under these conditions should result in the release of deacylated-tRNA following a pathway like pathway 3 in Scheme 4.1 (Refer to 4.3.5.3), where the deacylated-tRNA<sup>fMet</sup> moves away from the body of the ribosome with the L1-stalk before being released. This release from the E2-site, can be affected by the presence of deacylated-tRNAs in the solution. Figure 5.1 presents the binding curve for deacylated-tRNA<sup>fMet</sup> (Cy3) as measured by an increase in T202C-L1 (Cy5) FRET efficiency fluorescence upon addition of

increasing amounts of deacylated-tRNA<sup>fMet</sup> (Cy3) in an equilibrium FRET experiment. The initial amount of fluorescence without any tRNA<sup>fMet</sup> (Cy3) added back (0.0  $\mu$ M) accounts for the fluorescence seen from the translocated-tRNA<sup>fMet</sup> (Cy3). This experiment allowed the estimation of a  $K_D = 0.123 \mu$ M. To ensure E2-site occupancy in the following experiments, the equilibrium was shifted by preincubating the POST-1 complexes with 0.5  $\mu$ M deacylated-tRNA<sup>fMet</sup> (Cy3, unless otherwise specified).

### 5.3.2 The Extent of Competition Depends on the Concentration of the Added Deacylated-tRNA

The FRET efficiency between T202C-L1 (Cy5) on the 50S subunit and deacylated-tRNA<sup>fMet</sup> (Cy3) in the E2-site of a POST-1 complex (0.25  $\mu$ M) was measured as a result of stopped-flow addition of increasing concentrations of tRNA<sup>Lys</sup> (0.0, 0.1, 0.5, 0.75, 1.5, and 3.0  $\mu$ M; **Figure 5.2A**). The curves were fit to either a single or double exponential curve and, **Table 5.2** shows that the apparent rate constant of the major FRET efficiency decrease remains constant at  $\sim 1.5 \text{ s}^{-1}$ , independent of the concentration of deacylated-tRNA<sup>Lys</sup> added to the complex; however, the amplitude of the major FRET efficiency decrease is dependent on the concentration of the added deacylated-tRNA<sup>Lys</sup>. An apparent  $K_D$  of  $\sim 0.15 \mu$ M can be obtained by plotting the amplitude change after 30 sec versus the concentration of added deacylated-tRNA<sup>Lys</sup> (**Figure 5.2 B**, in agreement with the  $K_D$  obtained earlier by different methods using tRNA<sup>fMet</sup>). Further, although the rate constant of the

major change ( $k_{app1} = \sim 1.5 \text{ s}^{-1}$ ) is not affected by concentration (and is even present without addition of  $\text{tRNA}^{\text{Lys}}$ ), at concentrations above  $0.75 \text{ }\mu\text{M}$  the overall change becomes biphasic and introduces a slower ( $k_{app2} = \sim 0.13 \text{ s}^{-1}$ ) change of lesser magnitude.

In order to measure the binding of deacylated-tRNA to the ribosome, a T202C-L1 (Cy5) POST-1 complex was made from 70SICs with unlabeled deacylated-tRNA<sup>fMet</sup>, and purified as previously. In the POST-1 complex, the unlabeled deacylated-tRNA<sup>fMet</sup> is in the E2-site, and to ensure E2-site occupancy  $0.5 \text{ }\mu\text{M}$  unlabeled-tRNA<sup>fMet</sup> was added to the complex. tRNA<sup>Lys</sup> (Cy3) was then added to the T202C-L1 (Cy5) POST-1 complex via stopped flow, and an increase in FRET efficiency was measured when the tRNA<sup>Lys</sup> (Cy3) bound to the ribosome near L1 (Figure 5.3 A). This FRET efficiency increase was fit to a double exponential curve, with the major change occurring with an apparent rate constant of  $k_{app1} = 0.81 \text{ s}^{-1}$ , and a slower, lesser change occurring with an apparent rate constant of  $k_{app2} = 0.10 \text{ s}^{-1}$  for deacylated-tRNA<sup>Lys</sup> (Cy3) concentrations higher than  $0.75 \text{ }\mu\text{M}$  (Table 5.2). The rate constants for binding of deacylated-tRNA<sup>Lys</sup> (Cy3) are similar to the rate constants for the release of deacylated-tRNA<sup>fMet</sup> (Cy3) (Table 5.2, Figure 5.3 A versus Figure 5.3 B). It is difficult to obtain the actual FRET efficiencies because the amount of Cy3-tRNA bound to the ribosome is unknown. In the complexes containing labeled tRNA<sup>fMet</sup> (Cy3), it is not known how much remains bound to the E/E2-site after preincubation; further, it is unknown the amount of tRNA<sup>Lys</sup> (Cy3) that binds to the

ribosome in that experiment. By not knowing the amounts of deacylated-tRNA bound, it is impossible to measure accurate FRET efficiencies.

### 5.3.3 Competition is Not Codon Specific

Previous cryo-EM data has shown that tRNA in an E2-site has no contacts with the mRNA codon in the E-site (Fischer et al., 2010). In the POST-1 complexes used above, the mRNA codon in the E-site is AUG, and tRNA<sup>Lys</sup> has an anticodon that corresponds to a codon of AAA or AAG where there is at least one base pair possible. Therefore, in order to measure whether or not the competition is codon specific, a tRNA<sup>Tyr</sup> that has no bases in common with the mRNA in the E-site was used (codon: UAU or UAC). T202C-L1 (Cy5) POST-1 complexes (0.25  $\mu$ M) were preincubated with 0.5  $\mu$ M tRNA<sup>fMet</sup> (Cy3) as before, and then deacylated-tRNA<sup>Tyr</sup> (0.75 or 1.5  $\mu$ M) was added in a stopped flow. As seen in Figure 5.4, the release of E2-site tRNA<sup>fMet</sup> (Cy3) as measured by FRET efficiency loss upon addition of tRNA<sup>Tyr</sup>, is similar to the release upon addition of tRNA<sup>Lys</sup> in both rate constant and amplitude.

### 5.3.4 Addition of Ternary Complex Does Not Dramatically Enhance Deacylated-tRNA<sup>fMet</sup> Release

As alluded to in the introduction, an A- to E-site allosteric interaction has been shown in previous work (Rheinberger and Nierhaus, 1986; Rheinberger et al.,

1986; Gnirke et al., 1989, Nierhaus, 1990; Rheinberger, 1991; Chen et al., submitted manuscript); further, this allostery has also been held under scrutiny for the possibility that deacylated-tRNA inherent in the ternary complex is causing E-site competition resulting in release of E-site tRNA (Robertson and Wintermeyer, 1987). Above, it has been shown that deacylated-tRNA does indeed create a competition for the ribosome that is codon independent. Here, I explore whether the addition of a ternary complex has any additional effect on the release of tRNA. Because of the limits of artificial tRNA charging, any ternary complex added has an inherent amount of deacylated-tRNA that will create a competition for the E2-site. Lys-tRNA<sup>Lys</sup> charging efficiency has been optimized to ~35-40% resulting in deacylated-tRNA<sup>Lys</sup> concentrations of 0.5  $\mu$ M and 1.5  $\mu$ M for ternary complex concentrations of 0.39  $\mu$ M and 1.0  $\mu$ M, respectively. As seen in Figure 5.5 A/B, the addition of these ternary complexes to a POST-1 complex (made as above) only minor further deacylated-tRNA<sup>Met</sup> (Cy3) release as compared to the release seen upon addition of 0.5  $\mu$ M (Figure 5.5 A) or 1.5  $\mu$ M (Figure 5.5 B) deacylated-tRNA<sup>Lys</sup>.

Due to the low charging efficiency of tRNA<sup>Lys</sup>, creation of a ternary complex resulted in an approximate 2-fold excess of deacylated-tRNA : ternary complex. In order to increase the ratio of ternary complex : deacylated-tRNA, a more highly charged Phe-tRNA<sup>Phe</sup> (~72% charged) was used. A POST-1 complex had to be made using an mRNA sequence of MRFK, instead of MFKR, in order to put the codon for tRNA<sup>Phe</sup> in the open A-site of the complex. Using the MRFK mRNA sequence, a 70SIC complex was made with deacylated-tRNA<sup>Met</sup> (Cy3), and to it EF-

Tu.GTP.Arg-tRNA<sup>Arg</sup> and EF-G.GTP was added to create the POST-1 complex, which was then purified through sucrose, and preincubated with 0.5  $\mu\text{M}$  tRNA<sup>fMet</sup> (Cy3). Addition of EF-Tu.GTP.Phe-tRNA<sup>Phe</sup> (1.0  $\mu\text{M}$ , as measured by Phe-tRNA<sup>Phe</sup> concentration) to a POST-1 complex also resulted in 0.39  $\mu\text{M}$  deacylated-tRNA<sup>Phe</sup> being added. Therefore, if the addition of ternary complex to the POST-1 complex is a major contributor to the loss of tRNA<sup>fMet</sup> (Cy3) from the ribosome, the FRET efficiency loss from addition of ternary complex should be much greater than from the addition of 0.39  $\mu\text{M}$  deacylated-tRNA<sup>Phe</sup> alone. However, as seen in [Figure 5.5 C](#), the FRET efficiency loss is similar in both instances, meaning that the addition of ternary complex does not provide great enhancement of deacylated-tRNA<sup>fMet</sup> (Cy3) release from the ribosome. However, there is a slightly larger amplitude change for the complexes in which there is a ternary complex added; therefore, it is possible that ternary complex has some effect on the release of deacylated-tRNA<sup>fMet</sup>. Another possibility is that since there is no direct measurement of the amount of deacylated-tRNA present in the ternary complex solution, we may be imprecise in the amount of deacylated-tRNA leading to skewed amplitudes. Further experiments must be performed to better understand the exact scheme by which the release occurs.

## 5.4 Discussion

The slow rate of deacylated-tRNA release from the ribosomes that predominantly follow pathway 3 described above, would drastically hinder *in vivo* protein synthesis. However, in *in vivo* conditions, the cell has deacylated-tRNA and ternary complexes present in the solution; therefore, it is possible that this pathway is indeed followed, but the tRNA in the E2-site is subsequently released because of an equilibrium reached between bound and unbound deacylated-tRNA.

The equilibrium between bound and unbound deacylated-tRNA<sup>fMet</sup> was measured by both deacylated-tRNA<sup>fMet</sup> (Cy3) binding (Figure 5.1) and deacylated-tRNA<sup>fMet</sup> (Cy3) dissociation caused by competition with tRNA<sup>Lys</sup> (Figure 5.2 B), and allowed for an estimation of the dissociation constant of ~0.12-0.15  $\mu$ M. Further, as Figure 5.3 shows, the deacylated-tRNA<sup>Lys</sup> (Cy3) in solution binds to the ribosome in a position that allows FRET between it and the T202C-L1 (Cy5) ribosomes. As mentioned before, it is difficult to measure accurate FRET efficiencies for each complex.

As seen in Figure 5.2 A and Table 5.2, the major apparent rate constant for dissociation is not affected by the concentration of tRNA<sup>Lys</sup> added to the solution. Furthermore, even complexes without tRNA<sup>Lys</sup> added, have a small loss in FRET efficiency associated with release of tRNA<sup>fMet</sup> (Cy3). This apparent rate constant for release is similar to the smaller magnitude apparent rate constant for release seen in Chapter IV (Table 4.1, Exp. 30,  $k_{app2}$ ) and indicates that there is an inherent amount of deacylated-tRNA released at this rate that increases as a function of increasing



amounts of added deacylated-tRNA in solution. The data have been attempted to be fit into multiple general schemes but to this date have been unsuccessful. Therefore, unfortunately, at this time, it is not completely clear how the deacylated-tRNA from solution affects the release of deacylated-tRNA on the ribosome. Further t/t FRET and anisotropy experiments need to be completed in order to gain a better understanding of the mechanism.

Although the equilibrium between binding and dissociation cannot be specifically linked to the E2-site, it does occur at a position that is codon independent. In a translocated POST-1 ribosome, the mRNA codon in the E-site is AUG. The codon that is cognate for tRNA<sup>Lys</sup> is either AAA or AAG; therefore, there is at least near cognate coordination between the added tRNA<sup>Lys</sup> and the codon in the E-site. As seen in the cryo-EM images, when tRNA occupies the E2-site there is no longer any codon specificity, and thus, if the competition were for this site, there should not be a dependence on the identity of the deacylated-tRNA. Indeed this is what is seen when tRNA<sup>Lys</sup> is replaced with the completely non-cognate tRNA<sup>Tyr</sup> (codon: UAU or UAC). The competition for the site does not depend on the codon of the deacylated-tRNA because near cognate (tRNA<sup>Lys</sup>), and non-cognate (tRNA<sup>Tyr</sup>) compete at a similar level as seen in [Figure 5.4](#).

The idea of an A- and E-site allosteric interaction has been suggested numerous times; for example, the loss of codon-anticodon interaction at the E-site provokes high-efficiency frameshifting (**Trimble et al., 2004; Marquez et al., 2004**), the antibiotic ediene binds to the E-site on the 30S and induces misreading at the A-

site (**Dinos et al., 2004**), and weakening of E-site tRNA binding by mutations on the S7-S11 interface cause misincorporation and readthrough at the A-site (**Robert and Brakier-Gingras, 2003; Dinos et al., 2005**), however, it is not universally accepted. The major argument against one experiment that has been used as evidence for the allosteric interaction, that added ternary complex induces tRNA release from the E-site, is that the deacylated-tRNA inherent in the ternary complex is causing the E-site tRNA to release. In previous experiments by Nierhaus and coworkers, they dispute this criticism by suggesting that the deacylated-tRNA in the system cannot compete with the E-site tRNA because they do not share the same codon, and therefore do not affect the addition of non-cognate deacylated-tRNA (**Gnirke et al., 1989**). Above, I prove that this competition is not codon specific and any deacylated-tRNA can compete for the binding site. However, the question remained, as to whether or not the addition of a ternary complex can cause an allosteric release from the E-site, or E2-site in this case. As seen in **Figure 5.5**, the addition of ternary complexes with varying amounts of deacylated-tRNA in the mixture does not drastically change the amount of tRNA released from the ribosome. However, it cannot be overlooked that there is a slightly larger amplitude of FRET efficiency change associated with the complexes that have ternary complex added to them. It is possible that this increase in amplitude is only apparent because the concentration of deacylated-tRNA in the ternary complex solution cannot be accurately measured, or that the addition of ternary complex does indeed have a slight effect on release of E/E2-site tRNA. Further experiments need to be performed in order to obtain a full kinetic scheme for the competition between deacylated-tRNAs before any conclusions can be drawn

about the allosteric interactions. However, the drastic effects on deacylated-tRNA release from the E2-site seem to be the results of competition between binding of deacylated-tRNA from solution, and not from any allosteric interaction between the A- and E-sites.

Experiment	Figure	Cy3/POST-1	[ <sup>3</sup> H]-Phe/POST-1
--	5.1	0.22*	0.34
52,55,56,61	5.2 A	0.49	0.43
58	5.3 A	--	0.45
52	5.3 B	0.49	0.43
52, 57	5.4	0.49	0.43
49,52	5.5 A	0.49	0.43
60, 61	5.5 B	0.65	0.47
62, 63	5.5 C	0.74	0.41**

\*POST-1 complex was made with tRNA<sup>fMet</sup> (Cy3) labeled to only 0.33: 1, Cy3: tRNA<sup>fMet</sup>

\*\*[<sup>3</sup>H]-Arg/POST-1

### Table 5.1 tRNA Binding to POST-1 Complexes

T202C-L1 (Cy5) POST-1 complexes were made in Buffer B, starting with 70SICs (2 μM) containing highly labeled deacylated-tRNA<sup>fMet</sup> (Cy3, ~1:1). Addition of 3.0 μM ternary complex with Phe-tRNA<sup>Phe</sup> (unless otherwise specified) and EF-G.GTP (3.0 μM) resulted in a POST-1 complex that was purified through sucrose. Cy3/POST-1 indicates

the amount of tRNA<sup>fMet</sup> (Cy3) remaining bound to the POST-1 complex, and Phe/POST-1 indicates the amount of Phe-tRNA<sup>Phe</sup> remaining bound as measured by radioactive Phe, unless otherwise mentioned. These binding efficiencies were measured before the preincubation with excess deacylated-tRNAs.

Figure	Exp	Deacylated-tRNA	Ternary Complex	tRNA <sup>fMet</sup>	k <sub>app1</sub>	k <sub>app2</sub>
5.1	--	tRNA <sup>fMet</sup> (Cy3), (0.1, 0.2, 0.4, 1.0 $\mu$ M)	NO	Cy3	N/A	N/A
5.2	55	NO	NO	Cy3	1.88 $\pm$ 0.07 (0.13)	--
5.2	56	tRNA <sup>Lys</sup> , 0.10 $\mu$ M	NO	Cy3	1.45 $\pm$ 0.02 (0.18)	--
5.2, 5.5A	61	tRNA <sup>Lys</sup> , 0.50 $\mu$ M	NO	Cy3	1.61 $\pm$ 0.04 (0.36)	--
5.2, 5.3B, 5.4	52	tRNA <sup>Lys</sup> , 0.75 $\mu$ M	NO	Cy3	1.71 $\pm$ 0.05 (0.35)	0.190 $\pm$ 0.008 (0.08)
5.2, 5.5B	52	tRNA <sup>Lys</sup> , 1.50 $\mu$ M	NO	Cy3	1.21 $\pm$ 0.01 (0.38)	0.134 $\pm$ 0.002 (0.09)
5.2	52	tRNA <sup>Lys</sup> , 3.00 $\mu$ M	NO	Cy3	1.59 $\pm$ 0.05 (0.35)	0.130 $\pm$ 0.004 (0.09)
5.3A	58	tRNA <sup>Lys</sup> (Cy3) 0.75 $\mu$ M	NO	Unlabeled	0.73 $\pm$ 0.02 (-0.36) <sup>#</sup>	0.090 $\pm$ 0.001 (-0.06) <sup>#</sup>
5.4	57	tRNA <sup>Tyr</sup> , 0.75 $\mu$ M	NO	Cy3	1.37 $\pm$ 0.02 (0.38)	0.164 $\pm$ 0.006 (0.08)
5.5 A	60	tRNA <sup>Lys</sup> ,	0.27 $\mu$ M	Cy3	1.65 $\pm$ 0.03	0.21 $\pm$ 0.01

		0.50 $\mu\text{M}^*$			(0.40)	(0.043)
5.5 B	49	tRNA <sup>Lys</sup> , 1.50 $\mu\text{M}^{**}$	1.0 $\mu\text{M}$	Cy3	1.92 $\pm$ 0.04 (0.40)	0.317 $\pm$ 0.008 (0.12)
5.5 C	62	tRNA <sup>Phe</sup> , 0.39 $\mu\text{M}$	NO	Cy3	1.1 $\pm$ 0.1 (0.09)	--
5.5 C	63	tRNA <sup>Phe</sup> , 0.39 $\mu\text{M}^{***}$	1.0 $\mu\text{M}$	Cy3	1.79 $\pm$ 0.05 (0.10)	0.080 $\pm$ 0.002 (0.086)

# Rate constants for binding of tRNA<sup>Lys</sup> (Cy3)

\* based on using a Lys-tRNA<sup>Lys</sup> preparation that was **37% charged**

\*\* based on using a Lys-tRNA<sup>Lys</sup> preparation that was **40% charged**

\*\*\* based on using a Phe-tRNA<sup>Phe</sup> preparation that was **72%? charged**

**Table 5.2 Apparent Rate Constants of tRNA<sup>fMet</sup> (Cy3) Release Upon Addition of Deacylated-tRNA and/or Ternary Complex**

T202C-L1 (Cy5) POST-1 complexes were created in Buffer B, starting with 70SICs containing highly labeled deacylated-tRNA<sup>fMet</sup> (Cy3) unless otherwise mentioned. 0.50  $\mu\text{M}$  tRNA<sup>fMet</sup> (Cy3) or tRNA<sup>fMet</sup> (exp. 58) was added to the purified POST-1 complex (0.25  $\mu\text{M}$ ) in order to ensure E2-site occupancy. Labeled or unlabeled deacylated-tRNA or ternary complex was added to the POST-1 complexes as indicated in the text and the resulting traces were fit to either a single or double exponential curve using Scientist (Micromath).

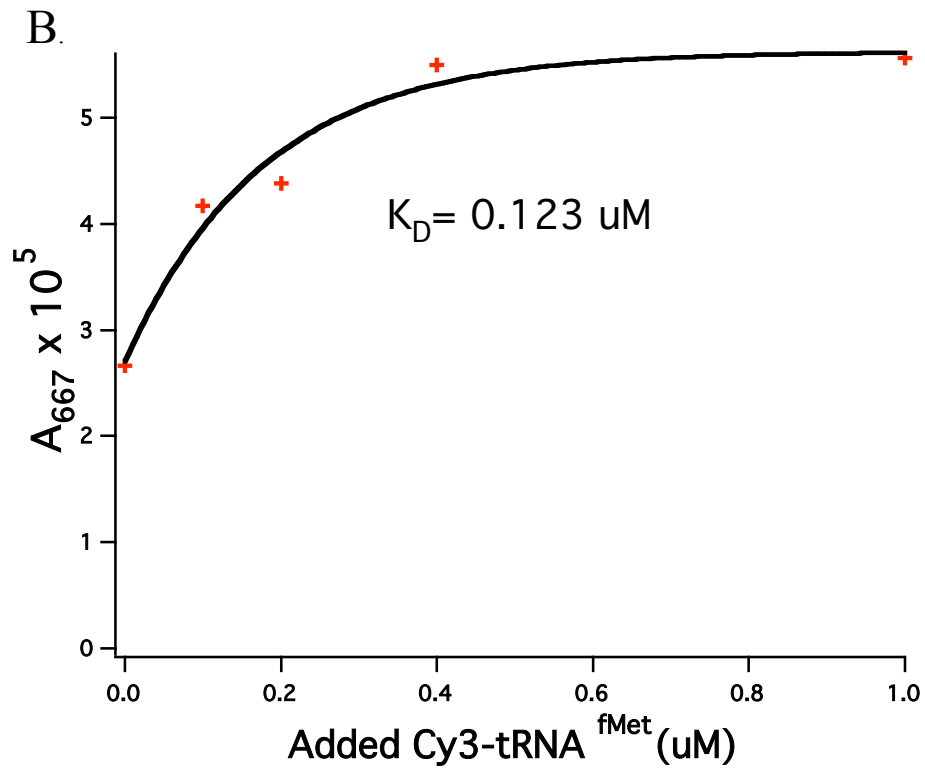
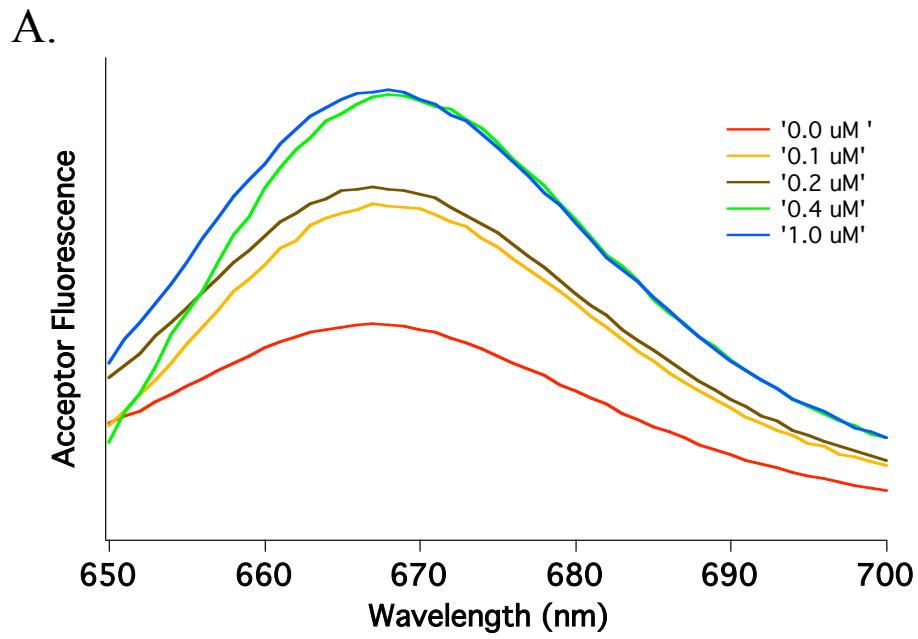
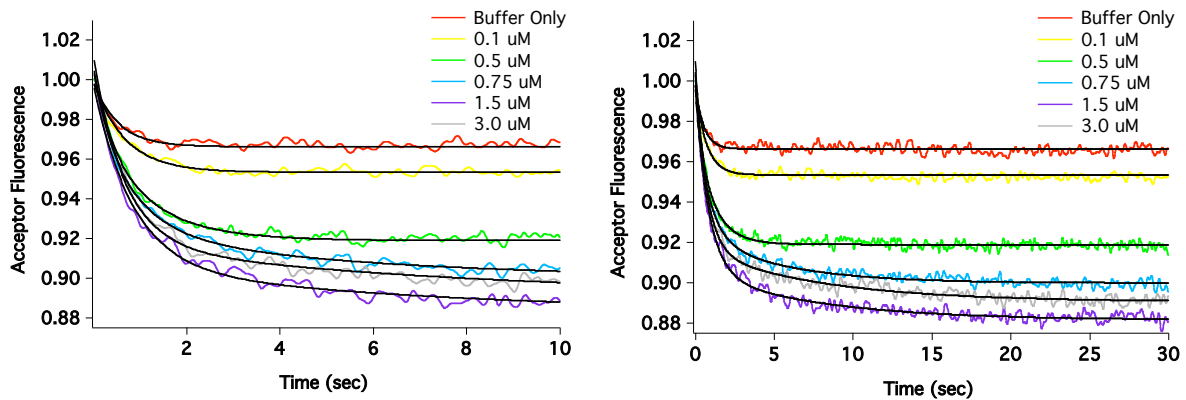


### **Figure 5.1 tRNA<sup>fMet</sup> (Cy3) Binding to a POST-1 Complex**

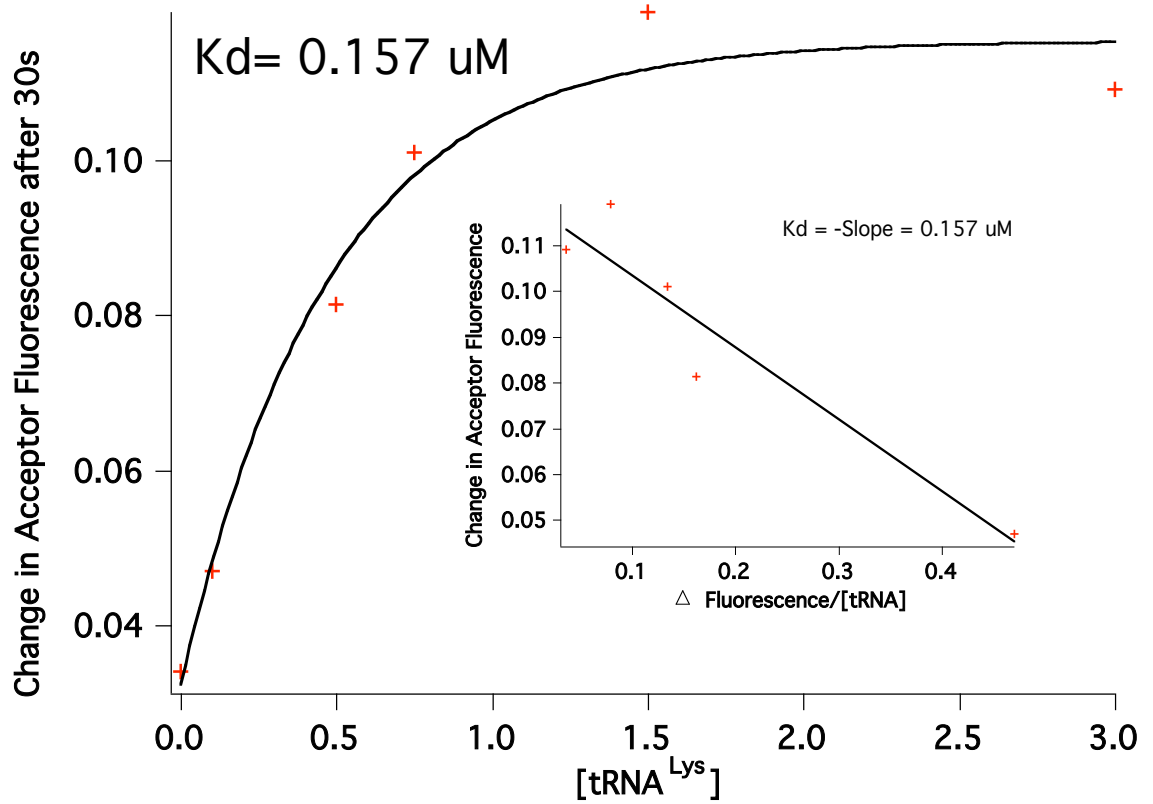
T202C-L1 (Cy5) POST-1 complexes were made in Buffer B starting with 70SICs containing deacylated-tRNA<sup>fMet</sup> (Cy3). The resulting POST-1 complexes were purified through sucrose and increasing concentrations of deacylated-tRNA<sup>fMet</sup> (Cy3) were titrated in an equilibrium FRET experiment. **A)** The increase in acceptor fluorescence signal upon addition of tRNA<sup>fMet</sup> (Cy3) at increasing concentrations. **B)** The binding curve for the increase in acceptor emission. The Cy3 donor was excited at 518 nm and the Cy5 acceptor emission was monitored at 667 nm. An increase in acceptor emission indicative of E/E2-site binding and a  $K_D$  value of 0.123  $\mu$ M was obtained.



A.

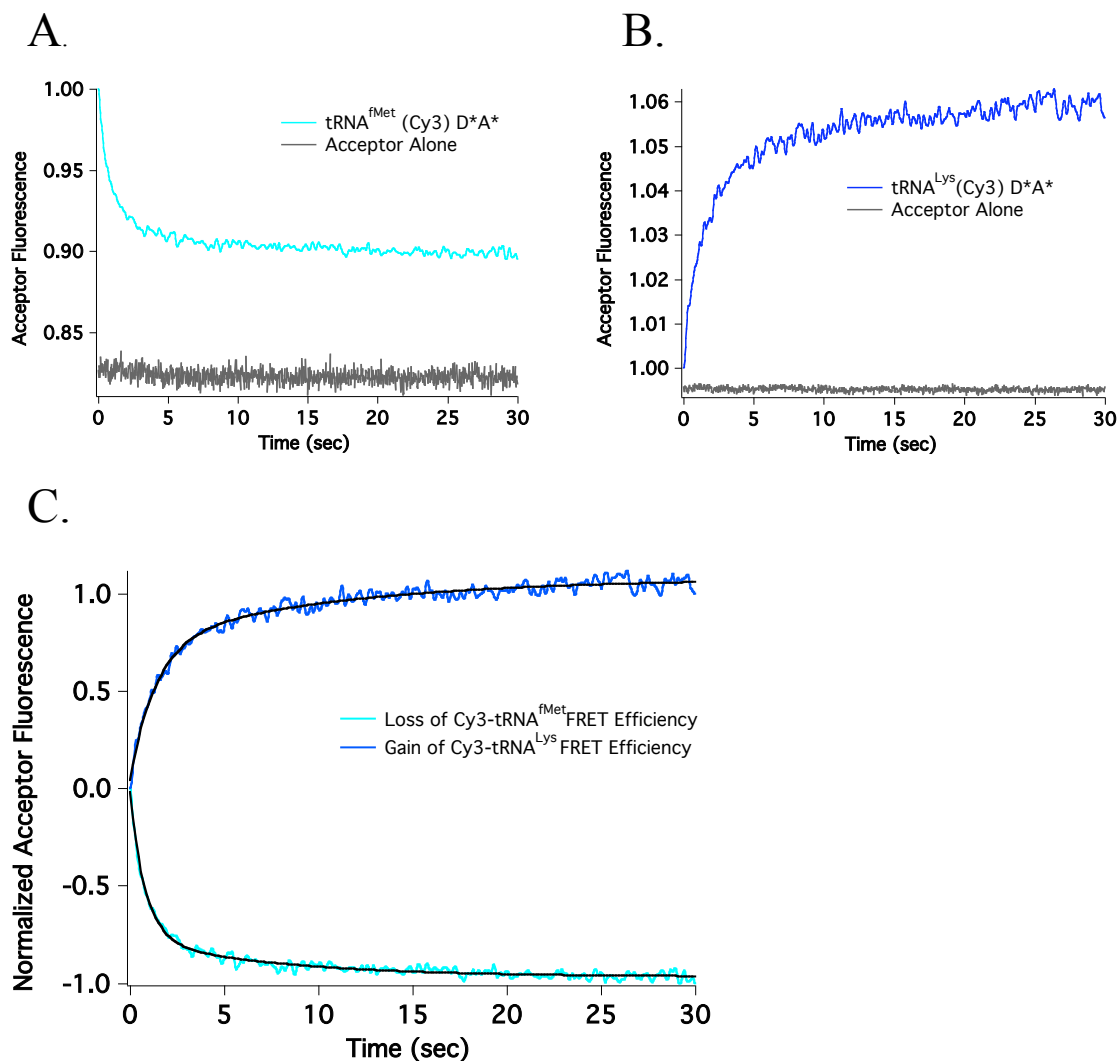


B.



**Figure 5.2 Release of Deacylated-tRNA<sup>fMet</sup> (Cy3) from the E2-site as a Function of Added Deacylated-tRNA<sup>Lys</sup> Concentration**

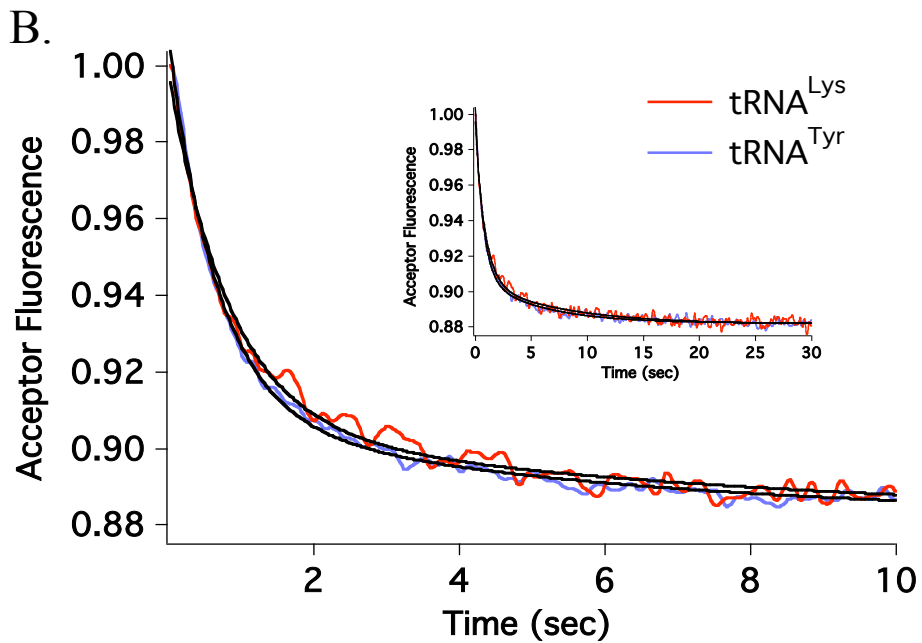
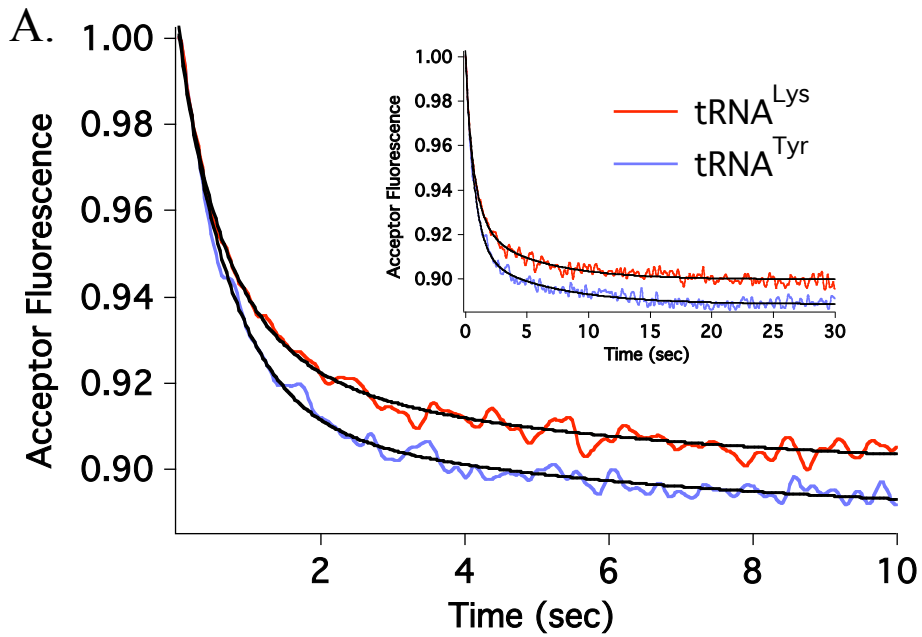
T202C-L1 (Cy5) POST-1 complexes were made in Buffer B, starting with 70SICs containing highly labeled deacylated-tRNA<sup>fMet</sup> (Cy3). 0.50  $\mu\text{M}$  tRNA<sup>fMet</sup> (Cy3) was added to the purified POST-1 complex (0.25  $\mu\text{M}$ ) in order to ensure E2-site occupancy with the labeled tRNA<sup>fMet</sup> (Cy3). In a stopped-flow experiment, increasing concentrations of tRNA<sup>Lys</sup> was added to POST-1 complexes, and the acceptor fluorescence was monitored as a measure of tRNA<sup>fMet</sup> (Cy3) release. The rate constants, as found by fitting to either single or double exponential equations in Scientist, for the major FRET efficiency decreases do not vary with concentration; however, the amplitude of the change does. Even at high concentrations of tRNA<sup>Lys</sup>, some amount of fluorescence remains because the binding and dissociation is indeed an equilibrium process, and there is still some tRNA<sup>fMet</sup> (Cy3) competing for the E2-site. By plotting the change in acceptor fluorescence versus tRNA<sup>Lys</sup> concentration (**B**) an apparent  $K_D$  for tRNA<sup>Lys</sup> binding can be obtained and is = 0.157  $\mu\text{M}$ . As determined by an Eadie-Hofstee plot (inset).



**Figure 5.3 Deacylated-tRNA Binding to and Release From the E2-Site**

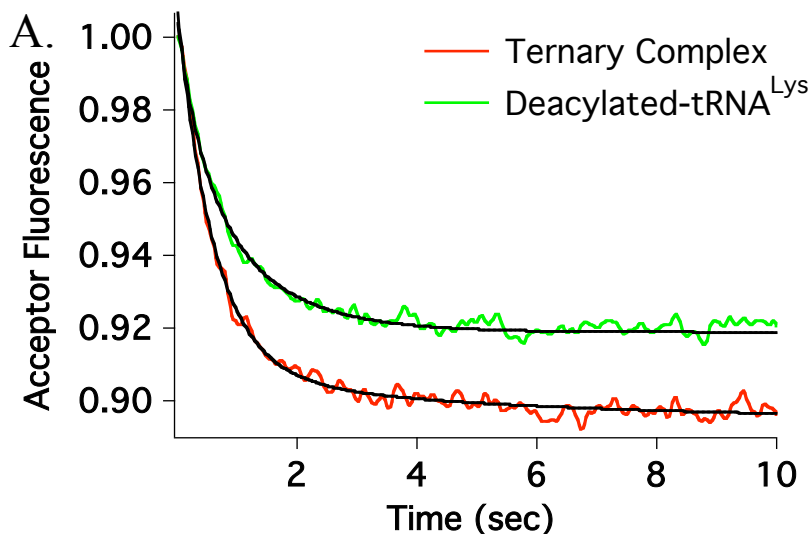
T202C-L1 (Cy5) POST-1 complexes were made from a 70SICs containing either highly-labeled tRNA<sup>fMet</sup> (Cy3) (0.49 Cy3/POST-1) (**A, ii**) or unlabeled tRNA<sup>fMet</sup> (**B, i**). **A, ii**: 0.75  $\mu$ M tRNA<sup>Lys</sup> as seen in **Figure 5.2**. **B, i**: 0.75  $\mu$ M tRNA<sup>Lys</sup> (Cy3) (0.52 Cy3/tRNA<sup>Lys</sup>) was added to 0.25  $\mu$ M POST-1 unlabeled tRNA<sup>fMet</sup> complexes that were preincubated with 0.5  $\mu$ M tRNA<sup>fMet</sup>, and FRET efficiency was monitored as acceptor

increase from the acceptor alone baseline upon tRNA<sup>Lys</sup> (Cy3) binding to ribosome near the L1-stalk. Apparent rate constants for the release and the binding were found by fitting both curves to double exponential equations as seen in [Table 5.2](#).



### Figure 5.4 Competition for the E2-site is Not Codon Specific

T202C-L1 (Cy5) POST-1 complexes were made in Buffer B, starting with 70SICs containing highly labeled deacylated-tRNA<sup>fMet</sup> (Cy3). 0.50  $\mu\text{M}$  tRNA<sup>fMet</sup> (Cy3) was added to the purified POST-1 complex (0.25  $\mu\text{M}$ ) in order to ensure E2-site occupancy with the labeled tRNA<sup>fMet</sup> (Cy3). In a stopped-flow experiment, 0.75  $\mu\text{M}$  or 1.5  $\mu\text{M}$  (A and B, respectively) of either tRNA<sup>Lys</sup> or tRNA<sup>Tyr</sup> was added to the POST-1 complex and the release of tRNA<sup>fMet</sup> from the E2-site of the ribosome was monitored by loss of acceptor FRET efficiency. The apparent rate constants for the loss of FRET efficiency were determined by fitting the curves to a double exponential equation as seen in [Table 5.2](#).



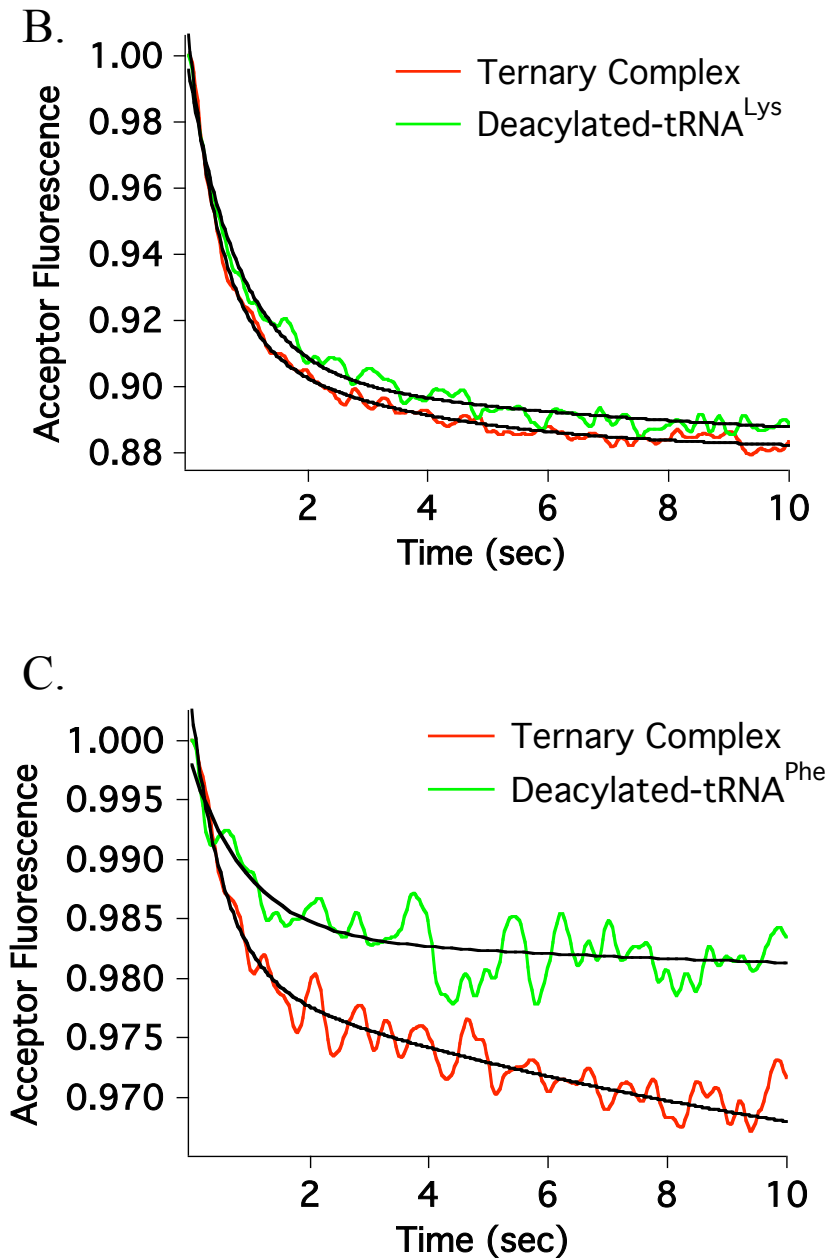


**Figure 5.5 Addition of Ternary Complex Does Not Significantly Promote Additional Deacylated-tRNA Release**

T202C-L1 (Cy5) complexes were made starting with deacylated-tRNA<sup>fMet</sup> (Cy3) in the 70SICs, and adding either EF-Tu.GTP.Phe-tRNA<sup>Phe</sup> (A and B; mRNA: MFKR) or

EF-Tu.GTP.Arg-tRNA<sup>Arg</sup> (C; mRNA: MRFK) plus EF-G.GTP in order to make the POST-1 complex. The POST-1 complexes were purified through sucrose cushion centrifugation and additional deacylated-tRNA<sup>Met</sup> (Cy3) was added to ensure E2-site occupancy, as seen above. **A)** Either addition of 0.5  $\mu\text{M}$  deacylated tRNA<sup>Lys</sup> or 0.27  $\mu\text{M}$  EF-Tu.GTP.Lys-tRNA<sup>Lys</sup> (as measured by Lys-tRNA<sup>Lys</sup> concentration), where the concentration of deacylated-tRNA<sup>Lys</sup> in the mixture is 0.5  $\mu\text{M}$  due to the low charging efficiency (37%) of the tRNA<sup>Lys</sup>, was added to a preincubated POST-1 complex. **B)** Either addition of 1.5  $\mu\text{M}$  deacylated tRNA<sup>Lys</sup> or 1.0  $\mu\text{M}$  EF-Tu.GTP.Lys-tRNA<sup>Lys</sup> (as measured by Lys-tRNA<sup>Lys</sup> concentration), where the concentration of deacylated-tRNA<sup>Lys</sup> in the mixture is 1.5  $\mu\text{M}$  due to the low charging efficiency (40%) of the tRNA<sup>Lys</sup>, was added to a preincubated POST-1 complex. **C)** POST-1 complexes were made using an MRFK message, putting the deacylated-tRNA<sup>Met</sup> (Cy3) in the E2-site, Arg-tRNA<sup>Arg</sup> in the P-site, and an open A-site coding for tRNA<sup>Phe</sup>. Either addition of 0.39  $\mu\text{M}$  deacylated tRNA<sup>Phe</sup> or 1.0  $\mu\text{M}$  EF-Tu.GTP.Phe-tRNA<sup>Phe</sup> (as measured by Phe-tRNA<sup>Phe</sup> concentration), where the concentration of deacylated-tRNA<sup>Phe</sup> in the mixture is 0.39  $\mu\text{M}$  due to the higher charging efficiency (72%) of the tRNA<sup>Phe</sup>, was added to a purified, preincubated POST-1 complex.

## References

- Agrawal, R.K., Penczek, P., Grassucci, R.A., Burkhardt, N., Nierhaus, K.H., Frank, J. (1999) Effect of Buffer Conditions on the Position of tRNA on the 70S Ribosome as Visualized by Cryoelectron Microscopy. *J Biol Chem* 274, 8723-8729.
- Amann, E., Brosius, J. (1985) "ATG vectors" for regulated high-level expression of cloned genes in *Escherichia coli*. *Gene* 40, 183-190.
- Amann, E., Brosius, J., Ptashne, M. (1983) Vectors bearing a hybrid trp-lac promoter useful for regulated expression of cloned genes in *Escherichia coli*. *Gene* 25, 167-178.
- Ban, N., Nissen, P., Hansen, J., Moore, P.B., Steitz, T.A. (2000) The Complete Atomic Structure of the Large Ribosomal Subunit at 2.4 Å Resolution. *Science* 289, 905-920.
- Baranov, V.I., Ryabova, L.A. (1988) Is the Three-site Model for the Ribosomal Elongation Cycle Sound? *Biochimie* 70, 259-65.
- Blanchard, S.C., Kim, H.D., Gonzalez, R.L., Puglisi, J.D., Chu, S. (2004) tRNA Dynamics on the Ribosome During Translation. *PNAS* 101, 12893-12898.



- Burkhardt, N., Jünemann, R., Spahn, C.M., Nierhaus, K.H. (1998) Ribosomal tRNA binding sites: three-site models of translation. *Crit Rev Biochem Mol Biol* 33, 95-149.
- Chandramouli, P., Topf, M., Ménétret, J., Eswar, N., Cannone, J.J., Gutell, R.R., Sali, A., Akey, C.W. (2008) Structure of the Mammalian 80S Ribosome at 8.7 Å Resolution.
- Chen, C., Stevens, B., Kaur, J., Cabral, D., Liu, H., Wang, Y., Zhang, H., Rosenblum, G., Smilansky, Z., Goldman, Y.E., Cooperman, B.S. (2011) Single-molecule fluorescence measurements of ribosomal translocation dynamics. *Mol Cell* 42, 367-377.
- Connell, S.R., Takemoto, C., Wilson, D.N., Wang, H., Murayama, K., Terada, T., Shirouzu, M., Rost, M., Schüler, M., Giesebrecht, J., Dabrowski, M., Mielke, T., Fucini, P., Yokoyama, S., Spahn, C.M.T. (2007) Structural Basis for Interaction of the Ribosome with the Switch Regions of GTP-bound Elongation Factors. *Mol Cell* 25, 751-764.
- Cornish P.V., Ermolenko, D.N., Staple, D.W., Hoang, L., Hickerson, R.P., Noller, H.F., Ha, T. (2009) Following Movement of the L1 Stalk Between Three Functional States in Single Ribosomes. *PNAS* 106, 2571-2576.
- Crick, F. H. (1970) Central Dogma of Molecular Biology. *Nature* 227, 561-563.

- Dabbs, E.R., Ehrlich, R., Hasenbank, R., Schroeter, B.H., Stöffler-Meilicke, M., Stöffler, G. (1981) Mutants of *Escherichia coli* lacking ribosomal protein L1. *J Mol Biol* 149, 553-578.
- Devaraj, A., Shoji, S., Holbrook, E.D., Fredrick, K. (2009) A role for the 30S subunit E site in maintenance of the translational reading frame. *RNA* 15, 255-265.
- Dinos, G., Wilson, D.N., Teraoka, Y., Szaflarski, W., Fucini, P., Kalpaxis, D., Nierhaus, K.H. (2004) dissecting the ribosomal inhibition mechanisms of edeine and pactamycin: the universally conserved residues G693 and C795 regulate P-site tRNA binding. *Mol Cell* 13, 113-124.
- Dinos, G., Kalpaxis, D.L., Wilson, D.N., Nierhaus, K.H. (2005) Deacylated tRNA is released from the E site upon A site occupation but before GTP is hydrolyzed by EF-Tu. *Nucleic Acids Res* 33, 5291-5296.
- Dong, H., Nilsson, N., Kurland, C.G. (1996) Co-variation of tRNA Abundance and Codon Usage in *Escherichia coli* at Different Growth Rates. *J Mol Biol* 260, 649-663.
- Fischer, N., Konevega, A.L., Wintermeyer, W., Rodnina, M.V., Stark, H. (2010) Ribosome Dynamics and tRNA Movement by Time-Resolved Electron Cryomicroscopy. *Nature* 466, 329-333.

- Frank, J., Agrawal, R.K. (2000) A Ratchet-like Inter-Subunit Reorganization of the Ribosome During Translocation. *Nature* 406, 318-322.
- Frank, J., Gao, H., Sengupta, J., Gao, N., Taylor, D.J. (2007) The Process of mRNA-tRNA Translocation. *PNAS* 104, 19671-19678.
- Fei, J., Kosuri, P., MacDougall, D.D., Gonzalez, R.L. (2008) Coupling of Ribosomal L1 Stalk and tRNA Dynamics During Translation Elongation. *Mol Cell* 30, 348-359.
- Gao, H., Sengupta, J., Valle, M., Korostelev, A., Eswar, N., Stagg, S. M., Van Roey, P., Agrawal, R.K., Harvey, S.C., Sali, A., Chapman, M. S., Frank, J. (2003) Study of the structural dynamics of E coli 70S ribosome using real-space refinement. *Cell* 113, 789-801.
- Gao, Y., Selmer, M., Dunham, C.M., Weixlbaumer, A., Kelley, A.C., Ramakrishnan, V. (2009) The Structure of the Ribosome with Elongation Factor G Trapped in the Posttranslocational State. *Science* 326, 694-699.
- Georgiou, G., Valax, P. (1996) Expression of correctly folded proteins in Escherichia coli. *Curr Opin Biotechnol* 7, 190-197.
- Gnirke A., Geigenmüller, U., Rheinberger, H.J., Nierhaus, L.H. (1989) The Allosteric Three-site Model for the Ribosomal Elongation Cycle. Analysis with a Heteropolymeric mRNA. *J Biol Chem* 264, 7291-7301.

- Gourse, R.L., de Boer, H.A., Nomura, M. (1986) DNA Determinants of rRNA Synthesis in *E. coli*: Growth Rate Dependent Regulation, Feedback Inhibition, Upstream Activation, Antitermination. *Cell* 44, 197-205.
- Halic, M., Becker, T., Frank, J., Spahn, C.M.T., Beckmann, R. (2005) Localization and Dynamic Behavior of Ribosomal Protein L30e. *Nat Struct Mol Biol* 12, 467-468.
- Harms, J., Schlutzen, F., Zarivach, R., Bashan, A., Gat, S., Agmon, I., Bartels, H., Franceschi, F., Yonath, A. (2001) High resolution structure of the large ribosomal subunit from mesophilic eubacterium. *Cell* 107, 679-688.
- Hartley, D.L., Kane, J.F. (1988) Properties of inclusion bodies from recombinant *Escherichia coli*. *Biochem Soc Trans* 16, 101-102.
- Hochuli, E. (1988) Large-scale chromatography of recombinant proteins. *J Chromatogr* 444, 293-302.
- Jewett, M.C., Swartz, J.R. (2004) Mimicking the *Escherichia coli* cytoplasmic environment activates long-lived and efficient cell-free protein synthesis. *Biotechnol Bioeng* 86, 19-26.
- Kemkhadze, K. S., Odintsov, V. B., Semenov, Y. P., and Kirillov, S. V. (1981) Quantitative study of the interaction of aminoacyl-tRNA with the A site of *Escherichia coli* ribosomes: equilibrium and kinetic parameters of binding in the absence of EF-Tu factor and GTP. *FEBS Lett.* 125, 10- 14.

- Kim, H.D., Puglisi, J.D., Chu, S. (2007) Fluctuations of transfer RNAs between classical and hybrid states. *Biophys J* 93, 3575-3582.
- Kisselev, L.L., Buckingham, R.H. (2000) Translational Termination Comes of Age. *Trends Biochem Sci* 25, 561-566.
- Köhler, C., Mayer, C., Neumair, O., Gröbner, P., Piendl, W. (1998) Interaction of ribosomal L1 proteins from mesophilic and thermophilic Archaea and Bacteria with specific L1-binding sites on 23S rRNA and mRNA. *Eur J Biochem* 256, 97-105.
- Kornberg, A. (1969) Active Center of DNA Polymerase. *Science* 163, 1410-1418.
- Korostelev, A., Ermolenko, D.N., Noller, H. F. (2008) Structural dynamics of the ribosome. *Curr Opin Chem Biol* 12, 674-683.
- Korostelev, A., Trakhanov, S., Laurberg, M., Noller, H.F. (2006) Crystal structure of a 70S ribosome-tRNA complex reveals functional interactions and rearrangements. *Cell* 126, 1065-1077.
- Lagerkvist, U., and Waldenstroem, J. (1964) Structure and Function of Transfer Rna. I. Species Specificity of Transfer Rna from E. Coli and Yeast. *J. Mol. Biol.* **37**, 28-37.

- Leger, M., Dulude, D., Steinberg, S.V., Brakier-Gingras, L. (2007) The three transfer RNAs occupying the A, P and E sites on the ribosome are involved in viral programmed-1 ribosomal frameshift. *Nucleic Acids Research* 35, 5581-5592.
- Li, W., Agirrezabala, X., Lei, J., Bouakaz, L., Brunelle, J.L., Ortiz-Meoz, R.F., Green, R., Sanyal, S., Ehrenberg, J.F. (2008) Recognition of Aminoacyl-tRNA: A Common Molecular Mechanism Revealed by Cryo-EM.
- Liao, P.Y., Gupta, P., Petrov, A.N., Dinman, J.D., Lee, K.H. (2008) A new kinetic model reveals the synergistic effect of E-, P- and A-sites on +1 ribosomal frameshifting. *Nucleic Acids Res* 36, 2619-2629.
- Lill, R., Schwägele, F., Sprinzl, M., Vogt, H., Wintermeyer, W. (1988) Specific Recognition of 3'-terminal Adenosine of tRNAPhe in the Exit Site of Escherichia coli Ribosomes. *J Mol Biol* 203, 699-705.
- Lill, R., Wintermeyer, W. (1987) Destabilization of Codon-Anticodon Interaction in the Ribosomal Exit Site. *J Mol Biol* 196, 137-148.
- Marston, F.A. (1986) The purification of eukaryotic polypeptides synthesized in Escherichia coli. *Biochem J* 240, 1-12.
- Marquez, V., Wilson, D.N., Tate, W.P., Triana-Alonso, F., Nierhaus, K.H. (2004) Maintaining the ribosomal reading frame: The influence of E site during translational regulation of release factor 2. *Cell* 118, 45-55.

- Marston, F.A., Hartley, D.L. (1989) Solubilization of protein aggregates. *Meth Enzymol* 182, 264-276.
- Mitra, K., Frank, J., (2006) Ribosome Dynamics: Insights From Atomic Structure Modeling into Cryo-Electron Microscopy Maps. *Annu Rev Biophys Biomol Struct* 35, 299-317.
- Moazed, D., Noller, H.F. (1989) Intermediate States in the Movement of Transfer RNA in the Ribosome. *Nature* 342, 142-148.
- Munro, J.B., Altman, R.B., O'Connor, N., Blanchard, S.C. (2007) Identification of Two Distinct Hybrid State Intermediates on the Ribosome. *Mol Cell* 25, 505-517.
- Munro J.B., Altman, R.B., Tung, C., Cate, J.H.D., Sanbonmatsu, K.Y., Blanchard, S.C. (2009) Spontaneous Formation of the Unlocked State of the Ribosome is a Multistep Process. *PNAS* 107, 709-714.
- Munro, J.B., Altman, R.B., Tung, C., Sanbonmatsu, K.Y., Blanchard, S.C. (2010) A Fast Dynamic Mode of the EF-G-bound Ribosome. *EMBO Journal* 29, 770-781.
- Nevskaya, N., Tishchenko, S., Volchkov, S., Kljashtorny, V., Nikonova, E., Nikonov, O., Nikulin, A., Köhrer, C., Piendl, W., Zimmermann, R., Stockley, P., Garber, M., Nikonov, S. (2006) New Insights into the Interaction of Ribosomal Protein L1 with RNA. *J Mol Biol* 335, 747-759.

- Nierhaus, K.H. (2006) Decoding errors and the involvement of the E-site. *Biochemie* 88, 1013-1019.
- Nikonov, S., Nevskaya, N., Eliseikina, I., Fomenkova, N., Nikulin, A., Ossina, N., Garber, M., Jonsson, B.H., Briand, C., Al-Karadaghi, S., Svensson, A., Aevansson, A., Liljas, A. (1996) Crystal Structure of the RNA Binding Ribosomal Protein L1 from *Thermus Thermophilus*. *EMBO Journal* 6, 1350-1359.
- Nikulin, A., Eliseikina, I., Tishchenko, S., Nevskaya, N., Davydova, N., Platonova, O., Piendl, W., Selmer, M., Liljas, A., Drygin, D., Zimmermann, R., Garber, M., Nikonov, S. (2003) Structure of the L1 Protuberance in the Ribosome. *Nat Struc Biol* 2, 104-108.
- Odom, O.W., Picking, W.D., Hardesty, B. (1990) Movement of tRNA but not the Nascent Peptide During Peptide Bond Formation on Ribosomes. *Biochemistry* 29, 10734-10744.
- Pan, D., Kirilov, S., Zhang, C., Hou, Y., Cooperman, B.S. (1996) Rapid ribosomal translocation depends on the conserved 18-55 base pair in P-site transfer RNA. *Nat Struct Mol Biol* 13, 354-359.
- Pan, D., Kirillov, S.V., Cooperman, B.S. (2007) Kinetically Competent Intermediates in the Translocation Step of Protein Synthesis. *Mol Cell* 25, 519-529.



- Pan, D, Qin, H., Cooperman, B.S. (2009) Synthesis and Functional Activity of tRNAs Labeled with Fluorescent Hydrazides in the D-Loop. *RNA* 15, 346-354.
- Pape, T., Wintermeyer, W., Rodnina, M.V. (1998) Complete Kinetic Mechanism of Elongation Factor Tu-dependent Binding of Aminoacyl-tRNA to the A Site of the *E. coli* Ribosome. *EMBO Journal* 17, 7490-7497.
- Porath, J., Carlsson, J., Olsson, I., Belfrage, G. (1975) Metal chelate affinity chromatography, a new approach to protein fractionation. *Nature* 258, 598-599.
- Rao, A.R., Varshney, U., (2001) Scientific interaction between the ribosome recycling factor and the elongation factor G from *Mycobacterium tuberculosis* mediates peptidyl-tRNA release and ribosome recycling in *Escherichia Coli*. *EMBO Journal* 20, 2977-2986.
- Rheinberger, H.J., Nierhaus, K.H. (1986) Allosteric Interactions Between the Ribosomal Transfer RNA-Binding Sites A and E. *J Biol Chem* 261, 9133-9139.
- Rheinberger, H.J., Sternbach, H., Nierhaus, K.H. (1986) Codon-anticodon Interaction at the Ribosomal E Site. *J Biol Chem* 261, 9140-9143.
- Robert, F. and Brakier-Gingras, L. (2003) A functional interaction between ribosomal proteins S7 and S11 within the bacterial ribosome. *J. Biol. Chem.* 278, 44913-44920.

- Robertson, J.M., Paulsen, H., Wintermeyer, W. (1986) Pre-steady-state kinetics of ribosomal translocation. *J Mol Biol* 192, 251-360.
- Robertson, J.M., Wintermeyer, W. (1987) Mechanism of Ribosomal Translocation. tRNA Binds Transiently to an Exit Site Before Leaving the Ribosome During Translocation. *J Mol Biol* 196, 525-540.
- Rodnina, M.V., Wintermeyer, W. (1995) GTP consumption of elongation factor Tu during translation of heteropolymeric mRNAs. *PNAS* 92, 1945-1949.
- Sambrook, J., Russell, D.W. (2001) *Molecular Cloning: A Laboratory Manual*, 3<sup>rd</sup> edn (New York: Cold Spring Harbor Press).
- Sander, G. (1982) Ribosomal Protein L1 from *Escherichia coli*. *J Biol Chem* 258, 10098-10103.
- Schein, C.H. (1991) Optimizing protein folding to the native state in bacteria. *Curr Opin Biotechnol* 2, 746-750.
- Schmeing, T.M., Ramakrishnan, V. (2009) What recent ribosome structures have revealed about the mechanism of translation. *Nature* 461, 1234-1242.
- Schmeing T.M., Voorhees, R.M., Kelley, A.C., Gao, Y., Murphy, F.V., Weir, J.R., Ramakrishnan, V. (2009) The Crystal Structure of the Ribosome Bound to the EF-Tu and Aminoacyl-tRNA. *Science* 326, 688-694.

- Schuwirth, B.S., Borovinskaya, M.A., Hau, C.W., Zhang, W., Vila-Sanjurjo, A., Holton, J.M., Cate, J.H.D. (2005) Structures of the Bacterial Ribosome at 3.5 Å Resolution. *Science* 310, 827-834.
- Selmer, M., Dunham, C.M., Murphy, F.V., Weixlbaumer, A., Petry, S., Kelley, A.C., Weir, J.R., Ramakrishnan, V. (2006) Structure of the 70S Ribosome Complexed with mRNA and tRNA. *Science* 313, 1935-1942.
- Seo, H., Abedin, S., Kamp, D., Wilson, D.N., Nierhaus, K.H., Cooperman, B.S. (2006) EF-G-dependent GTPase on the ribosome. Conformational change and fusidic acid inhibition. *Biochemistry* 45, 2504-2514.
- Semenkov, Y.P., Rodnina, M.V., Wintermeyer, W. (1996) The “Allosteric Three-site Model” of Elongation Cannot be Confirmed in a Well-defined Ribosome System from *Escherichia Coli*. *PNAS* 93, 12183-12188.
- Sergiev, P.V., Lesnyak, D.V., Kiparisov, S.V., Burakovsky, D.E., Leonov, A.A., Bogdanov, A.A., Brimacombe, R., Dontsova, O.A. (2005) Function of the ribosomal E-site: a mutagenesis study. *Nucleic Acids Research* 33, 6048-6056.
- Sørensen, H.P., Mortensen, K.K., (2005) Soluble Expression of Recombinant Proteins in the Cytoplasm of *Escherichia coli*. *Microb Cell Fact* 4, 1.
- Studier, F.W., Moffatt, B.A. (1986) Use of bacteriophage T7 RNA polymerase to direct selective high-level expression of cloned genes. *J Mol Biol* 189, 113-130.

Studier, F.W., Rosenberg, A.H., Dunn, J.J., Dubendorff, J.W. (1990) Use of T7 RNA polymerase to direct expression of cloned genes. *Meth Enzymol* 185, 60-89.

Subramanian, A.R., Dabbs, E.R. (1980) Functional Studies on Ribosomes Lacking Protein L1 from Mutant *Escherichia Coli*. *Eur J Biochem* 112, 425-430.

Tabor, S., Richardson, C.C. (1985) A bacteriophage T7 RNA polymerase/promoter system for controlled exclusive expression of specific genes. *PNAS* 82, 1074-1078.

Taylor, D.J., Nilsson, J., Merrill, A.R., Andersen, G.R., Nissen, P., Frank, J. (2007) Structures of Modified eEF2 80S Ribosome Complexes Reveal the Role of GTP Hydrolysis in Translocation. *EMBO Journal* 26, 2421-24231.

Trimble, M.J., Minnicus, A., Williams, K.P. (2004) tRNA slippage at the tmRNA resume codon. *RNA* 10, 805-812.

Valle, M., Zavialov, A., Sengupta, J., Rawat, U., Ehrenberg, M., Frank, J. (2003) Locking and Unlocking of Ribosomal Motions. *Cell* 114, 123-134.

Vesper, O., Wilson, D.N., (2006) Ribosome Recycling Revisited. *Mol Biol* 40, 742-750.

Voet, D., Voet, J.G., Pratt, C.W. (2006). *Fundamentals of biochemistry: life at the molecular level*, 2<sup>nd</sup> edn (New York: Wiley).

Watson, J.D., Crick, F.H. (1953a) Molecular Structure of Nucleic Acids; a Structure for Deoxyribose Nucleic Acid. *Nature* 171, 737-738.

Watson, J.D., Crick, F.H. (1953b) Genetical Implications of the Structure of Deoxyribonucleic Acid. *Nature* 171, 964-967.

Williams, D.C., Van Frank, R.M., Muth, W.L., Burnett, J.P. (1982) Cytoplasmic inclusion bodies in *Escherichia coli* producing biosynthetic human insulin proteins. *Science* 215, 687-689.

Wilson, D.N., Nierhaus, K.H. (2006) The E-site story: the importance of maintaining two tRNAs on the ribosome during protein synthesis. *Cellular and Molecular Life Sciences* 63, 2725-2737.

Wimberly, B., Brodersen, D., Clemons Jr., W. (2000) Structure of the 30S Ribosomal Subunit. *Nature* 407, 327-339.

Yusupov, M.M., Yusupova, G.Z., Baucom, A., Lieberman, K., Earnest, T.N., Cate, J.H., Noller, H.F. (2001) Crystal Structure of the Ribosome at 5.5 Å Resolution. *Science* 292, 883-896.

Zaher, H.S., Green, R. (2009) Fidelity at the molecular level: Lessons from protein synthesis. *Cell* 136, 746-762.

Zavialov, A.V., Mora, L., Buckingham, R.H., Ehrenberg, M. (2002) Release of Peptide Promoted by the GGQ Motif of Class 1 Release Factors Regulates the GTPase Activity of RF3. *Mol Cell* 10, 789-798.

# Appendix 1

## **Appendix 1: Fluorescent Studies of V177C-L1 (Cy3), V221C-L1 (Cy3), and K54C-L1 (Cy5)**

### **V177C-L1 (Cy3), V221C-L1 (Cy3)**

Fluorescently labeled mutant L1 50S were able to be prepared in an efficient manner. In order to probe the P- and E-site tRNA, steady-state spectrofluorometer experiments were used to determine the equilibrium FRET efficiency between the dye labeled mutant L1 50S and labeled fMet-tRNA<sup>fMet</sup> upon 70SIC to PRE-1 conversion, and PRE-1 to POST-1 conversion of the ribosome complex. Initially V177C-L1 (Cy3) 50S or V221C-L1 (Cy3) 50S were used as FRET acceptors with fMet-tRNA<sup>fMet</sup> (Rhd110) as the FRET donor. In these experiments, the donor was the limiting reagent, and therefore, the loss in donor signal was the main focus of the FRET efficiency measurements. In Buffer B, the purified 70SIC was incubated with ternary complex to create a PRE-1 complex in which the tRNA<sup>fMet</sup> (Rhd110) was free to sample the P/E hybrid state, and this resulted in an overall FRET efficiency increase between the deacylated-tRNA<sup>fMet</sup> and the labeled L1 as measured by decrease in donor fluorescence (Figure A1.1). Further, upon addition of EF-G.GTP to the PRE-1 complex, the donor fluorescence does not change, indicating a similar FRET efficiency for when deacylated-tRNA<sup>fMet</sup> occupies a P/E hybrid and a E/E translocated state, as expected from previous single molecule results (Fei et al., 2008). Although, initially these results were promising, we later decided that the Cy3 / Rhd110 FRET pair was not ideal for these L1 to tRNA (L/t) equilibrium FRET experiments, and by using a Cy5 / Cy3 pair, analysis by measuring acceptor fluorescence would also be possible due to decreased overlap of signals with



this dye pair. Further, during optimization of the L/t FRET experiments, the mutant T202C-L1, utilized by Fei and coworkers, was discovered and we decided to use this mutant because it was already shown to work well as an indicator for tRNA movement. However, we should not be hasty in ruling out the possibility that these other mutants would work just as well, and/or provide further information about the movements near the E-site.

### **K54C-L1 (Cy5)**

Munro and coworkers initially used the mutant S55C as an indicator of L1-tRNA FRET in single molecule experiments, and therefore, we decided to design the mutants K54C and S55C (**Munro et al, 2009; Munro et al., 2010**). Undergraduate (Adrienne Remiker) and rotation students (Chris Bryan, Cheryl McCullough, and Yanxin Wang) performed the majority of the experiments done with these mutants under my supervision. Primers for both mutants were designed, and Adrienne overexpressed the subsequent mutant protein. Chris and Cheryl labeled the K54C-L1 with Cy5-maleimide, and reconstituted the labeled L1 into the –L1 50S, and Yanxin performed the majority of the equilibrium FRET and stopped flow FRET experiments seen below. Equilibrium FRET studies were performed on two different complexes: 1) 70SICs created with highly charged fMet-tRNA<sup>fMet</sup> (Cy3); and 2) 70SICs created with deacylated-tRNA<sup>fMet</sup> (Cy3). The complexes were not purified through sucrose cushion, and either ternary complex (PRE-1) or ternary complex and EF-G.GTP (POST-1) were added to the 70SICs. The complexes created with highly charged fMet-tRNA<sup>fMet</sup> (Cy3) show very little change in the FRET efficiencies between all three complexes (**Figure A1.2 A**). The complexes

created with deacylated-tRNA<sup>fMet</sup> (Cy3) show a steady decrease in FRET efficiency from 70SIC to PRE-1 to POST-1. It is possible that this is due to deacylated-tRNA (not removed by sucrose cushion) non-specifically binding to the E-site creating high FRET efficiency in the 70SIC that is lost upon addition of ternary complex and/or EF-G.GTP (Figure A1.2 B). This decrease in FRET efficiency between the 3 complexes is also seen in time resolved stopped flow experiments seen below.

A 70SIC was created using deacylated-tRNA<sup>fMet</sup> (Cy3) and K54C-L1 (Cy5) (0.25  $\mu\text{M}$ ) and a ternary complex with Phe-tRNA<sup>Phe</sup>.EF-Tu.GTP (1.0  $\mu\text{M}$ ) was added in a stopped flow experiment. The resulting acceptor fluorescence change can be seen in Figure A1.3 A and can be fit to a double exponential curve with an initial rapid increase ( $k_{\text{app}1} = 25 \text{ s}^{-1}$ ) followed by a slower decrease ( $k_{\text{app}2} = 0.37 \text{ s}^{-1}$ ). The rapid FRET efficiency increase may be attributed to the ternary complex binding, whereas, the slow decrease (most likely what is seen in the equilibrium FRET) can be attributed to the loss of any deacylated-tRNA<sup>fMet</sup> (Cy3) from the E-site of the ribosome. Further, the donor channel signal (Figure A1.3 B) can be fit to a triple exponential, where the first phase is a mathematically induced donor decrease to accompany the acceptor increase described above. Analysis of the donor channel reveals a fluorescence change associated with inherent fluorescence change of the tRNA<sup>fMet</sup> (Cy3) upon tRNA accommodation, and occurs with an apparent rate constant of  $\sim 10 \text{ s}^{-1}$ . The final phase seen in the donor channel is a slow increase that is similar to the decrease seen in the acceptor channel and is most likely attributed to the loss of any tRNA that was initially bound to the E-site in

the 70SIC complex. Further studies with the K54C-L1 mutant must be performed in order to determine its true effectiveness as a probe for P- and E-site tRNA movement.

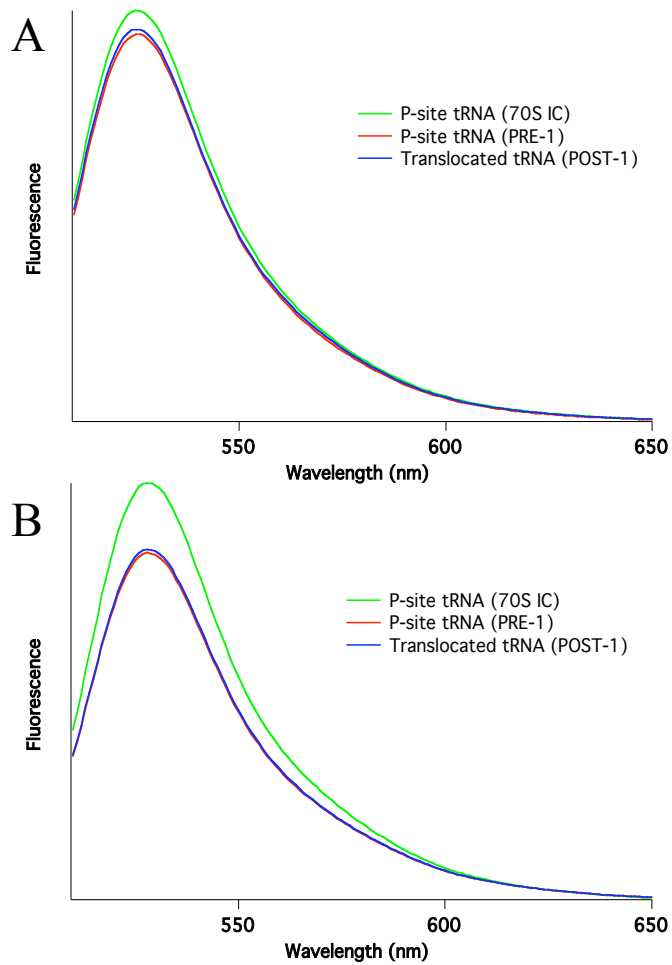


**Figure A1.1 Equilibrium FRET Traces of PRE and POST Translocation Ribosomes Using the Rhd110/Cy3 FRET Pair (V177C-L1, V221C-L1)**

70S initiation complexes were made for FRET analysis using fMet-tRNA<sup>fMet</sup> (Rhd110) as the donor and **A**) V177C-L1-50S (Cy3) or **B**) V221C-L1-50S (Cy3) as the acceptor. Equilibrium FRET measurements were taken using a Spectrofluorometer to determine the FRET at different stages of translocation. P-site / L1 FRET was measured in two ways; 1: using a P-site bound initiator tRNA (70SIC, 0.1 uM, green trace); and 2: by adding ternary complex containing Phe-tRNA<sup>Phe</sup>.EF-Tu.GTP (0.25 uM) to create a deacylated initiator tRNA that is free to sample the P/E hybrid state (PRE-1, red trace). The PRE-1 complexes were translocated by addition of EF-G.GTP (0.50 uM) and the FRET efficiency was measured by change in Donor wavelength fluorescence. The complexes were created using limiting donor (fMet-tRNA<sup>fMet</sup> (Rhd110)); therefore, the change in donor is used to determine FRET efficiency change. Because excess acceptor is used, it is possible that an acceptor molecule does not interact with a donor molecule; thus, the signal at the acceptor emission does not necessarily increase upon donor decrease since this is a bulk experiment. Further, the background caused by direct excitation of Cy3 in the experiment makes it very difficult to analyze the traces at the acceptor wavelength. Therefore, in all later experiments using T202C-L1 and K54C-L1 mutants, Cy3/Cy5 FRET efficiency is measured.

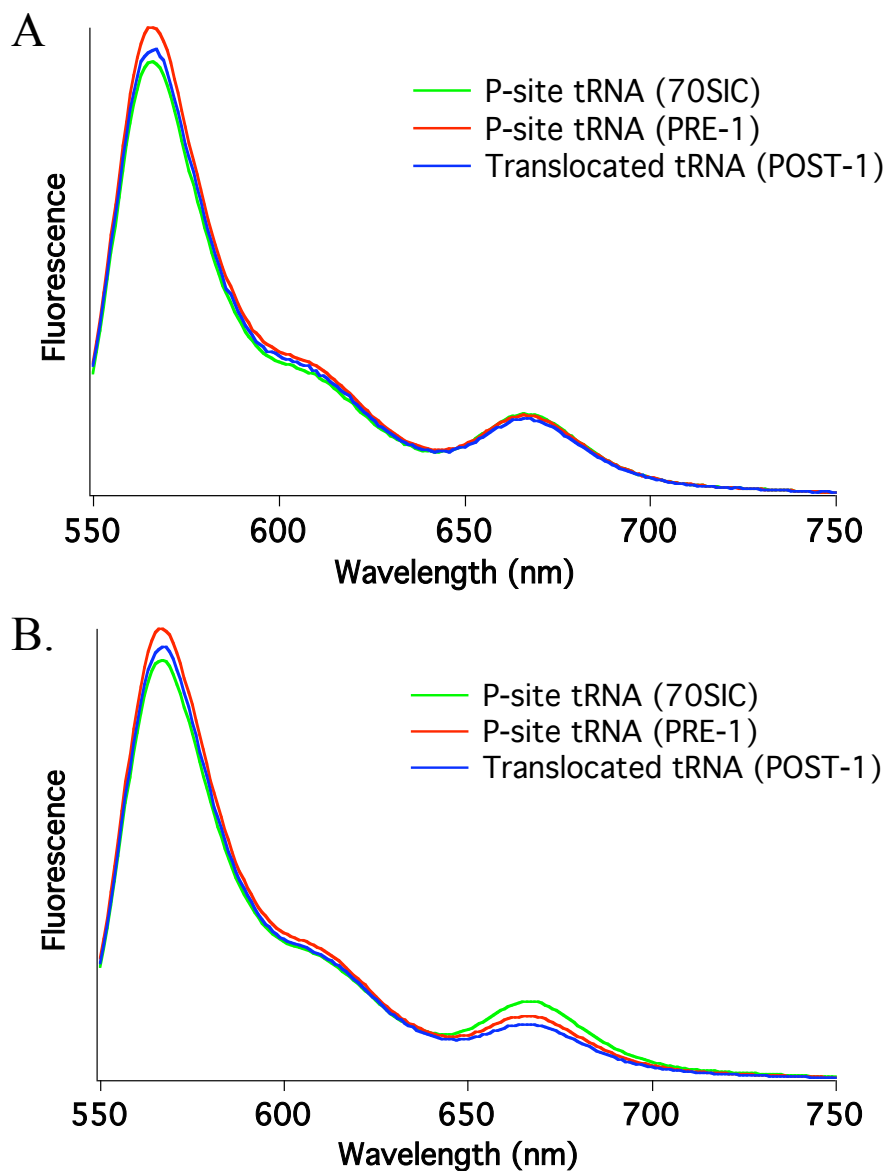
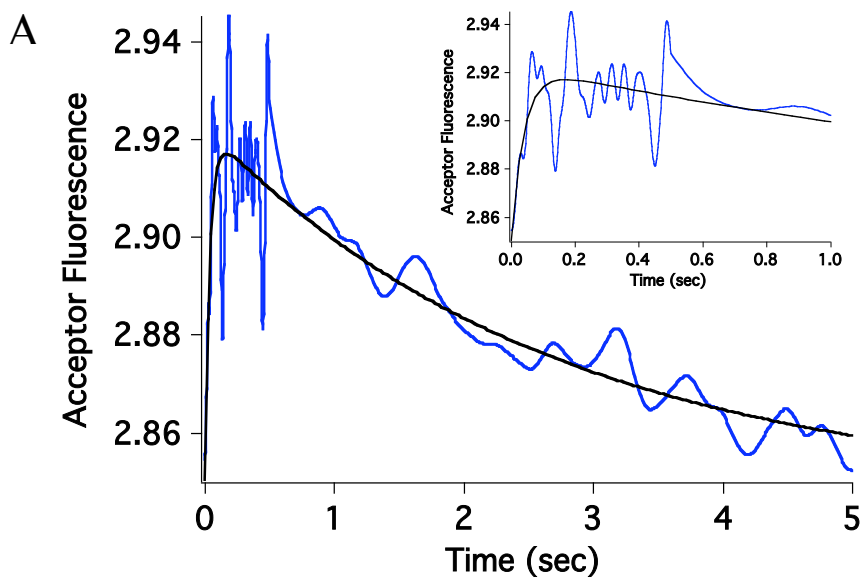


**Figure A1.2 Equilibrium FRET Traces of K54C-L1 (Cy5) Ribosomes**

**A and B:** 70S initiation complexes not purified through sucrose were made for FRET analysis using **A:** fMet-tRNA<sup>fMet</sup> (Cy3) or **B:** deacylated-tRNA<sup>fMet</sup> (Cy3) as the donor and K54C-L1-50S (Cy5) as the acceptor. Equilibrium FRET measurements were taken using a Spectrofluorometer to determine the FRET efficiency at different stages of

translocation. P-site / L1 FRET was measured in two ways; 1: using a P-site bound initiator tRNA (70SIC, 0.1 uM, green trace); and 2: by adding ternary complex containing Phe-tRNA<sup>Phe</sup>.EF-Tu.GTP (0.25 uM) to create a deacylated initiator tRNA that is free to sample the P/E hybrid state (PRE-1, red trace). The PRE-1 complexes were translocated by addition of EF-G.GTP (0.50 uM) and the FRET efficiency change was observed. The use of deacylated-tRNA<sup>Met</sup> (Cy3) in the 70SIC resulted in a decrease in FRET efficiency as measured by the acceptor decrease, and could be attributed to contaminating E-site deacylated tRNA<sup>Met</sup> (Cy3) leaving the E-site.

The complexes were created using limiting acceptor (Cy5-50S); therefore, the change in acceptor is used to determine FRET efficiency change. Because excess donor is used, it is possible that a donor molecule does not interact with an acceptor molecule; thus, it is possible that the signal at the donor emission does not necessarily decrease upon acceptor increase when FRET is seen since this is a bulk experiment.



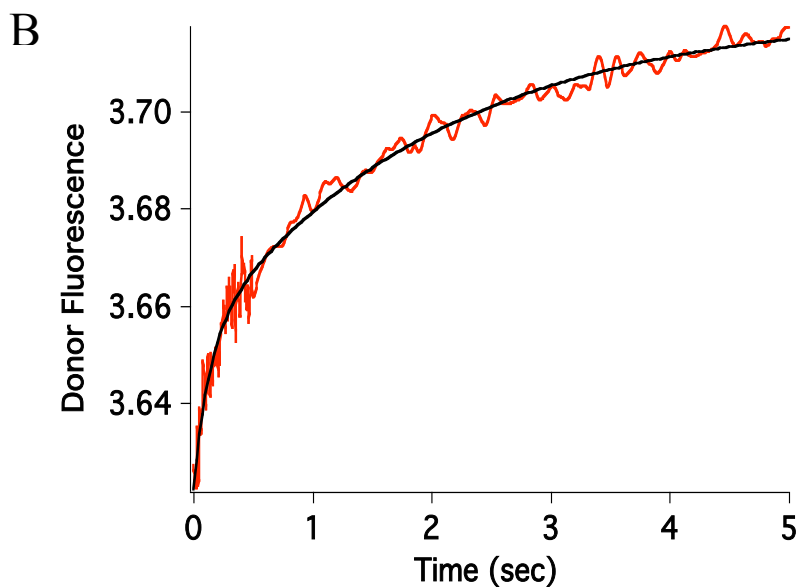


**Figure A1.3 FRET Efficiency Changes Associated With 70SIC to PRE-1 Complex as Viewed by Labeled K54C-L1**

70SIC complexes were made containing deacylated-tRNA<sup>fMet</sup> (Cy3) and K54C-L1 (Cy5) and not purified through sucrose cushion centrifugation. Ternary complex (Phe-tRNA<sup>Phe</sup>.EF-Tu.GTP, 1.0  $\mu$ M) was stopped flow added to the 70SIC (0.25  $\mu$ M) in order to create a PRE-1 complex. The donor Cy3 was excited at 540 nm, the acceptor channel emission (A) was observed at  $680 \pm 10$  nm, and the donor channel emission (B) was observed at  $570 \pm 10$  nm.

## **Appendix 2**

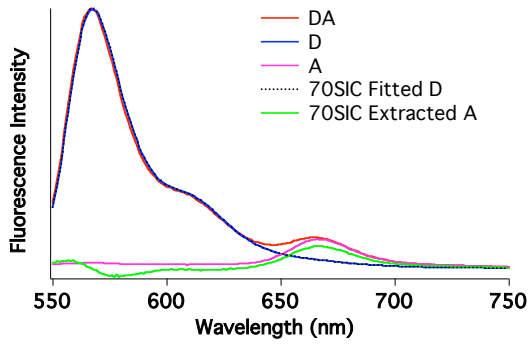


Buffer	Complex	Cy5/ 70S	Cy3/ 70S	D*A* (A) x10 <sup>5</sup>	D*A* (D) x10 <sup>6</sup>	D*A (A) x10 <sup>4</sup>	D*A (D) x10 <sup>6</sup>	Ext. A (A) x10 <sup>5</sup>	DA* (A) x10 <sup>5</sup>	FRET
<b>A1</b>	70SIC			1.95	1.54	4.85	1.51	1.45	1.62	~0
	PRE-1	0.64	0.78	2.66	1.41	4.85	1.51	2.21	1.62	<b>0.73</b>
	POST-1			1.79	1.54	4.85	1.51	1.29	1.62	~0
<b>A2</b>	70SIC			1.72	1.47	4.71	1.46	1.25	1.64	~0
	PRE-1	0.68	0.73	2.73	1.44	4.71	1.46	2.26	1.64	<b>0.77</b>
	POST-1			1.62	1.46	4.71	1.46	1.15	1.64	~0
<b>B1</b>	70SIC			1.66	1.46	4.84	1.50	1.90	1.53	~0
	PRE-1	0.66	0.75	2.68	1.45	4.84	1.50	2.21	1.53	<b>0.90</b>
	POST-1			2.35	1.43	4.84	1.50	1.89	1.53	<b>0.48</b>
<b>B2</b>	70SIC			1.56	1.39	4.97	1.40	1.07	1.46	~0
	PRE-1	0.67	0.70	2.60	1.37	4.97	1.40	2.12	1.46	<b>0.94</b>
	POST-1			2.27	1.36	4.97	1.40	1.79	1.46	<b>0.47</b>
<b>B3</b>	70SIC			1.53	1.23	4.49	1.41	1.13	1.54	~0
	PRE-1	0.55	0.69	2.50	1.37	4.49	1.41	2.06	1.54	<b>0.89</b>
	POST-1			2.37	1.43	4.49	1.41	1.91	1.54	<b>0.63</b>

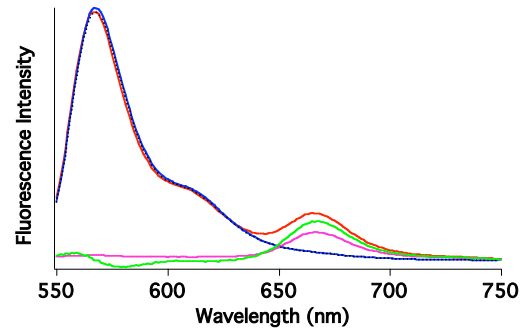
**Table A2.1 FRET Efficiency Calculations for Equilibrium FRET Experiments seen in Figure 4.1, 4.2 and A2.1**

## Buffer A, (Trial 2)

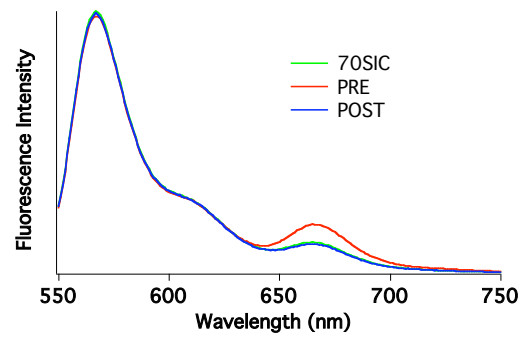
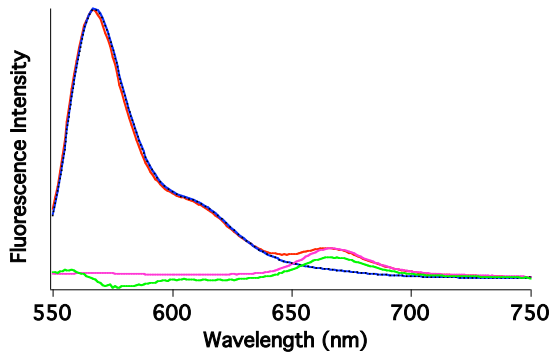
### 70SIC



### PRE-1

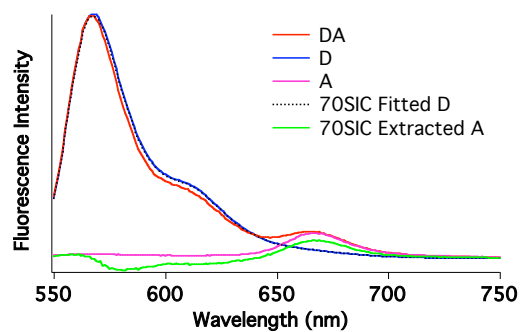


### POST-1

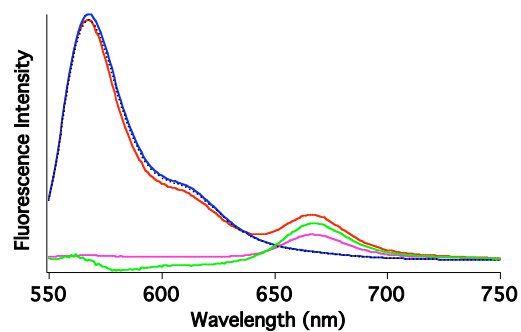


## Buffer B, (Trial 2)

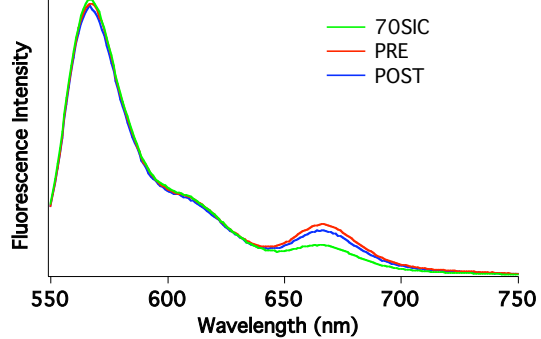
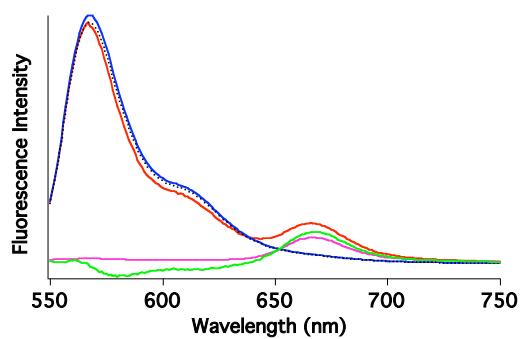
### 70SIC



### PRE-1



### POST-1



## Buffer B, (Trial 3)

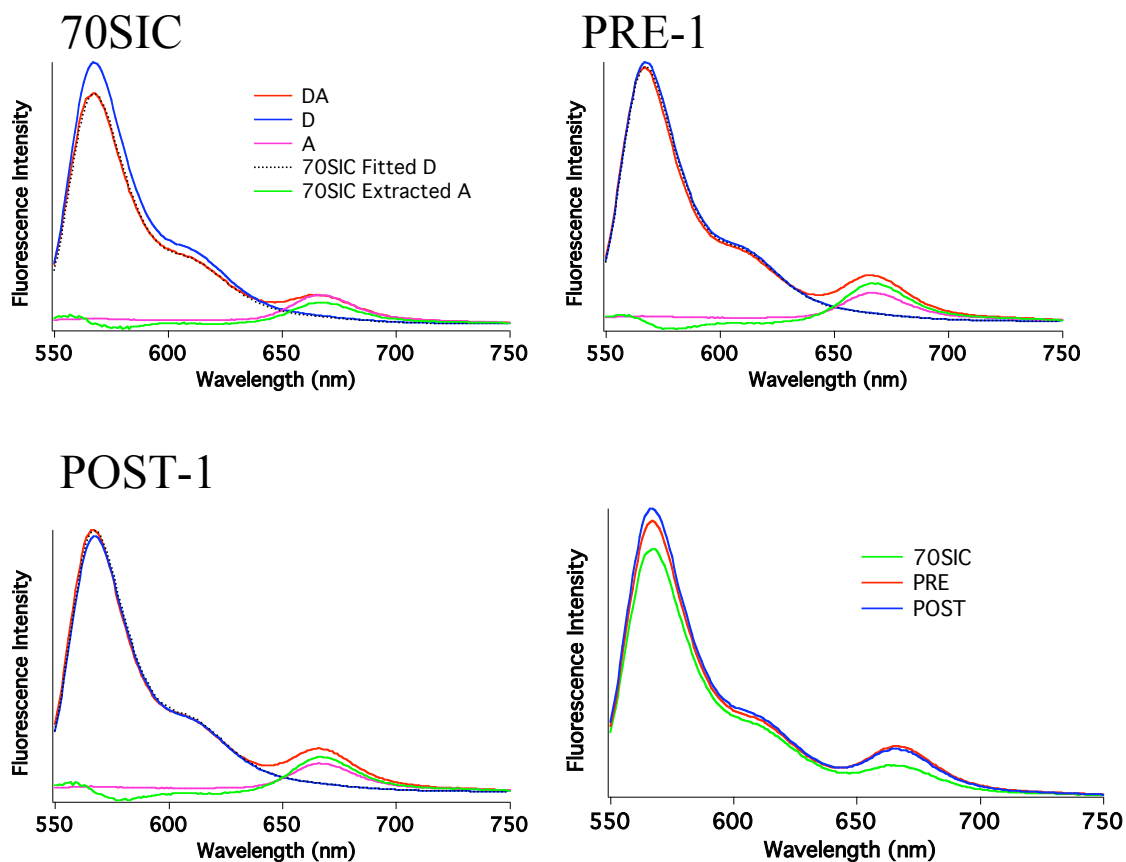


**Figure A2.1 Equilibrium FRET Efficiencies in Buffers A and B**

Complexes were made and equilibrium FRET was measured as in [Figure 4.1](#) (Buffer A) and [Figure 4.2](#) (Buffer B), however, instead of starting with highly charged initiator tRNA, ~25% charged initiator tRNA was used. FRET efficiency was determined and can be seen in [Table A2.1](#).